CATALYTIC OXIDATION PROCESSES USING FUNCTIONALISED *O,O'*-BIDENTATE LIGAND COPPER COMPLEXES

by

Pule Petrus Molokoane

A dissertation submitted to meet the requirements for the degree of

Magister Scientiae

in the

Department Of Chemistry
Faculty of Natural- and Agricultural Sciences

at the

University of the Free State

Supervisor: Prof. Gideon Steyl
Co-Supervisor: Prof. Andreas Roodt

December 2013

Acknowledgements

Revelations of Jesus Christ 1: 8

"I am the alpha and the Omega, the beginning and the end, who is and who was and who is to come, the almighty."

1Corinthians 15:10

"But by the grace of God I am what I am, and his grace which was bestowed upon me was not in vain; but I laboured more abundantly than they all, yet not I, but the grace of God which was with me."

With these two verses I would like to thank and Praise God almighty, his grace towards me has been overwhelming and humbling.

I would also like to thank my parents Nthabiseng Julia Molokoane and Moabi Joel Molokoane because without them none of this would be possible. Furthermore I would like to dedicate this to my late father Moabi Joel Molokoane, his selfless efforts to ensure that I will receive what he never got and thus ensuring a better future for me (he was truly devoted to us as his family and worked relentlessly for all of us including his grandchildren and always emphasized the importance of education. It's only unfortunate that he will never see this and ironically he's by far the one person who dreamed of seeing this).

Moabi Joel Molokoane (07-01-1950 to 22-10-2005)

To all my sisters for their support and for being my pillars of strength, thank you very much for everything. To my nephews and nieces for their patience and support, I know this endeavour has robbed you of a lot of precious time but nonetheless all of you were understanding and supportive. I hope this brings you all a sense of belief, that it creates the inspirational space that you all need to become what you all are destined to be (which in my opinion is "nothing short of phenomenal"). In a

sense this is an uncle trying to lead by example, so no one is pardoned in this regard and may his grace be with you in all your respective journeys.

To all my friends I would like to thank you all for your support and patience with me, I know I'm not the easiest person to be around but you all have embraced me regardless and for that I would like to express my most sincere gratitude.

To my colleagues at Inorganic Chemistry UFS for their support, help and for selflessly sharing all the knowledge and skills which contributed immensely to my development as a young scientist, thank you. Most importantly for leading by example and all the memorable times we shared together, special thanks to Dr Marietjie Schutte, Dr Cyril Young, Dr Theunis Jacobus Muller, Dr Ramakirushnan Suriya Narayanan, Dr Nagarajan Loganathan and Paul Severin Eselem Bungu.

To my supervisor and mentor Dr Gideon Steyl thank you for all the opportunities which you have provided to me and most importantly the support and encouragement ('at the very least always try'). What stands out for me about you was that you showed me a lot of faith which was overwhelming for me because I was an absolute stranger when I met you, and ever since then you have been nothing but kind and patient with me. Furthermore you were the first person who made me realize my capabilities as far as the applied sciences and research was concerned and you did this by example and for that I would like to express my gratitude.

To Prof Andreas Roodt, thank you for your enthusiasm and supervision with my project many of times your enthusiasm for science and research gave me reason to continue when I had stopped believing in this project. I would also like to commend you for your enthusiastic efforts in the group because I believe that's what keeps us all together at times. Furthermore also a big thank you for all the opportunities that you have provided for me in your research group and most importantly your patience with me.

'This work is based on the research supported in part by the following enterprises and or stakeholders;

- *The National Research Foundation of South Africa (Thrip), UID 84913.*
- *The Inkaba yeAfrica Foundation.*
- *Sasol.*
- *The University of the Free State.*

The opinions, findings and conclusions and/or recommendations expressed in this dissertation are that of the author, and the different enterprises/stakeholders mentioned here accept no liability whatsoever in this regard.

Table of Contents

Table of Contents

Table of Contents

ABBREVIATION

Abbreviation	Meaning
A_{obs}	Observed absorbance
ATR	Attenuated total reflectance
cm	centimeter
[Cu((EE(naltol))$_2$]	Bis(1,2-diethyl-3-hydroxy-4-pyridinonato)copper(II)
[Cu((EM(naltol))$_2$]	Bis(2-ethyl-3-hydroxy-1-methyl-4-pyridinonato)copper(II)
[Cu((EP(naltol))$_2$]	Bis(2-ethyl-3-hydroxy-1-isopropyl-4-pyridinonato)copper(II)
[Cu((ME(naltol))$_2$]	Bis(1-ethyl-3-hydroxy-2-methyl-4-pyridinonato)copper(II)
[Cu((MM(naltol))$_2$]	Bis(3-hydroxy-1,2-dimethyl-4-pyridinonato)copper(II)
[Cu((MP(naltol))$_2$]	Bis(3-hydroxy-2-methyl-1-isopropyl-4-pyridinonato)copper(II)
Eq.	Equation
(EE(naltol)H	1,2-Diethyl-3-hydroxy-4-pyridone
(EM(naltol)H	2-Ethyl-3-hydroxy-1-methyl-4-pyridone
(EP(naltol)H	2-Ethyl-3-hydroxy-1-isopropyl-4-pyridone
IR	Infra-red
K_x	Equilibrium constant for an equilibrium reaction
k_{obs}	Observed rate constant
M	mol.dm^{-3}
mg	Milligram
mmol	Millimol
(ME(naltol)H	1-Ethyl-3-hydroxy-2-methyl-4-pyridone
(MM(naltol)H	3-Hydroxy-1,2-dimethyl-4-pyridone
(MP(naltol)H	3-Hydroxy-2-methyl-1-isopropyl-4-pyridone
nm	Nanometer
TON	Turn over number
ppm	(Unit of chemical shift) parts per million
ν	IR stretching frequency
λ	UV/Vis wavelength
RMS	Root Mean Square
XRD	X-ray diffraction

Abstract

The aim of this study was to imitate the activity and behaviour of the enzyme catechol oxidase by employing simple copper nano molecular materials, and to investigate electronic and steric effects on this catalytic oxidation process. A range of *O,O'*-bidentate ligands were systematically synthesized by imparting different electronic properties to the ligand systems. These ligands were then coordinated to copper(II) metal ions to form the corresponding complexes. A total of six ligands were characterized and studied extensively, namely: MM(naltol)H, ME(naltol)H, MP(naltol)H, EM(naltol)H, EE(naltol)H and EP(naltol)H (3-hydroxy-1,2-dimethyl-4-pyridone, 1-ethyl-3-hydroxy-2-methyl-4-pyridone, 3-hydroxy-2-methyl-1-isopropyl-4-pyridone, 2-ethyl-3-hydroxy-1-methyl-4-pyridone, 1,2-diethyl-3-hydroxy-4-pyridone, 2-ethyl-3-hydroxy-1-isopropyl-4-pyridone). Only five crystal structures are reported: (MM(naltol)H, ME(naltol)H, EM(naltol)H, EE(naltol)H and EP(naltol)H). Six copper complexes were also synthesized and studied of which only two crystal structures were reported {[Cu(ME(naltol))$_2$] and [Cu(EP(naltol))$_2$]}, namely; [Cu(MM(naltol))$_2$], [Cu(ME(naltol))$_2$], [Cu(MP(naltol))$_2$], [Cu(EM(naltol))$_2$], [Cu(EE(naltol))$_2$] and [Cu(EP(naltol))$_2$].

Structural data revealed that all the ligands were in the keto-enol tautomeric form in the solid state and in all the cases where a clear packing order was observed, weak hydrogen bonding is present. These interactions result in the formation of dimers, which stabilizes the structures. This data also indicated a C=O bond length increase with increasing electron donation in the synthesized *O,O'*-bidentate ligands systems. The synthesized copper complexes were planar with slight deviations from planarity and in both the complexes the copper atoms lie on inversion centers. These complexes exhibit strong intramolecular hydrogen interactions.

The solution study results suggest that the complex with the least electron donating group on the ligand was the most effective catalyst; however, the same complex was coincidentally the most sterically demanding complex in the study. As the catechol oxidase is a macro-molecule which is very sterically crowded, the data suggests that steric effects play an important role in the catalytic

process and this was successfully demonstrated at a small-molecular level of detail *via* solution modelling experiments.

The two proposed mechanisms favour the process equally and none is preferred over the other. In the first mechanism the first step involves the coordination of 3,5-di-*tert*-butylcatechol to the copper which results in the subsequent loss of one of the coordinated ligands. In the second step the second 3,5-di-*tert*-butylcatechol coordinates to the copper with the subsequent loss of the second coordinated ligand. The third step involves the interaction with oxygen and the subsequent loss of one 3,5-di-*tert*-butylcatechol moiety. The fourth step is the rate determining formation of 3,5-di-*tert*-butylbenzoquinone, defined by the rate constants k_3 and k_{-3}, which also generates the catalytic species. The second mechanism is similar to the first and includes a reversible equilibrium between a two coordinated catechol species and a one catechol coordinated species, as well as a direct coordination of a new catechol molecule on the naltol-copper(II) species. The one catechol coordinated species oxidises the catechol to the corresponding quinone and the copper center is reduced in the process. An interaction with molecular oxygen re-oxidises the metal center and generates the catalytic species, which yields the product 3,5-di-*tert*-butylquinone. The rate constants in Mechanism 2 are defined by k_8 and k_{-8}. For the complexes $[Cu(ME(naltol))_2]$, $[Cu(MP(naltol))_2]$ and $[Cu(EP(naltol))_2]$ (in methanol at 25° C) the rate constants are k_f (= k_3 or k_8) and k_r(= k_{-3} or k_{-8}): (3.4±0.6) x 10^{-4} $M^{-1}.s^{-1}$ and (3.6±0.4) x 10^{-6} $M^{-1}.s^{-1}$), (4.8±0.9) x 10^{-4} $M^{-1}.s^{-1}$ and (3.2±0.6) x 10^{-6} $M^{-1}.s^{-1}$), (8.7±0.7) x 10^{-4} $M^{-1}.s^{-1}$ and (6.15±0.02) x 10^{-6} $M^{-1}.s^{-1}$).

Keywords; Catechol oxidase, 3,5-di-*tert*-butylcatechol, 3,5-di-*tert*-butylquinone, *O,O'*-bidentate ligand, structures, keto-enol tautomer.

Opsomming

Die doel van hierdie studie was die nabootsing van die aktiwiteit en gedrag van die ensiem katesjol oksidase deur die gebruik van eenvoudige koper nanomolekulêre materiale, en die ondersoek van elektroniese en steriese effekte op hierdie katalitiese oksidasieproses. `n Reeks *O,O'*-bidentate ligande is dus sistematies vervaardig deur verskillende elektroniese eienskappe aan die ligandstelsels te verleen. Hierdie ligande is aan koper(II) metaalione gekoördineer om die ooreenkomstige komplekse te vorm. `n Totaal van ses ligande is breedvoerig gekarakteriseer en bestudeer, naamlik: MM(naltol)H, ME(naltol)H, MP(naltol)H, EM(naltol)H, EE(naltol)H en EP(naltol)H (3-hidroksie-1,2-dimetiel-4-piridoon, 1-etiel-3-hidroksie-2-metiel-4-piridoon, 3-hidroksie-2-metiel-1-isopropiel-4-piridoon, 2-etiel-3-hidroksie-1-metiel-4-piridoon, 1,2-dietiel-3-hidroksie-4-piridoon en 2-etiel-3-hidroksie-1-isopropiel-4-piridoon). Slegs vyf kristalstrukture is geraporteer (MM(naltol)H, ME(naltol)H, EM(naltol)H, EE(naltol)H and EP(naltol)H). Ses koperkomplekse is ook vervaardig en bestudeer, waarvan twee kristalstrukture {[Cu(ME(naltol))$_2$] en [Cu(EP(naltol))$_2$]} geraporteer is: [Cu(MM(naltol))$_2$], [Cu(ME(naltol))$_2$], [Cu(MP(naltol))$_2$], [Cu(EM(naltol))$_2$], [Cu(EE(naltol))$_2$] en [Cu(EP(naltol))$_2$].

Strukturele data het onthul dat die ligande in die vaste toestand in `n keto-enol toutomeriese vorm voorkom en dat swak waterstofbindings voorkom in alle gevalle waar `n duidelike pakkingsorde waargeneem is. Hierdie waterstofbinding lei tot die vorming van dimere, wat die strukture stabiliseer. Hierdie data het ook `n verlenging van die C=O binding aangedui tydens `n toename in elektronskenking in die gesintetiseerde *O,O'*-bidentate ligandstelsels. Die gesintetiseerde koperkomplekse is planêr met effense afwykings uit planêriteit en beide die komplekse se koperatome lê op inversiesenters. Hierdie komplekse vertoon ook sterk intramolekulêre waterstofinteraksies.

Die resultate van die oplossingstudie stel voor dat die kompleks met die mins elektronskenkende groep die meer effektiewe katalis is, dieselfde kompleks is egter ook die mees steries veeleisende kompleks in die studie. Aangesien die katesjol oksidase `n steries beknopte makromolekuul is, stel die data voor dat die steriese effek `n belangrike rol in die katalitiese proses speel en hierdie

stelling is suksesvol gedemonstreer op `n molekulêre vlak *via* oplossingsmodulering eksperimente.

Die twee voorgestelde meganismes is ewe effektief en geeneen word bo die ander verkies nie. Die eerste stap van die eerste meganisme behels die koördinasie van 3,5-di-*tert*-butielkatesjol aan die koper wat lei tot die verlies van een van die gekoördineerde ligande. Tydens die tweede stap koördineer `n tweede 3,5-di-*tert*-butielkatesjol aan die koper met `n gepaardgaande verlies van `n tweede gekoördineerde ligand. Die derde stap behels die interaksie met suurstof en die gevolglike verlies van een 3,5-di-*tert*-butielkatesjol moïeteit. Die vierde stap is die tempobepalende vorming van 3,5-di-*tert*-butielbensokinoon, gedefinieer deur die tempokonstantes k_3 en k_{-3}, wat ook die katalitiese spesie genereer. Die tweede meganisme is soortgelyk aan die eerste, en sluit `n omkeerbare ewewig tussen `n twee gekoördineerde katesjolspesie en `n enkel gekoördineerde katesjol spesie in, asook direkte koördinasie van `n nuwe katesjol molekuul aan die naltol-koper(II) spesie. Die enkel gekoördineerde katesjol spesie oksideer die katesjol na die ooreenkomstige kinoon en die koper kern word in die proses gereduseer. `n Interaksie met molekulêre suurstof heroksideer die metaalkern en genereer die katalitiese spesie wat 3,5-di-*tert*-butielkinoon as produk lewer. Die tempokonstantes in Meganisme 2 word gedefinieer deur k_8 en k_{-8}. Vir die komplekse [Cu(ME(naltol))$_2$], [Cu(MP(naltol))$_2$] en [Cu(EP(naltol))$_2$] (in metanol teen 25° C) is die tempokonstantes k_f (= k_3 of k_8) en k_r(= k_{-3} of k_{-8}): (3.4±0.6) x 10^{-4} $M^{-1}.s^{-1}$ en (3.6±0.4) x 10^{-6} $M^{-1}.s^{-1}$), (4.8±0.9) x 10^{-4} $M^{-1}.s^{-1}$ en (3.2±0.6) x 10^{-6} $M^{-1}.s^{-1}$), (8.7±0.7) x 10^{-4} $M^{-1}.s^{-1}$ en (6.15±0.02) x 10^{-6} $M^{-1}.s^{-1}$).

Sleutelwoorde: Katesjol oksidase, 3,5-di-*tert*-butielkatesjol, 3,5-di-*tert*-butielkinoon, *O,O'*-bidentate ligand, strukture, keto-enol toutomeer.

1 Introduction and Aim of Study

1.1 Introduction

Emulating complicated biological activity with a simple synthetic molecule is a challenging attempt with various obstacles. To decrypt the biological code of reactivity, the biochemical process needs to be studied and examined thoroughly because a sound knowledge of the process by which the activity occurs is required. The next step is to determine functional reaction conditions for a model system, which is then followed by the development of functional and catalytic models and similar chemical architectures. This process is greatly aided by characterization methods (e.g. X-ray structural data) as they can reveal the character/identity of small/nano particles which can then be reproduced for modelling purposes. Functional models grant the opportunity to examine biological reactivity at a small-molecule level (metal complexes) of detail through systematic and comparative studies as opposed to at a macromolecular level of detail (enzymes etc.).

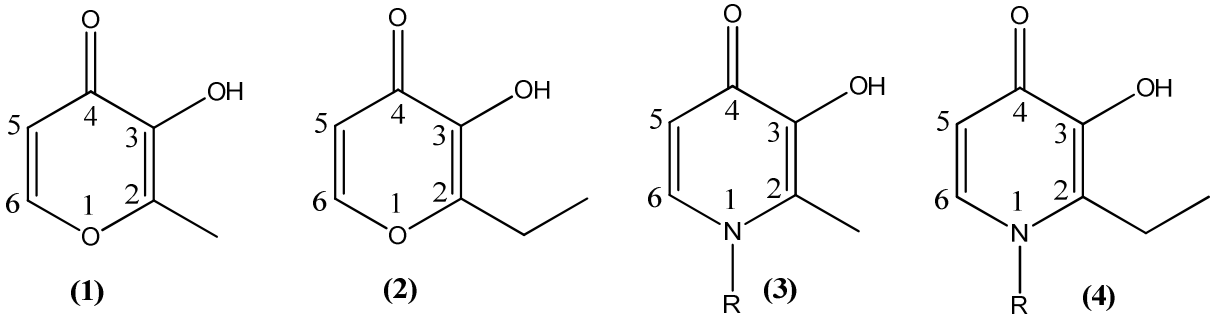

R = Me/Et/*iso*-propyl

Figure 1.1. 3-Hydroxy-4-pyranones (1 and 2) and the corresponding 3-Hydroxy-4-pyridones (3 and 4).

Copper containing enzymes are extremely important for their role of acting as oxygen carriers and in the oxidation reactions of many substrates.[1] In this study catechol oxidase activity of a series of Cu based complexes was studied as models to this enzyme which is responsible for the oxidation of phenolic compounds to quinones.[1] A series of *O,O'*-donor bidentate ligands were synthesized by fuctionalizing 3-hydroxy-2-methylpyran-4-one **(1)** and 3-hydroxy-2-ethylpyran-4-one (**2)** to yield the respective 3-hydroxy-2-methylpyrid-4-one **(3)** and 3-hydroxy-2-ethylpyrid-4-one **(4)** derivatives. The role of these ligands is very crucial as it tunes the O_2-binding process and the subsequent reactivity with substrates. For this reason functionalization was carried out in such a way that an array of different steric and electronic properties were brought about on the resulting structures in order to study their effects. These *O,O'* ligands were then coordinated to Cu(II) to form copper complexes which could be modelled for catechol oxidase activity. Furthermore the efficiency of the different complexes and factors influencing the efficiency should be determined as function is related to structure.

1.2 3-Hydroxy-4-pyranones

Pyrones maltol and ethyl maltol occur naturally in the bark and needles of certain conifers e.g. *Abies sibirica* (Siberian Fir) while they are also naturally obtained from malt, coffee, cocoa, milk, soya, etc.[2] These compounds are also formed during the pyrolysis of materials like cellulose, starch, and wood. They both are low-toxic compounds (LD_{50} 1400 mg/kg) and for this reason find application in the food and cosmetic industry.[2] However, it has been reported that maltol is a growth inhibitor.[3] These substances have a caramel like taste and induce the distinct scent of baking and roasting.[4] They also act as synergistic agents in flavour and sweetness enhancement of beverages, confections and chocolate products.

Of interest to this study is that these compounds are relatively cheap and are readily functionalized to various compounds and the fact that these compounds and their derivatives are biologically active compounds (specifically 3-hydroxy-4-pyridones (3,4-HPs)).[5] Furthermore these easy-to-functionalize heteroatomic rings are strong chelating ligands towards hard metal

[1] C. Eicken, B. Krebs, J. C. Sacchettini, *Curr. Opin. Struct. Biol. 9* ***(1999)*** 677.
[2] S. A. Mukha, I. A. Antipova, S. A. Medvedva, V. V. Saraev, L. I. Larina, A. V. Tsyrenzhapov, B. G. Sukhov, *Chemistry for Sustainable Development 15* ***(2007)*** 448.
[3] S. Patton, *J. Biol. Chem. 184* ***(1950)*** *131.*
[4] A. O. Pittet, P. Rittersbacher, R. Muralidhara, *J. Agr. Food Chem, 18* ***(1970)*** 929.
[5] M. A. Santos, S. M. Marques, S. Chaves, *Coord. Chem. Rev. 256* ***(2012)*** 240.

ions (e.g. Cu, Fe, Al, etc.).[6] This implies that using these compounds as basis, structural mutations can be performed strategically to investigate the influence of chemical properties such as the effect of electron withdrawing and donating groups and the effect of steric bulk while employing a hard metal like copper. For this reason 3-hydroxypyranones were functionalized to the corresponding 3-hydroxy-4-pyridinones (3,4-HPs) by substituting the cyclic oxygen with primary amines; methyl amine, ethyl amine and *iso*-propyl amine. From this series the electron donating ability of the alkyl groups is in this order; methyl > ethyl > *iso*-propyl. The effects of these substituents can be investigated in the resulting 3-hydroxypyridinone compounds.

1.3 3-hydroxy-4-pyridinones (3,4-HPs)

3,4-HPs are a group of N-heterocyclic core chelators. These compounds are easily functionalized and derivatized to a variety of compounds. This family of compounds is an important class of metal-related pharmaceutical drugs as they abstract/transfer hard metal ions (Fe^{3+}, Al^{3+}, etc.) from/into the human body.[6] These compounds are clinically used as iron chelating agents in patients suffering from metal overload related illnesses (β-Thalassemia, Alzheimer, etc.).[7] Biometals (Fe, Zn, Cu, Mo etc.) although important trace elements, can accumulate in the body as non-essential metal ions.[5] This can be attributed to either environmental exposure or the administration of metallodrugs to the human body.[7] This results in the disruption of several homeostatic mechanisms and buffering systems which regulate the low concentration of free metal ions.[5] 3,4-HPs are then administered orally to sequester dysfunctional metal ions in the body.[8] Because the resulting complexes are neutral they are readily partitioned across the cell membrane and in this way can facilitate the transportation of metals across the intestinal walls.

From synthesizing these compounds, a solid state study *via* x-ray crystallography of these ligands will show the effect of these substituents on the starting materials especially looking at changes in the carbonyl distances which might affect the coordination capacity of the newly synthesized ligands (3,4-HPs). These ligands will then aid in tuning the O_2-binding process and the subsequent reactivity of the resulting complexes with substrates. Furthermore, any intermolecular interactions that might also affect the coordination ability or the lability of the

[6] M. A. Barrand, B. A. Callingham, R. C. Hider, *J. Pharm. Pharmacol. 39* ***(1987)*** 203.
[7] G. Crisponi, M. Remelli, *Coord. Chem. Rev. 252* ***(2008)*** 1225.
[8] Z. D. Liu, R. C. Hider, *Coord. Chem. Rev. 232* ***(2002)*** 151.

resulting complexes can be determined as well as their respective strengths (the lengths in Angstrom of the different intermolecular interactions).

1.4 3,5-di-*tert*-butylcatechol

Catechol metabolism is essential both biologically and environmentally. Two main enzymes play a key role in these reactions, catechol dioxygenases and catechol oxidases. Catechol oxidases (found in bacteria, fungi, and plants) catalyze the oxidation of a variety of *o*-diphenols to the corresponding *o*-quinones.[9] Catechol oxidase is thought to be involved in plant protection as highly reactive *o*-quinones autopolymerize to brown polyphenolic catechol melanins, a process inferred to protect damaged plants from pathogens or insects.[10] This enzyme utilizes a dinuclear copper(II) center.[10] Catechol dioxygenase on the other hand are found in soil bacteria acting as intra- and extradiol cleaving enzymes that convert aromatic compounds to aliphatic compounds by cleaving them between the *ortho*-hydroxyls or outside the hydroxyl groups.[11] Intradiol-cleaving enzymes usually utilize an Fe(III) center, while the extradiol-cleaving enzymes usually utilize an Fe(II) center.[11]

This study is concerned with the oxidation of 3,5-di-*tert*-butylcatechol oxidation to 3,5-di-*tert*-butylquinone, a series of Cu(II) complexes will be synthesized in an attempt to reproduce the catechol oxidase activity with such complexes (see Figure 1.2).

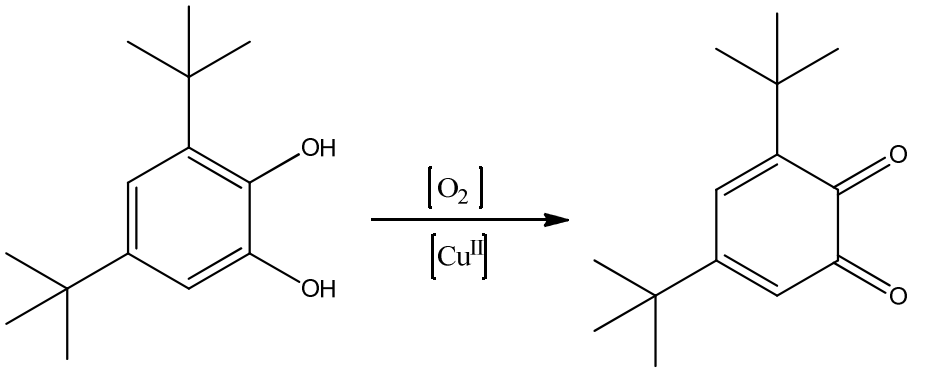

Figure 1.2. 3,5-di-*tert*-butylcatechol oxidation to 3,5-di-*tert*-butylquinone.

[9] B. K. Vimal, A. –A. Núria, C. Montserrat, H. Geeta, *Inorg. Chim. Acta. 363* ***(2010)*** 97.
[10] A. Majumder, S. Goswami, S. R. Batten, M. S. El Fallah, J. Ribas, S. Mitra, *Inorg. Chim. Acta. 359 (**2006**)* 2375.
[11] Kupán, J. Kaizer, G. Speier, M. Giorgi, M. Réglier, F. Pollreisz, *J. Inorg. Biochem. 103 (**2009**)* 389.

The aim is to emulate the complex biological reactivity produced by catechol oxidase by creating similar chemical architectures (simple synthetic molecules) to decode the biological code of reactivity. Furthermore from these modelling studies functional reaction conditions as well as optimum reaction conditions and the various parameters that can influence reactivity can be determined.

1.5 Aim of the study

Copper is an important trace element and finds wide application in many biochemical processes. These biochemical processes usually entail copper/oxygen systems as dioxygen carriers or as agents for selective and catalytic oxidative mutations. This implies that copper complexes can be modelled as oxidation catalyst and this provides interesting possibilities for systematic investigation. Compatible and versatile ligands aid in tuning the O_2-binding process and the subsequent reactivity with substrates in functional models.

The different aims for this study can therefore be summarized as follows:

1. The synthesis and characterisation of 3,4-HPs from the corresponding 3,4-hydroxypyranones.
2. The synthesis of copper(II) complexes by coordination of the synthesized 3,4-HPs to copper(II) metal ions.
3. Characterization of all the synthesized compounds using IR, NMR and X-ray diffraction.
4. The crystallographic characterization of the ligand systems and the resulting copper(II) complexes to study coordination modes, bond lengths, intra- and intermolecular interactions and distortions of the compounds.
5. Biomimetic modelling of catechol oxidase activity *via* reaction kinetics of the different copper(II) complexes which were synthesized (using 3,5-di-*tert*-butylchatechol as model substrate).
6. Analysis of results and comparison to literature.

2 Theoretical Aspects of Copper Catalysis

2.1 A brief history of copper

Copper (L. *cuprum*) previously known as *cyprium* (metal of Cyprus) was principally mined in Cyprus during the Roman era.[1] It has been mined for 5000 years and has been part of human civilization since ancient times to the modern day era.[1] In Mesopotamia during the time of the Sumerians and Chaldeans, specified use of the metal was established as considerable skills in copper handling were developed in this time. The copper manufactured in Mesopotamia was introduced to the Egyptian Empire where it was used to make ornaments, jewelry, armament and tools.[1] It was soon realized that pure copper, due to its softness, was not suitable for the manufacturing of tools used in agriculture. Later in the Roman era metals such as iron and bronze were used almost exclusively for tools and weaponry and it was during this time that copper was used in architecture for the first time.[1] A good illustration of its use can be witnessed in the roof sheathing of the Pantheon.[1]

Figure 2.1. The Roman Pantheon.[2]

[1] D. Rusjan, "Copper in Horticulture, Fungicides for Plant and Animal Diseases" (***2012***).
[2] http://romeinfo.files.wordpress.com/2011/12/roman_pantheon.jpg (last accessed 18/02/2014).

The use of copper(II) as an oxidizing agent for organic compounds dates back to Medieval practice involving what was known as Egyptian ointment. In 1815, the reddish brown precipitate was shown to be cuprous oxide.[3] In 1841 it was observed that D-glucose precipitated cuprous oxide from an alkaline solution of cupric sulphate, whereas sucrose did not react with this reagent.[4] Further work on carbohydrates by Barreswil led to his proposal of cupric tartrate as a qualitative test for reducing sugars.[4] A useful analytical procedure based on Barreswil's proposal by Fehling was developed a few years later.[5] Copper(II) is a useful oxidizing agent for a wide range of substrates because its highly selective and compatible with a variety of solvents.[6,7,8,9]

2.2 Copper in Organometallic Chemistry

2.2.1 Copper Metal

Copper is a chemical element with the symbol Cu, a freshly exposed surface of the metal is red-orange and shiny in colour. The metal is ductile, malleable and a good conductor of both heat and electricity (second only to silver in electrical conductivity). Some other notable chemical and physical properties of the element are summarized in Table 2.1.

[3] Vogel, Schweigger`s J. 13 (**1815**) 162.
[4] L. -C. Barreswil, *J. Pharm. 5* (**1844**) 425.
[5] H. Fehling, *Eur. J. Org. Chem. 72* (**1849**) 106.
[6] M. Bagherzadeh, M. Amini, A. Ellern, L. K. Woo, *Inorg. Chim. Acta. 383 (**2012**)* 46.
[7] T. Punniyamurthy, L. Rout, *Coord. Chem. Rev. 252 (**2008**)*134.
[8] S. M. Guo, C. L. Deng, J. H. Li, *Chin. Chem. Lett. 18 (**2007**)* 13.
[9] L. -H. Zou, A. J. Johansson, E. Zuidema, C. Bolm, *Chem. Eur. J. 19* (**2013**) 8144.

Table 2.1. Chemical and physical properties of copper[1,10]

Property	Value
Atomic Number	*29*
Relative Atomic Mass (g.mol^{-1})	*63.546(3)*
Ground State Electron Configuration	*[Ar]3d^{10} 4s^{1}*
Lattice type	*Face-centered cubic*
Melting Point (K)	*1357.77*
Boiling Point (K)	*2835*
Density (near r.t.) (g.cm^{-3})	*8.96*
Ionization Energy (kJ/mol)	*1st: 745.5*
	2nd: 1957.9
	3rd: 3555
Principal Oxidation States	*+1,+2,+3*
Fusion Heat (kJ/mol)	*13.26*
Evaporation Heat (kJ/mol)	*300.4*

Because of its electrical conductivity the electrical industry is one of the greatest users of copper and it is used for the production of wire, cable and electrical products for the electrical and building industries.[11] The construction industry accounts for the second most use of copper in areas such as pipes for plumbing, heating and ventilation as well as building wire and sheet metal facing.[11]

Cu^{2+} and Cu^{+} ions are soluble in water and provide antifungal and antibacterial effects (biostatic agents) at low concentration levels.[12] This intrinsic property is the main reason these ions are used in the production of fungicides. But high concentrations of copper salts affect physiological and biochemical processes in higher organisms.[13] This metal is an essential trace nutrient in

[10] R. C. Weast, M. J. Astle, "CRC Handbook of Chemistry and Physics", 60th ed. CRC Press: Boca Raton (***1980***).
[11] Copper Development Association: http://www.copper.org/publications/pub_list/pdf/a4095.pdf (last accessed 17/02/2014).
[12] N. Cioffi, L. Torsi, N. Ditaranto, G. Tantillo, L. Ghibelli, L. Sabbatini, T. Bleve-Zacheo, M. D'Alessio, P. G. Zambonin, E. Traversa, *Chem. Mater. 17 (**2005**)* 5255.
[13] M. C. Linder, M. Hazegh-Azam, *Am. J. Clin. Nutr. 63 (**1996**)* 7975.

plants, animals and humans. It is also an essential cofactor for many metalloproteins.[14,15] However, excess amounts of copper inhibits plant growth and impairs important cellular processes (i.e. photosynthetic electron transport) which leads to problems in cell function and metabolism.[16]

This metal was the first mineral to be extracted from the earth, and it has played a significant role in the history of man along with tin, as it gave rise to the Bronze Age. It is found in many minerals such as cuprite, malachite, azurite, chalcopyrite and bornite.[10] Large copper ore deposits are found in Canada, Chile, Peru, U.S., Zaire and Zambia.[10] The most significant copper ores are the carbonates, oxides and sulfides.[10] From these ore bodies, copper is acquired by smelting, leaching and electrolysis.[1]

2.2.2 Homogeneous Catalysis

By definition, homogenous catalysis refers to a catalytic system in which the substrates for a reaction and the catalyst components are brought together in one phase, mostly in the liquid phase. This process is important in industrial production of liquid fuels and bulk chemicals.[7] Furthermore, this process can also be used in the fine chemical industry to synthesize drugs and natural products; the petrochemical industry also employs some homogeneous catalytic systems.

By definition a catalyst is a substance that increases the rate at which a chemical reaction approaches equilibrium without itself becoming permanently involved. The catalyst or precursor can be activated or the actual catalytic species (active catalyst) can be generated *in situ*. During the catalytic cycle, the catalyst might exist in more than one form or states (molecular level) interconverting between the states and in a sense is therefore unaltered. Crucial properties that are influenced by a catalyst are the reaction rate and selectivity. This includes chemoselectivity, regioselectivity, diastereoselectivity and enatioselectivity. High selectivity implies a reduction of waste, a more effective use of feedstock and a less strenuous work-up procedure.

In this study a series of organometallic Cu(II) nano-complexes were synthesized by functionalizing maltol and ethyl maltol to their respective 3-hydroxy-4-pyridinones. These functionalized ligands were used to produced Cu(II) complexes. The ligand functionalization

[14] E. I. Solomon, R. G. Hadt, *Coord. Chem. Rev*. 255 (***2011***) 774.
[15] B. G. Malmström, P. Wittung-Stafshede, *Coord. Chem. Rev*. *185* (***1999***) 127.
[16] O. Farver, I. Pecht, *Coord. Chem. Rev. 255 (**2011**)* 757.

was carried out in a systematic manner to produce differing electronic and steric properties. The produced complexes were evaluated for catalytic activity and the influence that the induced functional groups had on catalysis.

In this chapter various applications of copper catalysis (mainly homogeneous) will be discussed to explain their insights and to draw a comparison in certain cases.

2.3 Oxidation

Catalytic oxidation plays a key role in transforming naturally available petroleum-based feed-stocks to more useful organic chemicals of a high oxidation state such as alcohols, alkenes and carbonyl compounds.[17,18] Millions of tons of these compounds are produced annually throughout the world and find various applications in the chemical industry ranging from agrochemicals to large scale commodities.[17-23] The processes of bulk chemical industries predominantly use molecular oxygen as primary oxidant for economic reasons (more cost effective). The efficiency of these processes depends mainly on the nature of the metal catalyst utilized to promote both the reaction rate and product selectivity. The fine chemical industry employs a variety of oxidizing reagents e.g. permanganate, dichromate etc.[24,25] However, these reagents are often required in stoichiometric quantities and generate hazardous by-products along with the target compounds demanding labour intensive work up procedures.[24-27]

The elimination of hydrogen from a substrate through the substitution of a hydrogen atom from a C–H bond with a more electronegative element in a chemical reaction is referred to as an oxidation reaction.[28] Oxidation reactions are reactions in which electrons are lost by one of the reagents (or substrates). The substrate losing the electron(s) is oxidised and the reagent causing

[17] G. W. Parshall, S. D. Ittel, "Homogeneous Catalysis: The Application and Chemistry of Catalysis by Soluble Transition Metal Complexes", 2nd ed, Wiley-Interscience, New York, (**1992**).
[18] R. A. Sheldon, J. K. Kochi, "Metal-catalyzed Oxidations of Organic Compounds", Academic Press, New York, (**1981**).
[19] A. E. Shilov, G. B. Shul'pin, *Chem. Rev. 97* (**1997**) 2879.
[20] C. L. Hill, *Nature 401* (**1999**) 436.
[21] L. Rout, T. Punniyamurthy, *Adv. Synth. Catal. 347* (**2005**) 1958.
[22] S. S. Stahl, *Angew. Chem. Int. Ed. 43* (**2004**) 3400.
[23] M. S. Sigman, M. J. Schultz, *Org. Biomol. Chem. 2* (**2004**) 2551.
[24] J. P. Collman, T. N. Sorrell, B. M. Hoffman, *J. Am. Chem. Soc. 97* (**1975**) 913.
[25] J. P. Collman, R. Boulatov, C. J. Sunderland, L. Fu, *Chem. Rev. 104* (**2004**) 561.
[26] M. Beller, C. Bolm, "Transition Metals for Organic Synthesis", *Wiley-VCH, Weinheim, 2* (**1998**).
[27] T. Punniyamurthy, S. Velusamy, J. Iqbal, *Chem. Rev. 105* (**2005**) 2329.
[28] J. E. Huheey, E. A. Keiter, R. L. Keiter, "Inorganic Chemistry", 4th Edition, Harper Collins, New York, (**1993)**.

oxidation is called an oxidant or an oxidizing agent and it is reduced in the process. Transition metal nano particles can act as catalysts in organic oxidation reactions (Figure 2.2).[28]

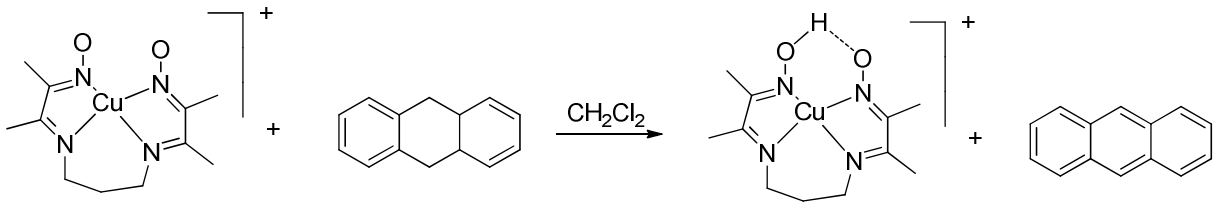

Figure 2.2. A Cu(II) complex oxidising 4a,9,9a,10-tetrahydroanthracene.

The transition metal catalysts of period four are of great use in oxidation chemistry because of their natural abundance, high reactivity and general application.[29] Among the first row transition metal complexes, copper complexes play a significant role in oxidation chemistry due to its relevance to abundance and biological chemistry.[30-34] This oxidation process usually involves a copper(II)-copper(I) couple.[35,36]

All catalytic oxidations can be classified into three categories:

(i) Catalytic oxygen transfer reactions: in this processes, the substrates react with an oxygen donor in the presence of a metal catalyst.[37-42]

[29] D. T. Sawyer, A. Sobkowaik, T. Matshumita, *Acc. Chem. Res. 29* (**1996**) 409.
[30] K. N. Kitajima, Y. Moro-oka, *Chem. Rev. 94* (**1994**) 737.
[31] K. D. Karlin, S. Kaderli, A. D. Zuberbuhler, *Acc. Chem. Res. 30* (**1997**) 139.
[32] J. -L. Pierre, *Chem. Soc. Rev. 29* (**2000**) 251.
[33] E. I. Solomon, P. Chen, M. Metz, S. -K. Lee, A. E. Palmer, *Angew. Chem. Int. Ed. Engl. 40* (**2001**) 4570.
[34] M. A. Halcrow, *Angew. Chem. Int. Ed. Engl. 40* (**2001**) 816.
[35] K. D. Karlin, Y. Gultneh, in: S. J. Lippard (Ed.), *Prog. Inorg. Chem. Wiley*, *35* (**1987**) 220.
[36] W. B. Tolman, *Acc Chem. Res. 30* (**1997**) 227.
[37] J. Smidt, W. Hafner, R. Jira, J. Sedlmeier, R. Sieber, H. Kojer, *Angew. Chem. Int. Ed. Engl. 1* (**1962**) 80.
[38] J. P. Collman, T. N. Sorrell, B. M. Hoffman, *J. Am. Chem. Soc. 97* (**1975**) 913.
[39] C. N. Satterfield, "Heterogeneous Catalysis in Practice", McGraw-Hill, New York, (**1980**).
[40] B. Meunier, S. P. de Visser, S. Shaik, *Chem. Rev. 104* (**2004**) 3947.
[41] J. P. Collman, R. Boulatov, C. J. Sunderland, L. Fu, *Chem. Rev. 104* (**2004**) 561.
[42] M. Costas, M. P. Mehn, M. P. Jensen, L. Que Jr., *Chem. Rev. 104* (**2004**) 939.

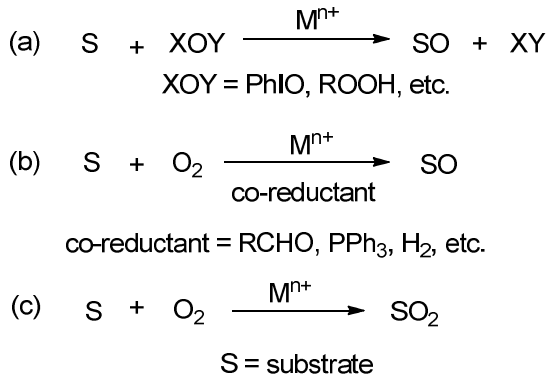

Figure 2.3. Catalytic oxygen transfer reaction.

(ii) Free radical oxidations: These oxidations are similar to autoxidation systems, it involves the generation of chain-initiating radicals through the metal-catalyzed decomposition of alkyl hydroperoxide.[43-46]

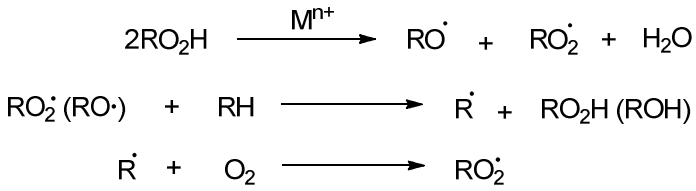

Figure 2.4. Free radical oxidation reactions.

(iii) Oxidations of a coordinated substrate by a metal ion: in this oxidation, the oxidized form of the metal is subsequently regenerated by the oxidation of the reduced form by dioxygen.[47-49]

[43] D. Mansuy, *Coord. Chem. Rev. 125* (**1993**) 129.
[44] J. E. Lyons, P. E. Ellis, H. K. Myers, *J. Catal. 155* (**1995**) 59.
[45] M. W. Grinstaff, M. G. Hill, J. A. Labinger, H. B. Gray, *Science 246* (**1994**) 1311.
[46] G. Yang, Y. Ma, J. Xu, *J. Am. Chem. Soc. 126* (**2004**) 10542.
[47] T. Mallat, A. Baiker, *Chem. Rev. 104* (**2004**) 3037.
[48] B. M. Stoltz, *Chem. Lett. 33* (**2004**) 362.
[49] J. Tsuji, "Palladium Reagents and Catalysts", Wiley, New York, (**1995**).

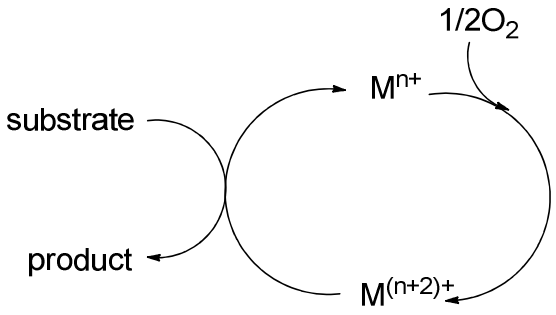

Figure 2.5. Metal ion oxidation of organic substrates.

2.4 Reactions with Molecular Oxygen

2.4.1 Epoxidation

Epoxides or oxiranes are three-membered-ring cyclic ethers. These compounds are adaptable synthetic compounds, making up convenient intermediates for the synthesis of many fine chemicals and commodities.[50,51] These compounds can be prepared from transition metal catalysts in the presence of terminal oxidants like NaOCI, PhIO, peracid, hydroperoxide and molecular oxygen. The latter is more attractive from an economic and environmental point of view as it is cheap and produces only water as a by-product in the absence of additives.[50,51] Copper(II) salts ($Cu(OH)_2$, $Cu(OMe)_2$ $CuCl_2$) and complex, $[Cu(OAc)_2]$, can be used for the epoxidation of alkenes with molecular oxygen employing aliphatic aldehydes as co-reductants (Table 2.2).[52] Terminal alkenes are less reactive in comparison to internal alkenes while *cis*-alkenes are isomerized to give a mixture of *cis* and *trans* epoxides.[52]

[50] K. A. Jorgensen, *Chem. Rev. 89* (**1989**) 431.
[51] T. Mukaiyama, T. Yamada, *Bull. Chem. Soc. Jpn. 68* (**1995**) 17.
[52] N. Komiya, T. Noata, Y. Oda, S.I. Murahashi, *J. Mol. Catal. A: Chem. 117* (**1997**) 21.

Table 2.2. Copper-catalyzed epoxidation of alkenes with cyclohexanal as a co-reductant.[52]

Entry	Substrate	Product	TON[a]
1	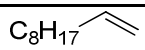	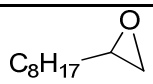	27
2		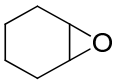	79
3	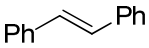		76
4	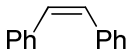	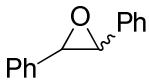 *trans* : *cis* = 22: 3	64

[a] ***Reactions studied at ambient temperature.***

Subsequently, copper(II) perchlorophthalocyanine has been used for the epoxidation of styrene, cyclohexene and 1-decene using 2-methylpropanal as a co-reductant at 40 °C with the following respective TONs: 798, 645 and 83.[53] The same study showed that under the same conditions using the same catalyst immobilized on HSi-MCM-41 increased the turnovers drastically with styrene and cyclohexene turnover numbers increasing to 3144 and 2532, respectively.[53]

2.4.2 Oxidation of Alkanes

The selective oxygenation of alkanes resulting in the corresponding oxygenated petrochemicals such as aldehydes, ketones, alcohols and carboxylic compounds is an important use of petroleum and natural gas based resources.[54-56] The oxidation process using copper as a catalyst and molecular oxygen as an oxidant is effective for the oxidation of higher alkanes yielding the corresponding alcohols and ketones in high turnovers. Copper(II) hydroxide ($Cu(OH)_2$) has been utilized for the oxidation of n-pentane, n-decane, cyclohexane and methylcyclohexane. It introduce OH and C=O functional groups in the respective structures to yield alcohols and

[53] P. Karandikar, M. Agashe, K. Vijayamohanan, A. J. Chandwadkar, *Appl. Catal. A: Gen. 257* (**2004**) 133.
[54] L. I. Simandi, "Catalytic Activation of Dioxygen by Metal Complexes", Kluwer Academic Publishers, Dordrecht, (**1992**).
[55] D. H. R. Barton, A. E. Martell, D. T. Sawyer, "The Activation of Dioxygen and Homogeneous Catalytic Oxidation", Plenum, New York, (**1993**).
[56] R. A. Sheldon, R. A. van Santen, "Catalytic Oxidation: Principles and Applications", World Scientific, Singapore, (**1995**).

ketones in the presence of ethanal (CH_3CHO) as a co-reductant in an oxygen atmosphere.[57,58] Replacement of $Cu(OH)_2$ with complexes derived from CuX_2 (X= Cl and OAc) and 18-crown-6 (**2**, in Figure 2.6.) or CH_3CN showed an enhancement in the efficiency of the oxidation (Table 2.3). Furthermore, copper(II) perchlorophthalocyanine (**1,** Figure 2.6) immobilized on NH_2-MCM-41 and $CuSO_4 \cdot 5H_2O$-**2** oxidises cyclohexane utilizing benzaldehyde and zinc respectively as co-reductants to yield a mixture of cyclohexanol and cyclohexanone.[59,60] The former was carried out at 50 °C yielding a product ratio of 32: 68 (cyclohexanol: cyclohexanone) with a turnover number of 297 based on the substrate (cyclohexane). The latter was carried out at room temperature yielding a product ratio of 77: 23 (cyclohexanol: cyclohexanone) with a turnover number of 134 based on cyclohexane. With the exception of the latter, these reactions occur *via* a radical process to yield ketones as the major products in comparison to alcohols (Table 2.3).

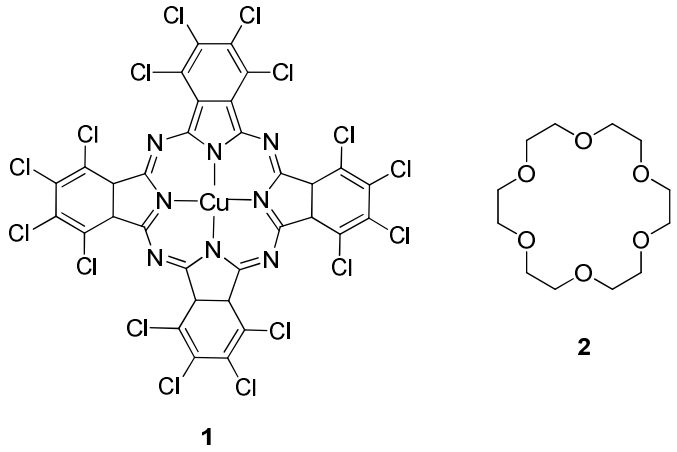

Figure 2.6. The structure of Cu(II) perchlorophthalocyanine [1] and 18-crown-6 [2].

[57] S. -I. Murahashi, N. Komiya, Y. Hayashi, T. Kumano, *Pure Appl. Chem. 73* (**2001**) 311.
[58] N. Komiya, T. Naota, S. -I. Murahashi, *Tetrahedron Lett. 37* (**1996**) 1633.
[59] P. Kanrandikar, A. J. Chandwadkar, M. Agashe, N. S. Ramgir, S. Sivasanker, *Appl. Catal. A: Gen. 297* (**2006**) 220.
[60] Y. Kurusu, D. C. Neckers, *J. Org. Chem. 56* (**1991**) 1981.

Table 2.3. Copper catalyzed oxidations of alkanes utilizing ethanal as a co-reductant.[61-63]

Entry	Catalyst	Temperature (°C)	Substrate	Products (ratio)	TON[a]
1	$CuCl_2$	70	Cyclohexane	Cyclohexanol (14), cyclohexanone (86)	16,200
2	$Cu(OAc)_2/CH_3CN$	70	Cyclohexane	Cyclohexanol (43), cyclohexanone (57)	27,000
3	$CuCl_2$	70	Cyclooctane	Cyclooctanol (11), cyclooctanone (89)	18,600
4	$CuCl_2$	70	*n*-Hexane	Hexan-2-ol (2.6), hexan-3-ol (2.6), hexan-2-one (46), hexan-3-one (48)	9,770
5	$Cu(OH)_2$	r.t.	*n*-Decane	Decan-2-ol (20), decan-3-ol (20), decan-2-one (27), decan-3-one (27)	1.5
6	$Cu(OH)_2$	r.t.	Adamandane	Adamantan-1-ol (27.7), adamantan-2-ol (1.6), adamantan-2-one (1)	9.6

[a] ***Based on co-reductant.***

The selectivity of cyclohexanol to cyclohexanone was increased to 50: 1 when the oxidation was carried out using a combination of $Cu(OAc)_2$ and quinone (in the ratio 5: 1), in acetonitrile as

[61] N. Komiya, T. Naota, S. -I. Muharashi, *Tetrahedron Lett. 37* (***1996***) 1633.
[62] S. -I. Muharashi, N. Komiya, Y. Hayashi, T. Kumano, *Pure Appl. Chem. 73* (***2001***) 311.
[63] N. Komiya, T. Naota, Y. Oda, S. -I. Muharashi, *J. Mol. Catal. A: Chem. 117* (***1997***) 21.

solvent, in the presence of tri-phenylphosphine (PPh_3) under irradiation.[64] The oxidation of n-hexane without the use of a co-reductant to a mixture of hexanol and hexanal with a 10.2 % conversion has been reported.[65] The reaction is catalyzed by the zeolite (NaY) supported copper-perchloropthalocyanine (**1)** under molecular oxygen (Figure 2.7).[65]

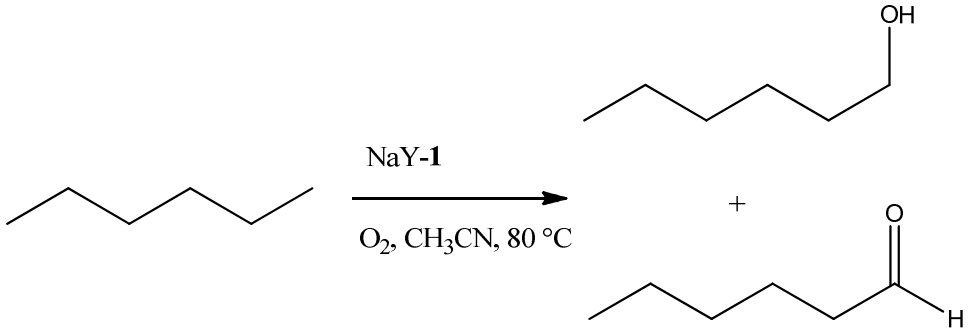

Figure 2.7. The oxidation of n-hexane without the use of a co-reductant.

The oxidation takes place only at the primary CH_3 group. This product distribution is not in favour of a free radical mechanism, which would typically be expected for a copper-catalyzed oxidation reaction. The application of $CuCl_2$ for the photocatalytic oxidation of cyclohexane without the use of a co-reductant with molecular oxygen was subsequently shown.[66,67] The reactions occurred with 70 % selectivity and 50 % conversion yielding a mixture of cyclohexanol and cyclohexanone under visible light.

2.4.3 Aromatic C—H oxidation

Aromatic C—H oxidation is one of the most difficult mutations in organic synthesis. The aromatic carbon nucleus is resistant to oxidation due to resonance stabilization and hence this reaction requires a very reactive oxidant under very harsh conditions.[68] Copper based catalytic systems with molecular oxygen are well documented in literature for this purpose.

[64] G. B. Shul'pin, M. M. Bockova, G. V. Nizova, *J. Chem. Soc., Perkin Trans. 2* (***1995***) 1465.
[65] R. Raja, P. Ratnasamy, *Stud. Surf. Sci. Catal. 100* (**1996**) 181.
[66] K. Takaki, j. Yamamoto, K. Komeyama, T. Kawabata, K. Takehira, *Bull. Chem. Soc. Jpn. 77* (**2004**) 225.
[67] G. B. Shul'pin, G. V. Nizova, *Petrol. Chem. 33* (**1993**) 107.
[68] A. H. Heines, "Methods for the Oxidation of Organic Compounds", Academic Press, London, **1985**.

2.4.3.1 Benzene to Phenol

Phenol is one of the significant chemical intermediates in the broad industrial field, and is manufactured mainly by the Cumene process.[69] This process produces phenol and acetone from benzene and propylene, however it consists of three steps and therefore direct insertion of oxygen into the benzene ring is much more practical from a synthetic point of view. CuCl has been utilized for the oxidation of benzene to yield a 3: 1 mixture of phenol and hydroquinone in the presence of molecular oxygen with a 32 % yield of the phenol.[69,70] A hydroxy radical is suggested to be the active species and is generated as shown below.

$$2Cu^{I} + O_2 + 2H^{+} \longrightarrow 2Cu^{II} + H_2O_2$$

$$Cu^{I} + H_2O_2 + H^{+} \longrightarrow Cu^{II} + HO^{\bullet} + H_2O$$

Figure 2.8. The generation of a hydroxy radical.

Nevertheless the reaction proceeds catalytically when Cu(II) is reduced to Cu(I) by molecular hydrogen in the presence of a palladium co-catalyst (Figure 2.9.).[7] Copper complexes immobilized on SiO_2, Al_2O_3, MCM-41, NaY, HZSM-5, $Ca_{10}(OH)_2(PO_4)_6$ and polyoxometalates were investigated for this purpose.[71-73] Catalysts prepared by co-precipitation and ion-exchange methods are more efficient in comparison to the catalysts prepared by impregnation. Ascorbic acid was used as a reducing agent in liquid phase reactions to obtain phenol with up to 9.2 % conversion and 91.8 % selectivity that corresponds to 25.8 TON.[71]

[69] A. Kunai, T. Wani, Y. Ueharan, Y. Iwasaki, S. Kuroda, K. Ito, K. Sasaki, *Bull. Chem. Soc. Jpn.* 67 (**1989**) 2613.
[70] S. Ito, T. Yamasaki, H. Okada, S. Okino, K. Sasaki, *J. Chem. Soc., Perkin Trans. 2* (**1988**) 285.
[71] H. Yamanaka, R. Hamada, H. Nibuta, S. Nishiyama, S. Tsuruya, *J. Mol. Catal. A: Chem. 178* (**2002**) 89.
[72] T. Miyahara, H. Kanzaki, R. Hamada, S. Kuroiwa, S. Nishiyama, S. Tsuruya, *J. Mol. Catal. A: Chem. 176* (**2001**) 141
[73] Y. Liu, K. Murata, M. Inaba, *Catal. Commun. 6* (**2005**) 679.

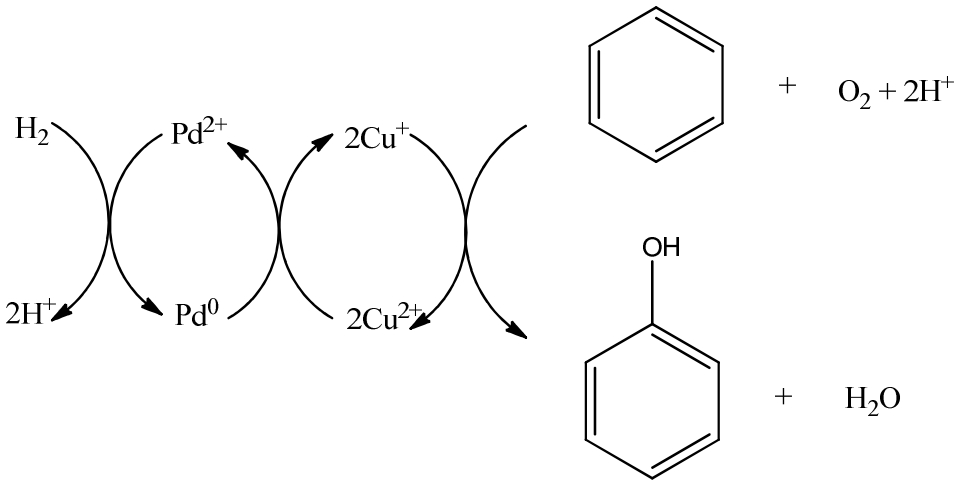

Figure 2.9. Phenol synthesis utilizing palladium as a co-catalyst.

2.4.3.1.1 Phenol to Quinone

Trimethyl-1,4-benzoquinone (TMQ) is a key intermediate in the synthesis of vitamin E.[74] The current industrial scale production method is para-sulfonation of 2,3,6-trimethylphenol (TMP) followed by MnO_2 oxidation.[75] Copper catalysts with molecular oxygen are effective for the single step preparation in the presence of co-catalysts such as LiCl and amine salts.[75] In the two phase system the oxidation could be repeated several times by recycling the catalyst, but the co-catalyst must be added at every run as it is lost. Recycling procedures have subsequently been studied by using polymer-supported copper catalysts, $CuCl_2$-**A** (Figure 2.10), and ionic liquids, $CuCl_2$-(BMIm)Cl.[76,77] These catalysts were effective and recyclable without loss of activity.[76,77]

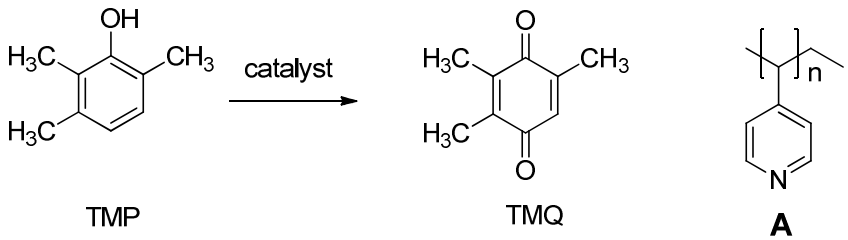

Figure 2.10. A schematic representation of the synthesis of TMQ from TMP.

[74] M. Yokoysama, T. Kitmura, Jpn. Kokai Tokkyo Koho JP 89-206349 (***1989***).
[75] K. Takehira, M. Shimizu, Y. Watanabe, H. Orita, T. Hayakawa, *Tetrahedron Lett. 30* (**1989**) 6691.
[76] K. Takaki, Y. Shimasaki, T. Shishido, K. Takehira, *Bull. Chem. Soc. Jpn. 75* (**2002**) 311.
[77] H. Sun, K. Harms, J. Sundermeyer, *J. Am. Chem. Soc. 126* (**2004**) 9550.

Table 2.4. Results of different catalysts employed in the synthesis of TMQ.

Catalyst (mol %)	Temp. (°C)	Time (h)	Yield (%)
$CuCl_2$-[BMIm]Cl (2.5)	60	5	86
$CuCl_2$-4 (10)	80	24	95

2.5 Oxidative Reactions of Copper Complexes as Co-catalysts

2.5.1 Wacker Oxidation

This process was discovered in 1959 and is one of the most essential industrial developments in the transformation of petrochemicals.[78,79] In this process alkenes are oxidized by a $Pd(II)Cl_2$ catalyst and an air-recyclable $CuCl_2$ co-oxidant.

$$C_2H_4 + H_2O \longrightarrow CH_3CHO + Pd(0) + 2HCl \quad (\mathbf{1})$$

$$Pd(0) + 2Cu(II)Cl_2 \longrightarrow Pd(II)Cl_2 + 2Cu(I)Cl \quad (\mathbf{2})$$

$$2Cu(I)Cl + 2HCl + 1/2O_2 \longrightarrow 2Cu(II)Cl_2 + H_2O \quad (\mathbf{3})$$

$$\text{Net: } C_2H_4 + 1/2\ O_2 \longrightarrow CH_3CHO \quad (\mathbf{4})$$

Scheme 2.1. The Wacker Process reaction equations.

In the first step (**1**) of scheme 2.1 the olefin is oxidised, the Pd(II) is reduced to Pd(0) and therefore the reaction is not catalytic without the Cu(II) co-oxidant. The second step (**2**) entails Cu(II) oxidation of Pd(0) to obtain the Pd(II) species. The third step (**3**) involves the oxidation of Cu(I) by molecular oxygen to Cu(II).

[78] J. Smidt, W. Hafner, R. Jira, J. Sedlmeier, R. Sieber, R. Ruttinger, H. Kojer, *Angew. Chem., Int. Ed. 71* (**1959**) 176.
[79] G. O. Spessard, G. L. Miessler, "Organometallic Chemistry"; Prentice Hall: Upper Saddle River, (**1997**).

The mechanism of the Wacker process depends on the reaction conditions, it consists of at least two competing pathways with different rate laws and product distributions dependent on $[Cl^-]$ and $[CuCl_2]$. There are four possible reaction conditions, each with distinct experimental data and rate laws.

- Industrial conditions (**LL**): Low $[Cl^-]$ and low $[CuCl_2]$, both $[Cl^-]$ and $[CuCl_2]$ < 1 M to exclusively provide aldehyde products through internal syn addition with the following rate law;

$$Rate_{LL} = \frac{k[PdCl_4^{2-}][olefin]}{[H^+][Cl^-]^2} \qquad (\mathbf{5})$$

- **HH** conditions: high $[Cl^-]$ (> 3.0 M) and high $[CuCl_2]$ (> 2.5 M) yield both aldehyde and chlorohydrin products through external anti-nucleophilic addition with the following rate law;

$$Rate_{HH} = \frac{k[PdCl_4^{2-}][olefin]}{[Cl^-]} \qquad (\mathbf{6})$$

- **HL** conditions: high $[Cl^-]$ and low $[CuCl_2]$ yielding no oxidation.
- **LH** conditions: low $[Cl^-]$ and high $[CuCl_2]$ provide syn and anti products, with a joint rate law involving equations **5** and **6**.

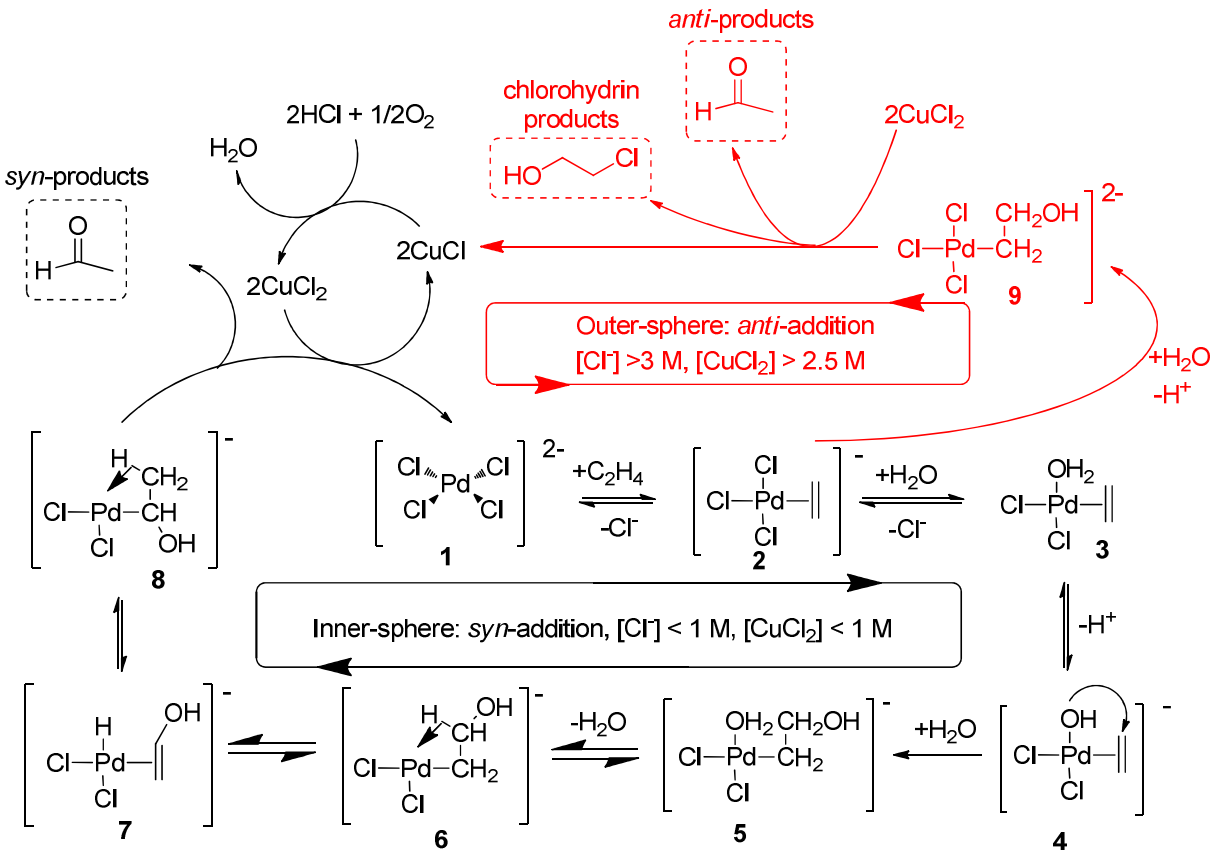

Figure 2.11. A composite mechanistic scheme for competitive syn (black) and anti (red) nucleophilic addition in the Wacker process (adapted from Keith *et al.*).[80]

The inner sphere pathway of the mechanism includes two rapid ligand exchange reactions (**1→3**) followed by a deprotonation step (**3→4**). This is succeeded by the rate determining syn hydroxypalladation step (**4→5**) with the rate law in Eq.5.[81] Subsequent to this are two facile hydride shifts (**6→8**) yielding an alkyl-alcohol specie that undergoes a water-assisted reductive elimination to afford acetaldehyde products.[82]

In the outer sphere process the mechanism entails the nucleophilic attack by the water species which takes place in an anti-fashion (**2→9**). The oxygen attacks from outside the palladium complex and the reaction are not an insertion of the ethene into the palladium oxygen bond. [83,84]

[80] J. A. Keith, R. J. Nielsen, J. Oxgaard, W. A. Goddard, *J. Am. Chem. Soc. 129* (**2007**) 12342
[81] P. M. Henry, *J. Am. Chem. Soc. 86* (**1964**) 3246.
[82] J. A. Keith, J. Oxgaard, W. A. Goddard, *J. Am. Chem. Soc. 128* (**2006**) 3132.
[83] J. E. Bäckvall, B. Akermark, S. O. Ljunggren, *J. Am. Chem. Soc. 101* (**1979**) 2411
[84] D. J. Nelson, R. Li, C. Brammer, *J. Am. Chem. Soc. 123* (**2001**) 1564.

This is then followed by the deprotonation of the $–CH_2\text{-}OH_2$ (+) cation **9-H**.[85] This step is considered to be the rate-determining step based on the rate law in Eq **6**. The process then yields chlorohydrin and acetaldehyde products. Under **HL** conditions an equilibrium between **2** and **9** is obtained without the formation of either products.[86] Under **LH** conditions both internal and external pathways are possible.

2.6 Copper Complexes in Oxidative Coupling Reactions

2.6.1 Glaser Reactions

The oxidative coupling reaction of terminal acetylenes in basic media to give conjugated diynes had its inception more than 100 year ago when Glaser noticed that the copper(I) derivative of phenyl-acetylene was oxidized in air to give 1,4-diphenyl-1,3-butadiyne. The cuprous derivative is used in trace amounts and it is not necessary to isolate it before oxidation. These synthetic transformations of terminal alkynes can be intermolecular or intramolecular with the reaction being a homo- or a hetero coupling between sp-carbon centers resulting in acetylinic or butadiyne derivatives.[87-89]

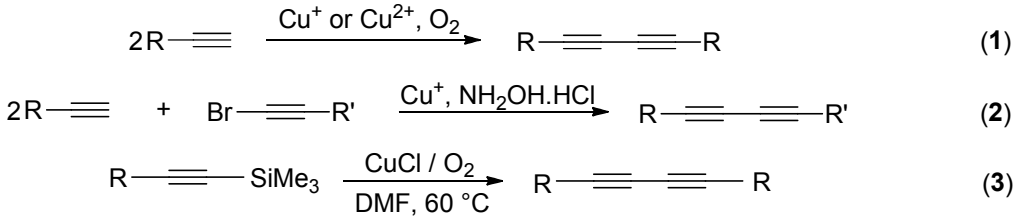

Figure 2.12. Oxidative homo- and heterocoupling reactions of terminal alkynes.

The coupling reactions between alkyne Grignard derivatives and 1-haloalkynes using Copper(I) salts are widely used.[89,90] As catalysts; organo-copper reagents are found to be very efficient for alkynides formation. In these types of reactions transmetalation of an alkynyl group to copper to generate an alkynylcopper species is considered to be a key step in the reaction. The following

[85] P. M. Henry, "Handbook of Organopalladium Chemistry for Organic Synthesis"; E. –I. Negishi, John Wiley & Sons, Inc.: New York 1 (**2002**).
[86] N. Gregor, K. Zaw, P. M. Henry, *Organometallics*. 3(**1984**) 1251.
[87] A. Puzari, J. B. Baruah, *J. Mol. Catal. A: Chem. 187* (**2002**) 149.
[88] K. Sonogashira, "Comprehensive Organic Synthesis": B. M. Trost (Ed.), Pergamon Press, New York, 3 (**1991**) 551
[89] A. S. Hay, *J. Org. Chem. 27* (**1962**) 3320.
[90] G. M. Whitesides, C. P. Casey, *J. Am. Chem. Soc. 88* (**1966**) 4541.

oxidative dimerization of the organic part on the metal-alkenyl complex yields the corresponding 1,3-butadiyne.[90] Under aerobic conditions, in a polar solvent and in the presence of cuprous chloride, alkynylsilanes (**3**) (in Figure 2.12) undergo an oxidative homocoupling which yields conjugated diynes and disubstituted ethynes in good yields.[91] The $[Cu(OH)TMEDA]Cl_2$ (TMEDA = *N, N, N', N'*-tetramethylethylenediamine) is a bi-nuclear complex which is very efficient for dimerising terminal olefins and acetylenes as well as naphthols and is widely used for this purpose.[92,93]

The elimination of solvent or the replacement of hazardous solvent with environmentally friendly solvents in chemical processes is considered one of the main subjects in green chemistry. For this reason polyethylene glycol (PEG) and compressed CO_2 amongst others have attracted much attention as alternative solvents in this process (Figure 2.13).

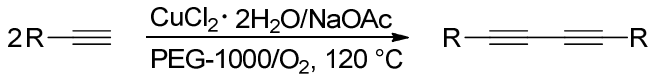

Figure 2.13. Oxidative coupling reactions employing PEG as solvent.[94]

Table 2.5. Results of oxidative terminal alkyne couplings of various substrates employing the reaction scheme in Figure 2.13.[94]

Entry	R	Time (h)	Conv. (%)	Yield[b] (%)
1	C_6H_5	1.5	99	99
2	*p*-$CH_3C_6H_4$	1.5	99	99
3	*m*-$CH_3C_6H_4$	1.5	70	68
4	*m*-$CH_3C_6H_4$	3	99	99
5	*p*-$CH_3OC_6H_4$	1.5	76	72
6	*p*-FC_6H_4	1.5	98	97
7	2-Thienyl	1.5	82	78
8	*n*-C_4H_9	1.5	29	28
9	*n*-C_4H_9	12	52	52
10	*n*-C_6H_{13}	6	62	60
11	*n*-C_6H_{13}	48	96	95
12	*n*-C_8H_{17}	48	75	73

[a] *Reaction conditions*: phenylacetylene (1 mmol, 0.112 mL), copper salts (0.1 mmol), NaOAc (1 mmol, 82 mg), PEG-1000 (3 g), 120 °C, Po_2 = 1 MPa, 1.5 h.
[b] GC yield.

[91] Y. Nishihara, K. Ikegashira, K. Hirabayashi, J. Ando, A. Mori, T. Hiyama, *J. Org. Chem. 65* (**2000**) 1780.
[92] M. Nakajima, I. Miyoshi, S. Hasimoto, M. Mori, K. Koga, *J. Org. Chem. 64* (**1999**) 2264.
[93] A. Mori, M. Nakajima, K. Koga, *Tetrahedron Lett. 35* (**1994**) 7983.
[94] Y. -N. Li, J. -L. Wang, L. -N. He, *Tetrahedron Lett. 52* (**2011**) 3485.

As can be seen in Table 2.5 the process employing PEG as solvent is very efficient (high yields and short reaction times) with the exception of entries 9-12. However, the process employs high temperatures (120 °C). Furthermore the efficiency of various copper sources was investigated with $CuCl_2 \cdot 2H_2O$ being the most effective. Interestingly a mixture of $CuCl_2$ and H_2O obtaining the same results suggesting that water promotes the reaction in the presence of anhydrous $CuCl_2$ as the same reaction without water gave lower yields.[95]

2.6.2 Ullmann Reactions and the Ullmann Ether Synthesis

A number of reactions go under this name. These reactions entail C-C and C-heteroatom bond formation to yield biaryls, di- or triaryl amines, phosphines, diaryl ethers and sulphides.[96] Although cross-coupling is closely associated with palladium catalysis despite the number of inherent deficiencies of palladium catalysis (high cost and essential restrictions in scope) this type of chemistry is much older and copper is the ancestor of palladium in this domain.[96,97] This chemistry has been known for a full century.[98]

2.6.2.1 C-C Bond Formation (Biaryl Synthesis)

Biaryl formation is achieved by coupling of two aromatic halide molecules in the presence of ground copper metal at temperatures of 100-200 °C with homocoupling yielding symmetrical compounds whereas heterocoupling yields unsymmetrical compounds (Figure 2.14).[96]

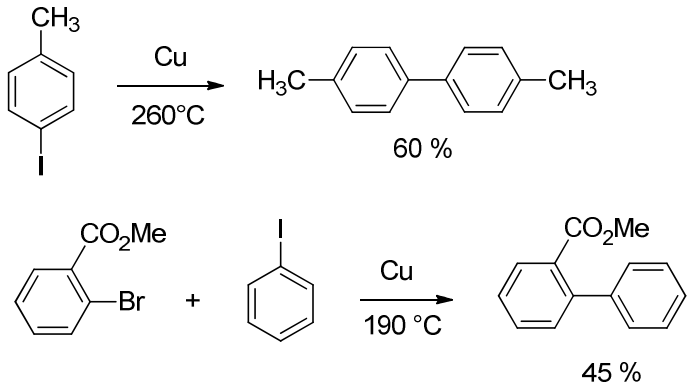

Figure 2.14. Biaryl formation (C−C bond formation).

[95] R. A. Fifer, J. J. Schiffer, *Chem. Phys. 50* (**1969**) 21.
[96] I. P. Beletskaya, A. V. Cheprakov, *Coord Chem Rev*. 248 (**2004**) 2337
[97] E. I. Negishi, Acc. *Chem. Res.* (**1982**) 15.
[98] J. Hassan, M. Sevignon, C. Gozzi, E. Schulz, M. Lemaire, *Chem. Rev. 102* (**2002**) 1359.

Intramolecular coupling is also possible and sometimes occurs much more readily than intermolecular coupling and is used for biphenylene and tetraphenylene synthesis.[99] These compounds and some of their substituted derivatives can be synthesized using the $CuCl_2$-mediated intramolecular coupling of an organozinc species prepared from 2,2-dilithiobiaryls with one or two molar equiv. of $ZnCl_2$ or $ZnBr_2$ in THF.[99] Although most of the reactions of 2,2-dilithiobiaryls with $CuCl_2$ in THF in the absence of $ZnCl_2$ or $ZnBr_2$ lead to biphenylenes as a major product, a similar reactions of the organozinc species with $CuCl_2$ in THF produced biphenylenes in much better yields, due to a smooth transmetallation and reductive elimination reactions.[100,101] In particular, the copper-mediated cyclization of benzannelated organozinc intermediates proceeded smoothly and selectively to afford the desired biphenylenes in 46–81% yield (Figure 2.15.). The reaction of the tetramethoxy-substituted organozinc species with $CuCl_2$ produced 2,3,6,7,10,11,14,15-octamethoxytetraphenylene as a major product in 67% yield.[102]

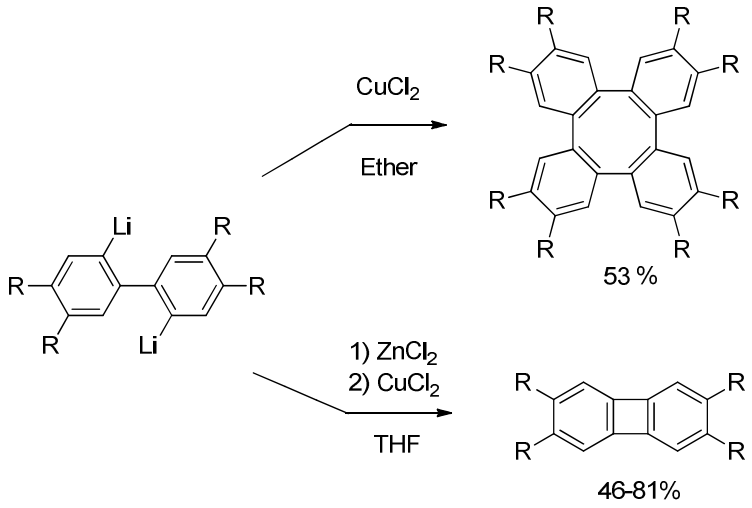

Figure 2.15. The formation of biphenylenes and tetraphenylenes.

2.6.2.2 Arylation of Aromatic Amines

The arylation of aromatic amines requires harsh and extended heating at 200 °C or higher, in the presence of copper salts, or copper oxides, or Cu Bronze, etc., with a base, in polar high

[99] A. Rajca, A. Safronov, S. Rajca, C. R. Ross, J. J. Stezowski, *J. Am. Chem. Soc. 118* (**1996**) 7272.
[100] R. Guilard, S. Brandes, A. Tabard, N. Bouhmaida, C. Lecomte, P. Richard, J. –M. Latour, *J. Am. Chem. Soc. 116* (**1994**) 10202.
[101] M. Iyoda, S. M. Humayun Kabir, A. Vorasingha, Y. Kuwatani, M. Yoshida, *Tetrahedron Lett. 39* (**1998**) 5393.
[102] S. M. H. Kabir, M. Hasegawa, Y. Kuwatani, M. Yoshida, H. Matsuyama, M. Iyoda, *J. Chem. Soc., Perkin Trans. 1* (**2001**) 159.

temperature boiling solvents (classical Ullmann method). However, reactions catalyzed by copper complexes are more efficient in non-polar solvents at reflux or lower temperatures.[103] Bidentate ligands such as bisphosphines, 8-hydroxyquinolines and 2,2-bipyridines can be utilized for the arylation of anilines by aryl iodides in the system CuI/L, t-BuOK, PhMe, 115 °C.[103,96] The use of 1,10-Phenanthroline is the most feasible method and the process shows good catalytic activity at moderate temperatures (50 °C). It can be applied to both monoarylation and diarylation.[104] In addition to this, some monodentate phosphines, such as tri-*o*-tolylphosphine P(*o*-tol)$_3$ and tri-*n*-butylphosphine PBu_3 are very efficient ligands for the arylation of anilines which is contrary to PPh_3, which is practically an ineffective agent for aryl iodides (Figure 2.16).

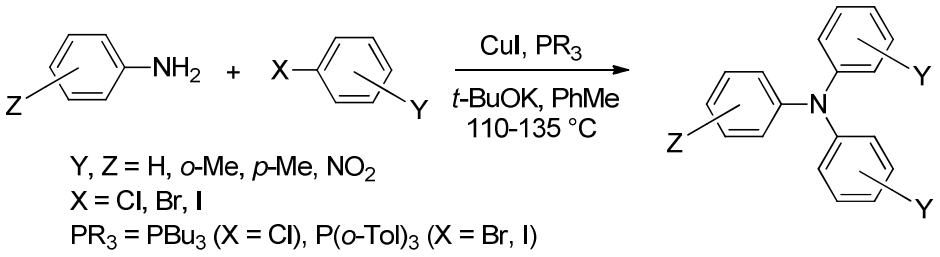

Figure 2.16. Arylation of substituted anilines.

2.6.2.3 Arylation of Aliphatic Amines

Arylation of secondary cyclic amines and primary aliphatic amines can also be obtained, currently the major restrain for copper catalysis in this domain is low reactivity of secondary non-cyclic amines.[105] This is most likely due to steric reasons and bases such as K_2CO_3, K_3PO_4, Cs_2CO_3 are employed in various solvents (both nonpolar and polar) for this process. Arylation of aliphatic amines in hydroxylic solvents employing K_3PO_4 as base and ethylene glycol used in two-fold excess over the amine was found to be very efficient (in the vicinal glycol ligand assisted method). This method has been used for the preparation of 6-aminoimidazo[1,2-*a*]pyridines from the appropriate iodo derivative.[105,106] Other ligands suitable for this process are amino acids and to prevent self-arylation of the ligand, amino acids with secondary amino-

[103] A. A. Kelkar, N. M. Patil, R. V. Chaudhari, *Tetrahedron Lett. 43* (**2002**) 7143.
[104] H. B. Goodbrand, N. X. Hu, *J. Org. Chem. 64* (**1999**) 670.
[105] F. Y. Kwong, A. Klapars, S. L. Buchwald, *Org. Lett. 4* (**2002**) 581.
[106] C. Enguehard, H. Allouchi, A. Gueiffier, S. L. Buchwald, *J. Org. Chem. 68* (**2003**) 4367.

groups are used e.g. *N*-methylglycine or proline, while *N*,*N*-dimethylaminoacids are less efficient as ligands.[107]

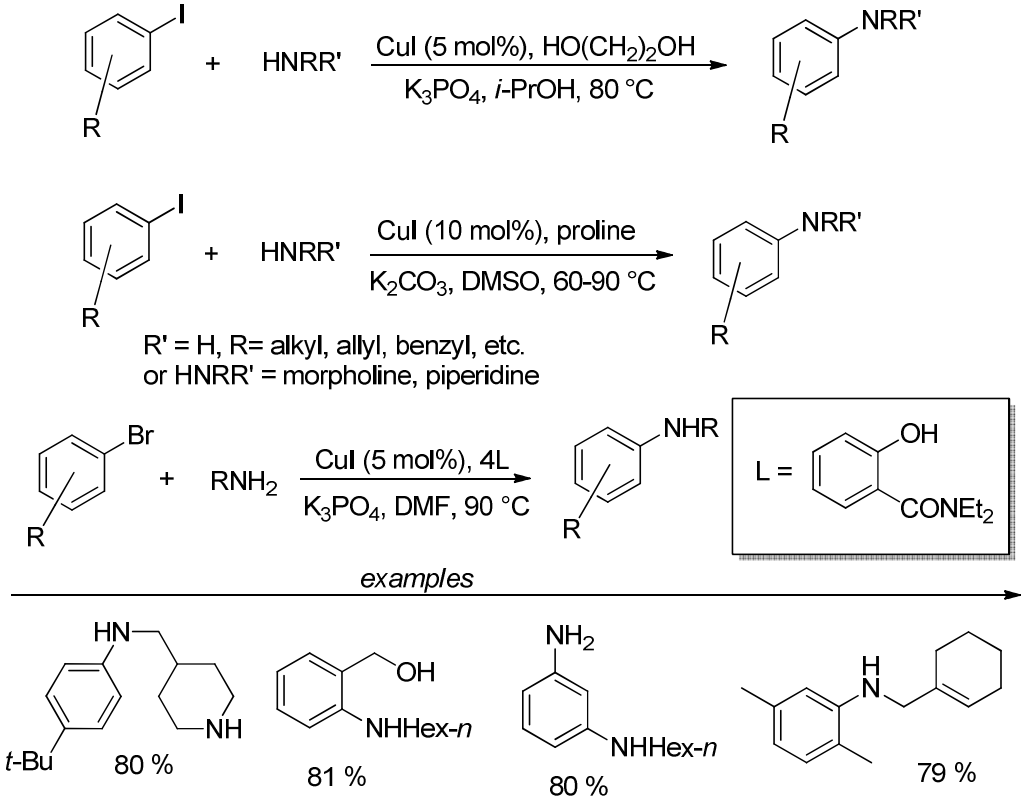

Figure 2.17. Copper catalyzed arylation of aliphatic amines in the presence of salicylamides, proline and ethylene glycol.[96]

2.6.2.4 Arylation of Functionally Substituted Alkylamines and Intramolecular Arylation

Amino acids can act as ligands for copper and the arylation of these compounds can be accomplished without utilizing additional ligands (ligand-assisted method). Both alpha and beta-aminoacids can be arylated in modest to good yields by aryl iodides or bromides.[108,109]The reaction is carried out under mild conditions using DMF as solvent. In some cases addition of

[107] D. W. Ma, Q. Cai, H. Zhang, *Org. Lett. 5* (**2003**) 2453.
[108] D. W. Ma, Y. D. Zhang, J. C. Yao, S. H. Wu, F. G. Tao, *J. Am. Chem. Soc. 120* (**1998**) 12459.
[109] D. W. Ma, C. F. Xia, *Org. Lett. 3* (**2001**) 2583.

small amounts of water favour the process.[108,110] However glycine is not reactive under these conditions (the simplest amino acid, Figure 2.18.).

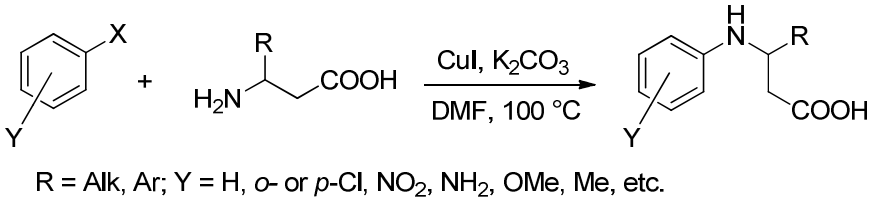

Figure 2.18. Arylation of amino acids.

Complex heterocycles can be synthesized by applying the intramolecular version of this reaction.[109] An interesting feature in this method is the ability to substitute only one halogen of two iodines or bromine atoms in *p*-dihalobenzene (see Figure 2.19.). Whereas in cross-coupling chemistry partial substitution is accomplished by using different halogens and this approach has been used for natural compound synthesis.[110]

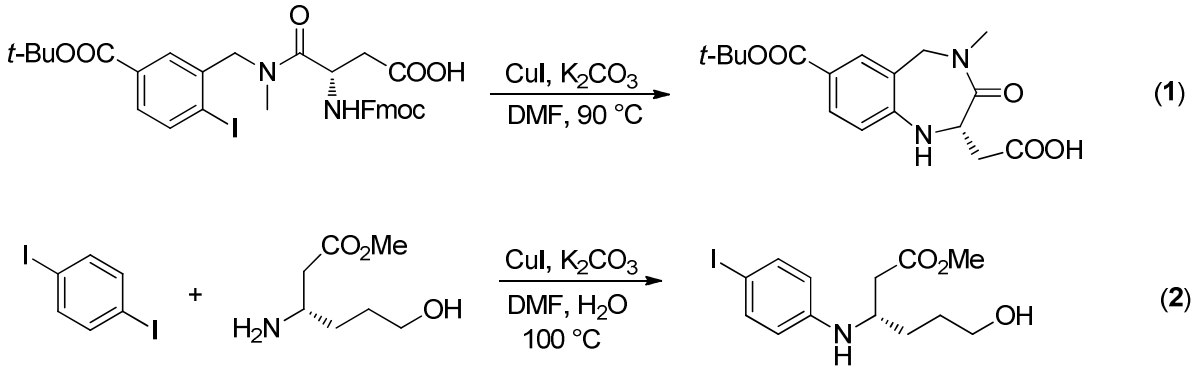

Figure 2.19. Intramolecular arylation and mono-substitution of *p*-dihalobenzene.

Intramolecular arylation is possible under mild conditions even with chlorides, however it is carried out under different conditions (see Figure 2.20.).[111] The preference for cyclisation is so high that halogen atoms present in the substrate in other positions are retained in the product.[112]

[110] D. W. Ma, C. F. Xia, J. Q. Jiang, J. H. Zhang, W. J. Tang, *J. Org. Chem. 68* (**2003**) 442.
[111] F. Y. Kwong, S. L. Buchwald, *Org. Lett. 5* (**2003**) 793.
[112] K. Yamada, T. Kubo, H. Tokuyama, T. Fukuyama, *Synlett* (**2002**) 231.

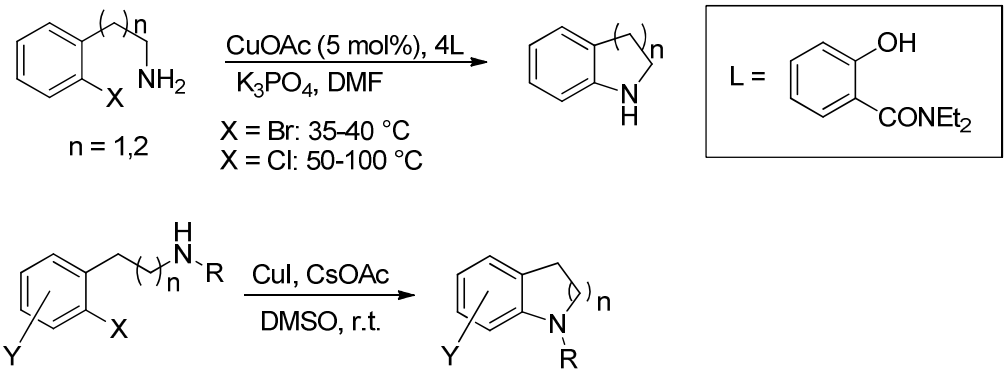

Figure 2.20. Ligand assisted and room temperature intramolecular arylation.

2.6.2.5 Arylation of Unsaturated Heterocyles

Arylation of unsaturated heterocyles is possible for a broad selection of azoles.[113] This includes pyrrole, pyrazole, imidazole and the respective benzo-derivatives. In addition to these, aryl bromides containing free amino groups can also be arylated.[113] The use of aryl bromides capable of intramolecular assistance (e.g. *o*-bromobenzoic acid) allows for less harsh reaction conditions.[113]Among the first systems suggested for this arylation was the rare organic-solvent-soluble copper(I) triflate process. This salt is commercially available as a benzene solvate $(CuOTf)_2 \cdot PhH$, however this catalytic method is a ligand assisted process and requires dibenzylideneacetone (dba) and 1,10-phenanthroline. This method enables the arylation of imidazoles in non-polar solvents.[114]

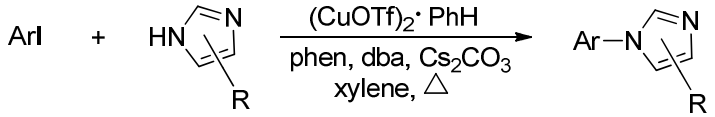

Figure 2.21. Arylation of imidazoles.

The same method can be applied for other aminations e.g. the reaction of 5-iodouracyl with various amines.[115] Although highly effective, this system is too complex and expensive.[115] Furthermore, the solubility of the Cu catalyst precursor and the choice of solvent is not a crucial

[113] T. Sugaya, Y. Mimura, N. Kato, M. Ikuta, T. Mimura, M. Kasai, S. Tomioka, *Synthesis* (**1994**) 73.
[114] A. Kiyomori, J. F. Marcoux, S. L. Buchwald, *Tetrahedron Lett. 40* (**1999**) 2657.
[115] J. B. Arterburn, M. Pannala, A. M. Gonzalez, *Tetrahedron Lett. 42* (**2001**) 1475.

parameter.[116] *trans*-Cyclohexyldiamine (CyDA) is an effecient ligand for this procedure and it enables arylation of mono- or dinitrogen azoles (including pyrroles, pyrazoles, indoles, indazoles, benzimidazoles, carbazoles, etc.).[117] In the case of indoles, dimethylated amines (DMEDA) and dimethylated cyclohexyldiamines (DMCyDA) are more suitable.[117]

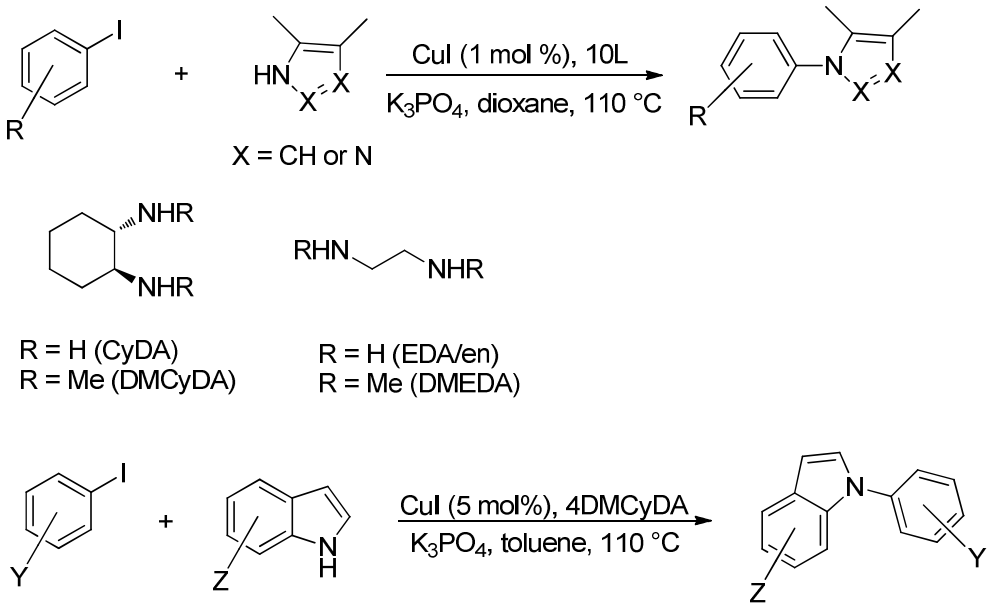

Figure 2.22. Copper-catalysed arylation of azoles and the ligands used in ligand assisted systems.

2.6.2.6 Arylation of Amides

Similarly, amides can be arylated using vicinal diamines especially EDA (en/ethylenediamine) and *rac*-*trans*-cyclohexanediamine (CyDA), as well as their *N*,*N*-dimethyl derivatives (DMEDA and DMCyDA), the latter pair being successful even for challenging tasks.[118] The CuI : diamine ligand system (1 mol%: 10 mol%) is highly effective for the amide arylation by aryl iodides with K_3PO_4 or Cs_2CO_3 as base, in a variety of solvents (toluene, dioxane, THF and DMF) at reflux or lower temperatures. Stronger bases hinder the reaction because the amidate formed binds to copper and prohibit the catalytic process.[117,119] The arylation is chemoselective (does not give disubstituted products for *N*-unsubstituted amides) and enables selective attack at the amide

[116] J. C. Antilla, A. Klapars, S. L. Buchwald, *J. Am. Chem. Soc. 124* (**2002**) 11684.
[117] A. Klapars, J. C. Antilla, X. H. Huang, S. L. Buchwald, *J. Am. Chem. Soc. 123* (**2001**) 7727.
[118] S. K. Kang, D. W. Kim, J. N. Park, *Synlett* (**2002**) 427.
[119] A. Klapars, X. H. Huang, S. L. Buchwald, *J. Am. Chem. Soc*. 124 (**2002**) 7421.

nitrogen even in the presence of a free aniline group (NH_2). Furthermore this method is not sensitive to functional groups in aryl iodides. In addition to this, the reactions are performed under mild conditions and at room temperature for more reactive substrates.[117,119]

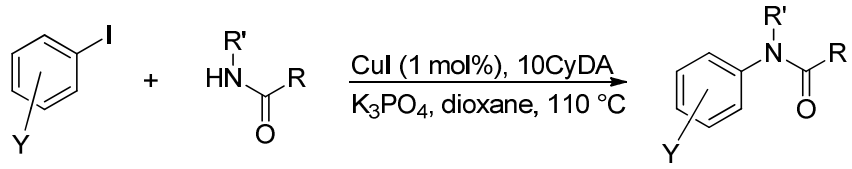

Figure 2.23. Arylation of amides.

An intramolecular version of this method gives a convenient approach for the synthesis of heterocycles.[119] Aryl chlorides, including electron rich *p*-chlorotoluene and *p*-chloroanisole can be utilized for the arylation provided that they are used as solvent (in excess) and DMCyDA is used as a ligand.[117] The method has also been applied to bromofurans, bromothiophenes and bromothiazoles.[120,121]

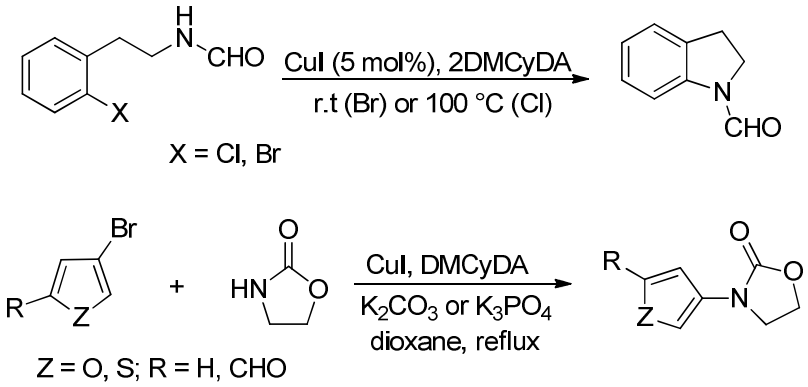

Figure 2.24. Intramolecular arylation of amides and cyclic carbamates.

Furthermore this method has also been applied to the arylation of carbamates (oxazolinones) with aryl bromides as a short pathway for the synthesis of potent antibacterial agents such as linezolid and toloxatone.[122]

[120] K. R. Crawford, A. Padwa, *Tetrahedron Lett. 43* (**2002**) 7365.
[121] A. Padwa, K. R. Crawford, P. Rashatasakhon, M. Rose, *J. Org. Chem. 68* (**2003**) 2609.
[122] B. Mallesham, B. M. Rajesh, P. R. Reddy, D. Srinivas, S. *Trehan, Org. Lett. 5* (**2003**) 963.

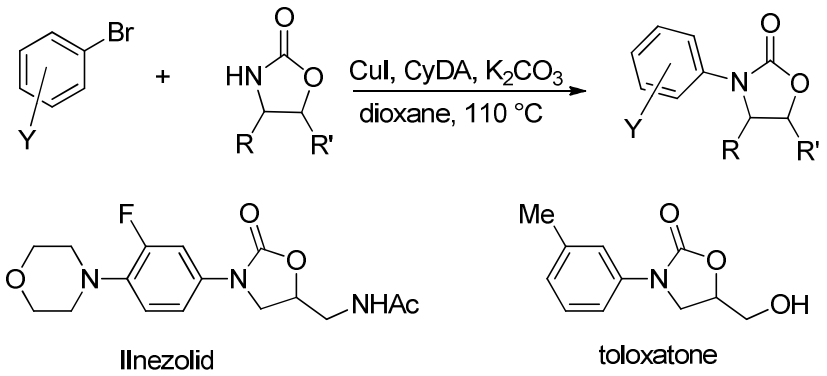

Figure 2.25. The synthesis of linezolid and toloxatone (antibacterial agents) employing the arylation of cyclic carbamates system.

Azobenzenes can also be synthesized by the arylation of Boc-protected (*N-tert*-butoxycarbonyl protected) phenylhydrazines.[123,124] In addition to this, both alkenylation and alkynylation of amides can be accomplished by utilizing ligand-assisted copper catalysis methods and therefore these methods are consequently used in complex natural product synthesis.[125-131]

2.6.2.7 C-O Bond Formation, Diaryl Ether Synthesis

The copper catalyzed condensation of aryl halides with phenols is also refered to as the Ullmann reaction. This reaction requires stoichiometric amounts of copper, phenols in excess and high temperatures due to the low nucleophilicity of the phenoxide and low reactivity of aryl halides.[132] For these reasons Buchwald and Hartwig introduced palladium-based methods to overcome these synthetic adversities.[133] However for large- and industrial-scale diaryl ether synthesis, copper-mediated aryl couplings are still reactions of choice in the pharmaceutical, agrochemical, fine and polymer chemistry industries.[133,134] Diaryl ethers can generally be synthesized by one of six ways:

[123] M. Wolter, A. Klapars, S. L. Buchwald, *Org. Lett. 3* (**2001**) 3803.
[124] K. -Y. Kim, J. -T. Shin, K. -S. Lee, C. -G. Cho, *Tetrahedron Lett*. 45 (**2004**) 117.
[125] R. C. Shen, J. A. Porco, *Org. Lett. 2* (**2000**) 1333.
[126] R. C. Shen, C. T. Lin, E. J. Bowman, B. J. Bowman, J. A. Porco, *J. Am. Chem. Soc. 125* (**2003**) 7889.
[127] A. Furstner, T. Dierkes, O. R. Thiel, G. Blanda, *Chem.-Eur. J. 7* (**2001**) 5286.
[128] L. Jiang, G. E. Job, A. Klapars, S. L. Buchwald, *Org. Lett. 5* (**2003**) 3667.
[129] M. O. Frederick, J. A. Mulder, M. R. Tracey, R. P. Hsung, J. Huang, K. C. M. Kurtz, L. C. Shen, C. J. Douglas, *J. Am. Chem. Soc. 125* (**2003**) 2368.
[130] Y. S. Zhang, R. P. Hsung, M. R. Tracey, K. C. M. Kurtz, E. L. Vera, *Org. Lett. 6* (**2004**) 1151
[131] J. R. Dunetz, R. L. Danheiser, *Org. Lett. 5* (**2003**) 4011.
[132] J. Lindley, *Tetrahedron. 40* (**1984**) 1433.
[133] H. B. Goodbrand, N. K. Hu, *J. Org. Chem. 64* (**1999**) 670.

- palladium-catalysed Buchwald-Hartwig reaction
- nucleophilic aromatic substitution
- coupling of phenols with an arylboronic acids
- oxidative coupling
- nucleophilic aromatic additions to metal-arene complexes
- Ullmann diaryl ether coupling

Under standard Ullmann conditions Wipf and Jung successfully synthesized a (+)-diepoxin σ precursor by coupling diol (**4**) (obtained by reduction of tetralone with lithium aluminum hydride) with 1-iodo-8-methoxynaphthalene (**2**). They used Cu_2O as the source of cuprous ions and pyridine as solvent at reflux temprature for 7h. Diaryl ether **5** was obatained with 63 % yield and was oxidized to the desired diaryl ether **3** (Figure 2.26).

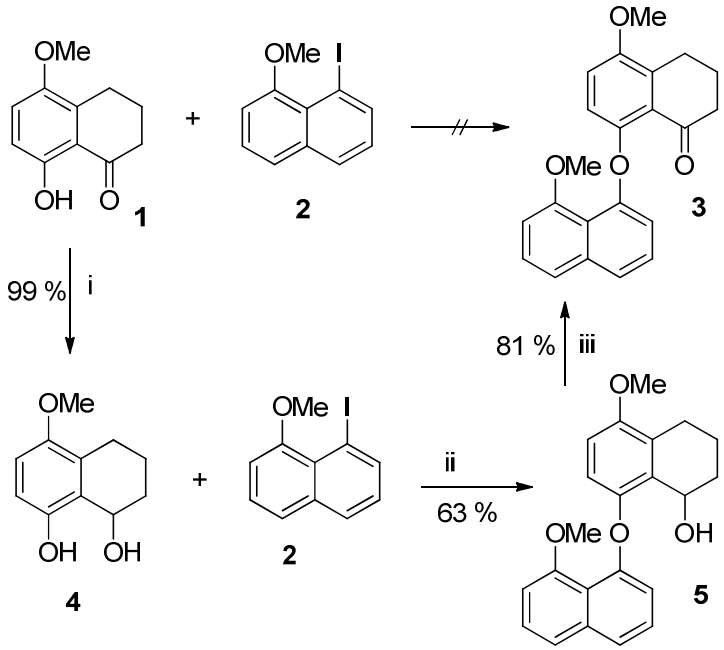

Reagents and conditions: **i) $LiAlH_4$, Et_2O; ii) Cu_2O, pyridine, reflux, 7h; iii) PCC, CH_2Cl_2, NaOAc, Celite.**

Figure 2.26. The synthesis of (+)-diepoxin σ precusor.

[134] P. J. Fagan, E. Hauptman, R. Shapiro, A. Casalnuovo, *J. Am. Chem. Soc. 122* (**2000**) 5043.

From this it was clear that changes in functional groups close to reacting centers can influence the Ullmann diaryl ether synthesis. The same deduction can be made from the work performed by Xing *et al*. In an attempt to synthesize the verbenachalcone precursor they did not obtain diaryl ether **8** by coupling of 2-benzyloxy-5-methylphenol (**6**) with i-bromo-2-methoxy-4-methylbenzene (**7**) in the presence of 5 mol% of $(CuOTf)_2PhMe$ and Cs_2CO_3 in pyridine at 110 °C (Illustrated in Figure 2.27). However using similar conditions **9** reacted with **10** to give the precursor **8** in modest yields.[135]

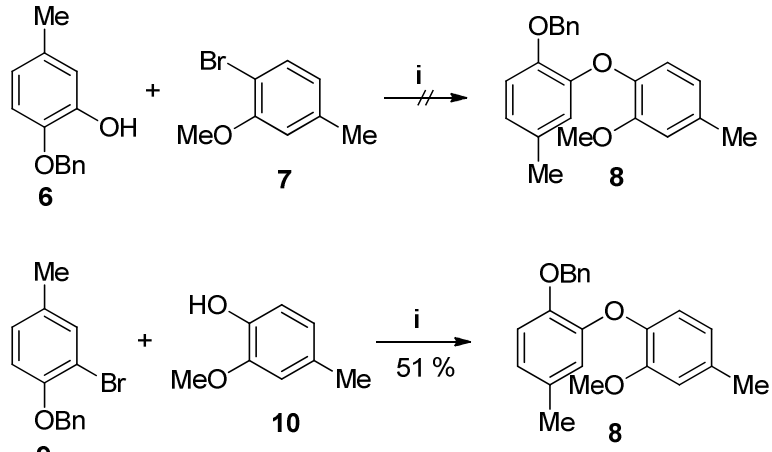

Reagents and conditions: **i) $(CuOTf)_2PhMe$, Cs_2CO_3, pyridine, 110 °C, 24 h.**

Figure 2.27. Preparation of verbenachalcone precursor.

2.6.2.8 Ligand Assisted Methods in Diaryl Ether Synthesis

Ligand assisted methods have also been reported for the synthesis of diaryl ethers. Cuprous ions are catalytic species in this reaction and addition of suitable ligands (in the presence of Cs_2CO_3) as base) enhances the solubility of these cuprous ions.[136] Subsequently more efficient catalysis compared to classical Ulmann coupling reactions can be obtained at lower reaction temperatures. In addition to enhanced solubility; cuprous ions are stabilized by complexation to aromatic compounds in solution.[137] Futhermore electron-donating groups on the phenol and electron-withdrawing groups on the halide makes the reaction favourable and fast. A series of aryl halides

[135] X. Xing, D. Padmannaban, L. A. Yeh, G. D. Cuny, *Tetrahedron. 58* (**2002**) 7903.
[136] A. J. Paine, *J. Am. Chem. Soc. 109* (**1987**) 1496.
[137] M. Saphier, A. Burg, S. Sheps, H. Cohen, D. Meyerstein, *J. Chem. Soc. Dalton Trans*. (**1999**) 1845.

and phenols formed ethers in *N*-methyl-2-pyrrolidone (NMP) as solvent, Cs_2CO_3 as base, and CuCl and 2,2,6,6-tetramethylheptane-3,5-dione (TMHD) as catalyst (see Figure 2.28 and Table 2.6). Furthermore this bidentate ligand accelerates the rate of the reaction and enables it to occur at moderate temperatures.[138]

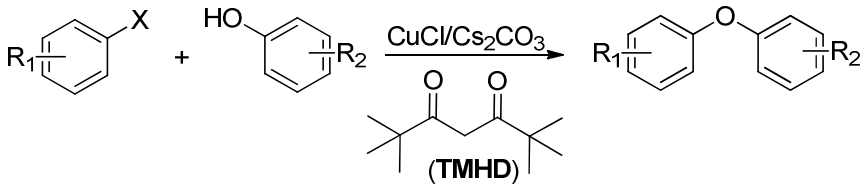

Figure 2.28. Ligand assisted (TMHD) diaryl ether synthesis.

Table 2.6. TMHD assisted diaryl ether synthesis.[138]

Entry	Ar-X	ArOH	Ether product	Reaction time (h)	Assay yield %	Isolated yield %
1	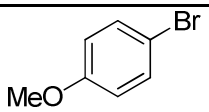	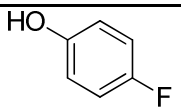	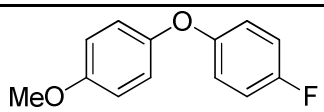	10	70	55
2	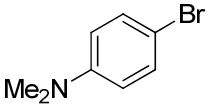	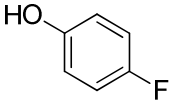	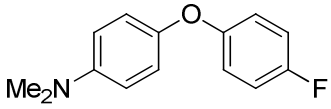	15	79	59
3	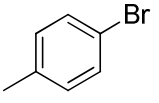	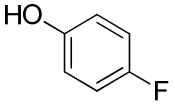	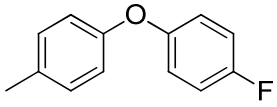	7.5	86	63
4	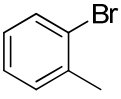	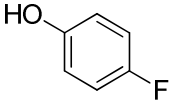	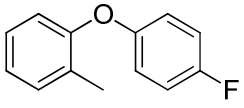	15	97	85
5	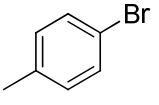	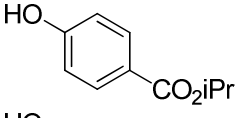	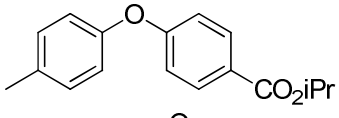	47	56	51
6	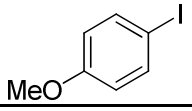	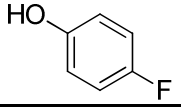	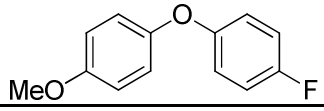	6	74	68

Inexpensive multidentate ligands like Chxn-Py-Al (Figure 2.30), salicylal-doxime (salox) and dimethylglyoxime (DMG) also optimized the process by increasing yields and lowering reaction

[138] E. Buck, Z. J. Song, D. Tschaen, P. G. Dormer, R. P. Volante, P. J. Reider, *Org. Lett.* 4 (**2002**) 1623.

temperatures to 80 °C (Figure 2.29., Table 2.7.). Of the three ligands, Chxn-Py-Al was more practical as it led to cleaner reaction, but they were overall equally effective.[139]

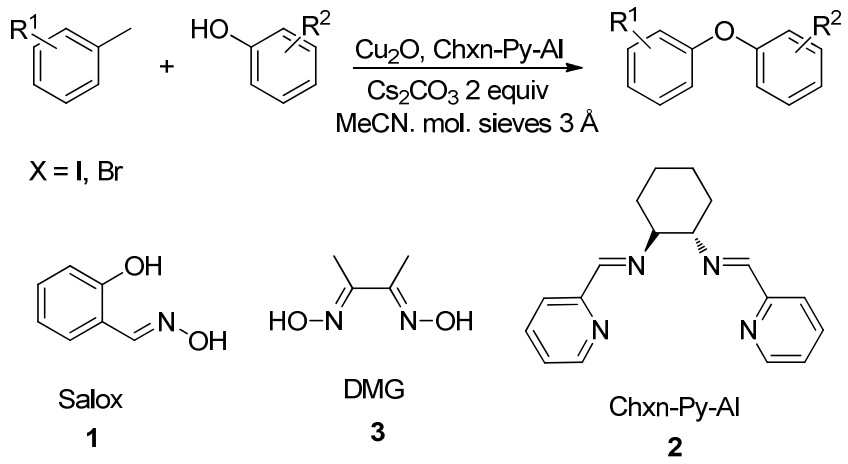

Figure 2.29. General mild Ullmann-type synthesis and chelating agents.

[139] H. -J. Cristau, P. P. Cellier, S. Hamada, J. -F. Spindler, M. Tailleter, *Org. Lett. 6* (**2004**) 913.

Table 2.7. Chxn-Py-Al assited Ullmann couplings.[139]

Entry	ArX	Phenol	Time (h)	T (°C)	Yield (%)
1	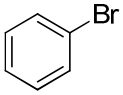	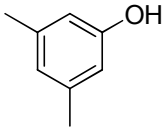	36	110	85
2	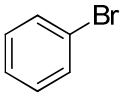	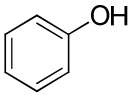	36	110	80
3	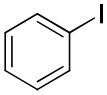	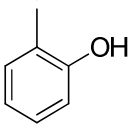	40	82	93
4	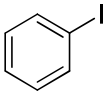	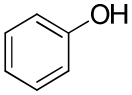	24	82	100
5	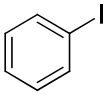	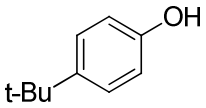	25	82	95
6	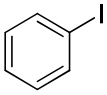	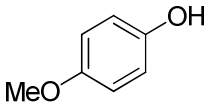	28	82	95
7	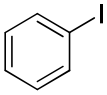	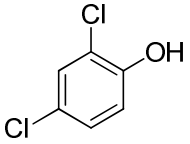	24	82	40
8	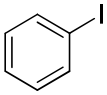	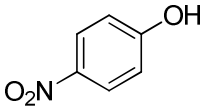	24	110	<1

Comparison of the two ligand systems shows that the TMHD system generally employs much higher temperatures (120 °C) and the reaction times are relatively short compared to the Chxn-Py-Al system. Furthermore the yields range from moderate to high (51-85 %). In contrast the Chxn-Py-Al system employs temperatures which are relatively lower (82-110 °C), the reaction times are generally longer and result in greater yields. The former TMHD system has the added advantage of tolerating electron-withdrawing groups on the phenols and electron-donating groups on the aryl halide.

2.6.2.9 Arylboronic Acid Diaryl Ether Synthesis

Chan and Evans independently reported the synthesis of diaryl ethers by employing a Cu(II)-promoted cross-coupling of phenols and arylboronic acids in the presence of molecular sieves

(Figure 2.30.).[140,141] The advantages of this method is that it's a room temperature synthesis, it tolerates a vast variety of substituents on both reagents and the yields are high. Further studies by Chan and Lam revealed that phenylboronic acid anhydride (boroxine) is more effective than coupling with phenyl boronic acid.[142] They also observed that phenylboronic acid is readily converted to $(PhBO)_3$, which could be the active species for arylation.

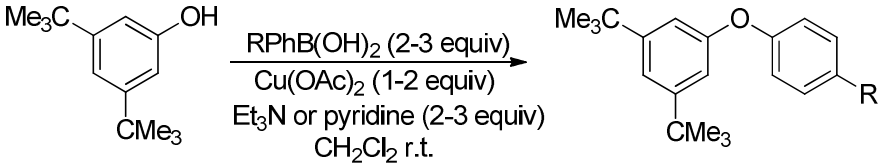

R = H (40 %), Me (73 %), OMe (73 %)

Figure 2.30. Coupling of arylboronic acids with phenols.

Petasis and co-workers and Sagar *et al*. reported the conversion of arylboronic acids to phenols and successive coupling of both species to form symmetrical diaryl ethers (Figure 2.31, **1**).[143,144]The advantage of this method is that it tolerates a variety of electron rich and poor substituents on the arylboronic acid, and the yields are good to excellent.

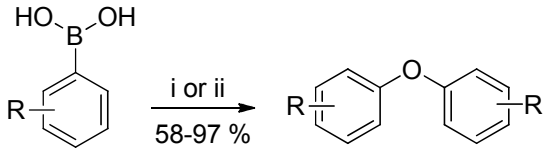

(**1**)

R = Me, t-Bu, OMe, COMe, Cl, F, Br, NO_2

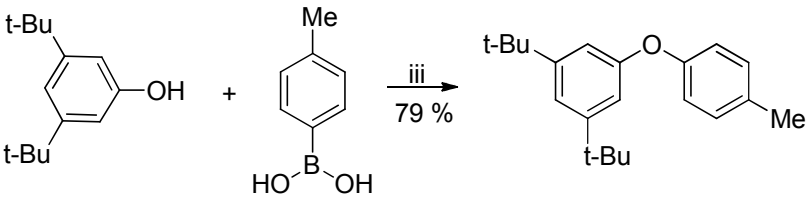

(**2**)

Reagents and conditions; **i) $Cu(OAc)_2$, Et_3N, CH_2Cl_2, 25 °C;**
ii) $Cu(OAc)_2$, Et_3N, H_2O, CH_2Cl_2-MeCN, 25 °C;
iii) $Cu(OAc)_2$ (0.1 equiv), O_2, pyridine, CH_2Cl_2, 50 °C

Figure 2.31. Homo-coupling of arylboronic acids and aerobic catalytic coupling to phenols.

[140] D. M. T. Chan, K. L. Monaco, R. Wang, M. P. Winters, *Tetrahedron Lett. 39* (**1998**) 2933.
[141] D. A. Evans, J. L. Katz, T. R. West, *Tetrahedron Lett. 39* (**1998**) 2937.
[142] D. M. T. Chan, K. L. Monaco, R. Li, D. Bonne, C. G. Clark, P. Y. S. Lam, *Tetrahedron Lett. 44* (**2003**) 3863.
[143] J. Simon, S. Salzbrunn, G. K. S. Prakash, N. A. Petasis, G. A. Olah, *J. Org. Chem. 66* (**2001**) 633.
[144] A. D. Sagar, R. H. Tale, R. N. Adude, *Tetrahedron Lett. 44* (**2003**) 7061.

Lam and Jadhav developed a catalytic system under oxidative conditions to synthesize diaryl ethers utilizing a $Cu(OAc)_2/O_2$ system with pyridine acting as base at 50 °C with 79 % yields (Figure 2.31 (**2**)).[145]A neutral protocol that was carried out at room temperature was reported by Batey and Quach.[146] This procedure utilized an aryltrifluoroborate salt which can be obtained by treatment of phenylboronic acid with potassium hydrogen fluoride (KHF_2). This system was catalyzed by Cu(II) acetate and 4-(dimethylamino)pyridine in the presence of molecular sieves under an oxygen atmosphere (Figure 2.32.).

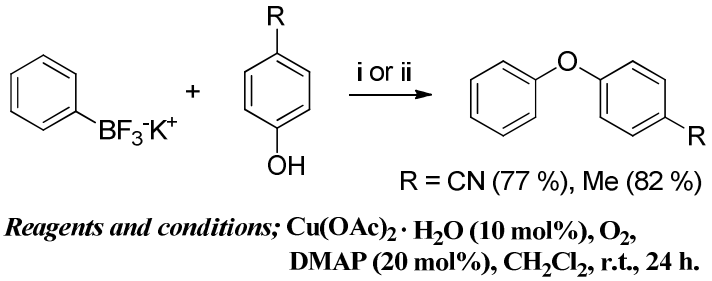

Figure 2.32. Aryltrifluoroborate ether synthesis.

Comparison of the four methods shows that they all produce the desired products in good yields. The latter (Batey, Quach, Chan and Evan's) methods requires high catalyst loadings compared to the two other methods (Lam *et al.* and Petasis *et al.*). Furthermore Lam and Jadhav's procedure is carried out at 50 °C whereas the other methods are carried out at 25 °C. Chan and Lam's procedure can also be used for intramolecular coupling of phenolic groups and intramolecular phenylboronic acid groups.[147,148]

2.6.2.10 Metal-free Diaryl Ether Synthesis

The catalytic reaction conditions for diaryl ether synthesis require high catalyst loadings, excess reagents, elevated temperatures, and long reaction times.[149-153] Although some arylboronic acid reactions occur at room temperature, excess amounts of reagents are often required. Pd-catalyzed

[145] P. Y. S. Lam, G. Vincent, C. G. Clark, S. Deudon, P. K. Jadhav, *Tetrahedron Lett. 42* (**2001**) 3415.
[146] T. D. Quach, R. A. Batey, *Org. Lett. 5* (**2003**) 1381.
[147] C. P. Decicco, Y. Song, D. A. Evans, *Org. Lett. 3* (**2001**) 1029.
[148] Y. Hitotsuyanagi, H. Ishikawa, S. Naito, K. Takeya, *Tetrahedron Lett. 44* (**2003**) 5901.
[149] G. Evano, N. Blanchard, M. Toumi, *Chem. Rev. 108* (**2008**) 3054.
[150] S. V. Ley, A. W. Thomas, *Angew. Chem., Int. Ed. 42* (**2003**) 5400.
[151] R. Frlan, D. Kikelj, *Synthesis* (**2006**) 2271.
[152] L. Ackermann, "Modern arylation methods", Ed.; Wiley-WCH: Weinheim, Germany, (**2009**).
[153] F. Monnier, M. Taillefer, *Angew. Chem., Int. Ed. 48* (**2009**) 6954.

cross-couplings of phenols and aryl halides were reported in 1999, and they give high yields of a range of diaryl ethers.[154,155] However, it relies on high reaction temperatures and expensive, noncommercial ligands. Furthermore, heteroaromatics and ortho-substituted coupling partners are often challenging in both Cu- and Pd-catalyzed reactions.[151] Olofsson *et al*. reported an improved diaryliodonium salt protocol that utilized substituted phenols and diaryliodonium triflates or tetrafluoroborates in aprotic solvents under mild conditions (Figure 2.33). This procedure tolerates bulky ortho-, and halo-substituents, racemization-prone amino acid derivatives and heteroaromatics.[156]

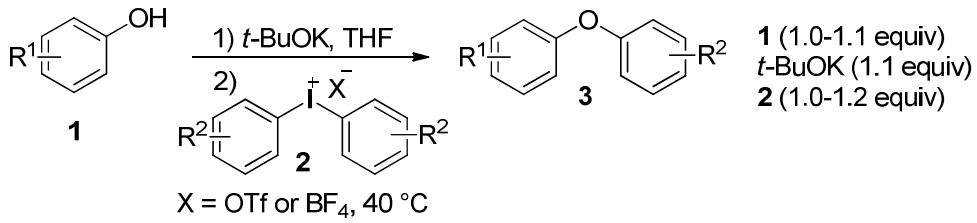

Figure 2.33. Arylation of functionalized phenol.[156]

[154] A. Aranyos, D. W. Old, A. Kiyomori, J. P. Wolfe, J. P. Sadighi, S. L. Buchwald, *J. Am. Chem. Soc. 121* (**1999**) 4369.
[155] G. Mann, C. Incarvito, A. L. Rheingold, J. F. Hartwig, *J. Am. Chem. Soc. 121* (**1999**) 3224.
[156] N. Jalalian, E. E. Ishikawa, L. F. Silva, B. Olofsson, *Org. Lett. 13* (**2011**) 1552.

Table 2.8. Results of Figure 2.33.[156]

Entry	Phenol 1	Diaryl Ether 3	Yield (%)
1	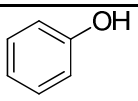	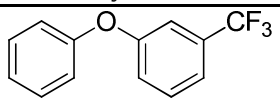	90
2	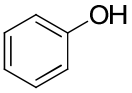	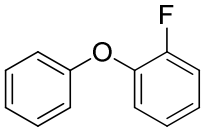	72
3	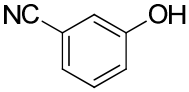	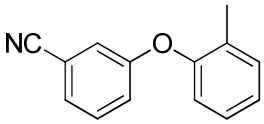	90
4	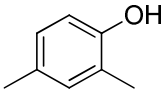	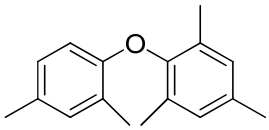	99
5	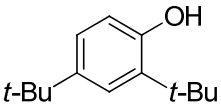	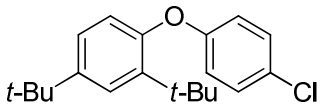	81
6	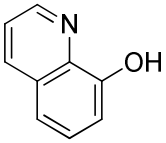	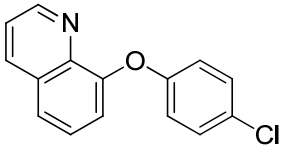	98

A comparison of this method to metal catalyzed processes shows that this method is faster (room temperature synthesis takes 2 h and 40 °C synthesis takes 15 min).[156] Furthermore the conditions are mild and this process is not sensitive to steric bulk.

2.7 Other Interesting Copper Mediated Reactions

2.7.1 Sonogashira Reaction

This process is a cross-coupling reaction of vinyl halides or aryl halides with terminal acetylenes under palladium catalysis and another transition metal, traditionally copper. This reaction forms a $C(sp^2)$—C(sp) bond at room temperature utilizing a palladium like $PdCl_2(PPh_3)_2$ in an amine solvent and using copper as a co-catalyst.[157-159] The Heck reaction allows substitution reactions on planar sp^2-hybridised carbon centers forming $C(sp^2)$—$C(sp^2)$ (for aryl and vinyl halides) and $C(sp^3)$—$C(sp^2)$ (for alkyl halides) provided that these halides do not possess any beta hydrogens. However it does not employ a copper co-catalyst and possesses the additional disadvantage of operating at high temperatures.

Another terminal unsaturated carbon coupling reaction is the Glazer reaction (see section 2.6.1) which couples two sp-carbons to form 1,3-butadiynes or acetylinic compounds. However it occurs at moderate temperatures and the process is catalyzed exclusively by copper and it requires molecular oxygen. For this reason the Sonogashira reaction must be carried out in the absence of oxygen gas or it will form the undesirable homo-coupling product (1,3-butadiyne derivative). This is what led to the so-called "copper free" Sonogashira reaction, in an attempt to address this particular problem. The term "Sonogashira reaction" is now used to refer to Pd-catalysed $C(sp^2)$—C(sp) bond formation between aryl halides or triflates with terminal alkynes regardless of whether copper(I) is used or not.

[157] K. Sonogashira, Y. Tohda and N. Hagihara, *Tetrahedron Lett. 16* (**1975**) 4467.
[158] A. D. Finke, E. C. Elleby, M. J. Boyd, H. Weissman, J. S. Moore, *J. Org. Chem. 74* (**2009**) 8897.
[159] A. Soheili, J. Albaneze-Walker, J. A. Murry, P. G. Dormer, D. L. Hughes, *Org. Lett. 5* (**2003**) 4191.

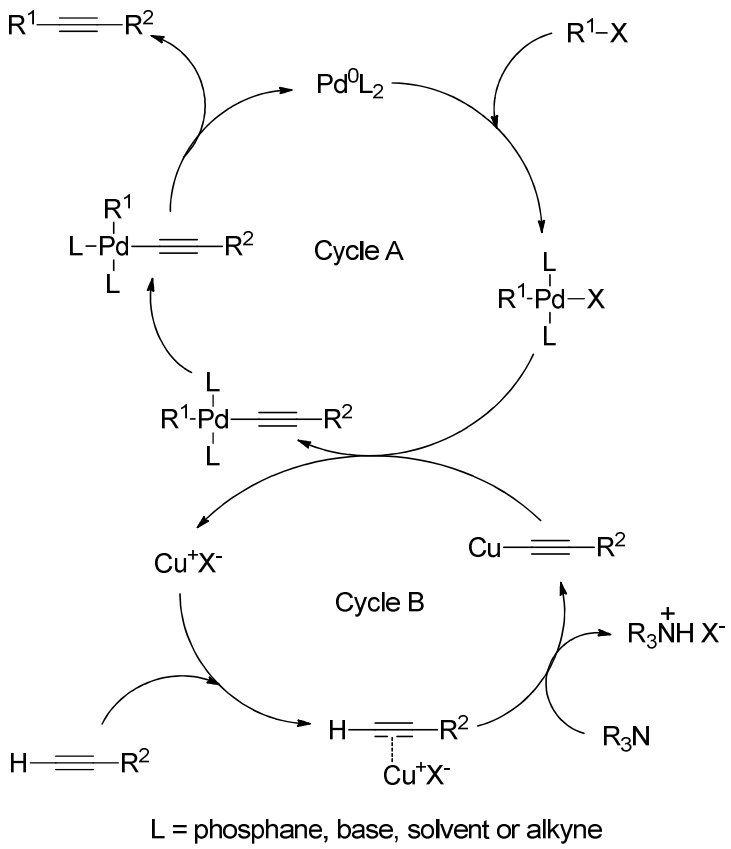

Figure 2.34. Sonogashira catalytic cycle.[160]

The proposed mechanism consists of two independent catalytic cycles. The palladium cycle (Cycle A) being classical for C—C bond formation and proceeding in the normal steps that can be expected for transitional metal catalysis e.g. oxidative addition which in this process it the rate determining step, copper mediated transmetallation, migratory insertion and reductive elimination with the generation of the Pd(0) catalyst. The copper cycle (cycle B) is poorly understood but the base is thought to assist the copper acetylide formation which transmetalates the acetylide to palladium and is eventually coupled to the aryl halide. Reactions where copper is used exclusively for the catalysis have also been reported but the process is carried out at high temperatures, inert conditions and the process is ligand assisted.

[160] R. Chinchilla, C. Najera, *Chem. Soc. Rev.*, *40* (**2011**) 5084.

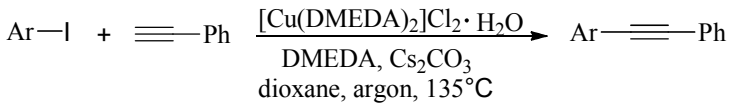

Figure 2.35. Sonogashira coupling.

Table 2.9. Results for the process depicted in Figure 2.35.[161]

Entry	Aryl iodide	Yield [%] after column chromatography
1	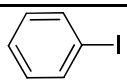	94
2	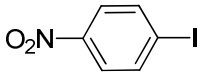	75
3	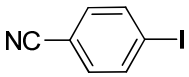	88
4	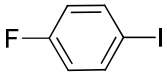	85
5	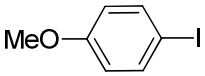	86
6	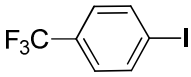	93
7	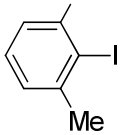	80

2.7.2 Diels-Alder Reaction

Conjugated dienes undergo an addition reaction with alkenes or alkynes (dienophiles) to yield cyclohexene or cyclohexadiene derivatives. This process is pericyclic and requires a cisoid conformation for the diene and a suprafacial-suprafacial mode of reaction (both ends of the diene attack from the same face of the dienophile in a *syn* fashion). In the cyclic transition state that forms, the two alkene carbons and carbon one and four of the diene rehybridize from sp^2 to sp^3 to form two new single bonds while carbons two and three of the diene remain sp^2-hybridized to form the new double bond in the cyclohexe product. The product is normally the endo product according to the *cis*-principle and the *endo* rule.[162-165] The first copper promoted Diels-Alder

[161] L. -H. Zou, A. J. Johansson, E. Zuidema, C. Bolm, *Chem. Eur. J. 19* (**2013**) 8144.
[162] J. Sauer, *Angew. Chem., Int. Ed. 5* (**1966**) 211.

reaction was reported by Bota *et al.* in 1961.[166] In 1969 Corey *et al*. utilized $Cu(BF_4)_2$ to synthesize a precursor for lactone (**4**, Figure 2.36) which was ultimately transformed to PGE_2.[167] This catalyst accelerated this reaction at 0 °C without isomerizing the diene [(5-methoxymethyl)cyclopenta-1,3-diene] and it also influenced the regioselectivity between methylcyclopentadienes and 2-chloro-acrylonitrile.[168]

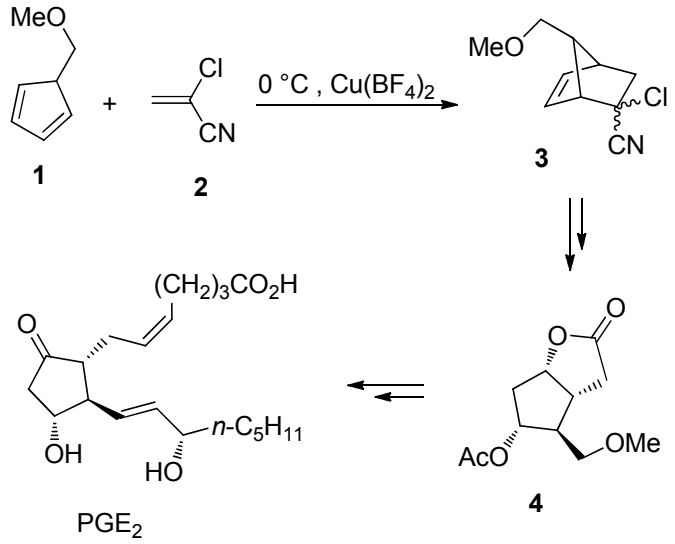

Figure 2.36. The synthesis of PGE_2.

Copper(II) complexes such as $Cu(OTf)_2$, $Cu(BF_4)_2 \cdot 6H_2O$, and $Cu(ClO_4)_2 \cdot 6H_2O$ give good stereocontrol (7/1) for similar transformations, but require longer reaction times and produce lower yields. For this reason a catalytic amount of quinone has to be added to accelerate the reaction, and a Cu(I) species is believed to catalyze this process.[169] $Cu(OTf)_2$ is generally regarded as the catalyst of choice for racemic Diels-Alder reactions.[170] However most enatioselective substrate-directed Diels-Alder reactions utilize aluminium- or titanium-Lewis acid catalysts and the chiral induction is achieved by attaching a chiral auxiliary to the dienophile unit.

[163] J. Sauer, *Angew. Chem., Int. Ed. 6* (**1967**) 16.
[164] K. Alder, G. Stein, *Angew. Chem. 50* (**1937**) 510.
[165] R. B. Woodward, T. J. Katz, *Tetrahedron 5* (**1959**) 70.
[166] T. Bota, C. Bucur, I. Drimus, L. Staˇnescu, D. Saˇndulescu, *Rev. Chim. (Bucharest, Rom.) 12* (**1961**) 503.
[167] E. J. Corey, N. M. Weinshenker, T. K. Schaff, W. Huber, *J. Am.Chem. Soc. 91* (**1969**) 5675.
[168] H. L. Goering, C. Chiu-Shan, *J. Org. Chem. 40* (**1975**) 2565.
[169] J. A. Moore, E. M. Partain, III *J. Org. Chem. 48* (**1983**) 1105.
[170] A. Behr, M. Fiene, F. Naendrup, K. Schu¨rmann, Eur. *J. Lipid Sci. Technol*. (**2000)**, 342.

2.8 Oxidation of 3,5-di-tert-butylcatechol

The oxidation of organic substrates with molecular oxygen under mild conditions is essential for industrial and synthetic processes, from an economical and environmental point of view.[171] 3,5-di-tert-butylcatechol in particular is oxidized by catechol dioxygenases and oxidase to the respective oxidized and cleaved products and 3,5-di-tert-benzoquinone, respectively.[171] Both these enzymes contain transition metal centers, Fe and Cu respectively. It is therefore important to design model systems that imitate the special structural and catalytic properties of these metalloenzymes (model compounds with catechol dioxygenases or catechol oxidase activity). Metal complexes because of their interesting magnetic, catalytic and electron transfer properties, make them suitable for this purpose. These compounds (metal complexes) can also serve as model compounds for oxygen-binding or oxygen-activating copper proteins.[172,173] Therefore identification and characterization of suitable coordination complexes and the investigation of their ability to influence reactivity patterns observed in metalloprotein chemistry, for the future exploitation of copper or iron (transition metal) oxygen systems as practical dioxygen carriers or as reagents for selective and catalytic oxidative transformations is very essential (more efficient catalysts for oxidation reactions).

[171] M. U. Triller, D. Pursche, W. -Y. Hsieh, V. L. Pecoraro, A. Rompel, B. Krebs, *Inorg. Chem. 42* (**2003**) 6274.
[172] S. K. Mandal, L. K. Thompson, M. J. Newlands, E. J. Gabe, *Inorg. Chem. 28* (**1989**) 3707.
[173] D. E. Wilcox, A. G. Porras, Y. T. Hwang, K. Lerch, M. E. Winkler, E. I. Solomon, *J. Am. Chem. Soc. 107* (**1985**) 4017.

2.8.1 Mechanistic Insights

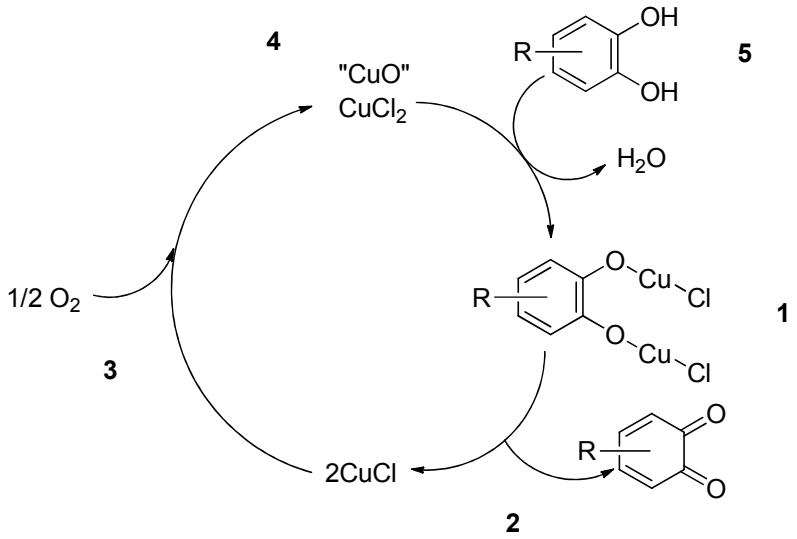

Figure 2.37. Catalytic cycle of catechol oxidation to quinone employing cupric chloride as catalyst.[174]

Figure 2.37 emphasizes the main features of the catalytic process:

- (**1**) Formation of dicopper(II) catecholate intermediate.
- (**2**) Electron transfer from the aromatic ring to two Copper(II) centers in the intermediate giving *o*-benzoquinone and two Copper(I) centers.
- (**3**) Irreversible reaction of the generated copper(I) species with oxygen to give copper(II)-oxygen "reagent" **4**.
- (**5**) Reaction of this "reagent" with catechol leading to regeneration of the dicopper(II) catecholate intermediate and formation of water as the byproduct.

2.9 Concluding Remarks

In this chapter the various applications and mechanistic insights of copper in catalytic oxidation were discussed. It is important to fully comprehend the various aspects associated with these systems in order to develop new and much more efficient processes, for this reason a parallel conclusion will be drawn here for copper and its counterpart palladium.

[174] T. R. Demmin, M. D. Swerdloff, M. M. Rogic, *J. Am. Soc.Chem 103* (**1981**) 5795.

Copper salts and complexes are adaptable reagents for cross-coupling reactions, with a wide range of application similar to that of palladium. This ranges from C—C, C—heteroatom (N, P, O, S, Se) to C—H and C—metal bond formation. Palladium based catalysts are derived from expensive phosphines whereas copper based catalysts are derived from cheaper and more trivial N or O ligands, many of which are common analytical or general purpose reagents. Interestingly copper assisted methods have applications where they are deemed much more effective than their palladium counter parts e.g. better tolerance to functional groups and double bonds, more flexible chemoselectivity (C—N, C—O cross-coupling, etc.). These methods extend the breath of scope for cross-coupling reactions where palladium based catalysts are not successful e.g. secondary alcohols in C—O coupling, sp^3–sp^2 and sp^3–sp^3 C—C coupling.

The most important shortcoming of copper assisted cross-coupling chemistry as a whole is a lack of understanding of the catalytic systems. This also includes the relation between catalyst efficiency and the integrity of the catalyst itself and the mechanism through which the process occurs. Furthermore the effect of various parameters associated with the catalyst is not well understood this includes ligand effects, solvent effects, etc. However in palladium based catalytic processes the initial complex is not the actual catalyst, the catalyst is generated *in situ* by a pre-activation process. The structure of which is mostly unknown due to the high liability of the palladium coordination shell.

Monodentate phosphines usually prohibit copper catalysed reactions and chelating diphosphines are not useful ligands for copper catalytic processes. In many cases heterogeneous copper salts which are partially soluble in the reaction media are generally more efficient than soluble complexes. High solubility normally means high ligation which implies a saturated coordination sphere of the metal and hardly any space for mutations involved in catalysis. The high sensitivity of copper to ligation may be the difference between Cu and Pd in catalysis. Palladium affords strict control of the coordination sphere by phosphine and similar heavily bonding ligands, while copper does not.

Although copper is more economical than palladium, most copper catalyzed processes are slow and have low turnover frequencies (TOFs). However Pd chemistry affords very high TONs and TOFs. Furthermore copper favors expensive organic iodides as reagents, with bromides being

lesser reactive, and only a few systems being dedicated to organic chlorides, whereas palladium can utilize inactivated reagents for chemical mutations.

Copper assisted chemistry is environmentally oblivious. In copper assisted chemistry no attempts have been made to develop green or sustainable methods. However in Pd-catalyzed chemistry a lot of sustainable methods have been developed and successfully implemented. This is arguably one of the reasons for carrying out this particular study.

3 Spectroscopic Characterization Techniques

3.1 Introduction

Characterization techniques entail the use of measurements based on light and other forms of electromagnetic radiation. The effect of the interaction of matter and radiation is measured or the amount of radiation absorbed or produced by molecular or atomic species of interest. These techniques can be classified by the region of the electromagnetic spectrum used in the particular measurement. For this study the following spectroscopic methods of characterization were used; infrared, nuclear magnetic resonance (NMR), ultraviolet, visible and X-ray.

3.2 Infrared Spectroscopy

The infrared region ranges from 1000 nm to 100 µm in the electromagnetic spectrum.[1] All molecules possess a certain amount of energy and are in constant motion. Their bonds stretch and contract, and their atoms move back and forth. Vibrations involve either a change in bond length (stretching) or bond angle (bending). Some bonds stretch in-phase (symmetrical) and others out-of-phase (asymmetric stretching). A molecule consisting of n atoms has a total of 3n degrees of freedom, corresponding to motions along any of the three Cartesian coordinate axes (x, y, z). In a nonlinear molecule, 3 of these degrees are rotational and 3 are translational (the motion of the entire molecule through space) and the remaining are true fundamental vibrations. In a linear molecule, 2 degrees are rotational, 3 are translational and the rest are fundamental vibrations. Among the 3n – 6 (non-linear) or 3n – 5 (linear) fundamental vibrations, those that produce a net change in the dipole moment may result in IR activity and those that give polarizability changes may give rise to Raman activity. The larger the dipole change, the stronger the intensity of the band in an IR spectrum.

[1] J. McMurry, *Organic Chemistry*, 7th ed, Thomson, Brooks/Cole (**2008**).

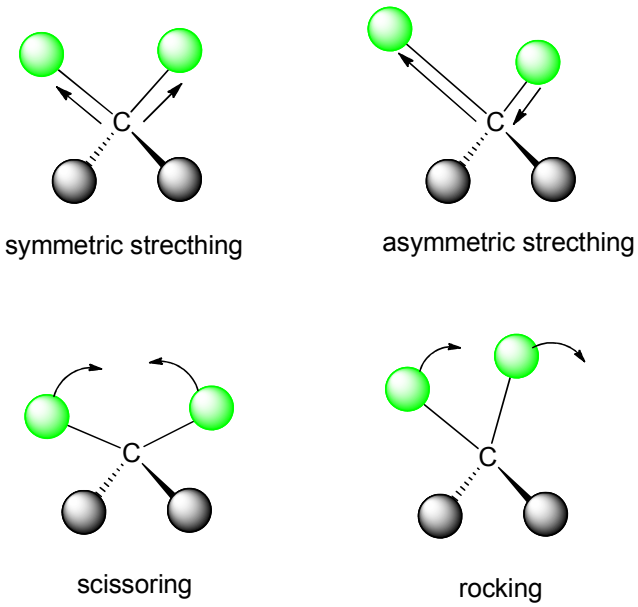

Figure 3.1. Types of molecular vibrations.

Vibrational transitions occur because a molecule has a number of quantized energy levels or vibrational states associated with the bonds in the molecule.[2] This means that a molecule can stretch or bend only at specific frequencies corresponding to specific energy levels. The total energy of a molecule is given by Eq. 3.1:

$$E = E_{\text{electronic}} + E_{\text{vibrational}} + E_{\text{rotational}} \qquad \text{Eq. 3.1}$$

with $E_{electronic}$ the energy associated with the electrons in the various outer orbitals of the molecules, $E_{vibrational}$ the energy of the molecule as a whole due to interatomic vibrations and $E_{rotational}$ accounts for the energy associated with rotation of the molecule about its center of gravity. This technique is not sufficiently energetic to cause electronic transitions, but it can induce vibrational and rotational transitions associated with the ground electronic state of the molecule.[3] For instance when a molecule is irradiated with electromagnetic radiation, energy is absorbed if the frequency of the radiation matches the frequency of the vibration or the frequency of the rotation. This can either result in the atoms of the molecule vibrating at greater

[2] D. A. Skoog, D. M. West, F. J. Holler, S. R. Crouch, *Fundamentals of Analytical Chemistry*, 8th ed, Brooks/Cole (**2007**).
[3] K. Nakamoto, *Infrared Spectra of Inorganic and Coordination Compounds*, 2nd ed, John Wiley & Sons, Inc., New York (**1970**).

amplitudes and the chemical bonds being slightly elongated or the molecule rotating at a higher frequency than before. The frequency (v) of this radiation is given by Eq. 3.2:

$$v = c/\lambda \qquad \text{Eq. 3.2}$$

where c is the speed of light = 3.00 x 10^8 m.s^{-1} and λ is the wavelength. The energy of this radiation will then be given by;

$$E = hv = hc/\lambda \qquad \text{Eq. 3.3}$$

where h is Planck's constant (6.63 x 10^{-34} J.s). This is an invaluable tool as almost all compounds absorb infrared radiation and have a unique absorption spectrum which is considered to be its fingerprint. This allows identification by comparison to compounds that have already been fully characterized by simply comparing their IR-spectra. If the two spectra in question are identical it implies that the two compounds are the same and that the particular compound was successfully synthesized. Furthermore, functional groups have characteristic IR absorption bands that don't change from one compound to another. For instance:

- The region from 2000 to 1500 cm^{-1} is where double bonds (C=O, C=N, C=C) absorb, carbonyl (C=O) absorption peaks are in the range of 1680 to 1750 cm^{-1} and alkene stretching in the range of 1640 to 1680 cm^{-1}.[4]
- From 2500 to 2000 cm^{-1} triple bonds (C$\equiv$N, C$\equiv$C) absorb.
- From 4000 to 2500 cm^{-1} corresponds to absorption due to N−H, C−H and O−H single bond stretching motions. N−H and C−H bonds absorb in the range 3300 to 3600 cm^{-1} while C−H bond-stretching occurs near 3000 cm^{-1}.

Thus by learning where functional group absorptions occur, structural information can be obtained from IR-spectra.

[4] J. Clayden, N. Greeves, S. Warren, P. Wothers, *Organic Chemistry*, Oxford University Press Inc., New York (**2001**).

3.3 Nuclear Magnetic Resonance Spectroscopy

NMR or nuclear magnetic resonance spectroscopy is a technique used to elucidate the structure of organic compounds. It identifies the carbon-hydrogen framework of the organic compound. In principle it can identify any nucleus with a nuclear spin in a molecule.

Protons and neutrons have a quantum property called spin (S) and are referred to as spin ½ particles. Two protons or two neutrons with opposite spins can pair up their spins to give an overall spin of zero and therefore the spin of a nucleus is dependent on the number of protons and neutrons that the nucleus is composed of. With even numbers of protons and neutrons pairing up to give an overall spin quantum number of zero (S = 0) occurs. Such nuclides do not have an overall spin and consequently no angular momentum. A non-zero spin is associated with a non-zero angular momentum (p) which is related to the magnetic moment (μ) of the charged spinning nucleus *via* the relation $\mu = \gamma p$ (γ = gyromagnetic ratio). This magnetic moment allows the observation of NMR absorption spectra caused by transitions between the nuclear spin levels.

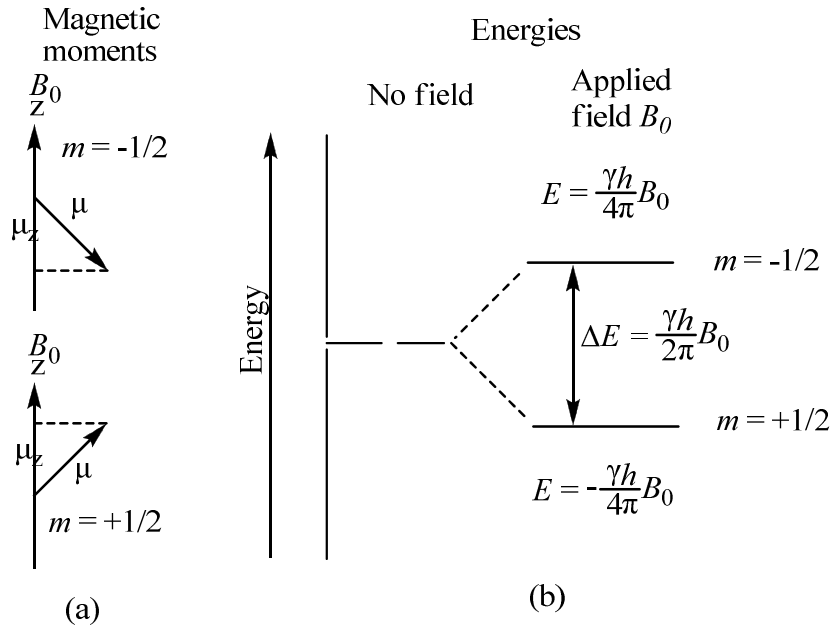

Figure 3.2. Magnetic moments and energy levels for a nucleus with a spin quantum number of ½.

If S = ½ the nucleus is dipolar and if S ≥ 1 it is quadrupolar. The prime difference between dipolar and quadrupolar nuclei is the spin-lattice relaxation times. In dipolar nuclei these relaxation times are generally greater in comparison to those of quadrupolar nuclei (very short

spin-lattice relaxation times). This results in readily detectable, high-resolution measurements in dipolar nuclei samples and line broadening in quadrupolar nuclei samples. This is due to the energy levels of quadrupolar nuclei splitting into multiple levels as opposed to only two in dipolar nuclei upon application of a magnetic field. Quadrupolar relaxation is therefore much more rapid.

Nuclides that possess a nuclear spin upon exposure to a magnetic field have their energy levels split. These nuclei absorb electromagnetic radiation as a result of the energy level splitting induced by the magnetic field. For nuclei with spin ½ only two possible spin states are possible e.g. +1/2 and -1/2. The nuclei with anti-parallel spin (-1/2) to the applied field will possess a greater energy than those spinning parallel to the field (+1/2). The molecular environment influences the absorption of the radio-frequency radiation by these nuclei and this effect can be correlated with molecular structure.

3.4 Ultraviolet-visible Spectroscopy (UV-Vis)

An ultraviolet spectrum is obtained by irradiating the sample with UV light of continuously changing wavelength. When the wavelength corresponds to the energy level required to excite an electron to a higher level, energy is absorbed.[5] This electronic absorption is detected and displayed on a plot of absorbance *vs.* wavelength and is defined as;

$$A = I_0/I \qquad \text{Eq. 3.4}$$

I_0 is the intensity of the incident beam and I is the intensity of the light transmitted through the sample. The wavelength necessary to accomplish the respective transitions in a conjugated molecule depends on the energy gap between HOMO and LUMO, which in turn depends on the nature of the conjugated system. Thus by measuring the UV spectrum of an unknown compound, structural information about the nature of any conjugated π or σ electron system present in a molecule can be obtained.[1] The extent of conjugation in a molecule affects the wavelength of UV absorption. As the extent of conjugation increases the energy difference between HOMO and LUMO decreases e.g. buta-1,3-diene absorbs at λ_{max} = 217 nm, hexa-1,3,5-triene absorbs at λ_{max} = 258 nm and 1,3,5,7-octatetraene absorbs at λ_{max} = 290 nm. The following molecular transition can be observed (* represents anti-bonding orbitals).

[5] J. Conradie, *Spectroscopy Lecture notes*, UFS Chemistry Department (**2010**).

- $\sigma \rightarrow \sigma^*$
- $\pi \rightarrow \pi^*$
- $n \rightarrow \sigma^*$
- $n \rightarrow \pi^*$

3.5 Theory of X-Ray Diffraction

The wavelength of X-ray radiation is suited for resolving atoms separated by the distance of a covalent bond. The energy of a quantum of this radiation is approximately 8000 eV which is approximately the energy of electrons in their orbitals. This equivalence of energy leads to interactions so that the electrons of an atom will primarily be responsible for the scattering of X-rays. The interference of the scattered X-rays leads to the general phenomenon of diffraction.

Single-crystal X-ray diffraction is a non-destructive analytical technique which provides detailed information about the internal lattice of crystalline substances, including unit cell dimensions, bond-lengths, bond-angles, and details of site-ordering. Directly related to it is single-crystal refinement, where the data generated from the X-ray analysis is interpreted and refined to obtain the crystal structure.

3.5.1 Diffraction

Scattering refers to the ability of objects to change the direction of a wave (in this case atoms). Huygen's principle states that every point along a wave front can be considered to be the origin of a new wave front (Figure 3.3).[6]

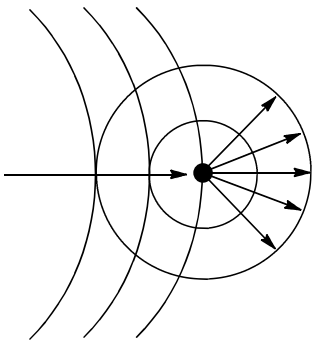

Figure 3.3. Huygen's principle of diffraction.

[6] B. Crowell, *Optics*, 2.1 ed, (**1999**). Also available at; www.lightandmatter.com

The velocity of this new wave front is equal to that of the original. Objects placed in the path of a wave front act as points of propagation for new wave fronts. The entirely new waves are called scattered waves. If two point objects (A and B) are placed in the path of the wave front, each of them will propagate a new wave front having identical wavelengths and velocities (Figure 3.4).

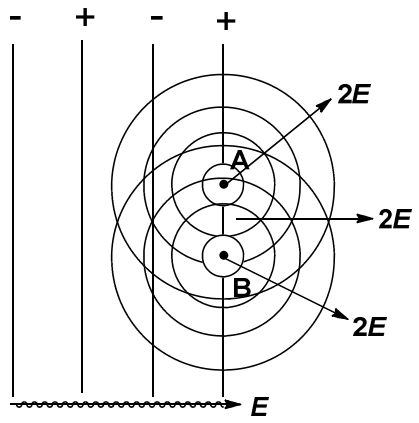

Figure 3.4. Constructive interference of scattered waves from two points placed in front of an incident wavefront.

The relative phases of these wave fronts depend on the positions of A and B relative to the origin of the initial wave front. At some position in space the wave propagating from A will reinforce the scattered wave from B through constructive interference if the two scattered waves are in phase or *vice versa*. Alternatively the wave from A will reduce the amplitude of the wave from B through destructive interference if the amplitudes are out of phase or *vice versa*. This is called diffraction; the sum of the two waves propagated from A and B result in an amplitude that is dependent on the relative positions of A and B and is also dependent on where the new wave fronts are being observed. If several observations of the amplitude of the new wave front at different positions is simultaneously made, information can be extrapolated to determine the relative positions of the diffracting objects A and B relative to the origin of the initial wave front. This is how x-ray diffraction is used to solve the structure of molecules in single crystals i.e. X-rays are scattered by atoms of molecules or regular repeating arrays of molecules (single crystal) to give a pattern that represents the molecular order and structure. Furthermore using mathematics as the lens, structure reconstruction to transform the pattern back into the original structure can be performed.

3.5.2 Bragg's Law

In 1912 W. L. Bragg developed a relationship to comprehend how diffraction relates to the relative positions of point objects in space.[7] In this model, lattice points in the crystal are viewed as parallel planes. Stacking the reflecting planes at regularly spaced intervals *d* creates a simple one dimensional model of a crystal. In this model, a wave of wavelength λ is incident on the reflecting plane at an angle *θ*.

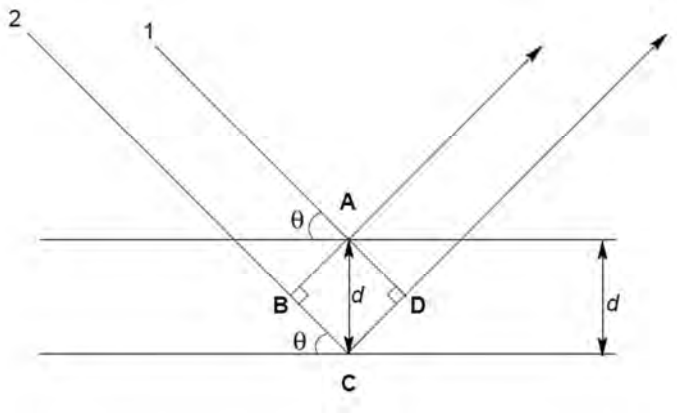

Figure 3.5. Diffraction of X-rays according to Bragg's law.

The individual paths of scattered light are parallel and constructive interference is only observed if the reflected waves are perfectly in phase. This only occurs when the difference in the length of the path of the incident and reflected waves of each plane (BC + CD) is equal to some integer value (*n*) of the wavelength of the incident X-rays (Eq. 3.5).

$$BC + CD = n\lambda \qquad \text{Eq. 3.5}$$

This path difference is related to the distance separating the reflecting planes by the following trigonometric relationship;

$$BC + CD/2 = d\sin\theta \qquad \text{Eq. 3.6}$$

This results in the following equation by combining Eq. 3.5 and Eq. 3.6;

$$2d\sin\theta = n\lambda \qquad \text{Eq. 3.7}$$

[7] D. Halliday, R. Resnick, J. Walker, *Fundamentals of Physics*, 4th ed, John Wiley & Sons, Inc., New York (**1994**).

There's a reciprocal relationship between the Bragg angle θ and the spacing between the reflecting planes *d*. This means that smaller spacing of repeating units in a crystal results in larger diffraction angles and *vice versa*.

3.5.3 Structure Factor

The position of atoms in a unit cell are expressed in terms of fractional coordinates called Miller indices (*h, k, l*) and the cell edges are defined by vectors x, y, z (Eq. 3.8).

$$\mathrm{r} = \mathrm{h}x + \mathrm{k}y + \mathrm{l}z \qquad \text{Eq. 3.8}$$

The structure factor *F*(*hkl*) of any X-ray reflection (diffracted beam) is the quantity that exhibits both the amplitude and the phase of that reflection.[8] It plays an essential part in the solution and refinement of crystal structures because it serves as the quantity related to the intensity of the reflection which depends on the structure giving rise to that reflection and is independent of the method and conditions of observation of the reflection.

$$F(\mathrm{hkl}) = \sum_{j=1}^{N} g_j \exp\left(i\phi_j\right) = \sum_{j=1}^{N} g_j \exp[i2\pi\left(\mathrm{h}x_j + \mathrm{k}y_j + \mathrm{l}z_j\right)] \qquad \text{Eq. 3.9}$$

In Equation 3.9, g_j = scattering factor of each of the N atoms and ϕ_j = the phase of the wave. The set of structure factors for all the reflections (*hkl*) are the prime quantities necessary for the derivation of the three-dimensional distribution of electron density, which is the image of the crystal structure, calculated by Fourier methods. The way in which the separate scattered or diffracted rays combine to form an image depends on three factors associated with each ray:

- Direction,
- amplitude and
- phase.

In X-ray crystallography, the diffracted beams are separately observed and their intensities measured as the blackness of spots on an X-ray film or by direct quantum counting in a diffractometer. By identifying the Miller indices (*hkl*) of the crystal plane giving rise to each

[8] M. J. Buerger, *Crystal-Structure Analysis*, Wiley, New York (**1960**).

diffracted beam, the direction of the beam is specified. From the measured intensity of the beam its amplitude may readily be deduced. Currently there is no method available for observing the phase of each diffracted beam, which is the third segment of data required before mathematical recombination is possible to produce an image of the structure. This forms what is known as the phase problem in crystallography.[9]

The structure factor therefore represents the resultant amplitude and phase of scattering of all the electron density distribution of one unit cell. The amplitude is calculated as the number of times that the amplitude is greater than that of an isolated electron. The phase is calculated relative to a phase of zero for hypothetical scattering by a point at the origin of the unit cell. The resultant is calculated as a superimposition of waves, one from each atom in the unit cell, each wave having an amplitude which depends on the number of electrons in the atom and a phase which depends on the position of the atom in the unit cell.

$$F(\mathrm{hkl}) = \sum_{j=1}^{N} f_j[\cos 2\pi(\mathrm{h}x_j + \mathrm{k}y_j + \mathrm{l}z_j) + i\sin 2\pi(\mathrm{h}x_j + \mathrm{k}y_j + \mathrm{l}z_j)] \qquad \text{Eq. 3.10}$$

The energy that is associated with a cosine wave is proportional to the square of the amplitude of the wave. In X-ray diffraction, it is expressed in terms of the intensity of the scattered wave, $I_o(hkl)$ (where the superscript 'o' signifies an experimentally observed quantity). Accordingly:

$$I_0(\mathrm{hkl}) \propto |F_0(\mathrm{hkl})|^2 \qquad \text{Eq. 3.11}$$

This is ideal and forms the basis of X-ray structure analysis, since it allows the experimental I_0(hkl) values to be directly related to the structure by IF(*hkl*)I. Atoms with high atomic numbers give a greater concentration of electrons than atoms with low atomic numbers. Electron density is a function of position and can be given as $\rho(x, y, z)$. The structure factor in terms of electron density is given by the following equation;

$$F(\mathrm{hkl}) = \int \rho(x, y, z) \exp[i2\pi(\mathrm{h}x_j + \mathrm{k}y_j + \mathrm{l}z_j)]\, dV \qquad \text{Eq. 3.12}$$

[9] R. Pepisky, J. M. Robertson, J. C. Speakman, Eds., *Computing Methods and the Phase Problem in X-ray Crystal Analysis*, Oxford, Pergamon (**1960**).

3.5.4 Solutions to the Phase Problem

The solution of a crystal structure therefore consists of applying some technique for obtaining the approximate phases of at least some of the X-ray reflections. Direct methods approximate the initial and expanding phases from measured X-ray intensities by using mathematical formulae. This method is used for structures comprised exclusively of light atoms.

Alternatively for compounds containing heavier atoms or compounds in which a major part of the structure is already known the Patterson function can be applied. This function is similar to an electron density map with peaks of positive electron density in various positions.

$$P(u,v,w) = V^{-1}\sum_h\sum_k\sum_l(F_{\mathrm{hkl}})^2\exp[-2\pi i(\mathrm{h}u+\mathrm{k}v+\mathrm{l}w)] \qquad \text{Eq. 3.13}$$

where *V* represents the volume of the unit cell. The positions of these peaks are not the positions of the atoms in the structure but a function of vectors between pairs of atoms in the structure. The implication being that the Patterson function only produces information on where the atoms lie relative to each other and not relative to the unit cell origin. The Patterson peaks are a proportional indication of the size of the atoms involved.

3.5.5 Least Squares Refinement

In the process of structure refinement, knowledge of phases is extended to all reflections and is made as accurate as possible for all reflections. Apart from the direct method of obtaining some initial phases, both the solution and refinement processes depend on the ability to calculate structure factors for a proposed approximate arrangement of some or all of the atoms in the crystal structure. The least square refinement is used to compare calculated data with experimental data to obtain a degree of similarity between them. For crystal structure refinement, the similarities between the experimental structural factor, (F_0), and calculated structural factor, (F_c), is compared in terms of the residual index or R-factor by the following equation;

$$R = \frac{\sum\left||F_0|-|F_c|\right|}{\sum|F_0|} \qquad \text{Eq. 3.14}$$

An R-factor of lower than 0.1 indicates a complete and correct structure determined from good experimental data. Better refinements can be obtained by incorporating a weighting factor for each reflection (*w*) which is a reliability factor of the different measured data. This gives rise to a new residual factor which is extensively used for determining crystal structures.

$$wR^2 = \frac{\sum w({F_0}^2 - {F_c}^2)^2}{\sum w({F_0}^2)^2} \qquad \text{Eq. 3.15}$$

3.6 Theoretical Aspects of Chemical Kinetics

3.6.1 Introduction

Chemical reaction kinetics is the study within which quantitative determination of reaction rates are made *i.e.* the speed of a reaction and its mechanism (reactions take place at various speeds). Chemical processes can be broken down into a sequence of one or more single-step processes (elementary process). These basic steps involve either a single reactive collision between two molecules (bimolecular process), or dissociation/isomerization of a single reactant molecule (unimolecular process) to yield a product or an intermediate. Under extremely high pressures, a termolecular process may occur, which involves simultaneous collision of three reactant molecules to yield a product or an intermediate.

Elementary processes involve a transition between two atomic or molecular states separated by a potential boundary. The potential boundary makes up the activation energy of the process, and determines the rate at which it occurs. If this boundary is low, the thermal energy of the reactants will generally be high enough to overcome the barrier and move to the products, and the reaction will be fast. However if the boundary is high, only a few reactants will have sufficient energy, and the reaction will be much slower. The presence of a potential boundary to the reaction is also the source of the temperature dependence of reaction rates.

The great variety of chemical species, types of reaction, and the accompanying potential energy surfaces involved implies that the timescale over which chemical reactions occur covers many orders of magnitude, from very slow reactions such as iron rusting, to extremely fast reactions

such as the electron transfer processes involved in many biological systems or the combustion reactions occurring in flames.

For chemical reactions, the speeds are measured in units of moles of reactant consumed per unit of time or moles produced per unit of time, and the term rate is used, rather than speed. When reactions take place in solutions, or for gases, then rate is given in units of moles per liter of reactant consumed per unit of time.

Chemical kinetics is a very complex subject, however it can be simplified significantly by selective manipulation of a few parameters concerning the process of interest e.g. the concentrations of the reagents and the reaction temperature, pressure, solvent, etc. Thus a kinetic study of these copper(II) nano-particles will help evaluate the efficiency of these complexes in homogeneous catalysis and to deduce a mechanism for the process. For the purposes of this study the rate of product formation was determined at constant temperature and in methanol as solvent. The technique used is defined by Beer-Lambert law;[10]

$$\log_{10}\frac{I_o}{I_{trs}} = \varepsilon c\iota = A \qquad \text{Eq. 3.16}$$

3.6.2 Reaction Rates and Rate Laws

For the reaction:

$$pP + uU \longrightarrow lL + eE$$

The rate can be expressed as;

$$\text{Rate of reaction} = -\frac{d[P]}{d\mathrm{t}} = -\frac{d[U]}{d\mathrm{t}} = \frac{d[L]}{d\mathrm{t}} = \frac{d[E]}{d\mathrm{t}} \qquad \text{Eq. 3.17}$$

Where $d[P]$ and $d[U]$, are changes in concentration of reactants (depletion) over a time dt, while the latter $d[L]$ and $d[E]$ are changes in concentration of products (formation).

[10] P. W. Atkins, *Physical Chemistry*, Oxford: Oxford University Press Inc, (**1994**).

The rate law can be defined as "the experimentally determined dependence of the reaction rate on the reactant concentrations".[11] The rate law of the above mentioned reaction will have the following generic form,

$$\text{Rate} = k[P]^{\alpha}[U]^{\beta} \qquad \text{Eq. 3.18}$$

Where *k* is the rate constant and components α, β are determined experimentally and represents the order of the reaction with respect to the concentrations of the respective reagents. The sum of these components gives the total order of the reaction. The rate constant is independent of the concentrations of *P* and *U* but can be influenced by temperature, solvent, catalyst, etc.

For this catalytic process the catalyst concentration was kept constant while the concentration of the substrate to be oxidised was varied. The rate of product formation was monitored and comparisons made between the different catalyst precursors. Temperature, solvent effects, or pressure studies were not analysed (rate constant dependence on the variables), however the effect of dissolved oxygen was investigated. The process is denoted below;

$$\text{A} \xrightarrow{k_1} \text{B}$$

A general rate equation can be determined for this nth-order single component process. The form of the rate expression is given below;

$$-\frac{d[A]}{d\text{t}}k_1[A]^n = \frac{d[B]}{d\text{t}} \qquad \text{Eq. 3.19}$$

This form can be integrated and the limits are taken as [A_0] = initial concentration at t = 0 and [A] = concentration at time t.

$$-\int_{[A_0]}^{[A]} \frac{d[A]}{[A]^n} = k\int_0^t d\text{t} \qquad \text{Eq. 3.20}$$

There are several possible reaction orders for a single component rate expression e.g. *n* = 0, 1, 2 (zero, first and second order reactions respectively). The integrated forms can be obtained from the above equation;

- Zero order in A:

$$[\text{A}] = [\text{A}_0] - k\text{t} \qquad \text{Eq. 3.21}$$

[11] R. B. Jordan, *Reaction Mechanisms of Inorganic and Organometallic Systems*, Oxford: Oxford University Press, Inc., (**1991**).

- First order in A:

$$\ln \frac{[A]}{[A_0]} = -k\text{t or } [\text{A}] = [A_0]e^{-k\text{t}} \qquad \text{Eq. 3.22}$$

- Second order in A:

$$\frac{1}{[A]} = k\text{t} + \frac{1}{[A_0]} \qquad \text{Eq. 3.23}$$

To obtain an acceptable rate equation, the experimentally determined absorbance-time data is fitted to each of the integrated expressions. A linear plot is obtained when the integrated form of the correct rate law is used. The rate constant, *k*, can then be determined from the slope of the line.

A useful technique employed to simplify rate equations in chemical kinetics is *pseudo*-order reactions. In this technique an n-order reaction can be carried out such that it is of the n-1 or lesser order (false order) to simplify its rate law. This is achieved by carrying out the reaction in such a way that one of the reagent concentrations is held constant throughout the reaction. For instance if the concentration of *P* (in section 3.6.2 above) is held constant, then this concentration will contribute to a factor in the rate law known as the observed rate constant (k_{obs}) and the reaction will be *pseudo* β order in *U* instead of the real order (α + β). In this sense a reaction has been transformed to a lower false order with a false rate constant referred to as the observed rate constant. This can be achieved by the following ways:

- By having an excess concentration of one of the reagents so that the change in concentration is only minute compared to the other reagent (remains essentially constant).
- Using a buffer, if the reaction medium is water and one of the reagents is either a hydronium ion or a hydroxide ion. The use of a buffer could hold the concentration of these ions reasonably constant.
- A first-order solution reaction of a substance in the presence of its solid phase also displays a *pseudo* process. If the dissolution rate of the solid is greater than the reaction rate of the dissolved solute, the solute concentration is maintained constant by the solubility equilibrium and the reaction becomes a *pseudo* zero-order reaction.

From Beer's law, the absorbance of the absorbing species is directly proportional to its concentration and to the path length of the absorbing medium. This relationship between concentration and absorbance is used to determine the rate equation. Furthermore reactions are

normally performed under *pseudo*-order conditions to simplify the process of determining the rate constant and to opt for the simple order reaction/process. The change in absorbance of a solution consisting of the reaction components is then plotted as a function of time after the components were mixed. The plots obtained show either increasing or decreasing limiting kinetics as the rate of product formation is monitored (or reagent depletion). The observed *pseudo*-order rate constants for the reaction is then determined from Eq. 3.24;

$$A_{obs} = A_{\infty} - (A_{\infty} - A_0)e^{-k_{obs}t} \qquad \text{Eq. 3.24}$$

where A_{obs} represents the experimentally observed absorbance at specific time t, A_{∞} is the absorbance maximum after the reaction has completed, A_0 represents the initial absorbance when the reaction was started and k_{obs}, the observed rate constant. The half-life ($t_{1/2}$) of a reaction is defined as the time required for the reactant concentration to decay by 50 % and is given by the following expression;

$$t_{1/2} = \frac{\ln 2}{k_{obs}} = \frac{0.693}{k_{obs}} \qquad \text{Eq. 3.25}$$

3.7 Conclusion

The transition state theory, thermodynamics and temperature dependence of reaction rates were not discussed in this section as the effect of temperature changes was not investigated in this study. These techniques will not only be used to elucidate the structure and identify the functional groups but also to identify the different species as they form in the studies carried out in the succeeding chapters.

4 Synthesis and Spectroscopic Characterization

4.1 Chemical Characterization and Instrumentation

All reagents used for synthesis and characterization were of analytical grade. If nothing else is stated, all commercially available reagents were used as received from Sigma-Aldrich. All organic solvents were dried and distilled before use. All infrared spectra were recorded as neat samples on a Bruker Tensor Standard System spectrophotometer with a laser range of 4000–370 cm^{-1} and reported in cm^{-1}. The UV-Vis spectra were collected on a Varian Carey 50 Conc spectrometer equipped with a Julabo F12-mV temperature cell regulator (accurate to within 0.1 °C) in a 1.00 cm quartz cuvette cell. The ^{1}H NMR spectra were obtained in $(CD_3)_2CO$ solutions on a 300 MHz Bruker spectrometer. ^{1}H chemical shifts are reported relative to TMS using the $(CD_3)_2CO$ peak (2.5 ppm). All chemical shifts are reported in ppm and coupling constants in Hz.

4.2 Synthesis of 3-Hydroxy-4-pyridones derivatives

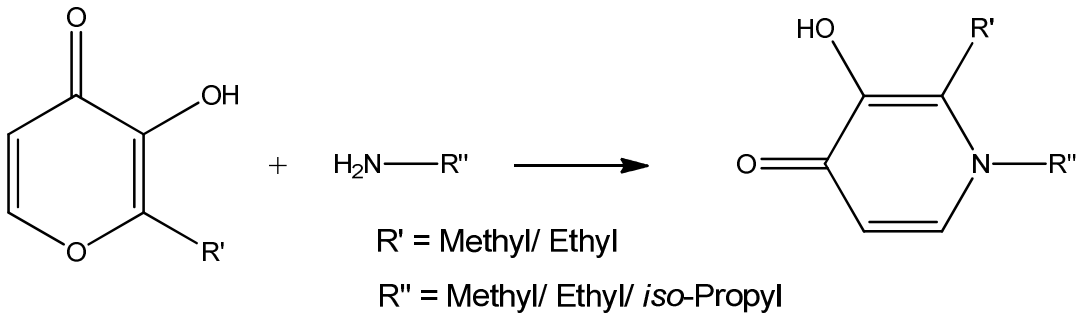

Figure 4.1. The synthesis of 3-hydroxy-4-pyridones from 3-hydroxy-pyran-4-ones.

4.2.1 3-Hydroxy-1,2-dimethyl-4-pyridone (MM(naltol)H)

3-Hydroxy-1,2-dimethyl-4-pyridone was prepared by refluxing 3-hydroxy-2-methyl-pyran-4-one (methyl maltol) (5.00 g, 39.65 mmol) with 3 equivalents of 40 % aqueous methylamine (4.10 ml,

119.00 mmol) in 100 ml of water overnight. The mixture turned dark brown. Decolourizing charcoal was added and the mixture was left to stand for 30 min. The mixture was filtered and the dark brown filtrate was evaporated *in vacuo* to yield a dark brown solid. Precipitation from cold acetone gave a white crystalline precipitate of 3-hydroxy-1,2-dimethyl-4-pyridone. IR (ATR) $\nu_{C=O}$ (cm^{-1}): 1567.0, 1630.7; $\nu_{C=C}$ (cm^{-1}): 1506.3, 1995.7. NMR (300 MHz, $(CD_3)_2CO$) ^1H: 2.25(s), 3.62(s), 6.08(d), 7.54(d). Yield: 3.50 g, 25.15 mmol, 70 %.

4.2.2 1-Ethyl-3-hydroxy-2-methyl-4-pyridone (ME(naltol)H)

1-Ethyl-3-hydroxy-2-methyl-4-pyridone was prepared by refluxing 3-hydroxy-2-methyl-pyran-4-one (methyl maltol) (10.03 g, 79.53 mmol) with 3 equivalents of 70 % aqueous ethylamine (12.64 ml, 240 mmol) in 200 ml of water overnight. The mixture turned dark brown. Decolourizing charcoal was added and the mixture was left to stand for 30 min. It was then filtered and the dark brown filtrate was evaporated *in vacuo* to yield a dark brown solid. After washing with acetone a brown precipitate of 1-ethyl-3-hydroxy-2-methyl-4-pyridone was obtained. IR (ATR) $\nu_{C=O}$ (cm^{-1}): 1565.3, 1625.1; $\nu_{C=C}$ (cm^{-1}): 1506.5, 1528.8; ν_{O-H}: 3155.7. NMR (300 MHz, $(CD_3)_2CO$) ^{13}C: 11.54, 16.43, 48.34, 111.36, 128.95, 137.28, 145.99, 160.49. NMR (300 MHz, $(CD_3)_2CO$) ^1H: 1.25(t), 2.29(s), 3.96(q), 6.12(d), 7.58(d). Yield: 8.01 g, 52.30 mmol, 79.7%.

4.2.3 3-Hydroxy-2-methyl-1-isopropyl-4-pyridone (MP(naltol)H)

3-Hydroxy-2-methyl-1-isopropyl-4-pyridinone was prepared by refluxing 3-hydroxy-2-methyl-pyran-4-one (methyl maltol) (5.01 g, 39.73 mmol) with 3.3 equivalents of aqueous isopropylamine (14.06 ml, 130.8 mmol, 99.0 %) in 100 ml of water overnight. The mixture turned dark brown. Decolourizing charcoal was added and the mixture was left to stand for 30 min. This was then filtered and the dark brown filtrate was evaporated *in vacuo* to yield a dark brown solid. Precipitation from cold acetone gave a pink precipitate of 3-hydroxy-2-methyl-1-isopropyl-4-pyridinone. IR (ATR) $\nu_{C=O}$ (cm^{-1}): 1568.0, 1623.7; $\nu_{C=C}$ (cm^{-1}): 1502.7, 1526.3; ν_{O-H} (cm^{-1}): 3125.7. NMR (300 MHz, $(CD_3)_2CO$) ^1H: 1.34(d), 2.32(s), 4.49(m), 6.18(d), 7.68(d). Theoretical mass percentage of $C_9H_{13}NO_2$: C = 64.6 %, H = 7.8 %, N = 8.4 %, O = 19.2 %. Elemental analysis (average %): C = 64 (1) %, H = 5.61 (8) %, N = 8.9 (2) %. Yield: 4.10 g, 32.30 mmol, 81.80 %.

4.2.4 2-Ethyl-3-hydroxy-1-methyl-4-pyridone (EM(naltol)H)

2-Ethyl-3-hydroxy-1-methyl-4-pyridone was prepared by refluxing 2-ethyl-3-hydroxy-pyran-4-one (ethyl maltol) (5.01 g, 39.73 mmol) with 3.3 equivalents of 40 % aqueous methylamine (18.29 ml, 117.70 mmol) in 100 ml of water overnight. The mixture turned dark brown. Decolourizing charcoal was added and the mixture was left to stand for 30 min. This was then filtered and the dark brown filtrate was evaporated *in vacuo* to yield a dark brown solid. After washing with cold acetone, a white crystalline precipitate of 2-ethyl-3-hydroxy-1-methyl-4-pyridone was obtained. IR (ATR) $\nu_{C=O}$ (cm^{-1}): 1568.8, 1623.7; $\nu_{C=C}$ (cm^{-1}): 1510.7; ν_{O-H} (cm^{-1}): 3149.8. NMR (300 MHz, $(CD_3)_2CO$) ^{13}C: 11.33, 19.15, 41.59, 110.55, 135.16, 145.64, 160.50. NMR (300 MHz, $(CD_3)_2CO$) ^{1}H: 1.11(t), 2.70(q), 3.67(s), 6.08(d), 7.53(d). Yield: 3.92 g, 25.57 mmol, 78.2 %.

4.2.5 1,2-Diethyl-3-hydroxy-4-pyridone (EE(naltol)H)

1,2-Diethyl-3-hydroxy-4-pyridone was prepared by refluxing 2-ethyl-3-hydroxy-pyran-4-one (ethyl maltol) (5.00 g, 39.65 mmol) with 3.3 equivalents of 40 % aqueous methylamine (6.18 ml, 117.50 mmol) in 100 ml of water overnight. The mixture turned dark brown. Decolourizing charcoal was added and the mixture was left to stand for 30 min. This was then filtered and the dark brown filtrate was evaporated *in vacuo* to yield a dark brown solid. After washing with cold acetone, a white crystalline precipitate of 1,2-diethyl-3-hydroxy-4-pyridone was obtained. IR (ATR) $\nu_{C=O}$ (cm^{-1}): 1573.7, 1618.2; $\nu_{C=C}$ (cm^{-1}): 1507.2, 1530.7; ν_{O-H} (cm^{-1}): 3153.9. NMR (300 MHz, $(CD_3)_2CO$) ^{13}C: 13.17, 17.26, 19.13, 47.85, 111.67, 134.07, 137.28, 145.67, 169.52. NMR (300 MHz, $(CD_3)_2CO$) ^{1}H: 1.13(t), 1.27(t), 2.69(q), 3.96(q), 6.12(d), 7.57(d). Yield: 4.80 g, 28.71 mmol, 96.0 %.

4.2.6 2-Ethyl-3-hydroxy-1-isopropyl-4-pyridone (EP(naltol)H)

2-Ethyl-3-hydroxy-1-isopropyl-4-pyridinone was prepared by refluxing 2-ethyl-3-hydroxypyran-4-one (ethyl maltol) (5.02 g, 39.81 mmol) with 6 equivalents of aqueous isopropylamine (12.65 ml, 214.10 mmol, 99%) in 100 ml of water overnight. The mixture turned dark brown. Decolourizing charcoal was added and the mixture was left to stand for 30 min. This was then filtered and the dark brown filtrate was evaporated *in vacuo* to yield a dark brown solid. Crystallization from cold acetone gave pink crystals of 2-ethyl-3-hydroxy-1-isopropyl-4-

pyridinone. IR (ATR) $\nu_{C=O}$ (cm^{-1}): 1571.2, 1619.2; $\nu_{C=C}$ (cm^{-1}): 1503.8, 1527.9; ν_{O-H} (cm^{-1}): 3155.7. NMR (300 MHz, $(CD_3)_2CO$) ^{13}C: 13.3, 18.5, 23.1, 51.5, 111.9, 133.4, 134.3, 145.2, 169.2. NMR (300 MHz, $(CD_3)_2CO$) ^{1}H: 1.11(t), 1.38(d), 2.77(q), 4.48(m), 6.18(d), 7.70(d). Yield: 2.5 g, 13.79 mmol, 49.8%.

4.3 Synthesis of Bis(pyridonato)copper(II) Complexes

In each case bis(O,O'-bidentate)copper(II) was prepared by dissolving the respective O,O'-bidentate ligand (3.00 mmol) in methanol (15 ml) and the mixture was heated to 60.0 °C while stirring. After the addition of copper acetate (1.50 mmol; 0.30 g) to the mixture, it was stirred for 4 hours at 60.0 °C. The solution was left to cool to room temperature, and a green precipitate appeared that was filtered. The precipitate was washed with cold ethanol and dried.

4.3.1 Bis(3-hydroxy-1,2-dimethyl-4-pyridinonato)copper(II) [Cu(MM(naltol))$_2$]

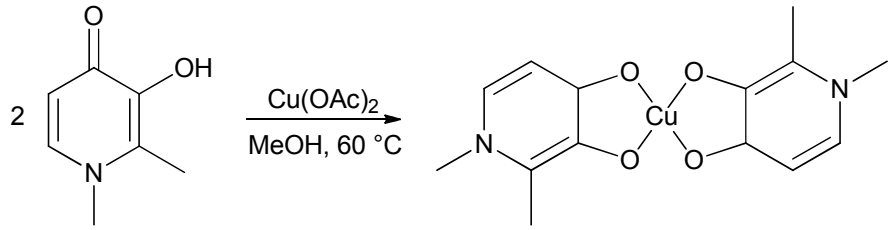

Figure 4.2. The synthesis of bis(3-hydroxy-1,2-dimethyl-4-pyridinonato)copper(II).

IR (ATR) $\nu_{C=C}$ (cm^{-1}): 1546.2, 1600.4; ν_{C-O} (cm^{-1}): 1258.1, 1282.8. Yield: 0.35 g, 1.26 mmol, 68.7 %.

4.3.2 Bis(1-ethyl-3-hydroxy-2-methyl-4-pyridinonato)copper(II) [Cu((ME(naltol))$_2$]

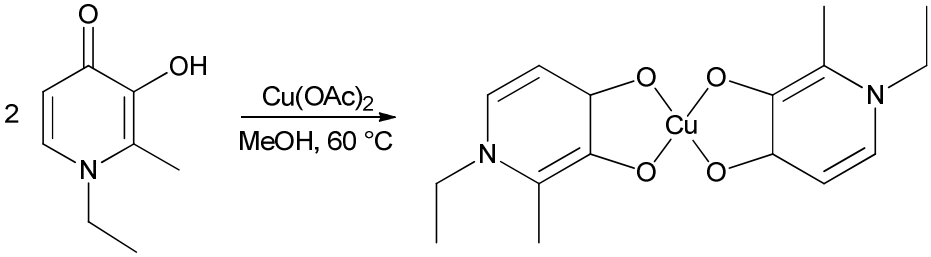

Figure 4.3. The synthesis of bis(1-ethyl-3-hydroxy-2-methyl-4-pyridinonato)copper(II).

IR (ATR) $\nu_{C=C}$ (cm^{-1}): 1542.3, 1593.1; ν_{C-O} (cm^{-1}): 1261.2, 1284.5. Yield: 0.42 g, 1.37 mmol, 76.10 %.

4.3.3 Bis(3-hydroxy-2-methyl-1-isopropyl-4-pyridinonato)copper(II) [Cu((MP(naltol))$_2$]

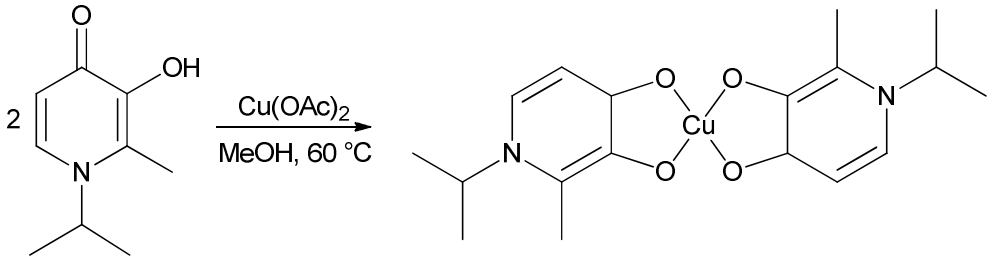

Figure 4.4. The synthesis of bis(3-hydroxy-2-methyl-1-isopropyl-4-pyridinonato)copper(II).

IR (ATR) $\nu_{C=C}$ (cm^{-1}): 1546.2, 1600.4; ν_{C-O} (cm^{-1}): 1258.1, 1282.8. Theoretical mass percentage of $CuC_{18}H_{26}N_2O_4$: Cu = 16.0 %, C = 54.6 %, H = 6.1 %, N = 7.1 %, O = 16.2 %. Elemental analysis (average %): C = 53 (2) %, H = 4.5 (1) %, N = 7.62 (3) %. Yield: 0.49 g, 1.47 mmol, 95.2 %.

4.3.4 Bis(2-ethyl-3-hydroxy-1-methyl-4-pyridinonato)copper(II) [Cu((EM(naltol))$_2$]

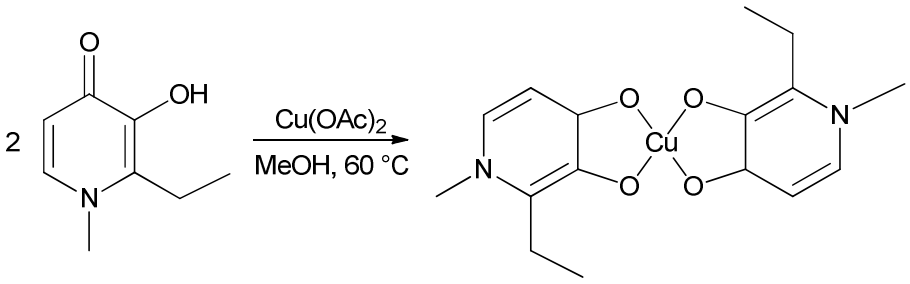

Figure 4.5. The synthesis of bis(2-ethyl-3-hydroxy-1-methyl-4-pyridinonato)copper(II).

IR (ATR) $\nu_{C=C}$ (cm^{-1}): 1543.9, 1596.0; ν_{C-O} (cm^{-1}): 1235.1, 1275.6. Yield: 0.45 g, 1.47 mmol, 81.6 %.

4.3.5 Bis(1,2-diethyl-3-hydroxy-4-pyridinonato)copper(II) [Cu((EE(naltol))$_2$]

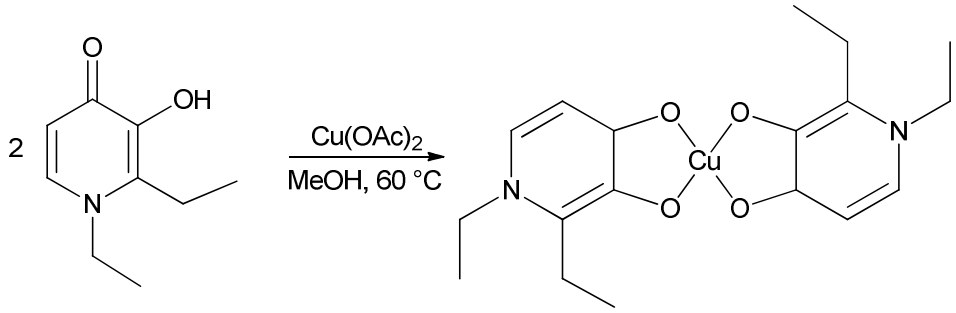

Figure 4.6. The synthesis of bis(1,2-diethyl-3-hydroxy-4-pyridinonato)copper(II).

IR (ATR) $\nu_{C=C}$ (cm^{-1}): 1546.6, 1591.4; ν_{C-O} (cm^{-1}): 1247.1, 1271.2. Yield: 0.5 g, 1.84 mmol, 84.2 %.

4.3.6 Bis(2-ethyl-3-hydroxy-1-isopropyl-4-pyridinonato)copper(II) [Cu((EP(naltol))$_2$]

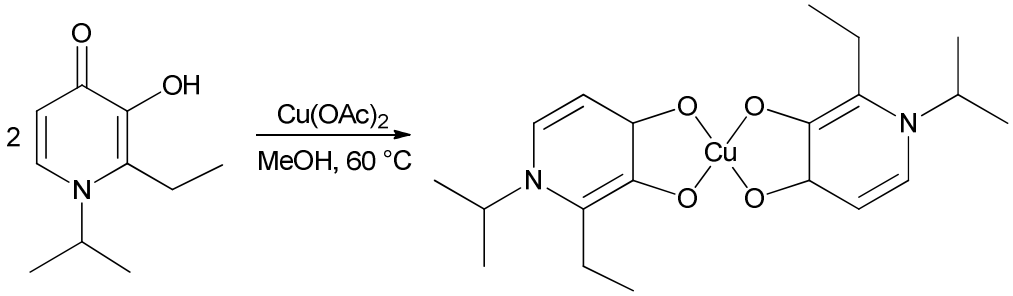

Figure 4.7. The synthesis of bis(2-ethyl-3-hydroxy-1-isopropyl-4-pyridinonato)copper(II).

IR (ATR) $\nu_{C=C}$ (cm^{-1}): 1542.2, 1591.7; ν_{C-O} (cm^{-1}): 1259.0, 1279.4. Yield: 0.58 g, 1.60 mmol, 91.2 %.

4.4 Conclusion

Cu(II) is a paramagnetic metal ion which generally interferes with the signal or chemical shift of copper(II) nuclei. This made it difficult to carry out Cu(II) characterisation using NMR. For the same reason literature characterization of these copper complexes was only by X-ray diffraction and elemental analysis. In this study IR characterization was performed on the six complexes, some crystal structures were also obtained and will be discussed in Chapters 5 and 6.

Furthermore, the NMR spectra of all six ligands obtained in this study agree with those reported in literature.[1,2] A kinetic study of three of these complexes follows in Chapter 7.

[1] G. J. Kontoghiorghes, L. Sheppard, *Inorg. Chim. Acta. 136* (**1987**) L11.
[2] L. Simpson, S. J. Rettig, J. Trotter, C. Orvig, *Can. J. Chem. 69* (**1991**) 893.

5 Crystallographic Characterization of 3-Hydroxy-4-pyridones

5.1 Introduction

In this chapter the solid state characterization of selected 3-hydroxy-4-pyridones is presented. The aim is not only to report the structures but to also give structural insights with regards to the effect of the respective functionalizations which were carried out on Maltol (3-hydroxy-2-methylpyran-4-one) and Ethyl Maltol (2-ethyl-3-hydroxy-pyran-4-one) based analogs. Due to the intrinsic properties of these six membered ring systems they should possess interesting conformations and interactions, while from solid state characterization different structural insights such as packing, orientation, hydrogen bonding, bond lengths and bond distances etc. can be obtained.

Apprehension of these properties, structural data and orientation of these bidentate ligands might assist to explain the subsequent effects observed in the metal complex as these parameters can influence the coordination ability of the ligands and the catalysis of the complexes. This analysis will hopefully provide some fundamental insights on catalyst efficiency and selectivity e.g. the effect of electron donating substituents and or steric bulk on the coordinating ligands etc. This will therefore also help determine the parameters for optimum selectivity and specificity.

5.2 Experimental

In this section the solid state characterization which has been carried out by single crystal X-ray diffraction is described. The reflection data collections and initial unit cell dimensions were determined on a Bruker X8 Apex II 4K Kappa CCD diffractometer equipped with graphite monochromated MoKα radiation (λ = 0.71073 Å) and the ω- and φ-scans collected at T = 100(2)

K.[1] The first 50 frames after completion of the data collection were repeated to analyse for any decay of the crystal and showed no significant decomposition during the data collection. The frame integrations were performed by utilizing the SAINT-Plus and XPREP software packages which also includes data reduction.[2] The data was treated for absorption effects by utilizing the multi-scan technique SADABS and the structure was solved with the ShelXS structure solution program using Direct Methods and refined with the ShelXL using and full-matrix least-squares refinement using Olex-2.[3-5] All non H-atoms were refined anisotropically. Aromatic H atoms were positioned geometrically and allowed to ride on their parent atoms, with U_{iso}(H) = 1.2U_{eq}(parent) of the parent atom with a C—H distance of 0.93 Å. The methyl and methene H atoms were placed in geometrically idealized positions and constrained to ride on its parent atoms with U_{iso}(H) = 1.5U_{eq}(C) and U_{iso}(H) = 1.2U_{eq}(C) and at a distance of 0.96 Å and 0.97 Å respectively. The methine hydrogen atoms were placed in geometrically idealized positions and constrained to ride on its parent atoms with U_{iso}(H) = 1.2 U_{eq}(C) and at a distance of 0.98 Å. Hydroxyl H atoms were placed from the electron density map and refined freely. All molecular graphics (crystal structures) were constructed using the program Diamond3.2i.[6] All structures are shown as thermal ellipsoids drawn at 70 % probability level unless otherwise stated.

[1] Bruker (2005). Apex2 (Version 1.0-27). Bruker AXS Inc., Madison, Wisconsin, USA.
[2] Bruker (2004b). SAINT-Plus. Version 7.12 (including XPREP). Bruker AXS Inc., Madison, Wisconsin, USA.
[3] O. V. Dolomanov, L. J. Bourhis, R. J. Gildea, J. A. K. Howard, H. Puschmann, J. Appl. Cryst. *42* ***(2009)*** 339.
[4] G. M. Sheldrick, *Acta Cryst. A64* ***(2008)*** 112.
[5] A. Altomare, G. Cascarano, C. Giacovazzo, A. Guagliardi, M. C. Burla, G. Polidori, M. Camalli, *J. Appl. Cryst. 27* ***(1994)*** 435.
[6] H. Putz, K. Brandenburg, "Crystal and Molecular Structure Visualization" GbR, Kreuzherrenstr. 102, 53227 Bonn, Germany.

5.3 Results and Discussion

Five crystal structures are presented in this section, these compounds are derived from 3-hydroxy-2-methylpyran-4-one (**3**) and 2-ethyl-3-hydroxy-pyran-4-one (**7**). The naming convention and the respective structures are presented in Fig. 5.1. The part in parenthesis (naltol) indicates that to the cyclic ring of the pyranone moiety, a nitrogen atom has been introduced (the cyclic oxygen has been substituted with a nitrogen atom), therefore the altol designation represents the unchanged form of the pyranone ring. The first letter in the name indicates whether the compound was derived from **3** (M) or **7** (E). The second letter denotes the alkyl group attached to the nitrogen atom M, E and P for methyl, ethyl and *iso*-propyl respectively. The terminal H indicates the hydroxyl proton in the structures (enol form).

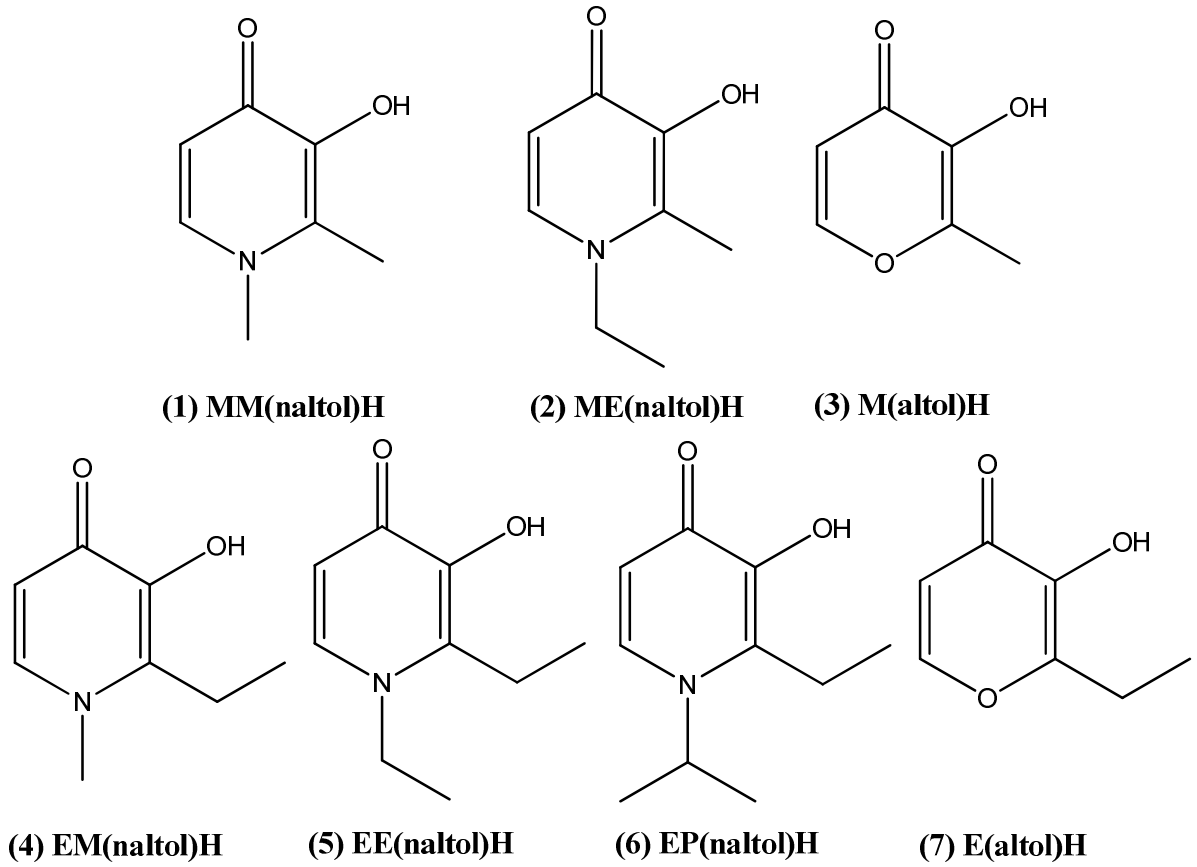

Figure 5.1. Chemdraw representation of the five *O,O'*-bidentate ligand crystal structures and their respective starting materials presented in this chapter and the naming convention used throughout this dissertation for these 3-Hydroxy-4-pyridinones.

Table 5.1. Crystallographic data and refinement parameters for M(altol)H (3) derivatives.

Compound	3-Hydroxy-1,2-dimethyl-4-pyridone {MM(naltol)H} (1)	1-Ethyl-3-hydroxy-2-methyl-4-pyridone {ME(naltol)H} (2)
Empirical formula	$C_7H_9NO_2$	$C_8H_{11}NO_2$
Formula weight	139.15	153.18
Temperature (K)	100 (2)	100 (2)
Crystal system	orthorhombic	orthorhombic
Space group	*Pbca*	*Pbca*
a (Å)	7.1770(3)	11.517(5)
b (Å)	12.9150(6)	11.149(5)
c (Å)	13.6960(6)	12.323(5)
α (°)	90	90
β (°)	90	90
γ (°)	90	90
Volume ($Å^3$)	1269.50(10)	1582.3(12)
Z	8	8
Density calc. ($g.cm^{-3}$)	1.456	1.286
μ (mm^{-1})	0.108	0.093
F(000)	592.0	656.0
Crystal size (mm^3)	0.564 × 0.124 × 0.114	0.362 × 0.31 × 0.148
Radiation (Å)	MoK_α (λ = 0.71073)	MoK_α (λ = 0.71073)
2Θ range for data collection (°)	5.95 to 56.63	6.07 to 56.58
Index ranges	$-9 \le h \le 9$, $-17 \le k \le 15$, $-17 \le l \le 18$	$-15 \le h \le 14$, $-14 \le k \le 13$, $-12 \le l \le 16$
Reflections collected	15982	18661
Independent reflections	1584 [R_{int} = 0.0338, R_{sigma} = 0.0148]	1966 [R_{int} = 0.0327, R_{sigma} = 0.0176]
Completeness to θ (°; %)	28.3 ; 99.9	28.3 ; 99.9
Data/restraints/parameters	1584/0/94	1966/0/103
Goodness-of-fit on F^2	1.083	1.071
Final R indexes [I>=2σ (I)]	R_1 = 0.0429, wR_2 = 0.1184	R_1 = 0.0361, wR_2 = 0.0925
Final R indexes [all data]	R_1 = 0.0467, wR_2 = 0.1215	R_1 = 0.0433, wR_2 = 0.0979
Largest diff. peak/hole ($e.Å^{-3}$)	0.44/-0.23	0.30/-0.22

5.3.1 3-Hydroxy-1,2-dimethyl-4-pyridone {MM(naltol)H (1)}

Colourless cuboidal crystals of the title compound crystallized in the orthorhombic space group *Pbca* with one independent molecule in the asymmetric unit. The numbering scheme of the compound is represented in Fig. 5.2, while atomic coordinates, complete lists of bond distances and angles, anisotropic displacement parameters and hydrogen coordinates are reported in the Supplementary Data (§ A). The most important bond distances and bond angles as well as torsion angles are given in Table 5.2.

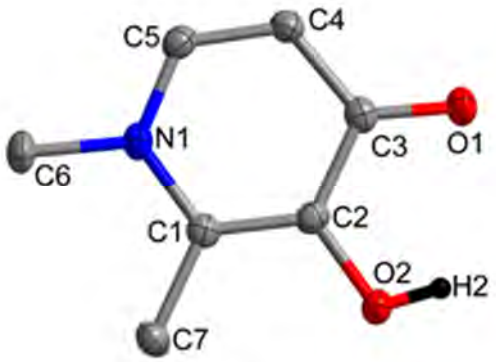

Figure 5.2. Molecular representation of MM(naltol)H (1) showing the atom numbering scheme. Hydrogen atoms are omitted for clarity except for the hydroxyl hydrogen, while displacement ellipsoids are drawn at 70 % probability level.

Table 5.2. Selected bond distances, bond angles and torsion angles for MM(naltol)H (1).

3-Hydroxy-1,2-dimethyl-4-pyridone {MM(naltol)H (1)}		
Bond no.	**Atoms**	**Bond distances (Å)**
(1)	O1-C3	1.272(2)
(2)	O2-C2	1.360(1)
(3)	N1-C6	1.471(2)
(4)	C1-C7	1.497(2)
(5)	C1-C2	1.376(2)
(6)	C4-C5	1.366(2)
(7)	O/N1-C1	1.378(2)
(8)	O/N1-C5	1.350(2)
(9)	C2-C3	1.423(2)
(10)	C3-C4	1.439(2)
Angle no.	**Atoms**	**Bond angles (˚)**
(1)	C2-C3-C4	115.0(1)
(2)	C1-N1/O-C5	120.8(1)
(3)	C2-C1-C7	122.4(1)
(4)	C1-N1-C6	120.1(1)
(5)	O2-C2-C1	118.7(1)
(6)	O1-C3-C4	124.3(1)
(7)	O/N1-C1-C7	118.7(1)
Torsion	**Atoms**	**Torsion angles (˚)**
(1)	O2-C2-C3-O1	0.6(2)
(2)	C6-N1-C1-C7	2.3(2)
(3)	C7-C1-C2-O2	-0.3(2)

Table 5.2 shows that the C=O bond lengths are increased by 0.04(2) Å in this compound when compared to the length of a pure ketone bond (C=O bond length = 1.23(1) Å).[7] The O2—C2 bond length is slightly shorter than a paraffinic C−O bond length by 0.07(1) Å (C−O bond length = 1.43(1) Å).[7] This indicates that there is a minimum delocalization of electrons between the carbonyl and the hydroxyl group and that the proton lies exclusively on O2 as the two bonds are very distinct. The C1—C2 and C4—C5 bond lengths are ≈ 1.37(3) Å and are slightly longer than a simple C=C bond distance (C=C bond distance = 1.337(6) Å).[7] The molecule itself is asymmetric and the bond lengths C1—C2 (1.376(2) Å) and C4—C5 (1.366(2) Å) indicate double bonds in the structure (C=C bond length ≈ 1.34 Å).[7] Furthermore this also indicates that

[7] R. C. Weast, M. J. Astle, "CRC Handbook of Chemistry and Physics", 60th ed. CRC Press: Boca Raton (***1980***).

although there are double bonds in the structure and they are not conjugated and as a result there is a minimum electron delocalization in the structure as delocalized C=C bond lengths are ≈ 1.4 Å. The rest of the bonds indicate single bond character with the cyclic N—C bond lengths being shorter than the acyclic N1—C6 bond length (C−N bond length is = 1.472(5) Å).[7] The two cyclic C—C bond distances (C2—C3 and C3—C4) are shorter than the acyclic C1−C7 bond distance (C—C bond length = 1.541(3) Å); the two cyclic C—C bonds have an average value of 1.431(3) Å whereas the acyclic C1−C7 has a value of 1.471(2) Å (this gives a difference of 0.04(4) Å between the cyclic and the acyclic bonds).[7] All the bond angles are ≈ 120 ˚ indicating the trigonal planar character of the central atom in each of the mentioned bond angles with slight deviations.

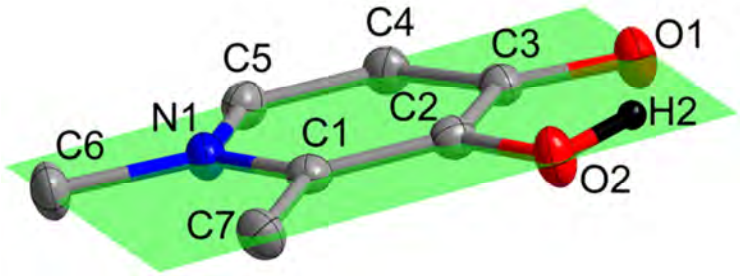

Figure 5.3. Molecular representation of MM(naltol)H (1) showing the atom numbering scheme and the planarity of the molecule. Hydrogen atoms are omitted for clarity except for the hydroxyl hydrogen, while displacement ellipsoids are drawn at 70 % probability level.

Very small torsion angles are observed in the structure which indicate that the structure is planar with almost negligible deviations from the plane, this can be seen from the following torsion angles O2—C2—C3—O1, C6—N1—C1—C7 and C7—C1—C2—O2 which are 0.6(2), 2.3(2) and -0.3(2) ˚ respectively. Furthermore, the H2 proton is clearly observed forming part of the plane as illustrated in Fig. 5.3. The various hydrogen interactions are summarized below in Table 5.3, Fig. 5.4 illustrates the different hydrogen bonds which occur in the structure with the colours green and purple indicating intermolecular hydrogen bonds and orange and turquoise indicating intramolecular hydrogen bonds.

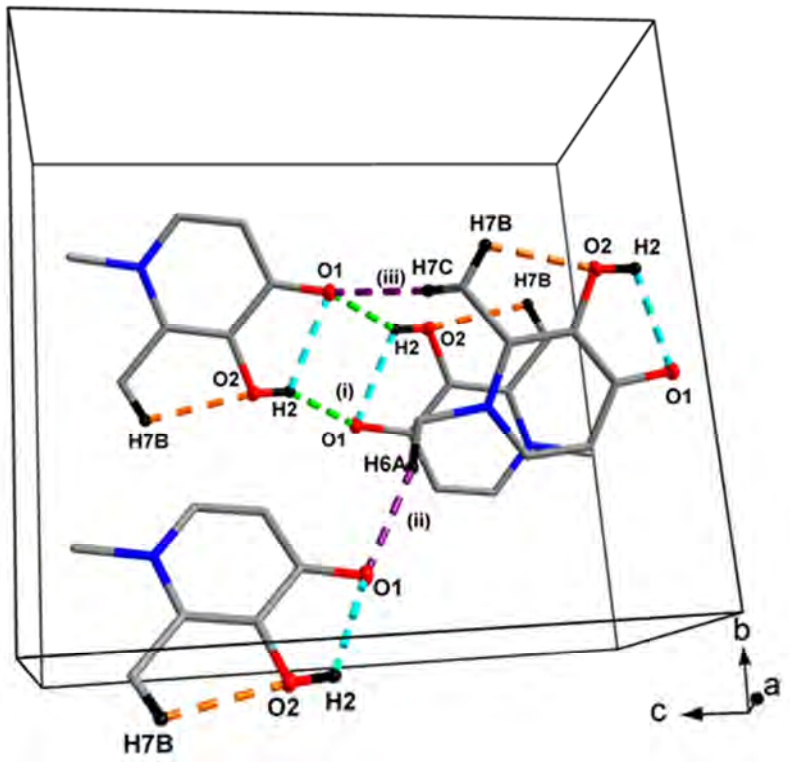

Figure 5.4. Hydrogen bonds observed in MM(naltol)H (1). Hydrogen atoms not taking part in the hydrogen bonds are omitted for clarity. Symmetry transformations used to generate equivalent atoms: 1.5-x, 0.5+y, z; x, 0.5-y, -0.5+z; -0.5+x, 0.5-y, 1-z.

Table 5.3. Summary of the hydrogen bond distances (Å) and angles (˚) observed in MM(naltol)H (1).

D-H…A	d(D-H) (Å)	d(H…A) (Å)	d(D…A) (Å)	ь (D-H…A)(˚)
O2-H2…O1	0.82	2.34	2.746(1)	112
O2-H2…O1$^{(i)}$	0.82	1.93	2.671(1)	151
C6-H6A…O1$^{(ii)}$	0.96	2.52	3.386(2)	150
C7-H7B…O2	0.96	2.39	2.832(2)	108
C7-H7C…O1$^{(iii)}$	0.96	2.51	3.457(2)	168

Symmetry codes, transformations used to generate equivalent atoms: (i) 1–x, 1-y, 1-z; (ii) x,1/2-y,-1/2+z; (iii) 1/2-x,1-y,-1/2+z

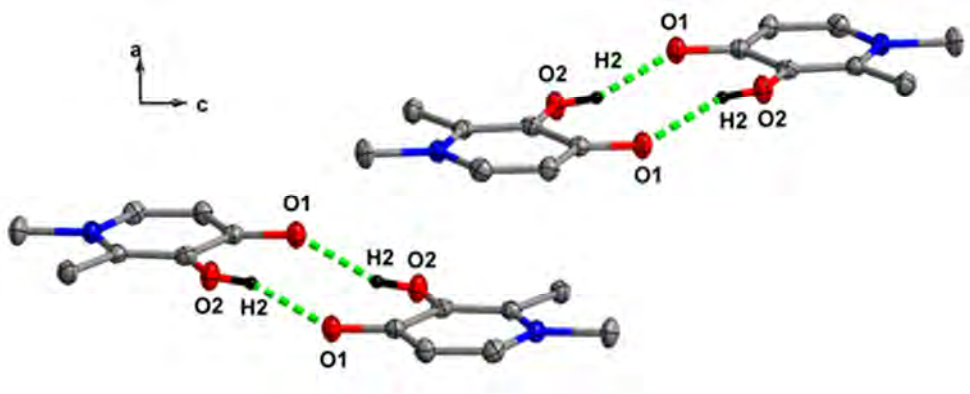

Figure 5.5. Molecular representation of MM(naltol)H (1) showing the dimeric pairs packing along the *ac*-plane. Hydrogen atoms are omitted for clarity except for the hydroxyl hydrogens involved in intermolecular hydrogen bonding, while displacement ellipsoids are drawn at 70 % probability level. Symmetry transformations used to generate equivalent atoms: 1-x, -y, -z; -1+x, y, -1+z; -1.5+x, x, 0.5-z; 0.5-x, -y, -0.5+z.

5.3.2 1-Ethyl-3-hydroxy-2-methyl-4-pyridone {ME(naltol)H (2)}

Colourless cubic crystals of the title compound crystallized in the orthorhombic space group *Pbca* with one independent molecule in the asymmetric unit. The atom labeling of the compound and some important bond distances and bond angles as well as torsion angles are given in Fig. 5.6 and Table 5.4 respectively, while atomic coordinates, all bond distances and angles, anisotropic displacement parameters and hydrogen coordinates are reported in the Supplementary Data (§ B).

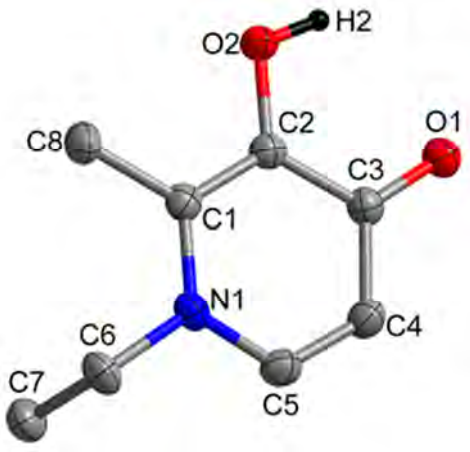

Figure 5.6. Molecular representation of ME(naltol)H (2) showing the atom numbering scheme. Hydrogen atoms are omitted for clarity except for the hydroxyl hydrogen, while displacement ellipsoids are drawn at 70 % probability level.

Table 5.4. Selected bond distances, bond angles and torsion angles for ME(naltol)H (2).

1-Ethyl-3-hydroxy-2-methyl-4-pyridone {ME(naltol)H (2)}		
Bond no.	**Atoms**	**Bond distances (Å)**
(1)	O1-C3	1.267(1)
(2)	O2-C2	1.356(1)
(3)	N1-C6	1.482(1)
(4)	C1-C8	1.499(2)
(5)	C1-C2	1.373(2)
(6)	C4-C5	1.364(2)
(7)	O/N1-C1	1.381(1)
(8)	O/N1-C5	1.355(1)
(9)	C2-C3	1.442(2)
(10)	C3-C4	1.419(2)
Angle no.	**Atoms**	**Bond angles (˚)**
(1)	C2-C3-C4	114.81(9)
(2)	C1-N1/O-C5	120.46(9)
(3)	C2-C1-C8	121.71(9)
(4)	C1-N1-C6	121.91(9)
(5)	O2-C2-C1	118.79(9)
(6)	O1-C3-C4	124.2(1)
(7)	O/N1-C1-C8	119.22(9)
(8)	N1-C6-C7	111.38(9)
Torsion	**Atoms**	**Torsion angles (˚)**
(1)	O2-C2-C3-O1	-0.4(2)
(2)	C6-N1-C1-C8	3.5(1)
(3)	C8-C1-C2-O2	-0.6(2)
(4)	C1-N1-C6-C7	89.8(1)

Table 5.4 shows that the C=O bond lengths are increased by 0.04(1) Å in this compound when compared to the length of a pure ketone bond (C=O bond length = 1.23(1) Å).[7] The O2—C2 bond length is slightly shorter than a paraffinic C−O bond length by 0.07(1) Å (C−O bond length = 1.43(1) Å).[7] This again indicates that there is a minimum delocalization of electrons between the carbonyl and the hydroxyl group and that the proton lies exclusively on O2 as the two bonds are very distinct. The C1—C2 and C4—C5 bond lengths are ≈ 1.37 Å and are slightly longer than a simple C=C bond distance (C=C bond distance = 1.337(6) Å).[7] The molecule itself is asymmetric and the bond lengths C1—C2 (1.373(2) Å) and C4—C5 (1.364(2) Å) indicate double bonds in the structure (C=C bond length ≈ 1.34 Å).[7] Furthermore this also indicates that

although there are double bonds in the structure and they are not conjugated and as a result there is a minimum electron delocalization in the structure as delocalized C=C bond lengths are ≈ 1.4 Å.7 The rest of the bonds indicate single bond character with the cyclic N—C bond lengths being shorter than the acyclic N1—C6 bond length (C−N bond length is = 1.472(5) Å).[7] The two cyclic C—C bond distances (C2—C3 and C3—C4) are shorter than the acyclic C1−C7 bond distance (C—C bond length = 1.541(3) Å), the two cyclic C—C bonds have an average value of 1.431(3) Å whereas the acyclic C1−C8 has a value of 1.499(2) Å (this gives a difference of 0.07(4) Å between the cyclic and the acyclic bonds).[7] All the bond angles are ≈ 120 ˚ indicating the trigonal planar character of the central atom in each of the mentioned bond angles with slight deviations. However C6 in the structure is very close to being tetrahedral as can be seen from the angle N1—C6—C7 which approaches 109.5 ˚ (111.38(9) ˚).

Very small torsion angles are observed in the structure which indicate that the structure is planar with almost negligible deviations from the plane from plane 1; this can be seen from the following torsion angles O2—C2—C3—O1, C6—N1—C1—C7 and C7—C1—C2—O2 which are -0.4(2), 3.5(1) and -0.6(2)˚ respectively. However, there is one large torsion angle C1—N1—C6—C7 which shows that the terminal methyl of the ethyl group is almost at a right angle to the plane of the ring (plane 1), as shown in Fig. 5.7. The dihedral angle (Between planes 1 and 2) is 85.57(4) ˚ and the H2 proton is clearly observed forming part of the plane as illustrated in Fig. 5.7.

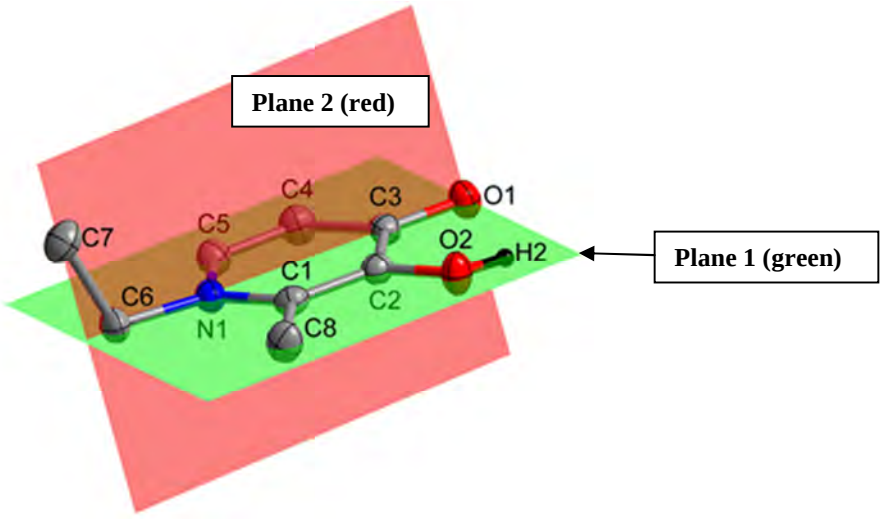

Figure 5.7. Molecular representation of ME(naltol)H (2) showing the atom numbering scheme and the different planes through the molecule. Hydrogen atoms are omitted for clarity except for the hydroxyl hydrogen, while displacement ellipsoids are drawn at 70 % probability level.

The molecules are arranged symmetrically in pairs along the *ac*-plane; these pairs alternate between tail first and head first in a row and also flip upside down between adjacent pairs when viewed along the *b*-axis. These alternating orientations are then packed along the *ac*-plane in rows, where no classic hydrogen bonding interactions were observed in this structure.

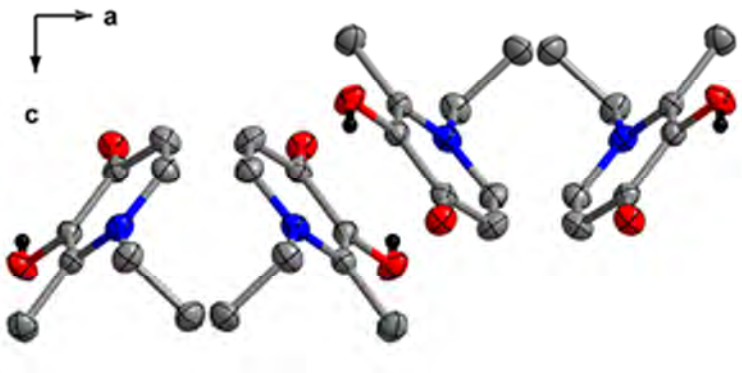

Figure 5.8. Molecular representation of ME(naltol)H (2) showing the packing along the *ac*-plane. Hydrogen atoms are omitted for clarity except hydroxyl hydrogens, while displacement ellipsoids are drawn at 70 % probability level. Symmetry transformations used to generate equivalent atoms: -x, 0.5+y, 0.5-z; -1.5+x, y, 0.5-z; -1.5+x, y, 0.5-z; 0.5-x, 1-y, -0.5-z; -1+x, 0.5-y, -0.5+z.

Table 5.5. Crystallographic data and refinement parameters for E(naltol)H (7) derivatives.

Compound	**2-Ethyl-3-hydroxy-1-methyl-4-pyridone {EM(naltol)H} (4)**	**1,2-Diethyl-3-hydroxy-4-pyridone {EE(naltol)H} (5)**	**2-Ethyl-3-hydroxy-1-isopropyl-4-pyridone {EP(naltol)H} (6)**
Empirical formula	$C_8H_{11}NO_2$	$C_9H_{13}NO_2$	$C_{10}H_{15}NO_2$
Formula weight	153.18	167.20	181.23
Temperature (K)	100 (2)	100 (2)	100 (2)
Crystal system	triclinic	monoclinic	orthorhombic
Space group	$P\bar{1}$	$P2_1/n$	*Pbca*
a (Å)	8.3014(5)	7.0919(2)	11.741(5)
b (Å)	8.4066(6)	9.3468(3)	13.355(5)
c (Å)	11.2927(7)	13.4308(4)	37.552(5)
α (°)	90.507(4)	90	90
β (°)	96.902(3)	93.0080(10)	90
γ (°)	95.241(4)	90	90
Volume (Å^3)	778.94(9)	889.05(5)	5888(3)
Z	4	4	24
Density calc. (g.cm^{-3})	1.306	1.249	1.227
μ (mm^{-1})	0.094	0.088	0.085
F(000)	328.0	360.0	2352.0
Crystal size (mm^3)	0.749 × 0.614 × 0.175	0.353 × 0.113 × 0.051	0.434 × 0.32 × 0.164
Radiation (Å)	MoKα (λ = 0.71073)	MoKα (λ = 0.71073)	MoKα (λ = 0.71073)
2Θ range for data collection (°)	3.634 to 56.714°	5.312 to 56.878°	4.092 to 56.694°
Index ranges	$-11 \le h \le 11$, $-11 \le k \le 11$, $-15 \le l \le 15$	$-9 \le h \le 7$, $-12 \le k \le 12$, $-17 \le l \le 17$	$-15 \le h \le 15$, $-17 \le k \le 14$, $-50 \le l \le 49$
Reflections collected	13499	16214	66795
Independent reflections	3866 [R_{int} = 0.0245, R_{sigma} = 0.0236]	2237 [R_{int} = 0.0199, R_{sigma} = 0.0111]	7343[R(int) = 0.0405]
Completeness to θ (°; %)	28.4 ; 99.3	28.5 ; 99.7	28.4 ; 100
Data/restraints/parameters	3866/0/205	2237/0/112	7343/0/364
Goodness-of-fit on F^2	1.089	1.059	1.021
Final R indexes [I>=2σ (I)]	R_1 = 0.0393, wR_2 = 0.1062	R_1 = 0.0348, wR_2 = 0.0933	R_1 = 0.0417, wR_2 = 0.0974
Final R indexes [all data]	R_1 = 0.0441, wR_2 = 0.1100	R_1 = 0.0394, wR_2 = 0.0979	R_1 = 0.0550, wR_2 = 0.1052
Largest diff. peak/hole (e.Å^{-3})	0.37/-0.27	0.35/-0.19	0.32/-0.28

5.3.3 2-Ethyl-3-hydroxy-1-methyl-4-pyridone {EM(naltol)H (4)}

Colourless plates of crystals of the title compound crystallized in the triclinic space group $P\overline{1}$ with two crystallographically independent molecules in the asymmetric unit. The numbering scheme of the compound is represented in Fig. 5.9, while atomic coordinates, all bond distances and angles, anisotropic displacement parameters and hydrogen coordinates are reported in the Supplementary Data (§ C). The most important bond distances and bond angles as well as torsion angles are given in Table 5.6.

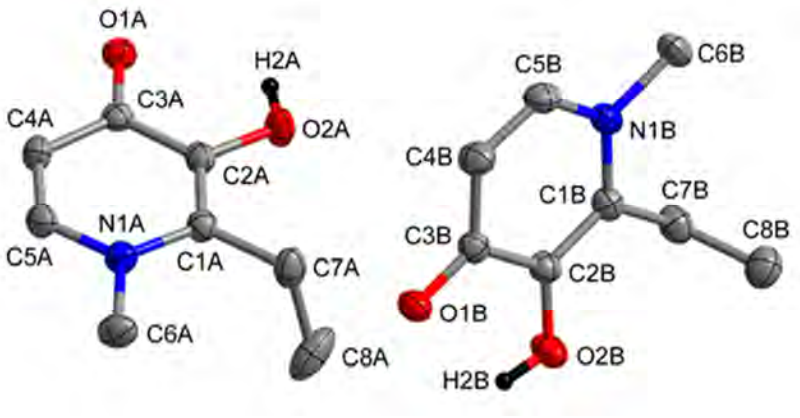

Figure 5.9. Molecular representation of EM(naltol)H (4) showing molecules A and B and the atom numbering scheme. Hydrogen atoms are omitted for clarity except for the hydroxyl hydrogens, while displacement ellipsoids are drawn at 70 % probability level.

Table 5.6. Selected bond distances, bond angles and torsion angles for EM(naltol)H (4).

2-Ethyl-3-hydroxy-1-methyl-4-pyridone			
		Molecule A	**Molecule B**
Bond no.	**Atoms**	**Bond distances (Å)**	
(1)	O1-C3	1.269(1)	1.265(1)
(2)	O2-C2	1.354(1)	1.355(1)
(3)	N1-C6	1.473(1)	1.473(1)
(4)	C1-C7	1.503(2)	1.510(2)
(5)	C1-C2	1.374(1)	1.376(1)
(6)	C4-C5	1.366(2)	1.366(2)
(7)	O/N1-C1	1.377(2)	1.380(1)
(8)	O/N1-C5	1.354(2)	1.355(2)
(9)	C2-C3	1.437(2)	1.442(2)
(10)	C3-C4	1.423(2)	1.419(2)
Angle no.	**Atoms**	**Bond angles (˚)**	
(1)	C2-C3-C4	114.68(9)	114.6(1)
(2)	C1-N1/O-C5	120.47(9)	120.62(9)
(3)	C2-C1-C7	120.8(1)	121.0(1)
(4)	C1-N1-C6	121.76(9)	121.12(9)
(5)	O2-C2-C1	118.09(9)	118.49(9)
(6)	O1-C3-C4	120.8(1)	124.6(1)
(7)	O/N1-C1-C7	120.5(1)	120.2(1)
(8)	O/N1-C6-C7	-	-
(9)	C1-C7-C8	112.4(1)	114.23(9)
Torsion no.	**Atoms**	**Torsion angles (˚)**	
(1)	O2-C2-C3-O1	-0.3(2)	1.8(2)
(2)	C6-N1-C1-C7	0.3(2)	-5.0(2)
(3)	C7-C1-C2-O2	-2.1(2)	4.3(2)
(4)	-	-	-
(5)	O1/N1-C1-C7-C8	82.9(1)	93.0(1)

Table 5.6 shows that the C=O bond lengths are increased by 0.04(1) Å in both molecules A and B when compared to the length of a pure ketone bond (C=O bond length = 1.23(1) Å).[7] The O2—C2 bond length is slightly shorter than a paraffinic C−O bond length by 0.08(1) Å in both molecules A and B (C−O bond length = 1.43(1) Å).[7] This indicates that there is a minimum delocalization of electrons between the carbonyl and the hydroxyl group and that the proton lies exclusively on O2 in both molecules A and B as the two bonds are very distinct. The C1—C2 and C4—C5 bond lengths are ≈ 1.37 Å in both molecules and are slightly longer than a simple

C=C bond distance (C=C bond distance = 1.337(6) Å).[7] The molecules themselves are asymmetric and the bond lengths C1—C2 (1.374(1) and 1.376(1) Å for molecules A and B respectively) and C4—C5 (1.366(2) Å for both molecules A and B) indicate double bonds in both molecules in the structure (C=C bond length ≈ 1.34 Å).[7] Furthermore this also indicates that although there are double bonds in the structure and they are not conjugated and as a result there is a minimum electron delocalization in the structure as delocalized C=C bond lengths are ≈ 1.4 Å.[7] The rest of the bonds indicate single bond character with the cyclic N—C bond lengths being shorter than the acyclic N1—C6 bond length in both molecules (C−N bond length is = 1.472(5) Å).[7] The two cyclic C—C bond distances (C2—C3 and C3—C4) are shorter than the acyclic C1−C7 bond distance (C—C bond length = 1.541(3) Å), the two cyclic C—C bonds (C2—C3 and C3—C4) have an average value of 1.430(3) and 1.431(3) Å for molecules A and B respectively whereas the acyclic C1−C7 bond length is 1.503(2) and 1.510(2) Å for molecules A and B respectively (this gives differences of 0.07(4) and 0.08(4) Å for molecules A and B respectively between the cyclic and the acyclic bonds in the respective independent molecules).[7] All the bond angles are ≈ 120 ˚ indicating the trigonal planar character of the central atom in each of the mentioned bond angles with slight deviations. However C7 in both molecules A and B is tetrahedral and this can be seen from the angle C1—C7—C8 which approaches 109 ˚.

Very small torsion angles are observed in the structures which indicate that the structures are planar with almost negligible deviations from the plane (plane 1), this can be seen from the following torsion angles O2—C2—C3—O1, C6—N1—C1—C7 and C7—C1—C2—O2. However there is one big torsion angle N1—C1—C7—C8 in both molecules which shows that the terminal methyl of the ethyl groups is almost at right angles to the plane of the ring (plane 1) in both molecules, this can be seen in Fig. 5.10 (molecule A is used to illustrate this).

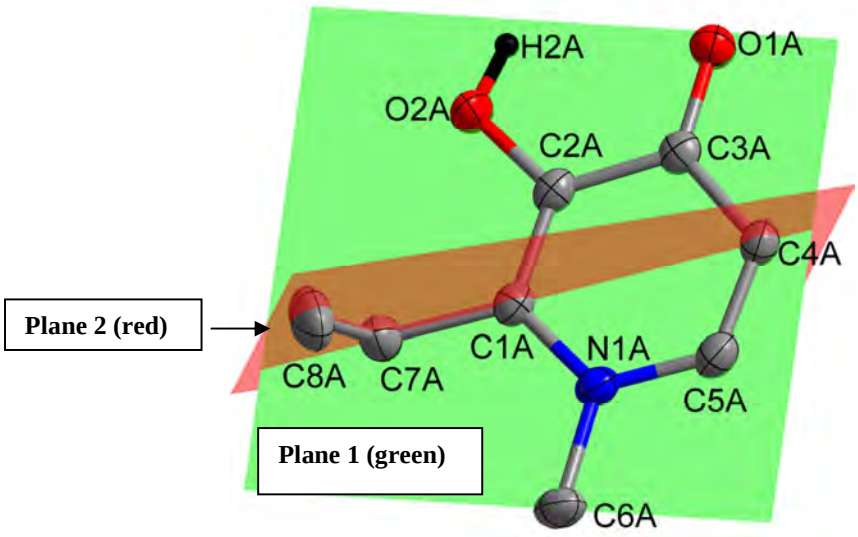

Figure 5.10. Molecular representation of EM(naltol)H (4) showing the atom numbering scheme and the different planes through molecule A, the same set of planes were drawn for molecule B and the resulting dihedral angles are reported below. Hydrogen atoms are omitted for clarity except for the hydroxyl hydrogens, while displacement ellipsoids are drawn at 70 % probability level.

The two molecules (A and B) are planar with the methyl groups (C8) protruding out of plane 1 and forming another plane (plane 2) which runs through C8, C7, C1 and C4. The dihedral angles between these planes are 83.71(6) and 88.52(5) ˚ for molecules A and B, respectively. The difference between the two dihedral angles in the two molecules is 4.81(8) ˚ showing that the respective molecules are distinct.

Figure 5.11. Least squares overlay of all the atoms in the two independent molecules (molecule A in red, molecule B in blue).

The picture above shows molecules A and B in the colours red and blue respectively. The RMS values for an overlay of the complete molecule A and B is 0.0835 Å, which shows that the

molecules are almost identical and the deviations in bond angles are very small and have no essential influence on the geometry of the molecules. The various hydrogen interactions are summarized below in Table 5.7 while Fig. 5.12 illustrates the different hydrogen bonds which occur in the structure with the colours green and purple indicating intermolecular hydrogen bonds and orange and turquoise indicating intramolecular hydrogen bonds.

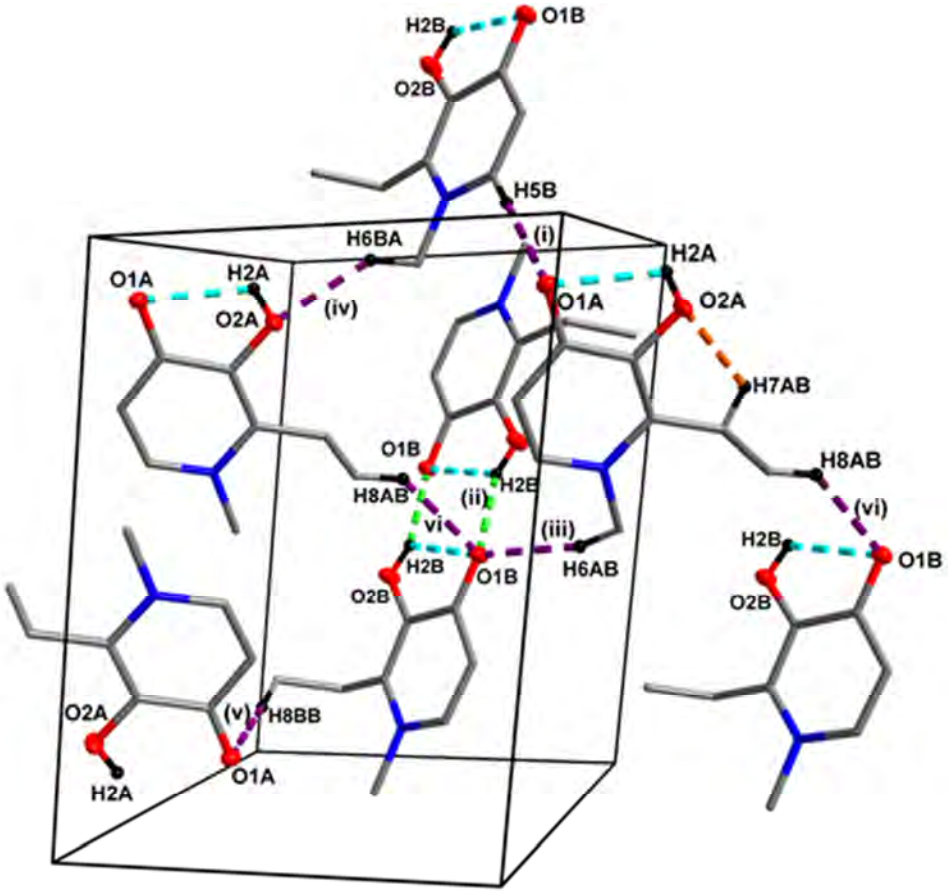

Figure 5.12. Hydrogen bonds observed in EM(naltol)H (4). Hydrogen atoms not taking part in the hydrogen bonds are omitted for clarity. Symmetry transformations used to generate equivalent atoms: 1+x, -1+y, -1+z; -x, 1-y, 1-z; -x, 1-y, 1-z; 1+x, -1+y, z; 1-x, 1-y, 1-z; 2+x, -1+y, z.

Table 5.7. Summary of the hydrogen bond distances (Å) and angles (˚) observed in EM(naltol)H (4).

D-H…A	D-H(Å)	H…A (Å)	D…A (Å)	D-H…A (˚)
O2A-H2A…O1A	0.84	2.29	2.738(1)	113
O2A-H2A…O1A$^{(i)}$	0.84	1.94	2.637(1)	140
O2B-H2B…O1B	0.84	2.31	2.748(1)	113
O2B-H2B…O1B$^{(ii)}$	0.84	1.91	2.651(1)	146
C6A-H6AB…O1B$^{(iii)}$	0.98	2.34	3.290(2)	163
C6B-H6BA…O2A$^{(iv)}$	0.98	2.36	3.194(2)	143
C5B-H5B-O1A$^{(i)}$	0.95	2.29	3.237(1)	173
C7A-H7AB-O2A	0.99	2.39	2.782(1)	103
C8B-H8BB-O1A$^{(v)}$	0.98	2.57	3.513(2)	161
C8B-H8AB-O1B$^{(vi)}$	0.98	2.54	3.336(2)	138

Symmetry codes, transformations used to generate equivalent atoms: (i) -x,1-y,-z; (ii) 1-x,2-y,1-z; (iii) -x,1-y,1-z; (iv) 1-x,1-y,-z; (v) 1+x,y,z; (vi) 1-x,1-y,1-z

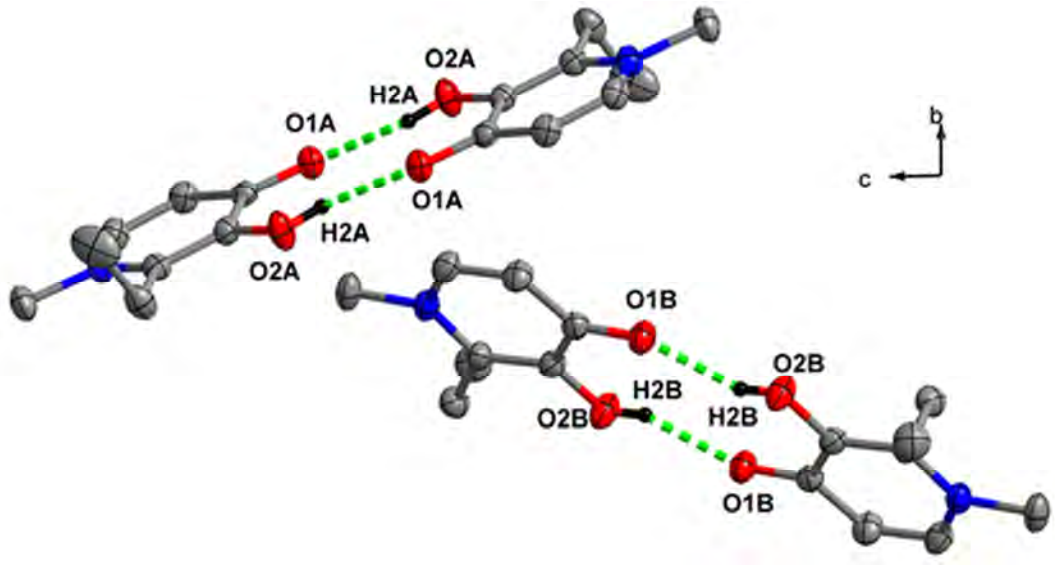

Figure 5.13. Molecular representation of EM(naltol)H (4) showing the packing along the *bc*-plane. Hydrogen atoms are omitted for clarity except for the hydroxyl hydrogens involved in intermolecular hydrogen bonding, while displacement ellipsoids are drawn at 70 % probability level. Symmetry transformations used to generate equivalent atoms: 1-x, 2-y, -z; 1+x, 1+y, -2+z; 2+x, y, -2+z; 1-x, 2-y, -1-z.

The main difference between the two molecules is the structural orientation in the solid-state. When viewed along the *a*-axis the A molecules form dimers with themselves *via* O—H…O hydrogen interactions and so do the B molecules. These dimers are lying at an angle towards each other and form two distinct rows of molecules A and B in the *bc*-plane. The intermolecular

O—H…O interactions seem to be stronger in the A molecules when compared to the B molecules.

5.3.4 1,2-Diethyl-3-hydroxy-4-pyridone {EE(naltol)H (5)}

Colourless cuboidal crystals of the title compound crystallized in the monoclinic space group $P2_1/n$ with one molecule in the asymmetric unit. The numbering scheme of the compound is represented in Fig. 5.14, while atomic coordinates, all bond distances and angles, anisotropic displacement parameters and hydrogen coordinates are reported in the Supplementary Data (§ D). The most important bond distances and bond angles as well as torsion angles are given in Table 5.8.

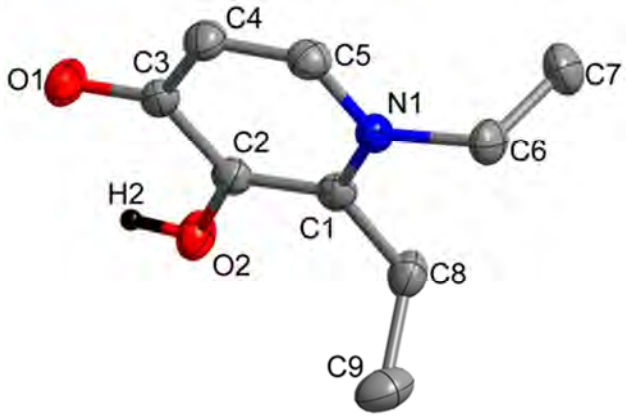

Figure 5.14. Molecular representation of EE(naltol)H (5) showing the atom numbering scheme. Hydrogen atoms are omitted for clarity except for the hydroxyl hydrogen, while displacement ellipsoids are drawn at 70 % probability level.

Table 5.8. Selected bond distances, bond angles and torsion angles for EE(naltol)H (5).

1,2-Diethyl-3-hydroxy-4-pyridone		
Bond no.	**Atoms**	**Bond distances (Å)**
(1)	O1-C3	1.265(1)
(2)	O2-C2	1.355(1)
(3)	N1-C6	1.484(1)
(4)	C1-C8	1.505(1)
(5)	C1-C2	1.375(1)
(6)	C4-C5	1.363(1)
(7)	O/N1-C1	1.379(1)
(8)	O/N1-C5	1.352(1)
(9)	C2-C3	1.438(1)
(10)	C3-C4	1.423(1)
Angle no.	**Atoms**	**Bond angles (˚)**
(1)	C2-C3-C4	114.42(8)
(2)	C1-N1/O-C5	120.09(8)
(3)	C2-C1-C7	119.92(8)
(4)	C1-N1-C6	121.74(7)
(5)	O2-C2-C1	117.89(8)
(6)	O1-C3-C4	124.68(8)
(7)	O/N1-C1-C8	121.74(7)
(8)	N1-C6-C7	111.32(8)
(9)	C1-C8-C9	111.92(8)
Torsion no.	**Atoms**	**Torsion angles (˚)**
(1)	O2-C2-C3-O1	-1.5(1)
(2)	C6-N1-C1-C8	4.9(1)
(3)	C8-C1-C2-O2	-0.9(1)
(4)	C1-N1-C6-C7	-82.9(1)
(5)	O1/N1-C1-C8-C9	98.0(1)

Table 5.8 shows that the C=O bond lengths are increased by 0.04(1) Å in this compound when compared to the length of a pure ketone bond (C=O bond length = 1.23(1) Å).[7] The O2—C2 bond length is slightly shorter than a paraffinic C−O bond length by 0.08(1) Å (C−O bond length = 1.43(1) Å).[7] This indicates that there is a minimum delocalization of electrons between the carbonyl and the hydroxyl group and that the proton lies exclusively on O2 as the two bonds are very distinct. The C1—C2 and C4—C5 bond lengths are ≈ 1.37 Å and are slightly longer than a simple C=C bond distance (C=C bond distance = 1.337(6) Å).[7] The molecule itself is asymmetric and the bond lengths C1—C2 (1.375(1) Å) and C4—C5 (1.363(1) Å) indicate

double bonds in the structure (C=C bond length ≈ 1.34 Å).[7] Furthermore this also indicates that although there are double bonds in the structure and they are not conjugated and as a result there is a minimum electron delocalization in the structure as delocalized C=C bond lengths are ≈ 1.4 Å.[7] The rest of the bonds indicate single bond character with the cyclic N—C bond lengths being shorter than the acyclic N1—C6 bond length (C−N bond length is = 1.472(5) Å).[7] The two cyclic C—C bond distances (C2—C3 and C3—C4) are shorter than the acyclic C1−C8 bond distance (C—C bond length = 1.541(3) Å), the two cyclic C—C bonds (C2—C3 and C3—C4) have an average value of 1.431(3) Å whereas the acyclic C1−C8 has a value of 1.505(1) Å (this gives a difference of 0.074(3) Å between the cyclic and the acyclic bonds).[7] All the bond angles are ≈ 120 ˚ indicating the trigonal planar character of the central atom in each of the mentioned bond angles with slight deviations. However bond angles N1—C6—C7 and C1—C8—C9 in the structure are tetrahedral, this can be seen from the values approaching 109 ˚ (see Table 5.8).

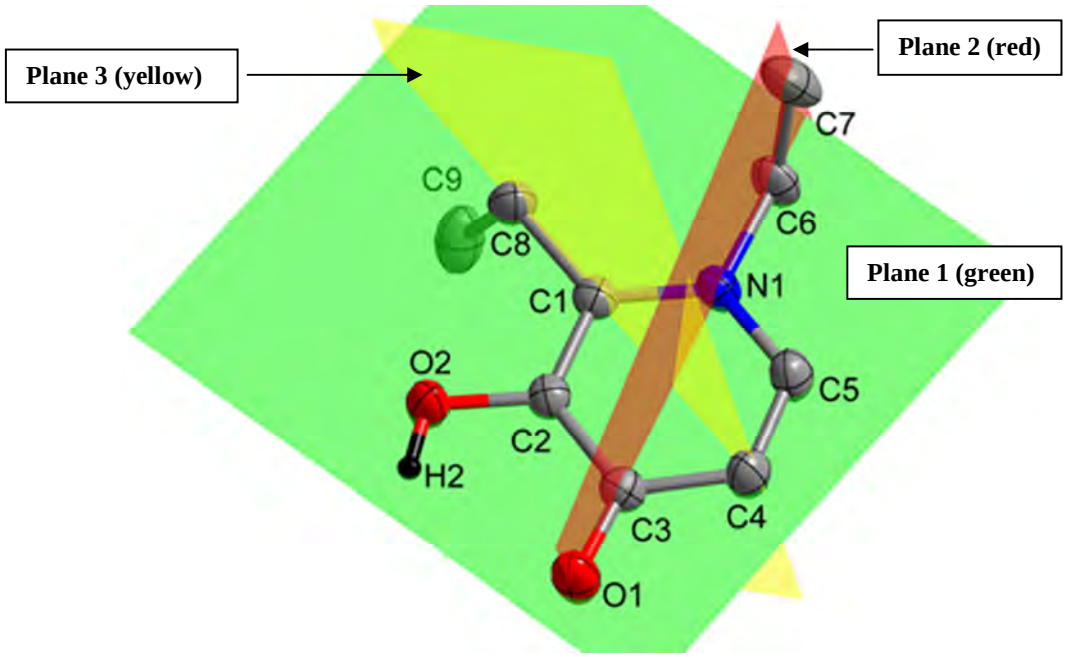

Figure 5.15. Molecular representation of EE(naltol)H (5) showing the atom numbering scheme and the different planes through the molecule. Hydrogen atoms are omitted for clarity except for the hydroxyl hydrogens, while displacement ellipsoids are drawn at 70 % probability level.

The numerical difference between the two torsion angles is 180.9(1) ˚. The dihedral angle between the first two planes (green and red) is 87.77(4) ˚. The second (green and yellow) and third (yellow and red) dihedral angles are 81.01(5) ˚ and 61.54(4) ˚ respectively, showing that C7 is almost at right angles to the plane formed by the cyclic part of the molecule. There are no

classic hydrogen interactions observed in this structure and the H2 proton is clearly observed forming part of the plane as illustrated in Fig. 5.15.

5.3.5 2-Ethyl-3-hydroxy-1-isopropyl-4-pyridone {EP(naltol)H (6)}

Pink cuboidal crystals of the title compound crystallized in the orthorhombic space group *Pbca* with three crystallographically independent molecules in the asymmetric unit. The numbering scheme of the compound is represented in Fig. 5.16, while atomic coordinates, all bond distances and angles, anisotropic displacement parameters and hydrogen coordinates are reported in the Supplementary Data (§ E). The most important bond distances and bond angles as well as torsion angles are given in Table 5.9.

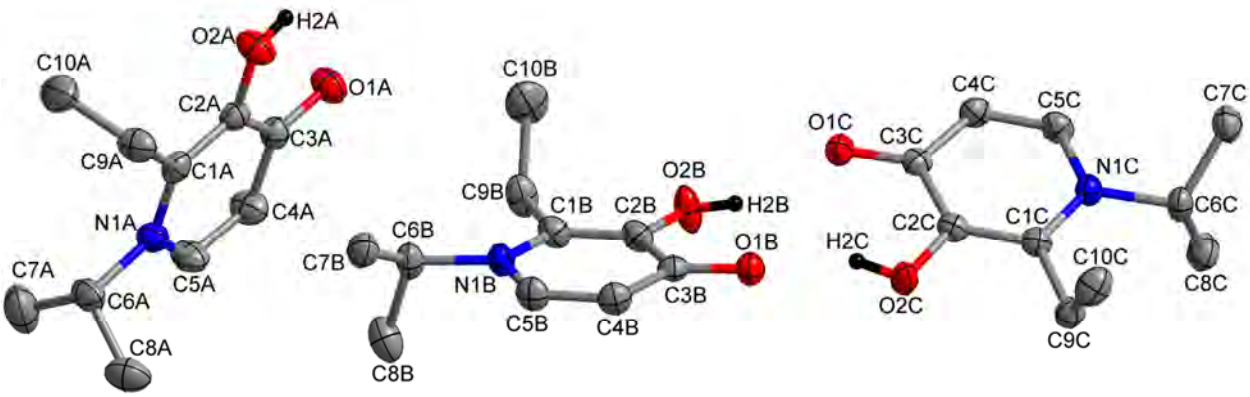

Figure 5.16. Molecular representation of EP(naltol)H (6) showing the three molecules A, B and C and the atom numbering scheme. Hydrogen atoms are omitted for clarity except for the hydroxyl hydrogens, while displacement ellipsoids are drawn at 70 % probability level.

Table 5.9. Selected bond distances, bond angles and torsion angles for EP(naltol)H (6).

2-Ethyl-3-hydroxy-1-isopropyl-4-pyridone				
		Molecule A	**Molecule B**	**Molecule C**
Bond no.	**Atoms**	**Bond distances (Å)**		
(1)	O1-C3	1.261(2)	1.264(2)	1.269(2)
(2)	O2-C2	1.353(2)	1.359(1)	1.354(1)
(3)	N1-C6	1.498(2)	1.496(2)	1.498(2)
(4)	C1-C9	1.500(2)	1.507(2)	1.503(2)
(5)	C1-C2	1.370(2)	1.373(2)	1.377(2)
(6)	C4-C5	1.360(2)	1.358(2)	1.362(2)
(7)	O/N1-C1	1.383(2)	1.385(2)	1.382(2)
(8)	O/N1-C5	1.355(2)	1.352(2)	1.354(2)
(9)	C2-C3	1.438(2)	1.438(2)	1.436(2)
(10)	C3-C4	1.422(2)	1.373(2)	1.420(2)
Angle no.	**Atoms**	**Bond angles (˚)**		
(1)	C2-C3-C4	114.0(1)	114.0(1)	114.3(1)
(2)	C1-N1/O-C5	119.5(1)	119.7(1)	119.7(1)
(3)	C2-C1-C9	119.5(1)	119.5(1)	119.8(1)
(4)	C1-N1-C6	122.5(1)	121.2(1)	121.2(1)
(5)	O2-C2-C1	118.2(1)	118.0(1)	117.5(1)
(6)	O1-C3-C4	124.4(1)	124.1(1)	123.9(1)
(7)	O/N1-C1-C9	120.8(1)	121.5(1)	120.6(1)
(8)	N1-C6-C7	109.8(1)	109.2(1)	109.3(1)
(9)	C1-C9-C10	111.3(1)	112.9(1)	112.0(1)
Torsion no.	**Atoms**	**Torsion angles (˚)**		
(1)	O2-C2-C3-O1	0.4(2)	-2.9(2)	0.4(2)
(2)	C6-N1-C1-C9	-0.6(2)	4.2(2)	2.4(2)
(3)	C9-C1-C2-O2	1.3(2)	-1.8(2)	0.1(2)
(4)	C1-N1-C6-C7	126.7(1)	150.6(1)	138.8(1)
(5)	O1/N1-C1-C9-C10	-87.9(1)	102.9(1)	86.5(1)
(6)	C1-N1-C6-C8	-109.2(1)	85.0(1)	95.6(1)

Table 5.9 shows that the C=O bond lengths are increased by 0.03(1) Å in molecules A and B and by 0.04(1) Å in molecule C when compared to the length of a pure ketone bond (C=O bond length = 1.23(1) Å).[7] The O2—C2 bond lengths in molecules A, B and C are slightly shorter than a paraffinic C−O bond length by 0.08(2), 0.07(1) and 0.08(1) Å respectively (C−O bond length = 1.43(1) Å).[7] This indicates that there is no delocalization of electrons between the carbonyl and the hydroxyl group and that the proton lies exclusively on O2 in all three molecules A, B and C as the two bonds are very distinct. The C1—C2 and C4—C5 bond lengths are ≈ 1.37

and ≈ 1.36 Å respectively in all three molecules and are slightly longer than a simple C=C bond distance (C=C bond distance = 1.337(6) Å).[7] The molecules themselves are asymmetric and the bond lengths C1—C2 (in all three molecules) and C4—C5 (in all three molecules) indicate double bonds in all the respective molecules (C=C bond length ≈ 1.34 Å).[7] Furthermore this also indicates that although there are double bonds in the structure and they are not conjugated and as a result there is no electron delocalization in the structure as delocalized C=C bond lengths are ≈ 1.4 Å.[7] The rest of the bonds indicate single bond character with the cyclic N—C bond lengths being shorter than the acyclic N1—C6 bond length in all molecules (C−N bond length is = 1.472(5) Å).[7] Furthermore the N1—C1 bond lengths are ≈ 1.38 Å whereas the N1—C5 bond lengths are ≈ 1.35 Å. Two cyclic C—C bond distances (C2—C3 and C3—C4) are shorter than the acyclic C1−C9 bond distance (C—C bond length = 1.541(3) Å) this can be seen in Table 5.7.[7] All the bond angles are ≈ 120 ˚ indicating the trigonal planar character of the central atoms in each of the mentioned bond angles with slight deviations. However bond angles N1—C6—C7 and C1—C9—C10 in all three molecules are tetrahedral and this can be seen from the values approaching 109 ˚.

Very small torsion angles (Torsion no. (1), (2) and (3)) are observed in the structures which indicate that the structures are planar with almost negligible deviations from the plane (plane 1), however the is three big torsion angles N1—C1—C6—C7, N1—C1—C9—C10 and N1—C1—C6—C8 in all three molecules which shows that the C8 and C10 methyl groups are protruding in opposite directions when compared to the other two molecules (molecules B and C). The dihedral angles between planes in all the three molecules are reported in Table 5.10 and molecule B is used to illustrate the three planes (Fig. 5.17). Furthermore the H2 proton is clearly observed forming part of the plane as illustrated in Fig. 5.17.

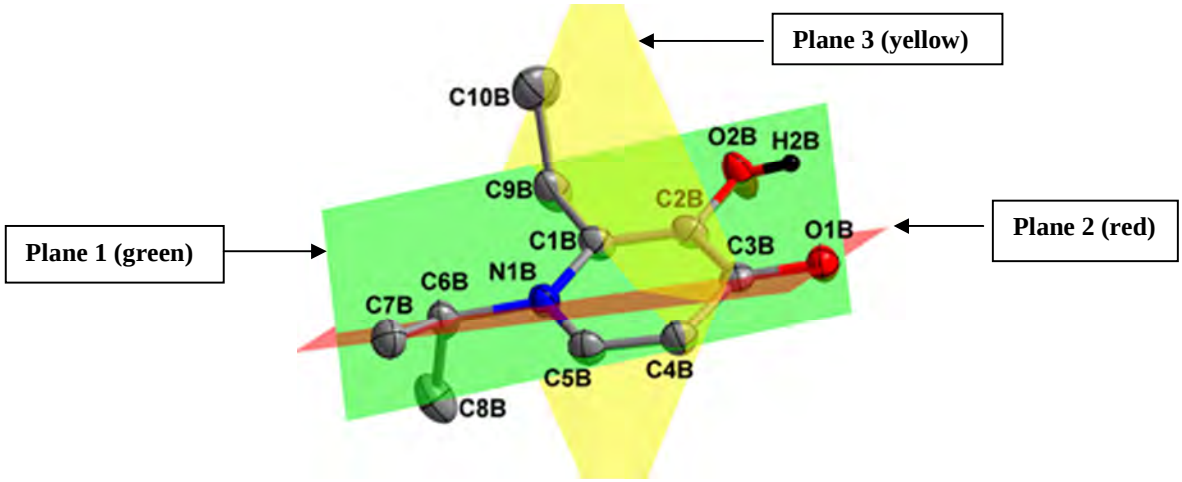

Figure 5.17. Molecular representation of EP(naltol)H (6) showing the atom numbering scheme and the different planes through the molecule B, the same set of planes were constructed for molecules A and C. Hydrogen atoms are omitted for clarity except for the hydroxyl hydrogen, while displacement ellipsoids are drawn at 70 % probability level.

Table 5.10. Dihedral angles between planes for EP(naltol)H (6) (molecule A, B and C).

	Dihedral Angles ˚		
Planes	**Molecule A**	**Molecule B**	**Molecule C**
C4-C5-C1-C2 & C7-C6-N1-O1 (Plane 1& Plane 2)	52.65(7)	30.32(7)	41.66(7)
C4-C5-C1-C2 & C10-C9-C1-O2 (Plane 1 & Plane 3)	89.38(7)	75.54(7)	87.71(6)
C7-C6-N1-O1 & C10-C9-C1-O2 (Plane 2 & Plane 3)	66.65(7)	89.32(7)	69.05(6)

The different dihedral angles vary in size and one dihedral angle varies between the three molecules. However the dihedral angle between the planes C4—C5—C1—C2 & C10—C9—C1—O2 is ≈ 90 ˚ in molecules A and C and the dihedral angle between the planes C7—C6—N1—O1 & C10—C9—C1—O2 in molecule B is also ≈ 90 ˚ indicating that the plane of C7 and the plane of the ring in each of the respective cases is at right angles to the plane of C10.

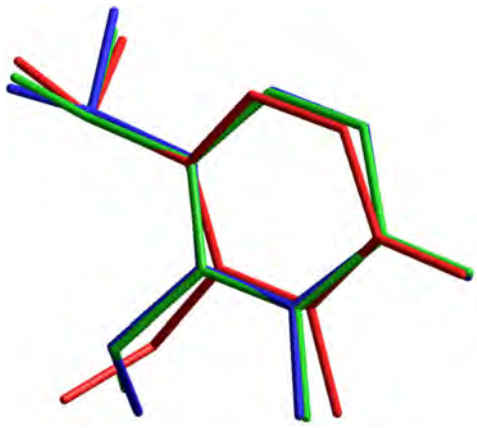

Figure 5.18. Least square overlay of all the atoms in the three independent molecules (molecule A in red, molecule B in blue and molecule C in green).

Figure 5.18 shows molecules A, B and C in the colours red, blue and green respectively. The RMS values for an overlay of the complete molecule A and B is 0.645 Å, for molecules B and C = 0.147 Å and for molecules A and C = 1.167 Å. Molecules B and C have the lowest r.m.s value because the ethyl group turns in the same direction as opposed to the overlay between A and B or A and C.

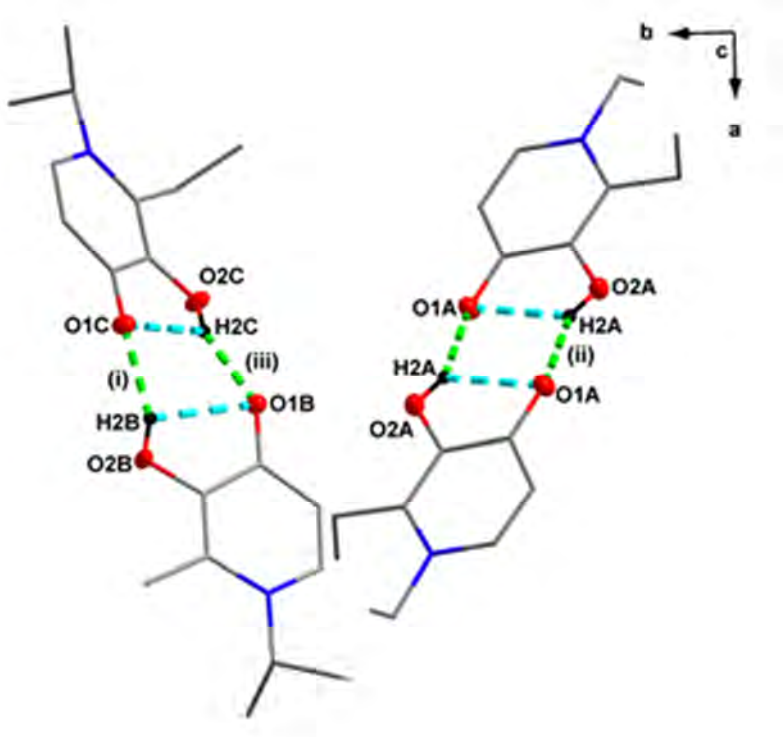

Figure 5.19. Hydrogen bonds observed in EP(naltol)H (6). Hydrogen atoms not taking part in the hydrogen bonds are omitted for clarity. Symmetry transformations used to generate equivalent atoms: 1.5-x, 1-y, 0.5+z; 1.5-x, 1-y, 0.5+z; x, 0.5-y, 0.5+z; 1-x, 0.5+y, 0.5-z.

The main difference between the three molecules is the structural orientation in the solid-state. These three molecules form dimers that are connected through O—H…O hydrogen bonds with $R^2_2(10)$ graph-set motifs. A molecules connect with each other to form inversion dimers, molecules B and C form dimers with local twofold symmetry with each other, but the two molecules are crystallographically distinct. These molecules (B and C) are linked to each other *via* O—H…O hydrogen bonds and this results in the formation of a three-dimensional network structure (see Fig. 5.20).

Table 5.11. Summary of the hydrogen bond distances (Å) and angles (˚) observed in EP(naltol)H (6).

D-H…A	D-H(Å)	H…A (Å)	D…A (Å)	D-H…A (˚)
O2B-H2B…O1B	0.88	2.34	2.7648	110
O2B-H2B…O1C[(i)]	0.88	1.86	2.6506	149
O2A-H2A…O1A	0.87	2.34	2.7580	110
O2A-H2A…O1A[(ii)]	0.87	1.87	2.6484	147
O2C-H2C…O1B[(iii)]	0.86	1.80	2.5871	150
O2C-H2C…O1C	0.86	2.38	2.7820	109

Symmetry codes, transformations used to generate equivalent atoms: (i) 1+x,y,z; (ii) 1-x,1-y,-z; (iii) -1+x,y,z

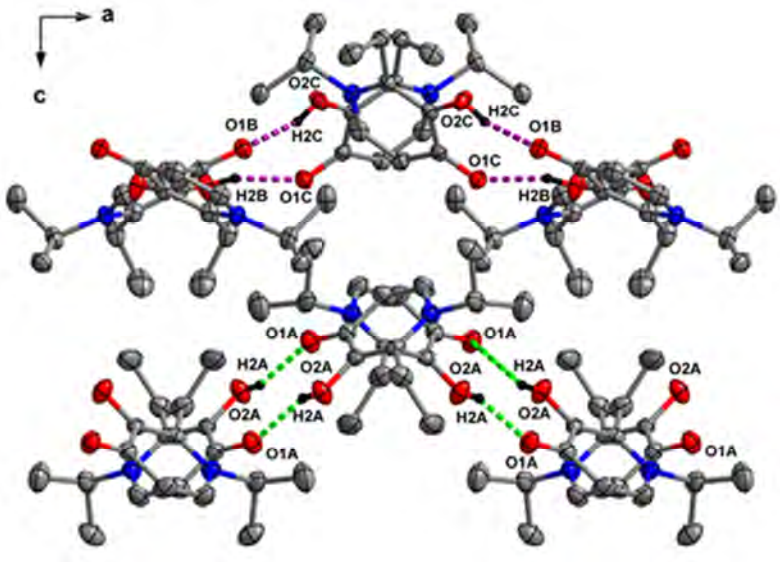

Figure 5.20. Molecular representation of EP(naltol)H (6) showing the packing along the *ac*-plane. Hydrogen atoms are omitted for clarity except for the hydroxyl hydrogens involved in intermolecular hydrogen bonding, while displacement ellipsoids are drawn at 70 % probability level. Symmetry transformations used to generate equivalent atoms: -1.5+x, -1+y, -0.5-z; -x, -0.5+y, -0.5-z; -1.5+x, -1+y, -0.5-z; 1-x, -0.5+y, -0.5-z; -0.5+x, -1+y, -0.5-z; 1-x, -0.5+y, -0.5-z; -1+x, -0.5-y, -0.5+z; -0.5-x, -y, -0.5+z; -0.5+x, -1+y, -0.5-z; -x, -0.5+y, -0.5-z; x, -0.5-y, -0.5+z; 0.5-x, -y, -0.5+z.

When viewed along the b-axis the molecules A, B and C are arranged in symmetrical pairs. One row is exclusively A pairs while the other row is both B and C pairs. These layers alternate along the *ac*-plane and form the packing of the molecules (Fig 5.20).

5.4 Comparative Study

Table 5.12 gives an overarching summary of all the compounds described in this chapter and compares the solid state behavior as observed from the single crystal X-ray studies.

A look at Table 5.12 reveals that the C=O bond lengths are increased by 0.026(4) Å in **1** compared to its parent compound **3**. Similarly in compound **2** the C=O bond is increased by 0.02(3) Å. This seems to indicate that the introduction of a methyl amine to **3** as in compound **1** has a much more significant influence than an introduction of an ethyl amine as in compound **2**, and may be attributed to the fact that a methyl group is more electron donating than an ethyl group. In addition to this the M(altol)H has a longer C=O bond distance compared to E(altol)H. The other bond lengths are similar as well as the bond angles and torsion angles. The E(altol)H (**7**) derivatives also show a similar pattern with C=O bond lengths decreasing in the order **4** > **5** > **6** >**7**. The other bond lengths are also similar in these structures as well as the bond angles and torsion angles.

The relative orientation of the two C-O bond moieties as defined the O2—C2—C3—O1 (torsion no. 1) torsion angle varies little (0 - 2˚) throughout all the structures reported, indicative of a fairly strong intramolecular hydrogen bond between the enol and the keto oxygen atoms.

Table 5.12. Comparison of bond data for all the (naltol)H and (altol)H compounds.

		MM(naltol)H	ME(naltol)H	M(altol)H	EM(naltol)H (4)		EE(naltol)H	EP(naltol)H (6)			E(altol)H
Bond	**Atoms**	**(1)**	**(2)**	**(3)[a]**	**Mol A**	**Mol B**	**(5)**	**Mol A**	**Mol B**	**Mol C**	**(7)[b]**
no.		**Bond distances (Å)**									
(1)	O1-C3	1.272(2)	1.267(1)	1.246(3)	1.269(1)	1.265(1)	1.265(1)	1.261(2)	1.264(2)	1.269(2)	1.235(3)
(2)	O2-C2	1.360(1)	1.356(1)	1.353(2)	1.354(1)	1.355(1)	1.355(1)	1.353(2)	1.359(1)	1.354(1)	1.348(3)
(3)	N1-C6	1.471(2)	1.482(1)	-	1.473(1)	1.473(1)	1.484(1)	1.498(2)	1.496(2)	1.498(2)	-
(4)	C1-C9	1.497(2)	1.499(2)	1.482(4)	1.503(2)	1.510(2)	1.505(1)	1.500(2)	1.507(2)	1.503(2)	1.471(2)
(5)	C1-C2	1.376(2)	1.373(2)	1.358(2)	1.374(1)	1.376(1)	1.375(1)	1.370(2)	1.373(2)	1.377(2)	1.343(3)
(6)	C4-C5	1.366(2)	1.364(2)	1.342(3)	1.366(2)	1.366(2)	1.363(1)	1.360(2)	1.358(2)	1.362(2)	1.319(3)
(7)	O/N1-C1	1.378(2)	1.381(1)	1.365(4)	1.377(2)	1.380(1)	1.379(1)	1.383(2)	1.385(2)	1.382(2)	1.354(3)
(8)	O/N1-C5	1.350(2)	1.355(1)	1.344(4)	1.354(2)	1.355(2)	1.352(1)	1.355(2)	1.352(2)	1.354(2)	1.335(3)
(9)	C2-C3	1.423(2)	1.442(2)	1.445(3)	1.437(2)	1.442(2)	1.438(1)	1.438(2)	1.438(2)	1.436(2)	1.434(2)
(10)	C3-C4	1.439(2)	1.419(2)	1.438(3)	1.423(2)	1.419(2)	1.423(1)	1.422(2)	1.373(2)	1.420(2)	1.428(4)
Angle		**Bond angles (˚)**									
(1)	C2-C3-C4	115.0(1)	114.81(9)	115.1(2)	114.68(9)	114.6(1)	114.42(8)	114.0(1)	114.0(1)	114.3(1)	113.9(2)
(2)	C1-N1/O-C5	120.8(1)	120.46(9)	119.4(2)	120.47(9)	120.62(9)	120.09(8)	119.5(1)	119.7(1)	119.7(1)	119.3(2)
(3)	C2-C1-C9	122.4(1)	121.71(9)	126.3(2)	120.8(1)	121.0(1)	119.92(8)	119.5(1)	119.5(1)	119.8(1)	126.9(2)
(4)	C1-N1-C6	120.1(1)	121.91(9)	-	121.76(9)	121.12(9)	121.74(7)	122.5(1)	121.2(1)	121.2(1)	-
(5)	O2-C2-C1	118.7(1)	118.79(9)	119.6(2)	118.09(9)	118.49(9)	117.89(8)	118.2(1)	118.0(1)	117.5(1)	118.5(2)
(6)	O1-C3-C4	124.3(1)	124.2(1)	124.0(3)	120.8(1)	124.6(1)	124.68(8)	124.4(1)	124.1(1)	123.9(1)	124.7(2)
(7)	O/N1-C1-C9	118.7(1)	119.22(9)	112.8(2)	120.5(1)	120.2(1)	121.18(8)	120.8(1)	121.5(1)	120.6(1)	112.0(2)
(8)	N1-C6-C7	-	111.38(9)	-	-	-	111.32(8)	109.8(1)	109.2(1)	109.3(1)	-
(9)	C1-C9-C10	-	-	-	112.4(1)	114.23(9)	111.92(8)	111.3(1)	112.9(1)	112.0(1)	112.4 (2)
Torsio		**Torsion angles (˚)**									
(1)	O2-C2-C3-O1	0.6(2)	-0.4(2)	-1.27(4)	-0.3(2)	1.8(2)	-1.5(1)	0.4(2)	-2.9(2)	0.4(2)	1.1(3)
(2)	C6-N1-C1-C9	2.3(2)	3.5(1)	-	0.3(2)	-5.0(2)	4.9(1)	-0.6(2)	4.2(2)	2.4(2)	-
(3)	C9-C1-C2-O2	-0.3(2)	-0.6(2)	-1.2(4)	-2.1(2)	4.3(2)	-0.9(1)	1.3(2)	-1.8(2)	0.1(2)	0.7(3)
(4)	C1-N1-C6-C7	-	89.8(1)	-	-	-	-82.9(1)	126.7(1)	150.6(1)	138.8(1)	-
(5)	O1/N1-C1-C9-C10	-	-	-	82.9(1)	93.0(1)	98.0(1)	-87.9(1)	102.9(1)	86.5(1)	-70.4(2)
(6)	C1-N1-C6-C8	-	-	-	-	-	-	109.2(1)	85.0(1)	95.6(1)	-

a) Ref 8
b) Ref 9

[8] J. Burgess, J. Fawcett, D. R. Russell, R. C. Hider, M. B. Hossain, C. R. Stoner, D. Van Der Helm, *Acta. Cryst. C52* ***(1996)*** 2917.
[9] S. D. Brown, J. Burgess, J. Fawcett, S. A. Parsons, D. R. Russell, E. Waltham, *Acta Cryst. C51* ***(1995)*** 1335.

A comparison of all the structures and the respective parent compounds shows many similarities and the only notable differences is that the derivatives have slightly longer C=O lengths compared to the parent compounds in each case. Some bond angles are missing from the parent compounds as those compounds are much more simpler (without N-atom substituents) but for those which are present in the structures they are comparable to these of the (naltol)H derivatives. Similarly some torsion angles are missing in the simpler structures and the first three torsion angles are comparable amongst all the structures with just a few molecules deviating significantly. In the more sterically demanding compounds there were much larger torsion angles and in some cases the methyl groups turn in the opposite direction compared to other structures, see e.g. torsion no. 4, 5 and 6.

5.5 Concluding Remarks

Five of six possible crystal structures were derived from 3-hydroxy-2-methylpyran-4-one (Maltol) and 2-ethyl-3-hydroxy-pyran-4-one (Ethyl Maltol) as starting materials (as reported in chapter 4). Some overarching observations are the following:

- All of them are in the ketone-enol tautomeric form in the solid state, as clearly seen from the basic molecular structures and the character of the O2—C2 and C3—O1 bond lengths.
- In all the cases where a clear packing order was observed, dimers were formed due to weak O—H…O hydrogen interaction (≈ 1.9 Å with bond angles ≈ 150 ˚) which primarily stabilized the structure.
- Most bond angles and bond lengths were comparable to the parent structures but indicated that the carbonyl length was slightly increased; assumed to be due to the functionalization brought about by synthetically manipulating the structure. The relative orientation of the two C-O moieties was only slightly altered as observed from the torsion angle of the parent molecule. Similar ligand geometry is therefore to be expected upon coordination to a metal centre.
- As a full set of the ethyl maltol derivatives was obtained, it indicated that the increase in C=O bond length was in this order: methyl amine (0.034(3) Å) > Ethyl amine (A =

0.031(3) Å and B = 0.031(3) Å) > *iso*-propyl amine (A = 0.027(3) Å, B = 0.030(3) Å and C = 0.034(3) Å). The same pattern is also observed in the derivatives of **3**.

- Finally, the fact that the range of structures varies very little, it is expected that the relative steric impact once coordinated to a metal centre will be very small, and will most probably primarily be electronic. This effect is then further investigated by the solid state structures reported in the next chapter, as well as the solution study which follows later.

6 Crystallographic Characterization of Bis(pyridinonato)copper(II) Complexes

6.1 Introduction

In this chapter the solid state characterization of selected bis(pyridinonato)copper(II) complexes will be presented. These two structures will be compared to similar structures reported in literature. Due to the inherent properties of these complexes which can be attributed to the ligands studied in Chapter 5 it is important to obtain structural insights such as packing, orientation, hydrogen bonding, bond angles and bond distances, etc. as these will influence the catalytic ability of these complexes. A sound knowledge of these properties will predict or even explain the behavior of these complexes in the latter chapters where they will be applied in catalytic oxidation.

6.2 Results and Discussion

Fig. 6.1 shows the structures and the naming convention of the two copper(II) complexes that will be presented in this chapter (**8** and **9**). The structures **10** and **11** are reported in literature and will be compared to **8** and **9**.

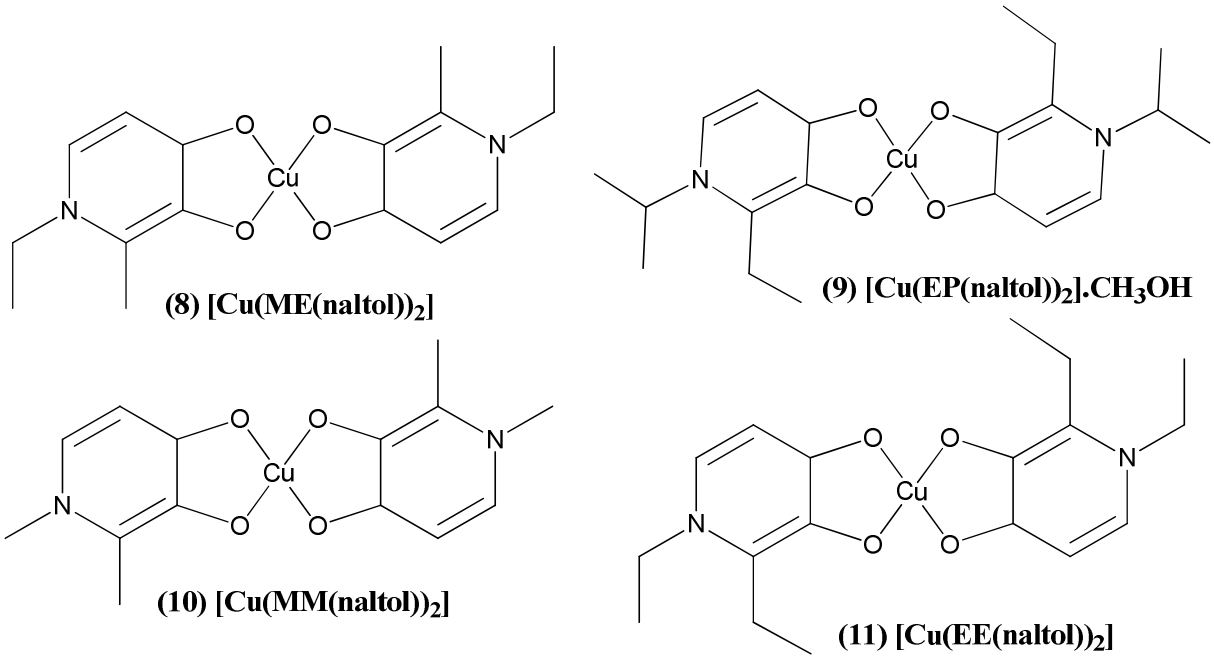

Figure 6.1. Chemdraw representation of the two crystal structures and their designated names that will be used throughout this chapter; for naming of ligands, see Figure 5.1.

Table 6.1. General X-ray crystallographic data and refinement parameters for [Cu(ME(naltol))$_2$] (8) and [Cu(EP(naltol)$_2$] (9).

Compound	[Cu(ME(naltol))$_2$] (8)	[Cu(EP(naltol))$_2$].CH_3OH (9)
Empirical formula	$C_{16}H_{20}N_2O_4Cu$	$C_{22}H_{36}N_2O_6Cu$
Formula weight	367.88	488.07
Temperature (K)	100(2)	100(2)
Crystal system	triclinic	monoclinic
Space group	$P\bar{1}$	$P2_1/c$
a (Å)	7.2250(2)	11.1150(2)
b (Å)	10.1460(2)	7.5560(2)
c (Å)	11.3160(8)	15.0120(2)
α (°)	89.6580(8)	90
β (°)	104.9800(9)	109.749(5)
γ (°)	89.7180(7)	90
Volume (Å^3)	801.30(6)	1186.62(5)
Z	2	2
Density calc. (g.cm^{-3})	1.525	1.366
μ (mm^{-1})	1.384	0.959
F(000)	382.0	518.0
Crystal size (mm^3)	0.264 × 0.156 × 0.061	0.251 × 0.181 × 0.17
Radiation (Å)	MoKα (λ = 0.71073)	MoKα (λ = 0.71073)
2Θ range for data collection (°)	3.726 to 56.862°	3.894 to 56.644°
Index ranges	$-9 \le h \le 8$, $-13 \le k \le 13$, $-15 \le l \le 13$	$-14 \le h \le 14$, $-10 \le k \le 8$, $-20 \le l \le 20$
Reflections collected	9686	19553
Independent reflections	3969 [R_{int} = 0.0234, R_{sigma} = 0.0343]	2938 [R_{int} = 0.0286, R_{sigma} = 0.0189]
Completeness to θ (°; %)	28.431 (98.3)	28.322 (99.6)
Data/restraints/parameters	3969/0/211	2938/0/147
Goodness-of-fit on F^2	1.046	1.038
Final R indexes [I>=2σ (I)]	R_1 = 0.0363, wR_2 = 0.0985	R_1 = 0.0249, wR_2 = 0.0628
Final R indexes [all data]	R_1 = 0.0475, wR_2 = 0.1057	R_1 = 0.0309, wR_2 = 0.0665
Largest diff. peak/hole (e.Å^{-3})	0.64/-0.65	0.45/-0.26

6.2.1 Bis(1-ethyl-3-hydroxy-2-methyl-4-pyridinonato)copper(II) [Cu(ME(naltol))$_2$] (8)

Green plates of the title compound crystallized in the triclinic space group $P\bar{1}$ with two independent molecules in the asymmetric unit. The numbering scheme of the compound is represented in Fig. 6.2, while atomic coordinates, bond distances and angles, anisotropic displacement parameters and hydrogen coordinates are reported in the Supplementary Data (§ F). The most important bond distances and bond angles are given in Table 6.2.

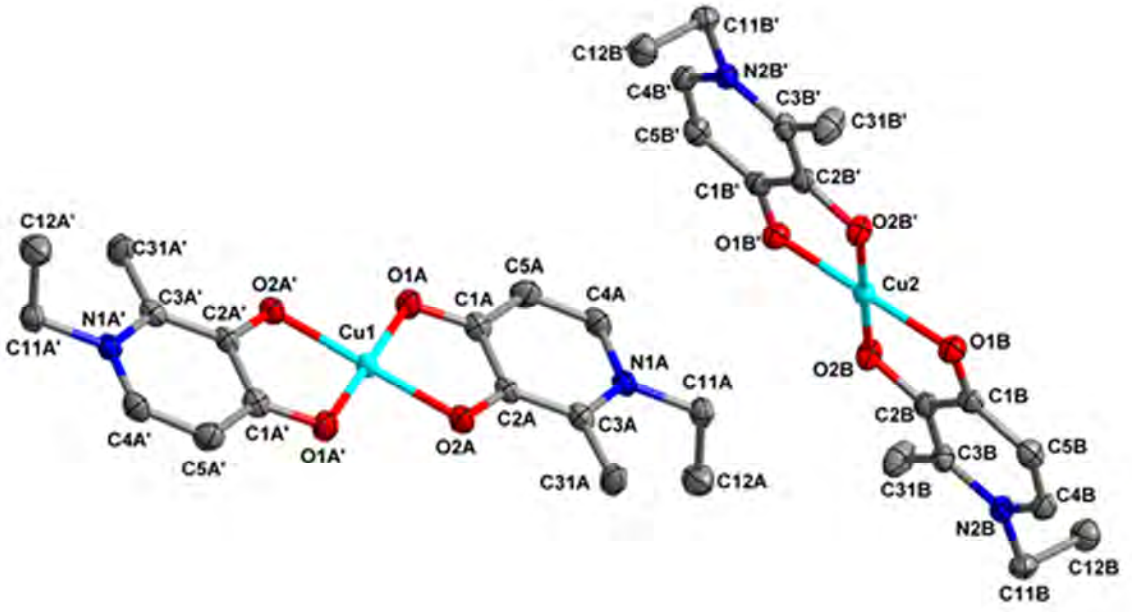

Figure 6.2. Molecular representation of [Cu(ME(naltol))$_2$] (8) showing molecules A and B and the atom numbering scheme, with displacement ellipsoids are drawn at 70 % probability level.

Table 6.2. Selected bond distances and bond angles for [Cu(ME(naltol))$_2$] (8).

		Cu(ME(naltol))$_2$ (8)	
		Molecule A	**Molecule B**
Bond no.	**Atoms**	**Bond distances (Å)**	
(1)	Cu-O1	1.943(2)	1.934(2)
(2)	Cu-O2	1.906(2)	1.908(2)
(3)	O2-C2	1.324(3)	1.328(3)
(4)	O1-C1	1.296(3)	1.303(3)
(5)	C2-C3	1.385(3)	1.385(3)
(6)	C4-C5	1.372(4)	1.363(3)
Angle no.	**Atoms**	**Bond angles (˚)**	
(1)	O2-Cu-O1	86.00(7)	86.69(6)
(2)	Cu-O2-C2	110.2(1)	109.18(1)
(3)	Cu-O1-C1	109.9(1)	109.5(1)
(4)	O2-C2-C3	122.8 (2)	122.4(2)
(5)	O1-C1-C5	125.0(2)	124.8(2)

In both molecules A and B the copper atoms lie on an inversion center, (see Fig. 6.2). The various hydrogen interactions are summarized below in Table 6.3, while Fig. 6.5 illustrates the hydrogen bonding which occurs in the structure with the colour purple indicating intermolecular hydrogen bonds.

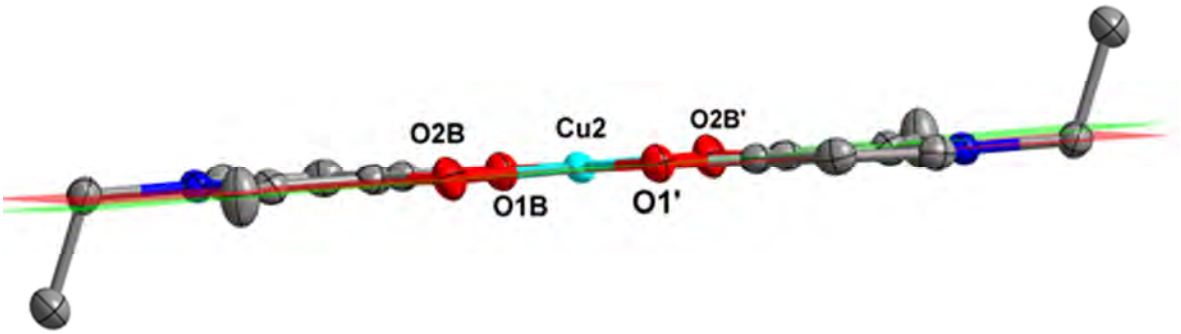

Figure 6.3. Molecular representation of [Cu(ME(naltol))$_2$] (8) showing the atom numbering scheme and the different planes through molecule B, the same set of planes were drawn for molecule A and the resulting dihedral angles are reported below. Hydrogen atoms are omitted for clarity, while displacement ellipsoids are drawn at 70 % probability level.

The two molecules are each virtually planar with a dihedral angle of 2.30(8) ˚ between planes O2−Cu−O1 and C3−C2−C1−C5 in molecule A and 1.20(8) ˚ in molecule B, which is almost a half of the dihedral angle of molecule A. This also indicates how distinct molecule A is from molecule B (refer to Fig. 6.3 for labeling).

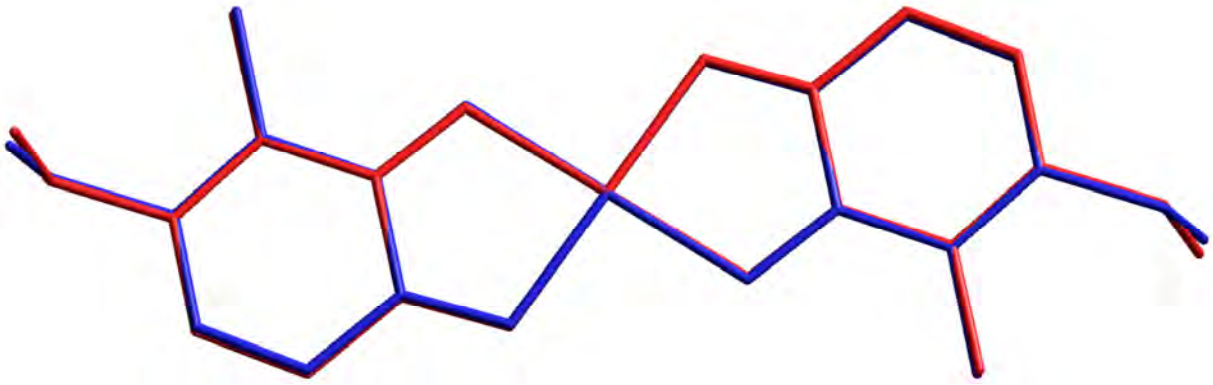

Figure 6.4. Least-squares overlay of all the atoms in the two independent molecules of [Cu(ME(naltol))$_2$] (8) (molecule A in red, molecule B in blue).

The r.m.s values for an overlay of the complete molecule A and B is 0.0743 Å, which shows that the molecules are almost identical and the deviations in bond angles and bond lengths are really very small and have no substantial influence on the geometry of the different molecules.

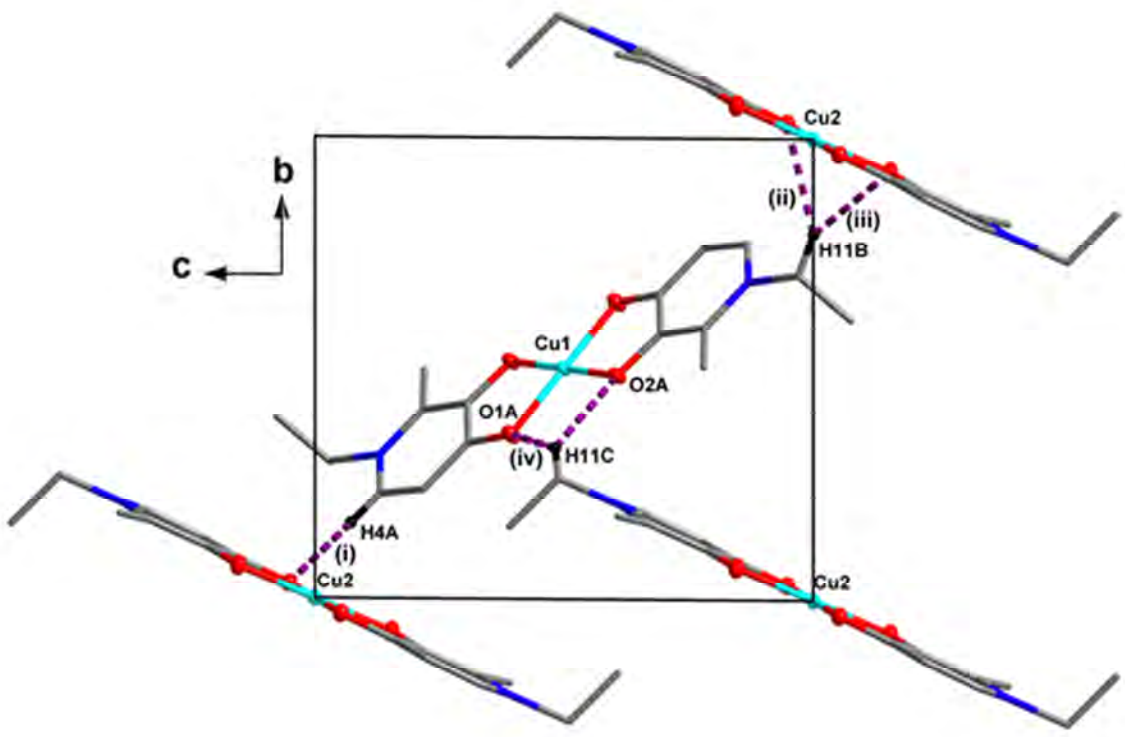

Figure 6.5. Hydrogen bonds observed in [Cu(ME(naltol)$_2$] (8). Hydrogen atoms not taking part in the hydrogen bonds are omitted for clarity. Symmetry transformations used to generate equivalent atoms: x, y, 1+z; -x, 1-y, 1-z; x, 1+y, z.

Table 6.3. Selected bond distances, bond angles and torsion angles for [Cu(ME(naltol)$_2$] (8).

D-H…A	d(D-H) (Å)	d(H…A) (Å)	d(D…A) (Å)	∟ (D-H…A)(°)
C4A-H4A…O1B$^{(i)}$	0.93	2.39	3.201(3)	146
C11A-H11B…O1B$^{(ii)}$	0.97	2.50	3.355(3)	146
C11A-H11B…O2B$^{(iii)}$	0.97	2.54	3.302(3)	136
C11B-H11C…O2A	0.97	2.44	3.250(3)	140
C11B-H11C…O2A$^{(iv)}$	0.97	2.42	3.234(3)	142

Symmetry codes, transformations used to generate equivalent atoms: (i) -x,1-y,-z; (ii) x,1+y,z; (iii) 1-x,1-y,-z; (iv) -x,1-y,1-z

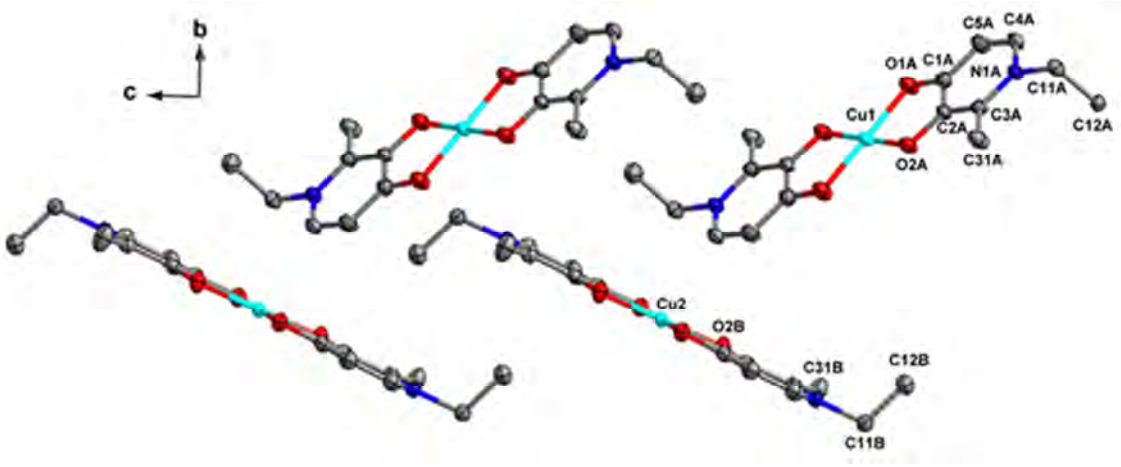

Figure 6.6. Molecular representation of [Cu(ME(naltol))$_2$] (8) showing the A and B molecules packing along the *bc*-plane. Hydrogen atoms are omitted for clarity except for the hydroxyl hydrogens involved in intermolecular hydrogen bonding, while displacement ellipsoids are drawn at 70 % probability level. Symmetry transformations used to generate equivalent atoms: 1-x, 1-y, 1-z; 1-x, 1-y, -z; 2-x, -y, 1-z; 2-x, -y, -z.

Along the *bc*-plane the A and B molecules pack in rows, forming overlapping zigzags of A and B molecules.

6.2.2 Bis(2-ethyl-3-hydroxy-1-isopropyl-4-pyridinonato)copper(II) methanol solvate [Cu(EP(naltol))$_2$].CH$_3$OH (9)

Green cubic crystals of the title compound crystallized in the monoclinic space group $P2_1/c$ with one independent molecule in the asymmetric unit. The numbering scheme of the compound is represented in Fig. 6.7, while atomic coordinates, bond distances and angles, anisotropic displacement parameters and hydrogen coordinates are reported in the Supplementary Data (§ G). The most important bond distances and bond angles are given in Table 6.3.

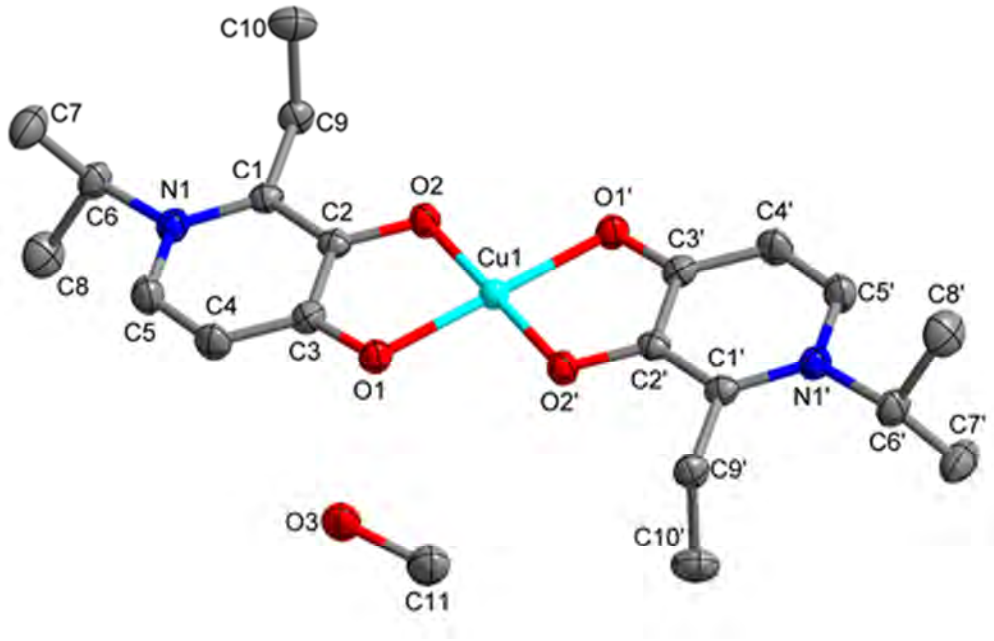

Figure 6.7. Molecular representation of [Cu(EP(naltol))$_2$].CH$_3$OH (9) showing the atom numbering scheme, while displacement ellipsoids are drawn at 70 % probability level.

Table 6.4. Selected bond distances and bond angles for [Cu(EP(naltol))$_2$].CH$_3$OH (9).

		[Cu(EP(naltol))$_2$].CH$_3$OH (9)
Bond no.	**Atoms**	**Bond distances (Å)**
(1)	Cu-O1	1.930 (1)
(2)	Cu-O2	1.9094 (10)
(3)	O2-C2	1.3244 (18)
(4)	O1-C3	1.3050 (18)
(5)	C1-C2	1.3921 (20)
(6)	C4-C5	1.3733 (22)
Angle no.	**Atoms**	**Bond angles (˚)**
(1)	O2-Cu-O1	86.369 (42)
(2)	Cu-O2-C2	109.526 (82)
(3)	O2-C2-C1	122.498 (123)
(4)	Cu-O1-C3	109.569 (88)
(5)	O1-C3-C5	124.571 (128)

This molecule has a copper atom lying on an inversion center, (see Fig. 6.7). The various hydrogen interactions are illustrated below in Table 6.5, while Fig. 6.9 shows the different hydrogen bonds which occur in the structure with the colours green, turquoise and purple indicating intermolecular hydrogen bonds and orange indicating intramolecular hydrogen bonds.

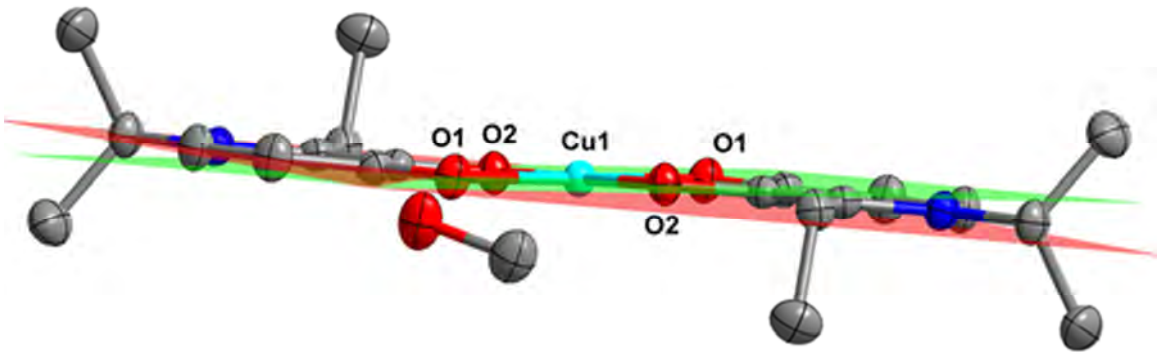

Figure 6.8. Molecular representation of [Cu(EP(naltol))$_2$].CH$_3$OH (9) showing the different planes through the molecule Hydrogen atoms are omitted for clarity except for the hydroxyl hydrogens, while displacement ellipsoids are drawn at 70 % probability level.

This molecule is also planar with a dihedral angle of 4.10(6) ˚ between planes O2-Cu-O1 and C1-C2-C3-C4 in the molecule. This molecule is however more bent than **8** (see Fig. 6.6 for numbering).

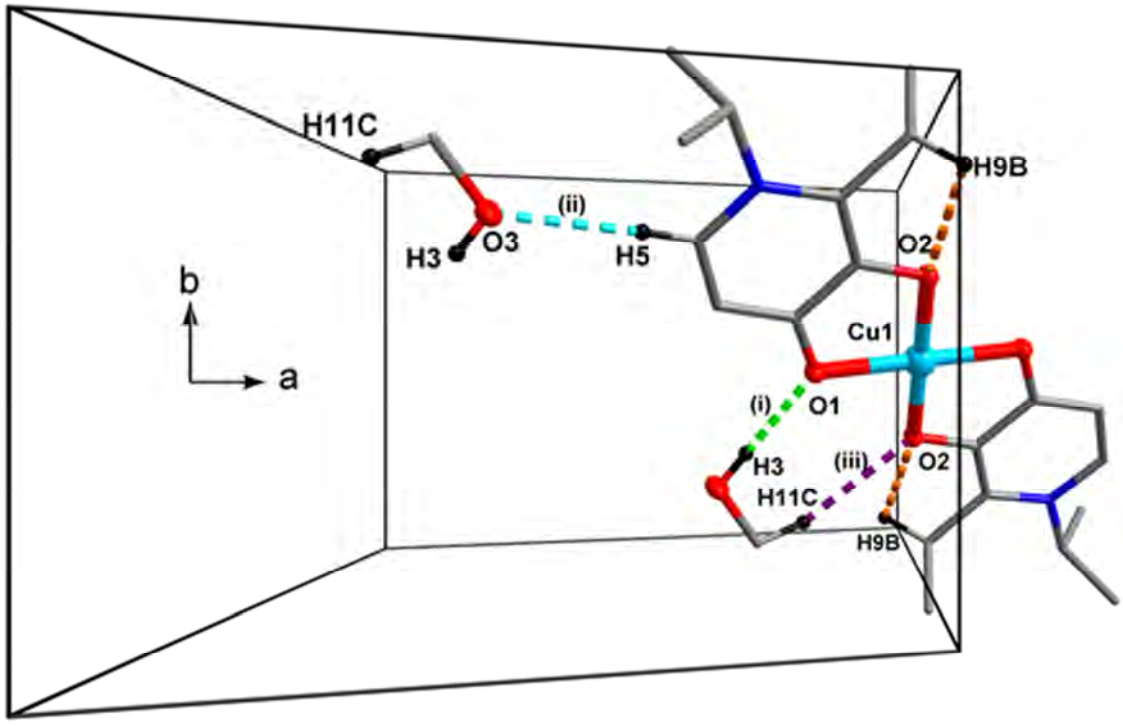

Figure 6.9. Hydrogen bonds observed in [Cu(EP(naltol))$_2$].CH$_3$OH (9), also that to the methanol solvate. Hydrogen atoms not taking part in the hydrogen bonds are omitted for clarity. Symmetry transformations used to generate equivalent atoms: 1-x, 0.5+y, 0.5-z.

Table 6.5. Hydrogen bonds observed in [Cu(EP(naltol))$_2$].CH$_3$OH (9). Hydrogen atoms not taking part in the hydrogen bonds are omitted for clarity.

D-H…A	d(D-H) (Å)	d(H…A)(Å)	d(D…A) (Å)	D-H…A (˚)
O3-H3…O1$^{(i)}$	0.84	2.29	2.7379(11)	113
C5-H5…O3$^{(ii)}$	0.98	2.34	3.2903(15)	163
C9-H9…O2	0.98	2.36	3.1943(15)	143
C11-H11C-O2$^{(iii)}$	0.95	2.29	3.2372(13)	173

Symmetry codes, transformations used to generate equivalent atoms: (i) x,3/2-y,-1/2+z; (ii) 1-x,-1/2+y,1/2-z; (iii) -x,1/2+y,1/2-z

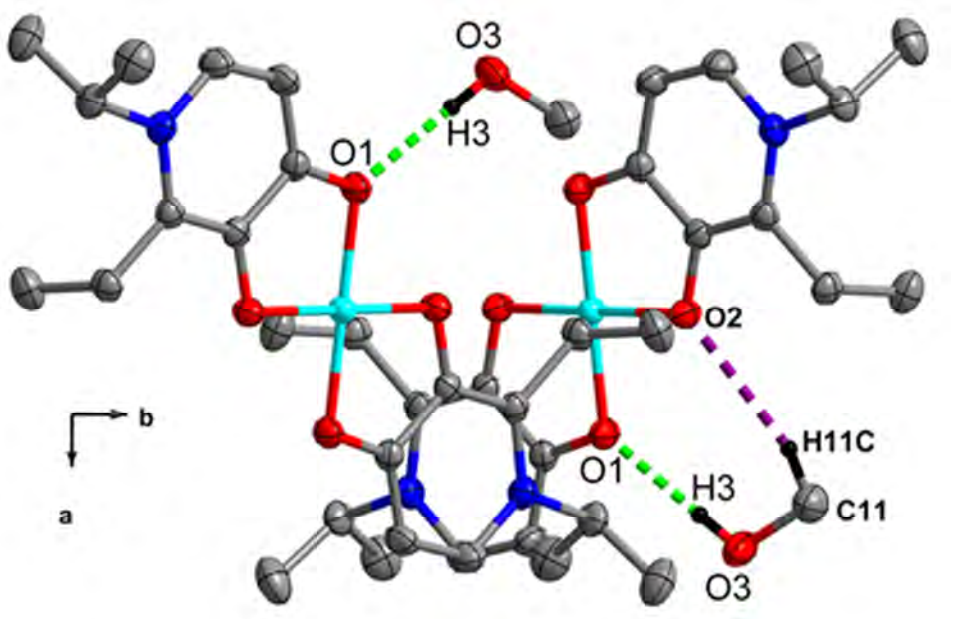

Figure 6.10. Molecular and hydrogen bonding in [Cu(EP(naltol))$_2$].CH$_3$OH (9) showing the molecules packing along the *ab*-plane. Hydrogen atoms are omitted for clarity except for the hydroxyl hydrogens involved in intermolecular hydrogen bonding, also that to the methanol solvate, while displacement ellipsoids are drawn at 70 % probability level. Symmetry transformations used to generate equivalent atoms: x, -1+y, z; x, -0.5-y, -0.5+z.

This structure is packed in a zigzag pattern along the *ab*-plane when viewed along the *c*-axis. This pattern is stabilized by the solvent molecules by forming intermolecular hydrogen bonds with the compound (see Fig. 6.9 and Table 6.4).

6.3 Comparative study

The known structures of these type of complexes are compared in Table 6.6, which indicates that although **8** and **10** are different (at opposite ends one has an ethyl group whereas the other a methyl group) they are very similar as almost all their bond angles and bond distances are almost identical. This suggests that even their spatial arrangements, apart from the periphery of the coordination shere, are identical. Both molecules are planar and the O2-Cu-O1 bond angle is ≈ 86 ˚, which shows that the square planar geometry is slightly distorted in both cases. Furthermore, the Cu-atoms act as inversion centers in both molecules. Compound **8** is being compared to **10** because they are both M(naltol)H derivatives, the only difference is the substituent on the nitrogen atom (**8** has a methyl whereas **10** has an ethyl group).

Table 6.6. Comparison of bond data for compounds 8, 9, 10, 11.

		[Cu(ME(naltol))$_2$] (8)		[Cu(MM(naltol))$_2$] (10) [a]	[Cu(EP(naltol))$_2$] (9)	[Cu(EE(naltol))$_2$] (11) [b]
		Molecule A	Molecule B			
Bond no.	**Atoms**	**Bond distances (Å)**				
(1)	Cu-O1	1.943(2)	1.934(2)	1.928(3)	1.930 (1)	1.923(4)
(2)	Cu-O2	1.906(2)	1.908(2)	1.913(3)	1.909(1)	1.913(3)
(3)	O2-C2	1.324(3)	1.328(3)	1.344(5)	1.324(2)	1.313(5)
(4)	O1-C3	1.296(3)	1.303(3)	1.300(5)	1.305(2)	1.310(5)
(5)	C1-C2	1.385(3)	1.385(3)	1.391(6)	1.392(2)	1.3916)
(6)	C4-C5	1.372(4)	1.363(3)	1.361(6)	1.373(2)	1.356(8)
Angle no.		**Bond angles (˚)**				
(1)	O2-Cu-O1	86.00(7)	86.69(6)	86.1(1)	86.37(4)	86.0(1)
(2)	Cu-O2-C2	110.2(1)	109.18(1)	108.5(2)	109.53(8)	109.9(2)
(3)	O2-C2-C1	109.9(1)	109.5(1)	110.3(3)	109.57(9)	110.4(3)
(4)	Cu-O1-C3	122.8 (2)	122.4(2)	120.9 (4)	122.5(1)	123.5(4)
(5)	O1-C3-C5	125.0(2)	124.8(2)	124.5(4)	124.6(1)	125.7(4)

a,=Ref 1. *b*=Ref 1

The two E(naltol)H derivatives, although slightly different (at opposite ends, one has an ethyl group whereas the other an *iso*-propyl group) display almost identical bond angles and bond lengths. Moreover, the bond lengths Cu-O1 and Cu-O2 are almost the same in both structures showing that the O1'-O2'-O1-O2 is almost a square. Both molecules are planar and the O2-Cu-O1 bond angle is ≈ 86 ˚, similar to **8**. Similarly this also shows that the square planar geometry is

[1] A. El-Jammal, P. L. Howell, M. A. Turner, N. Li, D. M. Templeton, *J. Med. Chem 37* (***1994***) 461.

slightly distorted and the Cu-atoms act as inversion centers in the molecule with the two ethyl groups protruding in opposite directions in the case of **11**.

A comparison of **2** and **8** shows that bond no. 1 has increased in **8** and bond no. 2 has decreased in **8**. The bond angles on the other hand remain roughly the same with slight deviation. The torsion angles are also similar with just torsion no. 2 showing a significant difference between the two compounds.

A comparison of **6** and **9** shows the same changes in structure, with bond no. 1 increase in **9** and bond no. 2 decreasing in **9**. The rest of the selected bond lengths and angles are similar with slight deviations. The torsion angles show that there is a significant change in the coordination site (torsion no. 1) with **9** having a smaller angle compared to **6**. Most of the torsion angles differ significantly with the greatest differences in torsion no. 5 and 6. This is due to molecule A in **6** which has the terminal methyl of the ethyl group turning in the opposite direction when compared to molecules B and C. Based on this data one can clearly see that only the orientation of molecule A is maintained when coordinated to the copper (II) center to form **9**.

Similarly, a comparison of **8** and **9** shows that the bond lengths are very similar and show the same patterns with regard to the changes when compared to the respective ligands (2 and 6). The bond lengths and angles are also similar between the two compounds and only the torsion angles differ by significant amounts.

Table 6.7. Comparison of bond data for the free ligand (naltol)H compounds (2 and 6) and the corresponding [Cu(naltol)$_2$] compounds (8 and 9).

		ME(naltol)H (2) [a]	[Cu(ME(naltol))$_2$] (8)		EP(naltol)H (6) [a]			[Cu(EP(naltol))$_2$].CH_3OH (9)
			Molecule A	Molecule B	Molecule A	Molecule B	Molecule C	
Bond no.	**Atoms**	**Bond distances (Å)**						
(1)	O1-C3	1.267(1)	1.296(3)	1.303(3)	1.261(2)	1.264(2)	1.269(2)	1.305(2)
(2)	O2-C2	1.356(1)	1.324(3)	1.328(3)	1.353(2)	1.359(1)	1.354(1)	1.324(2)
(3)	N1-C6	1.482(1)	1.478(4)	1.485(3)	1.498(2)	1.496(2)	1.498(2)	1.501(2)
(4)	C1-C9	1.499(2)	1.496(4)	1.492(3)	1.500(2)	1.507(2)	1.503(2)	1.505(2)
(5)	C1-C2	1.373(2)	1.385(4)	1.385(3)	1.370(2)	1.373(2)	1.377(2)	1.392(2)
(6)	C4-C5	1.364(2)	1.372(4)	1.363(3)	1.360(2)	1.358(2)	1.362(2)	1.373(2)
(7)	O/N1-C1	1.381(1)	1.379(3)	1.372(3)	1.383(2)	1.385(2)	1.382(2)	1.379(2)
(8)	O/N1-C5	1.355(1)	1.352(3)	1.350(3)	1.355(2)	1.352(2)	1.354(2)	1.353(2)
(9)	C2-C3	1.442(2)	1.437(3)	1.431(3)	1.438(2)	1.438(2)	1.436(2)	1.426(2)
(10)	C3-C4	1.419(2)	1.402(3)	1.401(3)	1.422(2)	1.373(2)	1.420(2)	1.392(2)
Angle no.		**Bond angles (˚)**						
(1)	C2-C3-C4	114.81(9)	117.8(2)	118.0(2)	114.0(1)	114.0(1)	114.3(1)	118.2(1)
(2)	C1-N1/O-C5	120.46(9)	121.4(2)	121.3(2)	119.5(1)	119.7(1)	119.7(1)	120.9(1)
(3)	C2-C1-C9	121.71(9)	120.6(2)	120.4(2)	119.5(1)	119.5(1)	119.8(1)	118.4(1)
(4)	C1-N1-C6	121.91(9)	121.1(2)	121.2(2)	122.5(1)	121.2(1)	121.2(1)	122.5(1)
(5)	O2-C2-C1	118.79(9)	122.8(2)	122.4(2)	118.2(1)	118.0(1)	117.5(1)	122.5(1)
(6)	O1-C3-C4	124.2(1)	125.0(2)	124.8(2)	124.4(1)	124.1(1)	123.9(1)	124.6(1)
(7)	O/N1-C1-C9	119.22(9)	120.5(2)	120.7(2)	120.8(1)	121.5(1)	120.6(1)	122.6(1)
(8)	N1-C6-C7	111.38(9)	112.4(2)	110.7(2)	109.8(1)	109.2(1)	109.3(1)	110.0(1)
(9)	C1-C9-C10	-	-	-	111.3(1)	112.9(1)	112.0(1)	111.3(1)
Torsion		**Torsion angles (˚)**						
(1)	O2-C2-C3-O1	-0.4(2)	-0.4(3)	0.7(3)	0.4(2)	-2.9(2)	0.4(2)	0.0(2)
(2)	C6-N1-C1-C9	3.5(1)	5.9(3)	0.1(3)	-0.6(2)	4.2(2)	2.4(2)	-3.6(2)
(3)	C9-C1-C2-O2	-0.6(2)	-1.9(3)	1.1(3)	1.3(2)	-1.8(2)	0.1(2)	3.0(2)
(4)	C1-N1-C6-C7	89.8(1)	82.5(3)	91.4(2)	126.7(1)	150.6(1)	138.8(1)	113.7(1)
(5)	O1/N1-C1-C9-C10	-	-	-	-87.9(1)	102.9(1)	86.5(1)	-88.0(2)
(6)	C1-N1-C6- C8	-	-	-	109.2(1)	85.0(1)	95.6(1)	-121.7(1)

[a] See Table 5.12

6.4 Concluding remarks

The–complexes reported here are planar, and the dihedral angles between the plane of the aromatic ring and the O1-Cu-O2 plane are very small, with the largest being ≈ 4 ˚ deviation of ≈ 4 ˚ from planarity, and the O1-Cu-O2 bond angle being ≈ 86 ˚. These complexes lie on an inversion center at the Cu atom, while the nitrogen atoms are inaccessible for coordination as in all the complexes there was no such coordination or even interaction observed. This might be due to the steric bulk in the case of the second structure as it has an *iso*-propyl attached to the nitrogen atom and thus rendering the lone pair on the nitrogen inaccessible.

These compounds also show strong intermolecular hydrogen bonding. As these hydrogen bonds tend to determine the properties of compounds their effects will be seen in the succeeding chapter when applied in catalysis.

The rates of different reactions, and the ability to act as oxidation catalysts, will be highlighted, and the structural aspects relevant to the catalytic behavior will be pointed out and discussed.

7 Catalytic activity of mononuclear [Cu(naltol)$_2$] complexes in the catechol oxidation by dioxygen

7.1 Introduction

The oxidation of organic or aromatic substrates is essential from both an economical and an environmental point of view. Two major enzymes that play a key role in these mutations are catechol dioxygenases and catechol oxidases.[1] The former being a natural means of breaking down aromatic precursors to aliphatic compounds (both intradiol and extradiol scission of catechols) and contains Fe, Mn, Mg or Cu in their active site. The latter is found in bacteria, fungi and plants catalyzing the oxidation of phenolic compounds to quinones as a protective mechanism.[2] Catechol oxidase has a type three copper center with an inter-nuclear distance of 2.9 Å in the oxidized form (*met* form) between the two copper (II) centers and a bridging hydroxyl group between them.[3] The reduced form (*deoxy* form) of the enzyme has an inter-nuclear distance of 4.4 Å between the two copper centers. Therefore most of its functional mimics are dinuclear Cu(II) complexes. However, other catalytically active complexes containing various transition metal ions such as Mn, Co, or Ni are also known.

Mononuclear metalloenzymes in which the copper center is the site of oxygen binding and activation belong to the type 2 copper protein family.[4] In this section the catalytic oxidation of 3,5-di-*tert*-butylcatechol by a number of Cu(II) complexes with varying electronic and steric

[1] A. Majumder, S. Goswami, S. R. Batten, M. S. El Fallah, J. Ribas, S. Mitra, *Inorg. Chim. Acta. 359* (***2006***) 2375.
[2] M. U. Triller, D. Pursche, W. –Y. Hsieh, V. L. Pecoraro, A. Rompel, B. Krebs, *Inorg. Chem. 42* (***2003***) 6274.
[3] Á. Kupán, J. Kaizer, G. Speier, M. Giorgi, M. Réglier, F. Pollreisz, *J. Inorg. Biochem. 103 (**2009**)* 389.
[4] A. C. Rosenzweig, M. H. Sazinsky, *Curr. Opin. Struct. Biol. 16* (***2006***) 729.

properties is discussed in detail. The aim is to evaluate the complex biological reactivity produced by catechol oxidase and to create similar chemical architectures and simple synthetic molecules to decode the biological code of reactivity. This will help to determine functional reaction conditions for model systems and the mechanistic pathways. These studies will also help in determining the ability of such complexes to influence reactivity patterns observed in metalloprotein chemistry, for the future exploitation of copper/oxygen systems as practical dioxygen carriers or as reagents for selective and catalytic oxidative mutations.

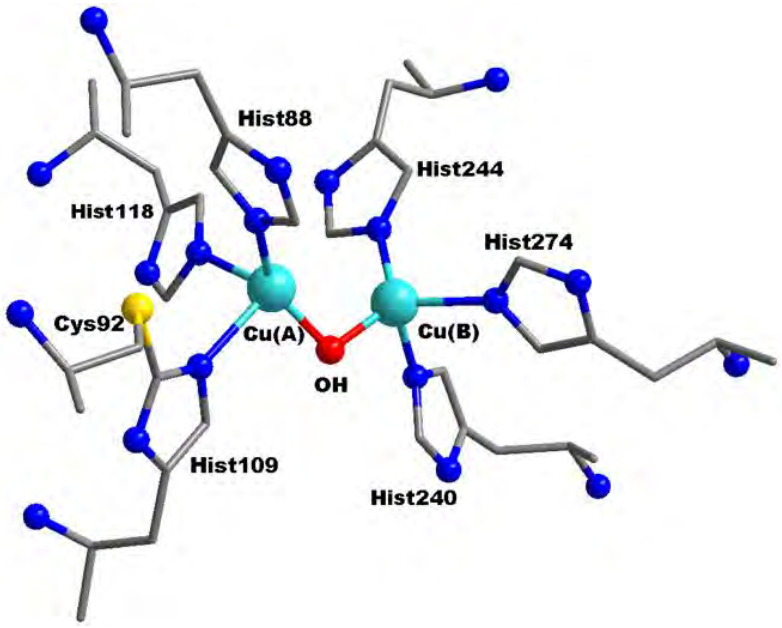

Figure 7.1. The coordination sphere of the dinuclear copper(II) center of catechol oxidase in the *met* state.[8]

To mimic the behavior in larger proteins, this study has identified three metal complexes which were investigated for the catalytic activities. The complexes utilized are $[Cu(EP(naltol))_2]$, $[Cu(MP(naltol))_2]$ and $[Cu(ME(naltol))_2]$; see previous chapters for description of the ligands.

7.2 Experimental

All reagents were of analytical grade. All organic solvents were pre-dried over calcium hydride and then distilled before use under an inert atmosphere (N_2 gas). The copper complexes were prepared as described in Chapter 4. Kinetic measurements were conducted on a UV-Vis Varian

Carey 50 Conc Spectrometer equipped with a Julabo F12-mV temperature cell regulator (accurate within 0.1°C) in a 1.00 cm quartz cuvette cell. The oxygen concentration was measured with a JENWAY Model 970 dissolved oxygen meter. Reactions of 3,5-di-*tert*-butylcatechol with O_2 catalyzed by [Cu(naltol)$_2$] were performed under pseudo-first-order conditions in a thermostatically controlled reaction vessel which was kept at 25 °C using oxygen saturated methanol as solvent. The reactions were sometimes slow taking ≈ 6 days. This posed a number of problems such as the leakage of oxygen from the system and the evaporation of the solvent.

The methanol was placed under a vacuum in a sonic bath to completely degas the solvent; molecular oxygen was then bubbled in the solvent at 25 °C producing different concentrations of dissolved oxygen which were dependent on the time intervals of exposure. An attempt was made to do the reaction without any oxygen, but there is a minimum of 3 ppm of oxygen in all gasses commercially available. The % dissolved oxygen varied between 15.1 % and 25.0 %. The reaction was monitored by following the rate at which 3,5-di-*tert*-butylbenzoquinone, the oxidation product of 3,5-di-*tert*-butylcatechol, forms. From literature the product formation is followed at ≈ 395 nm, however for this MSc study product formation was monitored at 560 nm as the absorption peak for the concentrations at λ = 395 nm used was > 1 which meant that Beer's law was not obeyed any more.

A concentration of 1 x 10^{-2} M 3,5-di-*tert*-butylcatechol and 1.9 x 10^{-5} M of the copper complex was used for the effect of varied oxygen investigation on the catalysis. The 3,5-di-*tert*-butylcatechol concentration ([DTBC]) for the rate constant determination varied between 1 x 10^{-2} M and 1 x 10^{-3} M while the complex concentration was kept at 1.9 x 10^{-5} M. A stock solution of 2 x 10^{-2} M of 3,5-di-*tert*-butylcatechol was prepared and this was diluted to obtain the correct concentration for the kinetic runs. All the solutions were prepared with O_2 saturated methanol. Extreme care was taken to ensure that all the glassware was clean to prevent any further oxidation of the 3,5-di-*tert*-butylbenzoquinone (DTBQ).

7.3 Biomimetic Modelling of Catechol Oxidase Activity

In this section the concentration of 3,5-di-*tert*-butylcatechol will be referred to as [DTBC] and that of 3,5-di-*tert*-butylbenzoquinone as [DTBQ]. In order to construct the complete reaction

mechanism, logical arguments based on literature, preliminary measurements and characterization studies need to be presented to reason for this particular approach. The following aspects were considered in this study:

1. T. R. Demmin *et al*. reported that in anaerobic conditions 3,5-di-*tert*-butylcatechol does not react with the various copper(II) complexes that they prepared to form the corresponding quinone.[5] However, in the presence of cupric chloride and 1 molar equiv. of triethylamine under anaerobic conditions 60 % yields of the quinone were obtained. This was arguably the reason why oxygen saturated solvent was used as no base or copper salts were used in this study. The dioxygen oxidizes the reduced form of the catalyst and makes the overall process catalytic.
2. In the same study, they reported that anaerobic oxidation of catechols with active copper(II) reagents in pyridine was a reversible process.[5] The degree of the reversible electron transfer from catechol to copper(II) species and from copper(I) species to *o*-benzoquinones is determined by the nature of both copper(II) and copper(I) species. Therefore, high/ low yields are a direct repercussion of the different thermodynamic stabilities of the Cu(II)/ Cu(I) pairs which are solvent dependent.
3. In aerobic conditions the copper(II) complexes that they synthesized efficiently catalyzed 3,5-di-*tert*-butylcatechol to the corresponding 3,5-di-*tert*-butylquinone with quantitative yields.[5] This was also in favour of an aerobic process and suggested that perhaps the degree of oxygen saturation may also have an effect on the overall process.
4. The wavelength of maximum absorption for 3,5-di-*tert*-butylbenzoquinone is 400 nm but the formation of 3,5-di-*tert*-butylbenzoquinone was monitored at 560 nm on the UV-Vis (Figure 7.2). This was due to the absorbance values exceeding one at 400 nm for the prepared concentrations with the implication that Beer's law could not be employed to analyze the data.

[5] T. R. Demmin, M. D. Swerdloff, M. M. Rogic, *J. Am. Chem. Soc. 103* (***1989***) 5795.

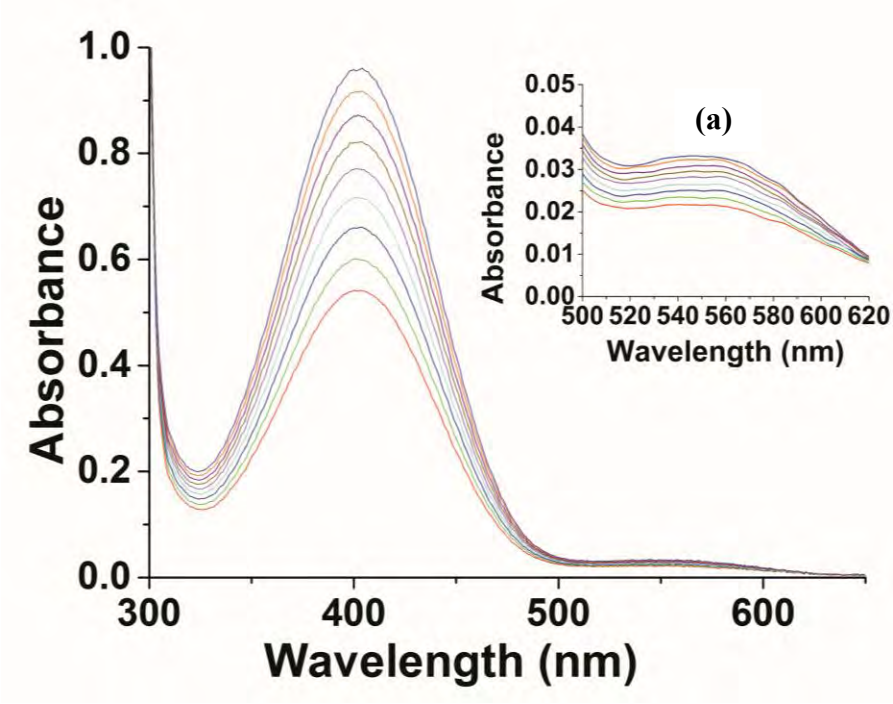

Figure 7.2. UV-Vis spectra for the formation of 3,5-di-*tert*-butylquinone at the wavelength of maximum absorption (400 nm) and minimum absorption (560 nm, insert a) at 25 °C in methanol. [Cu(naltol)$_2$] = 1.89 x 10^{-5} M, [O$_2$] = 9.25 x 10^{-3} M and t(initial) = 540 min, Δt = 60 min, t(final) = 1080 min. Insert (a) shows peak growth at the same rate at 560 nm.

5. Figure 7.2 shows the absorption profile of 3,5-di-*tert*-butylbenzoquinone as it forms at two different wavelengths (400 nm and 560 nm). Calculations show that the product absorbs much more at 400 nm than at 560 nm as the molar extinction coefficients for complexes [Cu(EP(naltol))$_2$], [Cu(MP(naltol))$_2$] and [Cu(ME(naltol))$_2$], are; 1125, 875 and 950 M^{-1}.cm^{-1} respectively at 400 nm. At 560 nm the molar extinction coefficients are 50, 75 and 75 M^{-1}.cm^{-1} respectively. Comparison to literature shows that at 400 nm the molar extinction coefficient of DTBQ ≈ 1560 M^{-1}.cm^{-1}.[6]
6. The most crucial internal factors that influence the catalytic activity of model compounds include;[7]
    a. The flexibility of the coordinating ligands, i.e. the greater the flexibility the higher the activity. The ligands were simple structures with single bonds that allowed various rotational movements and double bonds were only in the plane of the square planar conformation of the respective complexes.

[6] K. Selmeczi, M. Réglier, M. Giorgi, G. Speier, *Coord. Chem. Rev. 245* (**2003**) 191.
[7] K. S. Banu, M. Mukherjee, A. Guha, S. Bhattacharya, E. Zangrando, D. Das, *Polyhedron 45* (***2012***) 245.

b. The coordination environment of the copper centers, unsaturation or the presence of very labile ligands e.g. water molecules enhances the activity of the catalyst. The presence of a positive charge center close to the active site may also enhance the activity. In this case the axial positions perpendicular to the square planar are available for coordination and the availability of the metal centers was not an issue.

c. In dinuclear model compounds the best activity can be achieved when the Cu–Cu inter-nuclear distance is ≈ 3 Å.[6]

7. The most crucial external factors that influence the catalytic activity of model compounds include;[7]

   a. The nature of the model substrate; the presence of electron withdrawing group(s) makes the degree of oxidation difficult compared to the presence of bulky electron donating group(s) which makes oxidation of the substrate easy. In this case the substrate had two *tert*-butyl functional groups at positions 3 and 5 which made the process easy.

   b. The pH of the medium; the higher the pH the greater the activity. The activity of the enzyme is observed in the pH range of 5-8 (optimum at pH = 8), with an irreversible loss of activity below pH 4 and above pH 10.[8] For the current MSc study the reaction was carried out in methanol.

   c. The nature of the solvent; the lower the coordination power of the solvent, the higher the activity of the complexes in that solvent in catalyzing the oxidation.

8. In literature, various authors propose different mechanisms, ranging from bimetallic centers to mono metallic centers.[8,9] In Chapter 2 a brief discussion emphasizing the main features of the catalytic process was presented.[8,9]

9. The mononuclear copper complexes employed in the current MSc study have been well characterized by IR, elemental analysis and X-ray crystallography (Chapter 4, 5 and 6). The complexes fall in a range mimicking the Cu(II) protein family of enzymes.

[8] C. Belle, K. Selmeczi, S. Torelli, J. –L. Pierre, *C. R. Chimie. 10* (***2007***) 271.
[9] V. Mahadevan, R. J. M. K. Gebbink, T. D. P. Stack, *Curr. Opin. Chem. Bio. 4 (**2000**) 228.*

7.4 Possible Reaction Mechanisms for the Catalytic Cycle

By evaluating literature and the above mentioned arguments the following two possible mechanisms were considered to be plausible for the catalytic oxidation of 3,5-di-*tert*-butylcatechol:

Mechanism 1:

On the basis of Scheme 7.1, a rate law for the catalytic oxidation of 3,5-di-*tert*-butylcatechol by [Cu(naltol)$_2$] and molecular oxygen can be derived.

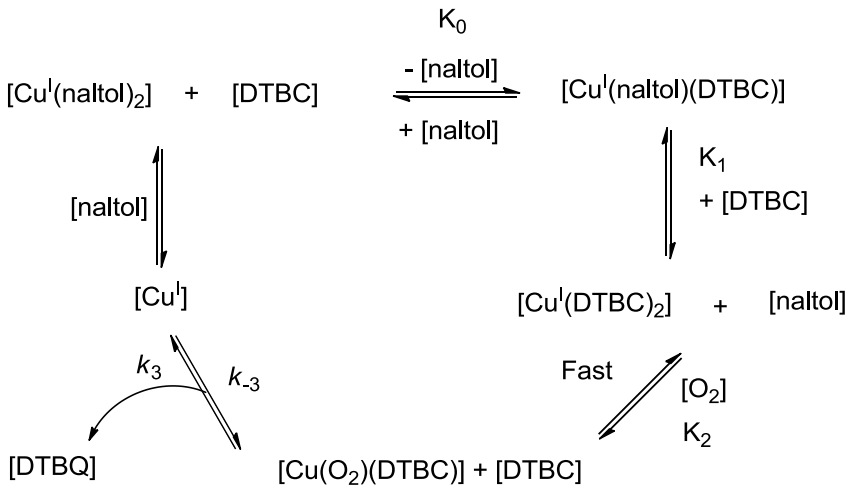

Scheme 7.1. Possible reaction scheme for the catalytic oxidation of 3,5-di-*tert*-butylcatechol by a Cu(naltol)$_2$ *in situ* generated species and molecular oxygen to form the corresponding 3,5-di-*tert*-butylbenzoquinone.[10]

The rate expression for the formation of 3,5-di-*tert*-butylbenzoquinone (DTBQ), as well as the equilibrium governing the third reaction in scheme 7.1, are given by Eq. 7.1 and Eq. 7.2, respectively:

$$Rate = \frac{d[DTBQ]}{dt} = k_3[Cu(O_2)(DTBC)] - k_{-3}[Cu^I] \qquad \text{Eq. 7.1}$$

$$K_2 = \frac{[Cu(O_2)(DTBC)][DTBC]}{[Cu^I(DTBC)_2][O_2]} \qquad \text{Eq. 7.2}$$

[10] T. J. Muller, "Copper Based Nanomaterials for Oxidation Catalysis" MSc dissertation, Department of Chemistry, University of Free State, Bloemfontein 9301, South Africa (***2009***).

The total metal concentration is known and is given by Eq. 7.3 and it can be converted into Eq. 7.4 and converted to Eq. 7.5.

$$[Cu]_{tot} = [Cu(O_2)(DTBC)] + [Cu^{I}(DTBC)_2]$$
$$= [Cu(O_2)(DTBC)] + \frac{[Cu(O_2)(DTBC)][DTBC]}{K_2[O_2]} \quad \text{Eq. 7.3}$$

$$[Cu(O_2)(DTBC)] = \frac{[Cu]_{tot}}{1 + \frac{[DTBC]}{K_2[O_2]}} \quad \text{Eq. 7.4}$$

$$Therefore, \quad [Cu(O_2)(DTBC)] = \frac{[Cu]_{tot} K_2[O_2][DTBC]}{[DTBC] + K_2[O_2]} \quad \text{Eq. 7.5}$$

By substituting Eq. 7.5 into Eq. 7.1, the rate equation becomes Eq. 7.6 and this gives the pseudo first-order rate constant ($[O_2] >> [Cu]_{tot}$), k_{obs} expression in Eq. 7.7:

$$Rate = \frac{k_3 K_2[O_2][Cu]_{tot}\,[DTBC]}{[DTBC] + K_2[O_2]} \quad \text{Eq. 7.6}$$

$$k_{obs} = \frac{k_3 K_2[O_2][DTBC]}{[DTBC] + K_2[O_2]} + k_{-3} \quad \text{Eq. 7.7}$$

Or, when $[DTBC] << 1$ ($K_2[O_2] >> [DTBC]$),

$$k_{obs} = k_3[DTBC] + k_{-3} \quad \text{Eq. 7.7a}$$

Mechanism 2:

Similarly, on the basis of scheme 7.2, a rate law for the catalytic oxidation of 3,5-di-*tert*-butylcatechol by [Cu(naltol)$_2$] and molecular oxygen can also be derived.

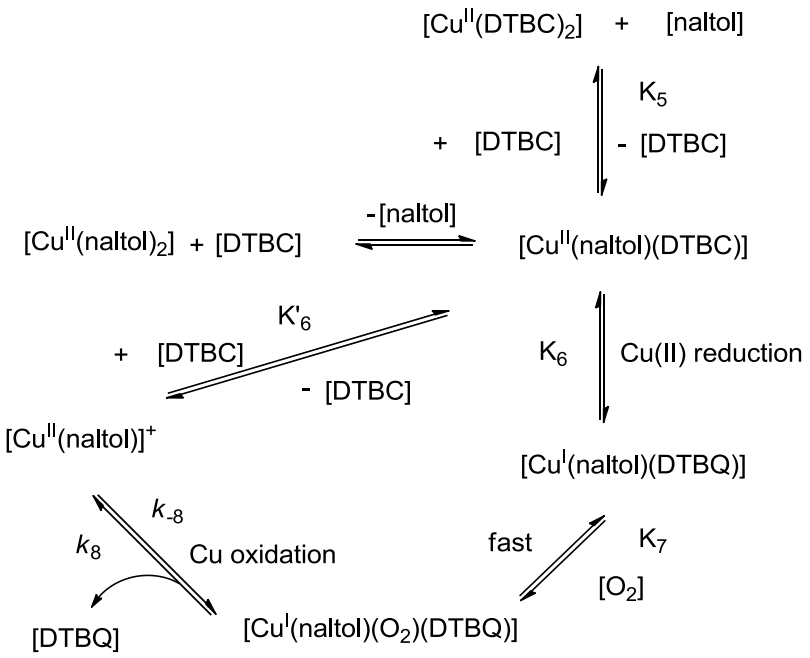

Scheme 7.2. Possible reaction scheme for the catalytic oxidation of 3,5-di-*tert*-butylcatechol by a Cu(II) *in situ* generated species and molecular oxygen to form the corresponding 3,5-di-*tert*-butylbenzoquinone.[10]

It has a different form from the one derived in the first mechanism as the equilibrium governing this mechanism is different. The form of the rate expression and the equilibrium constant in the 3rd reaction is illustrated in Eq. 7.8 and Eq. 7.9 respectively:

$$Rate = \frac{d[DTBQ]}{dt} = k_8[Cu^I(naltol)(O_2)(DTBQ)] - k_{-8}[Cu^{II}(naltol)] \qquad \text{Eq. 7.8}$$

Defining the simple equilibrium constants for K_6', K_{6R}, K_7, as in Eq. 7.9, Eq. 7.10 and Eq. 7.11, and rearrangement of Eq. 7.10 yields Eq. 7.12. From K_5 Eq. 7.13 is obtained.

$$K_6' = [Cu^{II}(naltol)(DTBC)] / ([Cu^{II}(naltol)]^+ [DTBC]) \qquad \text{Eq. 7.9}$$

$$K_{6R} = \frac{[Cu^{I}(naltol)(DTBQ)]}{[Cu^{II}(naltol)(DTBC)]} \quad \text{Eq. 7.10}$$

$$K_{7} = \frac{[Cu^{I}(naltol)(DTBQ)(O_2)]}{[Cu^{I}(naltol)(DTBQ)][O_2]} \quad \text{Eq. 7.11}$$

$$[Cu^{II}(naltol)(DTBC)] = \frac{[Cu^{I}(naltol)(DTBQ)]}{K_{6R}} \quad \text{Eq. 7.12}$$

$$[Cu^{II}(DTBC)_2] = \frac{K_5[Cu^{II}(naltol)(DTBC)][DTBC]}{[naltol]} \quad \text{Eq. 7.13}$$

The total metal concentration is known and is given by Eq. 7.14.

$$[Cu]_{tot} = \overbrace{[Cu^{II}(naltol)]}^{1} + \overbrace{[Cu^{II}(naltol)(DTBC)]}^{2} + \overbrace{[Cu^{I}(naltol)(DTBQ)]}^{3} + [Cu^{I}(naltol)(DTBQ)(O_2)] \quad \text{Eq. 7.14}$$

Combining the terms 1, 2 and 3 from Eq. 7.14 with Eq. 7.15, Eq. 7.16 and Eq. 7.17 gives Eq. 7.18.

$$[Cu^{I}(naltol)(DTBQ)] = \frac{[Cu^{I}(naltol)(O_2)(DTBQ)]}{K_7[O_2]} \quad \text{Eq. 7.15}$$

$$[Cu^{II}(naltol)(DTBC)] = \frac{[Cu^{I}(naltol)(DTBQ)(O_2)]}{K_{6R}K_7[O_2]} \quad \text{Eq. 7.16}$$

$$[Cu^{II}(naltol)] = \frac{[Cu^{I}(naltol)(O_2)(DTBQ)]}{[DTBC]K'_6K_{6R}K_7[O_2]} \quad \text{Eq. 7.17}$$

$$[Cu^{I}(naltol)(O_2)(DTBQ)] = \frac{[Cu]_{tot}}{1+\frac{1}{K_7[O_2]}+\frac{1}{K_{6R}K_7[O_2]}+\frac{1}{[DTBC]K'_6K_{6R}K_7[O_2]}} X \frac{[DTBC]K'_6K_{6R}K_7[O_2]}{[DTBC]K'_6K_{6R}K_7[O_2]} \quad \text{Eq. 7.18}$$

Eq. 7.18 then simplifies to Eq. 7.19.

$$[Cu^{I}(naltol)(O_2)(DTBQ)] = \frac{[DTBC]K'_6K_{6R}K_7[O_2][Cu]_{tot}}{1+[DTBC]K'_6+[DTBC]K'_6K_{6R}+[DTBC]K'_6K_{6R}K_7[O_2]} \quad \text{Eq. 7.19}$$

The pseudo first-order rate constant , k_{obs} for the formation of DTBQ may be obtained from Eq. 7.8 and Eq. 7.19 and is given in Eq. 7.20 for conditions where [$DTBC$] and $[O_2]$ >> $[Cu]_{tot}$

$$k_{obs} = \frac{k_8 K'_6 K_{6R} K_7 [DTBC][O_2]}{1 + [DTBC]K'_6 + [DTBC]K'_6 K_{6R} + [DTBC]K'_6 K_{6R} K_7 [O_2]} + k_{-8} \quad \text{Eq. 7.20}$$

Assuming an expected energy barrier for the formation of [Cu^I(naltol)(DTBQ)] and also a lower thermodynamic drive, Eq. 7.20 simplifies to Eq. 7.21, provided $[O_2]$ << 1.

$$k_{obs} = \frac{k_8 K'_6 K_{6R} K_7 [DTBC][O_2]}{1 + [DTBC]K'_6 + [DTBC]K'_6 K_{6R} + [DTBC]K'_6 K_{6R} K_7 [O_2]} + k_{-8} \quad \text{Eq. 7.21}$$

$$k_{obs} = k_8 K'_6 K_{6R} K_7 [O_2][DTBC] + k_{-8} \quad \text{Eq. 7.22}$$

Or, $$k_{obs} = k_8 \boldsymbol{K_A} [DTBC] + k_{-8} \quad \text{Eq. 7.23}$$

at constant $[O_2]$, since $\boldsymbol{K_A} = K'_6 K_{6R} K_7 [O_2]$ = constant.

Similarly, at fixed [DTBC], a variation of the $[O_2]$, assuming again an expected energy barrier for the formation of [Cu^I(naltol)(DTBQ)] and also a lower thermodynamic drive, Eq. 7.22 may be simplified to Eq. 7.24.

$$k_{obs} = \frac{k_8 K'_6 K_{6R} K_7 [DTBC][O_2]}{1 + [DTBC]K_7 [O_2]} + k_{-8} \quad \text{Eq. 7.24}$$

Or

$$k_{obs} = \frac{k_8 K_7 \boldsymbol{K_B} [O_2]}{1 + [DTBC]K_7 [O_2]} + k_{-8} \quad \text{Eq. 7.25}$$

at constant [DTBC], since $\boldsymbol{K_B} = K'_6 K_{6R}$[DTBC] = constant.

Finally, at higher [DTBC], the equilibrium defined by K_5 can come into play, which presumes a decrease in catalytic activity and therefore a corresponding decrease in the observed rate constant.

7.5 Results and Discussion

The catalytic process of 3,5-di-*tert*-butylcatechol oxidation by the different Cu-*O,O'* ligand systems to form 3,5-di-*tert*-butylbenzoquinone is slow and the reaction with all three complexes was monitored by UV-Vis. This constant temperature study was also used to compare the efficiency of the different [Cu(naltol)$_2$] complexes. Typical kinetic data, as illustrated in Figure 7.3 below, was fitted to Eq. 3.24 in order to determine the observed rate constant, k_{obs}.

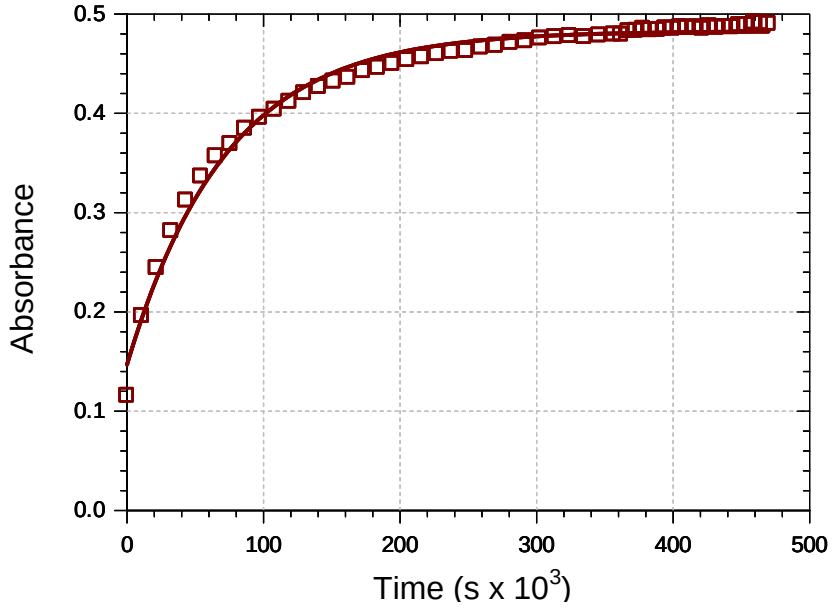

Figure 7.3. Typical UV-Vis absorbance vs. time data for the oxidation of 3,5-di-*tert*-butylcatechol catalyzed by [Cu(naltol)$_2$] to form the corresponding 3,5-di-*tert*-butylbenzoquinone at 560 nm in oxygen saturated methanol at 25.0 °C. [Cu(naltol)$_2$] = 1.89 x 10^{-5} [DTBC] = 0.008 M and k_{obs} 1.38(4) x 10^{-5} s^{-1}, experimental points observed as well as fitted line are illustrated.

Most of the fits are not perfect and the experimental points deviate from the fit, particularly in the latter parts of the reactions, as to suggest that perhaps there is another process occurring at the latter stages of the reaction. This is mainly thought to be due to decomposition of the 3,5-di-*tert*-butylbenzoquinone formed or even racemization of the product. Furthermore this can also be attributed to the leaking of molecular oxygen from the system or due to evaporation, resulting in undesired effects on the data towards completion of the process as the experiment takes ≈ 6 days.

7.5.1 Bis(1-ethyl-3-hydroxy-2-methyl-4-pyridinonato)copper(II) [Cu(ME(naltol))$_2$]

It was evident from the kinetic plots (see Fig. 7.4 for an example) that the 3,5-di-*tert*-butylcatechol was converted in a single step process to 3,5-di-*tert*-butylbenzoquinone catalyzed by [Cu(ME(naltol))$_2$]. It has also been reported in literature that the process is first-order in the substrate and second order in Cu(II). There was no clear evidence of any other intermediates that formed during the reaction or that suggested that the reaction took part in several steps. The data shows the slow formation of the product until the monitoring of the process was terminated after *ca*. 6 days.

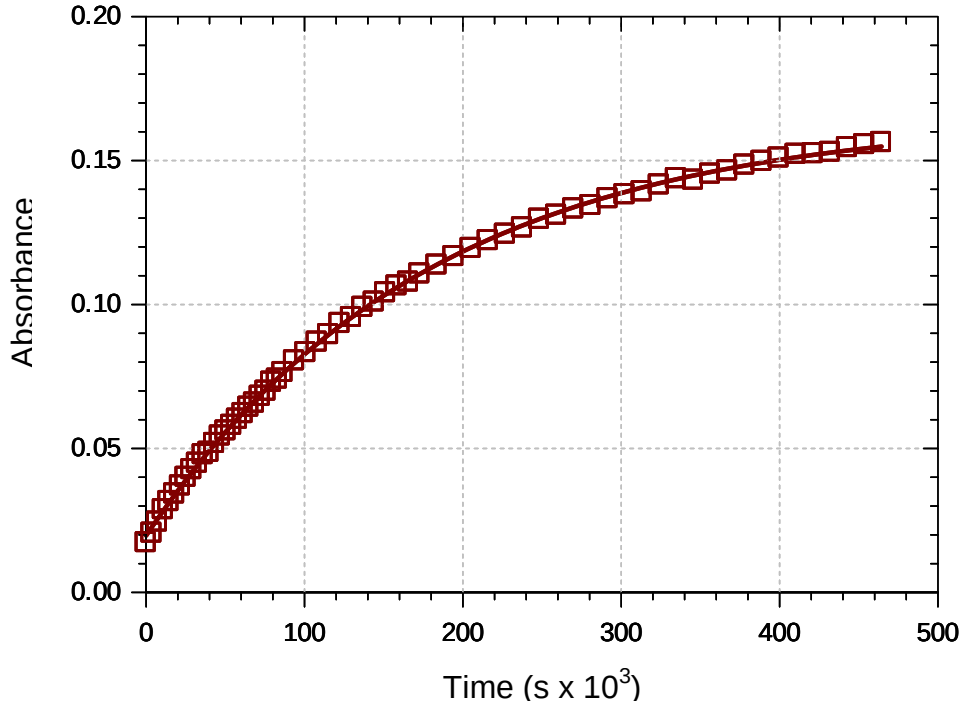

Figure 7.4. UV-Vis absorbance vs. time data for the oxidation of 3,5-di-*tert*-butylcatechol catalyzed by [Cu(ME(naltol))$_2$] to form the corresponding 3,5-di-*tert*-butylbenzoquinone in oxygen saturated methanol at 25.0 °C, λ = 560 nm. [Cu(ME(naltol))$_2$] = 1.88 x 10^{-5} M, [DTBC] = 0.004 M and k_{obs} = 5.52(7) x 10^{-6} s^{-1}, experimental points observed as well as fitted line are illustrated.

The influence of the pseudo first-order rate constant for the oxidation of 3,5-di-*tert*-butylcatechol by [Cu(ME(naltol))$_2$] is shown in Fig. 7.1. The plot of the different k_{obs} at different substrate ([DTBC]) concentrations shows a linear relationship as the substrate concentration increases, in agreement with Eq. 7.7a or 7.23. The rate data are reported in Table 7.1.

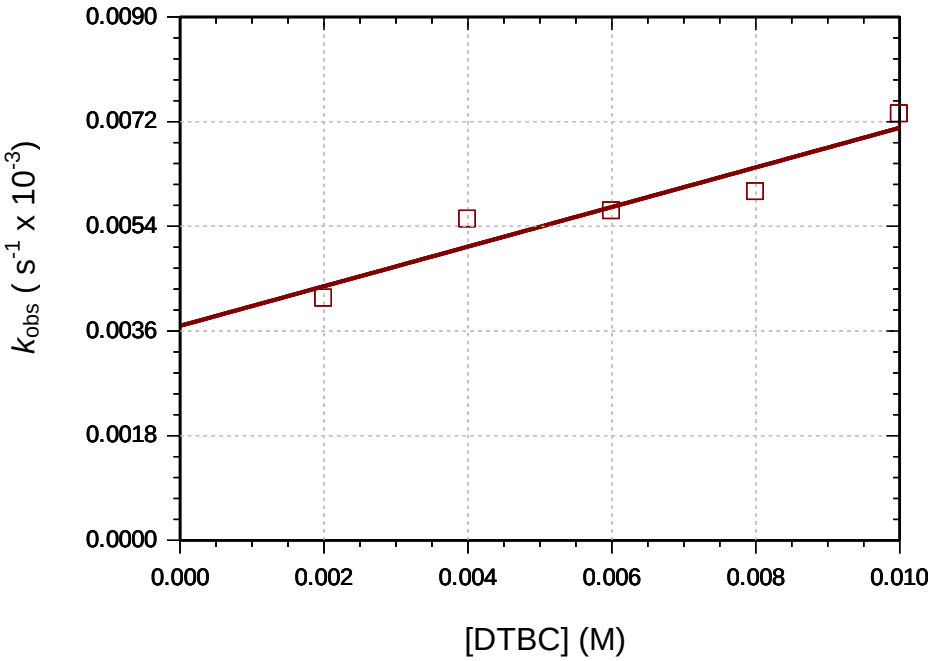

Figure 7.5. Pseudo first-order rate constant vs. [DTBC] in the oxidation of 3,5-di-*tert*-butylcatechol under pseudo first-order conditions in oxygen saturated methanol at 25.0 °C catalyzed by ([Cu(ME(naltol))$_2$]. ([Cu(ME(naltol))$_2$] = 1.9 x 10^{-5} M.

Table 7.1. UV-Vis kinetic data for the oxidation of 3,5-di-*tert*-butylcatechol catalyzed by ([Cu(ME(naltol))$_2$] in oxygen saturated methanol at 25.0 °C.

[3,5-di-*tert*-butylcatechol] (mol.dm^{-3})	[Cu(ME(naltol))$_2$] (mol.dm^{-3})	k_{obs} (s^{-1})		k_1 (M^{-1} .s^{-1})	k_{-1} (s^{-1})	K (M^{-1})
0.010	1.88 x 10^{-5}	7.33(1) x 10^{-6}		3.4(6) x 10^{-4}	3.6(4) x 10^{-6}	94(18)
0.008	1.89 x 10^{-5}	5.99(7) x 10^{-6}				
0.006	1.87 x 10^{-5}	5.66(5) x 10^{-6}				
0.004	1.88 x 10^{-5}	5.52(7) x 10^{-6}				
0.002	1.89 x 10^{-5}	4.16(7) x 10^{-6}				

7.5.2 Bis(2-ethyl-3-hydroxy-1-isopropyl-4-pyridinonato)copper(II) [Cu(EP(naltol))$_2$]

It was evident from the kinetic plots (see Fig. 7.6 for an example) that the 3,5-di-*tert*-butylcatechol was converted in a single step process to 3,5-di-*tert*-butylbenzoquinone catalyzed by [Cu(EP(naltol))$_2$].

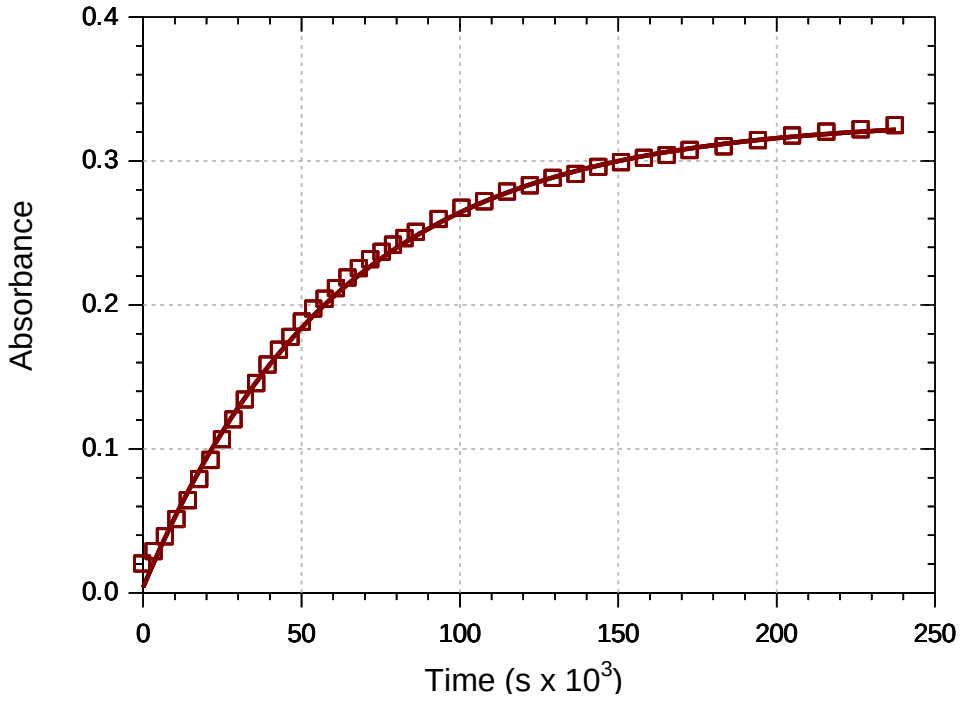

Figure 7.6. UV-Vis absorbance vs. time data for the oxidation of 3,5-di-*tert*-butylcatechol catalyzed by [Cu(EP(naltol))$_2$] to form the corresponding 3,5-di-*tert*-butylbenzoquinone in oxygen saturated methanol at 25.0 °C, λ = 560 nm. [Cu(EP(naltol))$_2$] = 1.88 x 10^{-5} M, [DTBC] = 0.006 M and k_{obs} = 1.07(2) x 10^{-5} s^{-1}, experimental points observed as well as fitted line are illustrated.

The influence of the pseudo first-order rate constant for the oxidation of 3,5-di-*tert*-butylcatechol by [Cu(EP(naltol))$_2$] is shown in Fig. 7.7. The plot of the different k_{obs} at different substrate ([DTBC]) concentrations shows a linear relationship as the substrate concentration increases, in agreement with Eq. 7.7a or 7.23. The rate data are reported in Table 7.2.

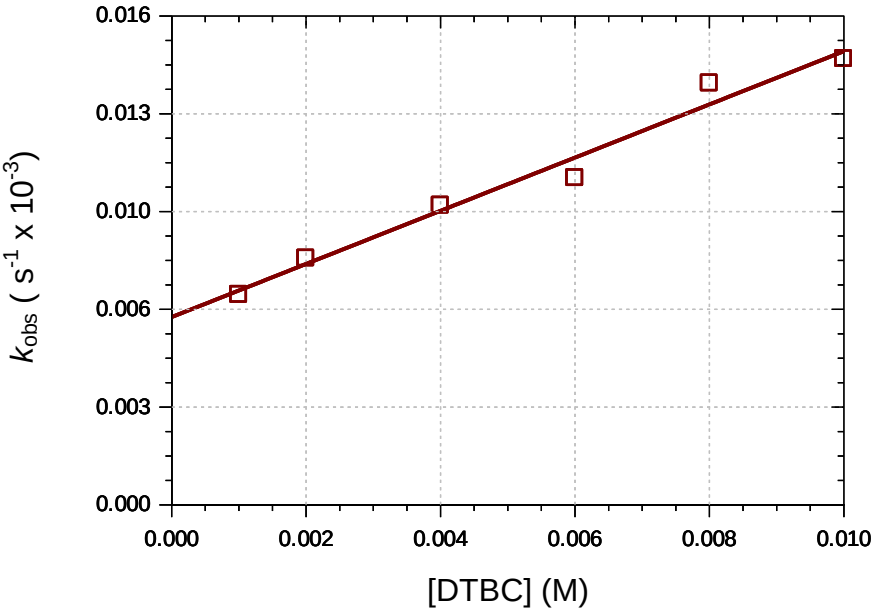

Figure 7.7. Pseudo first-order rate constant vs. [DTBC] in the oxidation of 3,5-di-*tert*-butylcatechol under pseudo first-order conditions in oxygen saturated methanol at 25.0 °C catalyzed by [Cu(EP(naltol))$_2$]. [Cu(EP(naltol))$_2$] = 1.9 x 10^{-5} M.

The same behavior is observed for [Cu(EP(naltol))$_2$] under the same conditions when compared to [Cu(ME(naltol))$_2$]. However this complex increased the rate threefold compared to [Cu(ME(naltol))$_2$] described above.

Table 7.2. UV-Vis kinetic data for the oxidation of 3,5-di-*tert*-butylcatechol catalyzed by [Cu(EP(naltol))$_2$] in oxygen saturated methanol at 25.0 °C.

[3,5-di-*tert*-butylcatechol] (mol.dm^{-3})	[Cu(EP(naltol))$_2$] (mol.dm^{-3})	k_{obs} (s^{-1})	k_1 (M^{-1} .s^{-1})	k_{-1} (s^{-1})	K (M^{-1})
0.010	1.89 x 10^{-5}	1.46(3) x 10^{-5}	8.7(7) x 10^{-4}	6.15(1) x 10^{-6}	141(11)
0.008	1.88 x 10^{-5}	1.38(4) x 10^{-5}			
0.006	1.88 x 10^{-5}	1.07(2) x 10^{-5}			
0.004	1.89 x 10^{-5}	9.80(1) x 10^{-6}			
0.002	1.89 x 10^{-5}	8.07(1) x 10^{-6}			
0.001	1.90 x 10^{-5}	6.88(2) x 10^{-6}			

A study employing [Cu(EP(naltol))$_2$] of 4.7 x 10^{-4} M and [DTBC] ranging from 0.010 to 0.225 M showed that in this range the k_{obs} gradually decreases and at a substrate concentration of 0.18 M the k_{obs} of the reaction becomes constant and is independent of the substrate concentration, $k_{obs} \approx 1.31 \times 10^{-5}$ s^{-1} (see Figure 7.8).

As discussed above, this decrease is assumed to be due to the K_5 equilibrium (Mechanism 2) or as defined in Mechanism 1 and illustrated in Eq. 7.7.

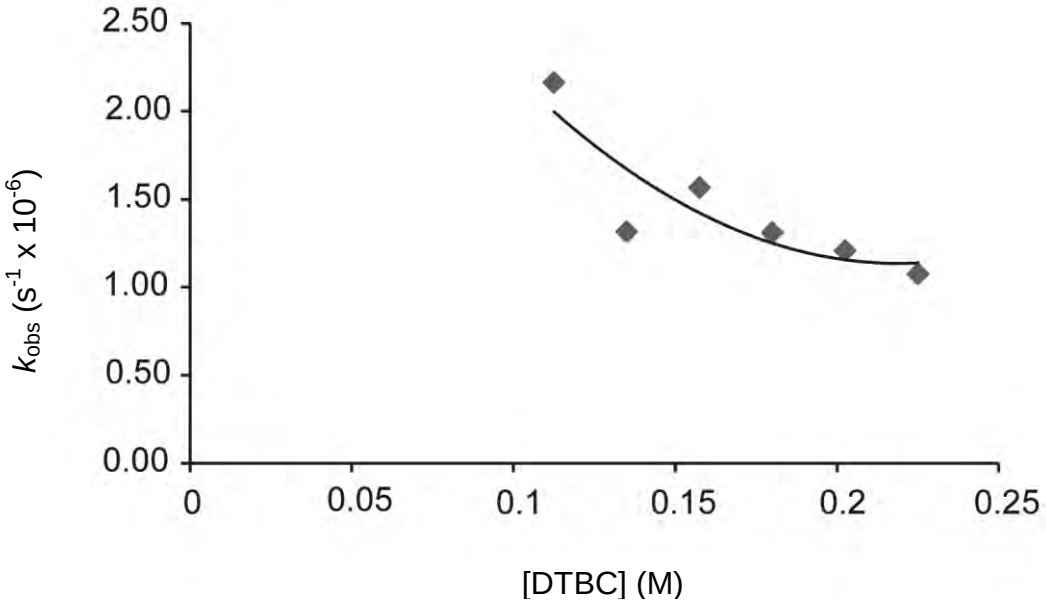

Figure 7.8. Pseudo first-order rate constant vs. [DTBC] in the oxidation of 3,5-di-*tert*-butylcatechol under pseudo first-order conditions in oxygen saturated methanol at 25.0 °C catalyzed by [Cu(EP(naltol))$_2$]. [Cu(EP(naltol))$_2$] = 4.7 x 10^{-4} M. [DTBC] > 0.1 M.

7.5.3 Bis(3-hydroxy-2-methyl-1-isopropyl-4-pyridinonato)copper(II) [Cu(MP(naltol))$_2$]

Next, the effect of different variables on [Cu(MP(naltol))$_2$] as catalyst was investigated. Preliminary experiments showed that [Cu(MP(naltol))$_2$] was the second most effective catalyst and for this reason it was chosen for further studies to determine the effect of oxygen concentration on the process and to give a general estimation as to what the degree of oxygen saturation will have on the three catalysts described in Par 7.5.1-7.5.3.

It was evident from the kinetic plots (see Fig. 7.9) that the 3,5-di-*tert*-butylcatechol was converted in a single step process to 3,5-di-*tert*-butylbenzoquinone catalyzed by [Cu(MP(naltol))$_2$].

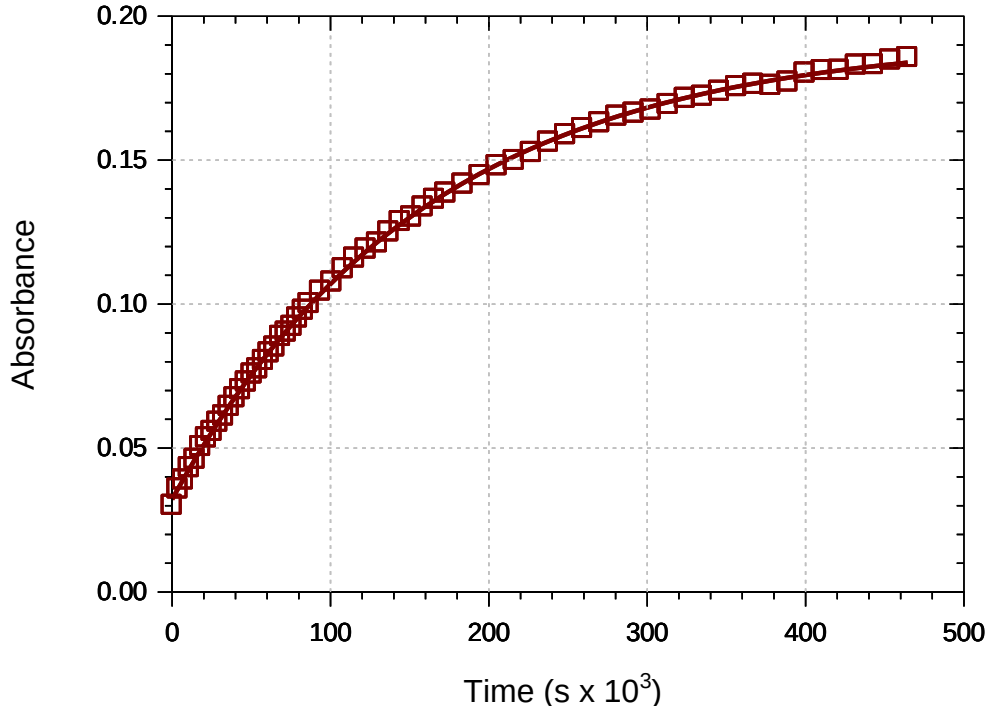

Figure 7.9. UV-Vis absorbance vs. time data for the oxidation of 3,5-di-*tert*-butylcatechol catalyzed by [Cu(MP(naltol))$_2$] to form the corresponding 3,5-di-*tert*-butylbenzoquinone in oxygen saturated methanol at 25.0 °C, λ = 560 nm. [Cu(MP(naltol))$_2$] = 1.88 x 10^{-5} M, [DTBC] = 0.004 M and k_{obs} = 4.78(8) x 10^{-6} s^{-1}, experimental points observed as well as fitted line are illustrated.

The influence of the pseudo first-order rate constant for the oxidation of 3,5-di-*tert*-butylcatechol by [Cu(MP(naltol))$_2$] is shown in Fig. 7.10. The plot of the different k_{obs} at different substrate ([DTBC]) concentrations shows a linear relationship as the substrate concentration increases, in agreement with Eq. 7.7a or 7.23. The rate data are reported in Table 7.3.

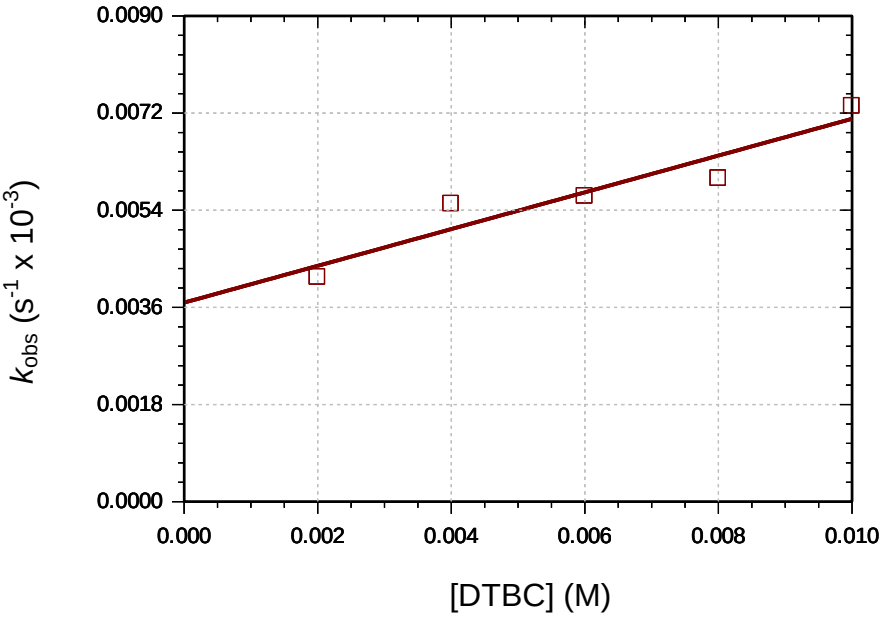

Figure 7.10. Pseudo first-order rate constant vs. [DTBC] in the oxidation of 3,5-di-*tert*-butylcatechol under pseudo first-order conditions in oxygen saturated methanol at 25.0 °C catalyzed by $[Cu(MP(naltol))_2]$. $[Cu(MP(naltol))_2] = 1.9 \times 10^{-5}$ M.

Table 7.3. UV-Vis kinetic data for the oxidation of 3,5-di-tertbutylcatechol catalyzed by $[Cu(MP(naltol))_2]$ in oxygen saturated methanol at 25.0 °C.

[3,5-di-*tert*-butylcatechol] ($mol.dm^{-3}$)	$[Cu(MP(naltol))_2]$ ($mol.dm^{-3}$)	k_{obs} (s^{-1})		k_1 ($M^{-1}.s^{-1}$)	k_{-1} (s^{-1})	K (M^{-1})
0.01	1.89×10^{-5}	$8.51(1) \times 10^{-6}$		$4.8(9) \times 10^{-4}$	$3.2(6) \times 10^{-6}$	150(39)
0.008	1.88×10^{-5}	$6.38(5) \times 10^{-6}$				
0.006	1.88×10^{-5}	$6.29(4) \times 10^{-6}$				
0.004	1.88×10^{-5}	$4.78(8) \times 10^{-6}$				
0.002	1.88×10^{-5}	$4.52(7) \times 10^{-6}$				

The pseudo first-order rate constants for the formation of DTBQ, k_{obs} of the different reactions with varying oxygen concentrations show increasing rates in a limiting process, see Fig. 7.11 (data in Table 7.4), as predicted by Eq. 7.7 and Eq. 7.25. The k_{obs} increases with an increase in dissolved oxygen and seem to approach a point where the degree of dissolved oxygen does not have an effect on the observed rate constant of the oxidation process. This point was not determined as the electrode used in this study had an upper detecting limit of 25 % oxygen (which is the point of saturation) and is $\approx 9.25 \times 10^{-3}$ M.

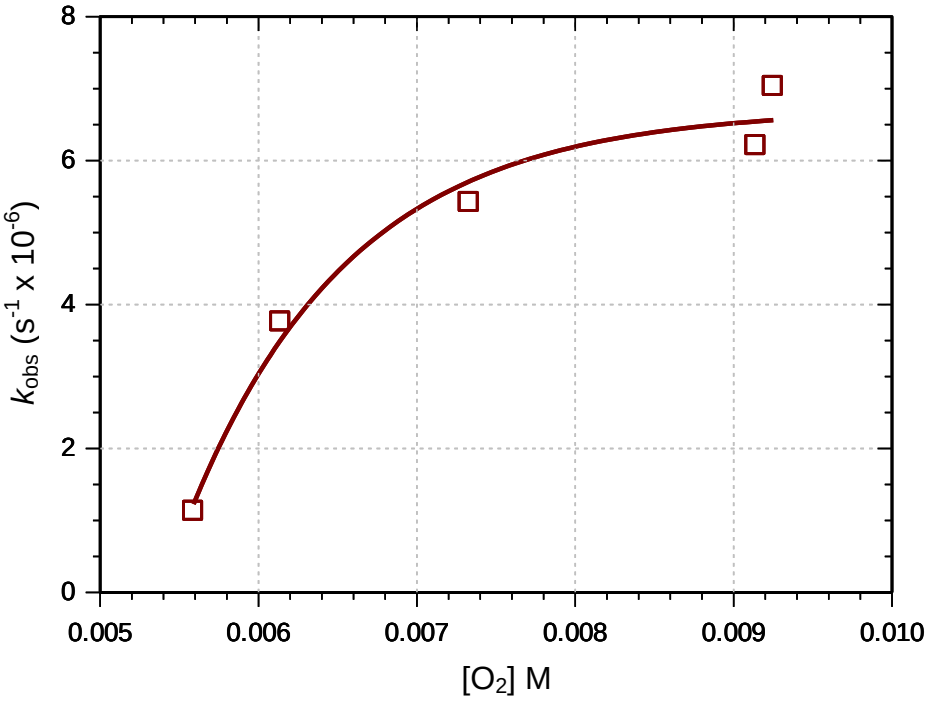

Figure 7.11. The effect of varied oxygen concentration in the oxidation of 3,5-di-*tert*-butylcatechol under pseudo first-order conditions in methanol at 25.0 °C, λ = 560 nm catalyzed by [Cu(MP(naltol))$_2$]. [Cu(MP(naltol))$_2$] = 1.9 x10^{-5} M, [DTBC] = 0.01 M. K_2 (Scheme 1; Eq. 7.7) or K_7 (Scheme 7.2; Eq 7.25) obtained from a L.S. fit of the data to Eq. yields $K_{2/7}$ = 150 M^{-1}

Table 7.4. The effect of varied oxygen concentration in the oxidation of 3,5-di-*tert*-butylcatechol catalyzed by [Cu(MP(naltol))$_2$] in methanol at 25.0 °C, λ = 560 nm. [Cu(MP(naltol))$_2$] = 1.9 x 10^{-5} M, [DTBC] = 0.01 M.

[3,5-di-*tert*-butylcatechol] (mol.dm^{-3})	[Cu(MP(naltol))$_2$] (mol.dm^{-3})	[O_2] (mol.dm^{-3})	k_{obs} (s^{-1})
0.0101	1.89 x 10^{-5}	5.59 x 10^{-3}	1.1(1) x 10^{-6}
0.0100	1.88 x 10^{-5}	6.14 x 10^{-3}	3.76(5) x 10^{-6}
0.0102	1.87 x 10^{-5}	7.33 x 10^{-3}	5.42(4) x 10^{-6}
0.0104	1.86 x 10^{-5}	9.14 x 10^{-3}	6.21(5) x 10^{-6}
0.0103	1.88 x 10^{-5}	9.25 x 10^{-3}	7.03(1) x 10^{-6}

7.6 Comparative Study

The complexes utilized and evaluated in this M.Sc. study are $[Cu(EP(naltol))_2]$, $[Cu(MP(naltol))_2]$ and $[Cu(ME(naltol))_2]$; see previous chapters for description of the ligands. It is clear that both mechanisms as proposed (1 and 2) are reasonable, based on the kinetic and synthetic experiments performed and reported.

A plot of the different k_{obs} at different substrate ([DTBC]) concentrations for all three complexes shows a linear relationship as the substrate concentration increases ($[Cu(II)(naltol)_2] = 1.9 \times 10^{-5}$ M). This catalyst ($[Cu(ME(naltol))_2]$) was however the least effective one compared to the three employed in this study (see Fig. 7.12 below).

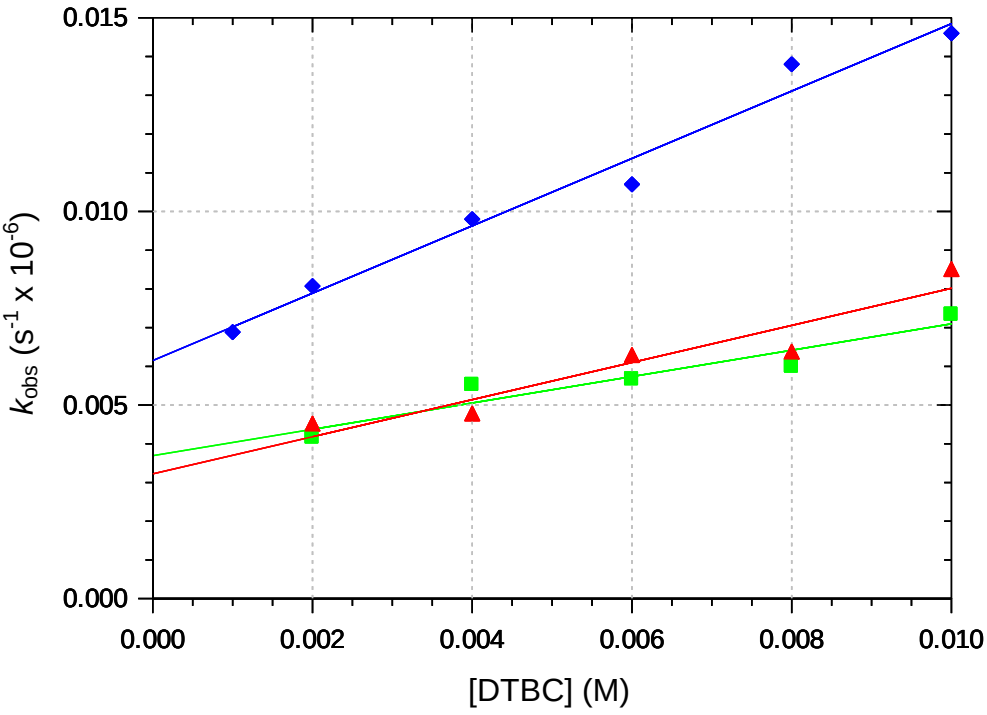

Figure 7.12. The effect of various Cu(II) complexes on the oxidation of 3,5-di-*tert*-butylcatechol under pseudo first-order conditions in oxygen saturated methanol at 25.0 °C. $[Cu(naltol)_2] = 1.9 \times 10^{-5}$ M. (Blue=$[Cu(EP(naltol))_2]$, Red=$[Cu(MP(naltol))_2]$, Green =$[Cu(ME(naltol))_2]$)

Table 7.5. Second order rate constants for the catalytic oxidation of DTBC concentration in the oxidation of 3,5-di-*tert*-butylcatechol catalyzed by the three complexes used in this study, in methanol at 25.0 °C, λ = 560 nm.

Complex	k_1 ($M^{-1}.s^{-1}$)
[Cu(MP(naltol))$_2$]	4.8(9) x 10^{-4}
[Cu(EP(naltol))$_2$]	8.7(7) x 10^{-4}
[Cu(ME(naltol))$_2$]	3.4(6) x 10^{-4}

Figure 7.12 above shows the direct comparison of the three complexes for the oxidation of 3,5-di-*tert*-butylcatechol to the corresponding 3,5-di-*tert*-butylquinone. The colours blue, red and green (fitted line and experimental points) indicate the complexes [Cu(EP(naltol))$_2$], [Cu(MP(naltol))$_2$] and ([Cu(ME(naltol))$_2$]). In general, the activities of these complexes are disappointingly low. However they compare well with the complexes studied by Muller (Ref 10); see also Table 7.6.

Comparison of these studied complexes with other mononuclear copper(II) complexes under similar conditions, [Cu(II)] = 1.4 x 10^{-5} M and [DTBC] ranging from 1.4 x 10^{-3} to 1.4 x 10^{-4} M yields k_{obs} of the order 10^{-5} (Figure 7.13).[10] These observed rate constants are generally higher than the ones obtained in this M.Sc. study and this can be attributed to the lower substrate concentrations used in the M.Sc. study of T. J. Muller with the highest concentration being tenfold less than what was used for this M.Sc. study (see Table 7.6).[10] Furthermore his studies indicated decreasing limiting kinetics whereas this was only observed in [Cu(EP(naltol))$_2$] at higher [DTBC] ([DTBC] > 0.1 M, see Figure 7.8)

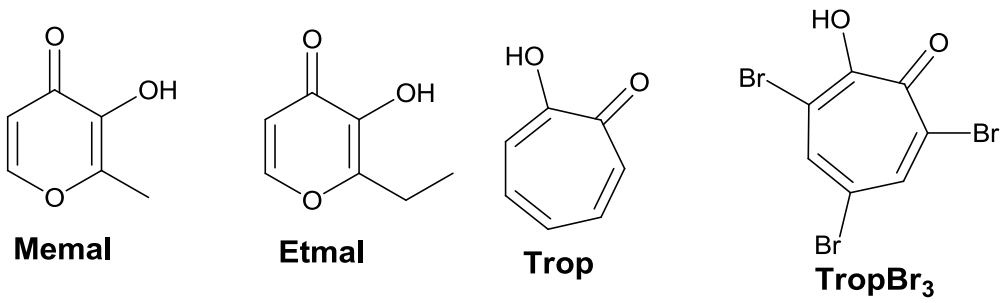

Figure 7.13. Ligand systems employed in T.J. Muller MSc dissertation. [10]

Table 7.6. Kinetic data for the oxidation of 3,5-di-*tert*-butylcatechol by different copper complexes [Cu(*O,O'*)$_2$] = 1.4 x 10^{-5} M at [O$_2$] = 1 x 10^{-3} M in methanol at 25.0 °C (sourced from T. J. Muller MSc dissertation), and Comparison with the current MSc study.[10] k_f indicates the second order rate constant for the formation of the DTBQ.

Complex	k_f (x10^{-6} M^{-1} s^{-1})
[Cu(MP(naltol))$_2$] [a]	480 ± 90
[Cu(EP(naltol))$_2$] [a]	870 ± 70
[Cu(ME(naltol))$_2$] [a]	340 ± 60
[Cu(Memal)$_2$] [b]	370 ± 60
[Cu(Etmal)$_2$] [b]	423 ± 20
[Cu(Trop)$_2$] [b]	5.0 ± 8
[Cu(TropBr$_3$)$_2$] [b]	1.7 ± 10

[a] This work; [b] Ref. 10

Dinuclear model complexes reported by V. K. Bhardwaj *et al.* show that their systems are much more effective for this process.[11] Under pseudo-first order conditions they obtained rates that are two orders-of-magnitude larger than the ones reported in this study (see Figure 7.14 and Table 7.7).

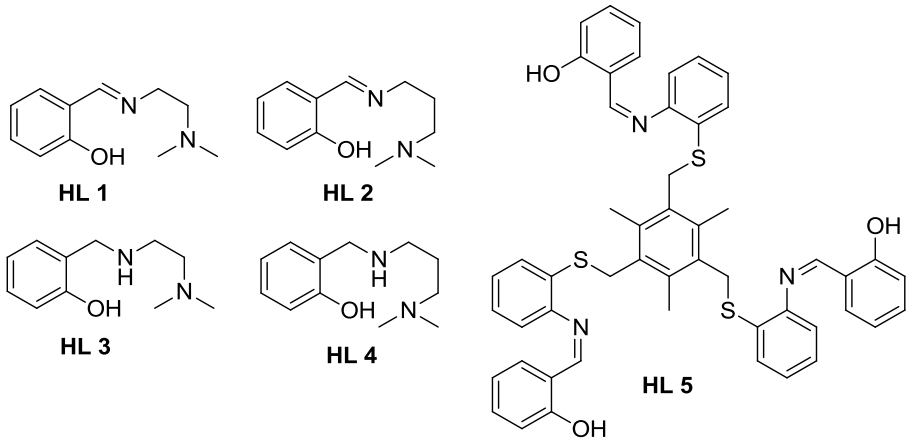

Figure 7.14. Various ligand systems employed in V. K. Bhardwaj *et al.* studies.

[11] V. K. Bhardwaj, N. Aliaga-Alcalde, M. Corbella, G. Hundal, *Inorg. Chim. Acta. 363 (**2010**)* 97.

Table 7.7. Rate constants for the oxidation of DTBC catalyzed by various dinuclear Cu(II) complexes (resourced from V. K. Bhardwaj *et al.*) .[11]

Complex	Rate constant (s^{-1}) x 10^{-4}
[{Cu(L1)}$_2$(l-$CH_3COO)_2$] (1)	7.72
[(CuL2)(CH_3COO)] (2)	6.08
[{Cu(CH_3COO)}$_2$(l-L3)$_2$] (3)	6.95
[{Cu(L4)}$_2$(l-($CH_3COO)_2$] (4)	13.53
[Cu_3(L5)($CH_3COO)_3$]. $3H_2O$ (5)	6.78

However, K. S. Banu *et al*. also reports dinuclear model complexes with observed rate constants of the order 10^1 which are highly catalytic (see Figure 7.15 and Table 7.8). [12]

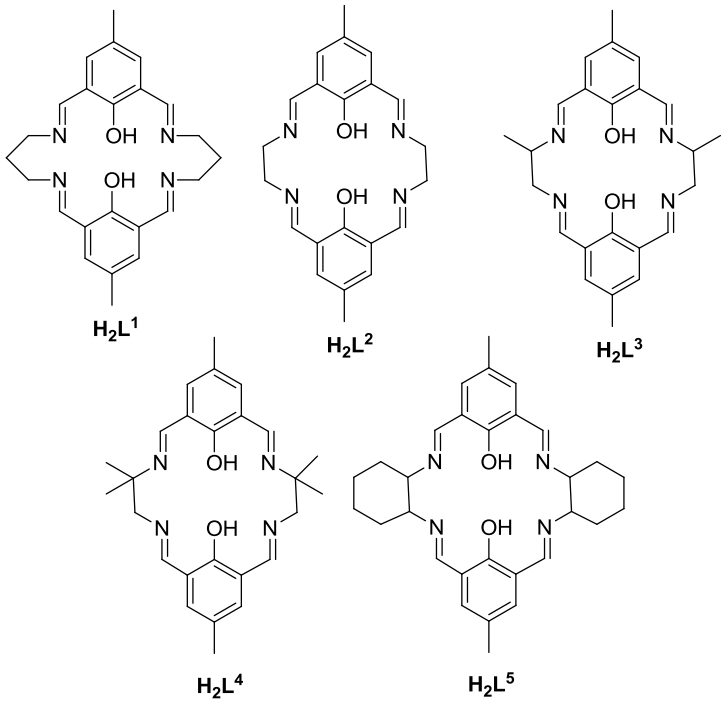

Figure 7.15.Various ligand systems employed in K.S. Banu *et al.* studies.

[12] K. S. Banua, T. Chattopadhyay, A. Banerjee, S. Bhattacharya, E. Zangrando, D. Das, *J. Mol. Catal. A Chem. 310 (2009)* 34.

Table 7.8. Observed rate constants for the oxidation of DTBC catalyzed by various dinuclear Cu(II) complexes (resourced from K. S. Banu *et al.*).[12]

Complex	Solvent	k_{cat} (s^{-1})
$[Cu_2L^1(N^3)_2 \cdot 2H_2O]$ (**1**)	Methanol	(5 ± 0.02)
$[Cu_2L^1(N^3)_2 \cdot 2H_2O]$ (**1**)	Acetonitrile	(6 ± 0.03)
$[Cu_2L^3(N^3)_2 \cdot 2H_2O]$ (**3**)	Acetonitrile	(3 ± 0.03)
$[Cu_2L^4(N^3)_2 \cdot 2H_2O]$ (**4**)	Acetonitrile	(5 ± 0.13)
$[Cu_2L^5(N^3)_2 \cdot 2H_2O]$ (**5**)	Acetonitrile	(6 ± 0.03)
$[Cu_2L^5(N^3)_2 \cdot 2H_2O]$ (**5**)	Methanol	(2 ± 0.18)

7.7 Conclusion

We have synthesized and characterized six copper(II) complexes which can act as potential catalysts for the oxidation of catechols to the corresponding quinones. These mononuclear copper(II) compounds imitate the catecholase activity of catechol oxidase, which is a type III Cu(II) protein. This activity was measured by monitoring the rate of the oxidation process of 3,5-di-*tert*-butylcatechol and a comparison was done between the complexes to determine which was more effective. This comparison showed that $[Cu(EP(naltol))_2]$ was the most active catalyst (although only twice as active as the other two), which implies that steric bulk or possibly less electron donating ability might enhance the process as the other complexes have substituents which were more electron donating, and the only other difference was that this particular complex was much more steric.

Another factor might be the hydrogen interactions observed in the two reported structures as ($[Cu(EP(naltol))_2]$) showed stronger interactions when compared to $[Cu((ME(naltol))_2]$ (d(H…A) ≈ 2.32 Å as opposed to d(H…A) ≈ 2.46 Å in $[Cu((ME(naltol))_2]$).

Comparison of the data obtained from this study strongly suggest that steric bulk has very significant effect on this oxidation process, which would make sense as the enzyme itself is a very sterically demanding molecule. If so we were successfully able to demonstrate this with simple nano materials at a smaller-molecular level of detail. At this point we cannot say with

absolute certainty which parameter(s) enhances the process. Further studies have to be conducted.

Based on the data observed both mechanisms reported are possible and none is favoured over the other.

However, the knowledge and experience gained with this study can be utilized to design more effective ligands and complexes in future.

8 Critical Evaluation of Study

8.1 Introduction

The scientific relevance and results of this M.Sc. study, as well as some future research possibilities are discussed in this chapter in terms of the pre-set aims outlined in chapter 1. One of the main objectives for this study was to obtain insights on the catalytic process by which copper oxidizes organic substrates. This required the synthesis of model compounds and the identification of suitable ligand systems for the synthesis which was then followed by the subsequent modelling of the complexes.

8.2 Results Obtained

8.2.1 Synthesis

Six *O'O*-bidentate ligands were successfully synthesized and characterized by IR, UV-VIS, NMR, elemental analysis and X-ray diffraction. Of the six two of the *O'O*-bidentate ligands have never been reported in literature namely; 3-Hydroxy-2-methyl-1-isopropyl-4-pyridone (MP(naltol)H) and 2-Ethyl-3-hydroxy-1-isopropyl-4-pyridone (EP(naltol)H). The crystal structure for the latter has already been published from this MSc study. The remaining four ligands are either polymorphs or different solvate compounds which can still be published as the completeness in these structures are very high and hence indicating good quality data.

Six copper(II) complexes were also synthesized in this study (from the corresponding six ligands). Four of these compounds have never been reported in literature; Bis(1-ethyl-3-hydroxy-2-methyl-4-pyridinonato)copper(II) [Cu((ME(naltol))$_2$], Bis(3-hydroxy-2-methyl-1-isopropyl-4-pyridinonato)copper(II) [Cu((MP(naltol))$_2$], Bis(2-ethyl-3-hydroxy-1-methyl-4-pyridinonato)copper(II) [Cu((EM(naltol))$_2$] and Bis(2-ethyl-3-hydroxy-1-isopropyl-4-pyridinonato)copper(II) [Cu((EP(naltol))$_2$]. Of the four compounds only two crystal structures

were obtained namely; [Cu((ME(naltol))$_2$] and [Cu((EP(naltol))$_2$]. In summary a total of six new compounds were synthesized for this MSc study.

8.2.2 Structural Insights

- All of the synthesized ligands were found to be in the ketone-enol tautomeric form in the solid state, this was observed from the basic molecular structures and the character of the O2—C2 and C3—O1 bond lengths) (see chapter 5).
- In all the cases where a clear packing order was observed, dimers were formed due to weak O—H…O hydrogen interactions (≈ 1.9 Å with bond angles ≈ 150 ˚) which primarily stabilized the structure.
- Most bond angles and bond lengths were comparable to the parent structures but indicated that the carbonyl length was slightly increased; assumed to be due to the functionalization brought about by synthetically manipulating the structure. The relative orientation of the two C—O moieties was only slightly altered as observed from the torsion angle of the parent molecule.
- As a full set of the ethyl maltol derivatives was obtained, it indicated that the increase in C=O bond length was in this order: methyl amine (0.034(3) Å) > Ethyl amine (A = 0.031(3) Å and B = 0.031(3) Å) > iso-propyl amine (A = 0.027(3) Å, B = 0.030(3) Å and C = 0.034(3) Å). The same pattern is also observed in the derivatives of M(altol)H.
- The complexes reported in this study are planar, and the dihedral angles between the plane of the aromatic ring and the O1-Cu-O2 plane are very small, with the largest being ≈ 4 ˚ deviation of ≈ 4 ˚ from planarity, and the O1-Cu-O2 bond angle being ≈ 86 ˚. These complexes lie on an inversion center at the Cu atom, while the nitrogen atoms are inaccessible for coordination as in all the complexes there was no such coordination or even interaction observed. This was assumed to be due to the steric bulk in the case of the [Cu(EP(naltol)$_2$)] as it has an *iso*-propyl attached to the nitrogen atom and thus rendering the lone pair on the nitrogen inaccessible. These compounds also show strong intermolecular hydrogen bonding.

8.2.3 Insights from Catalytic Modeling

The data from the solution studies indicates that either the least electron donating group in the series employed here (*iso*-propyl), steric bulk or the strength of the hydrogen bonding observed in the structures enhances the catalytic process. This is because the most effective complex [Cu((EP(naltol))$_2$] had an *iso*-propyl group and between the two crystal structures reported it had the strongest hydrogen interactions (d(H…A) ≈ 2.32 Å as opposed to d(H…A) ≈ 2.46 Å in [Cu((ME(naltol))$_2$]). From the data we conclude that both proposed mechanisms are possible as the data did not show any preference towards either one of them.

8.2.4 Shortcomings of the Study

Because the reactions took ≈ 6 days to run to completion it was impossible to prevent methanol evaporation at 25.0 °C over such a lengthy period of time. The same can also be said about the leakage of oxygen from the system or maintaining the oxygen concentration for ≈ 6 days. Due to time constraints as these reactions take a long time all the complexes were not modelled for catechol oxidase activity. However a credible selection ensured that all the aspect which were investigated could be illustrated in the complexes e.g. electron donating, steric bulk, etc. also due to time constraints temperature studies were not carried out in this study.

8.3 Future Research

An interesting result in the reactivity of the three complexes was observed during the oxidation of 3,5-di-*tert*-butylcatechol in this study. To fully comprehend this observed result additional experiments, as listed below, should be conducted.

- An extended kinetic evaluation to study the catalytic ability of the remaining complexes.
- Temperature studies to evaluate the effect of increased temperatures on the catalytic rates of the complexes
- The effect of various solvents on this catalytic process while employing these complexes, such a study would give further insight into a possible solvent effect in this process.

- Computational analyses to determine which parameter; steric or electronic, is the dominant factor in the enhancement of reaction rates.
- *In situ* analyses to identify the catalytic species in order to verify the actual mechanism.
- To investigate the capacity of electron donating groups and their influence in the catalytic oxidation to fully comprehend copper and its ability to act as an oxidising agent.
- Process optimization to enhance the catalytic process.

APPENDIX

A. Data for 3-Hydroxy-1,2-dimethyl-4-pyridone (1)

Table A. 1: Atomic coordinates (x 10^4) and equivalent isotropic displacement parameters ($Å^2$x 10^3) for 3-Hydroxy-1,2-dimethyl-4-pyridone (**1**). U(eq) is defined as one third of the trace of the orthogonalized U^{ij} tensor.

	x	y	z	U(eq)
O(1)	8694(1)	973(1)	5250(1)	16(1)
O(2)	9802(1)	-576(1)	6495(1)	16(1)
N(1)	8577(2)	1444(1)	8198(1)	13(1)
C(1)	9166(2)	502(1)	7840(1)	12(1)
C(2)	9240(2)	358(1)	6845(1)	12(1)
C(3)	8680(2)	1147(1)	6164(1)	12(1)
C(4)	8083(2)	2093(1)	6596(1)	13(1)
C(5)	8061(2)	2212(1)	7587(1)	13(1)
C(6)	8525(2)	1629(1)	9257(1)	17(1)
C(7)	9675(2)	-333(1)	8549(1)	14(1)

Table A. 2: Bond lengths [Å] and angles [°] for 3-Hydroxy-1,2-dimethyl-4-pyridone (**1**).

O(1)-C(3)	1.2715(15)
O(2)-C(2)	1.3596(14)
O(2)-H(2)	0.8200
N(1)-C(5)	1.3496(16)
N(1)-C(1)	1.3782(15)
N(1)-C(6)	1.4707(15)
C(1)-C(2)	1.3762(16)
C(1)-C(7)	1.4968(16)
C(2)-C(3)	1.4387(17)
C(3)-C(4)	1.4231(17)
C(4)-C(5)	1.3658(17)
C(4)-H(4)	0.9300
C(5)-H(5)	0.9300
C(6)-H(6A)	0.9600

C(6)-H(6B) 0.9600

C(6)-H(6C) 0.9600

C(7)-H(7A) 0.9600

C(7)-H(7B) 0.9600

C(7)-H(7C) 0.9600

C(2)-O(2)-H(2) 109.5

C(5)-N(1)-C(1) 120.81(10)

C(5)-N(1)-C(6) 119.06(11)

C(1)-N(1)-C(6) 120.12(10)

C(2)-C(1)-N(1) 118.90(11)

C(2)-C(1)-C(7) 122.39(11)

N(1)-C(1)-C(7) 118.71(11)

O(2)-C(2)-C(1) 118.72(11)

O(2)-C(2)-C(3) 118.85(10)

C(1)-C(2)-C(3) 122.40(11)

O(1)-C(3)-C(4) 124.32(11)

O(1)-C(3)-C(2) 120.71(11)

C(4)-C(3)-C(2) 114.95(11)

C(5)-C(4)-C(3) 120.91(11)

C(5)-C(4)-H(4) 119.5

C(3)-C(4)-H(4) 119.5

N(1)-C(5)-C(4) 122.01(11)

N(1)-C(5)-H(5) 119.0

C(4)-C(5)-H(5) 119.0

N(1)-C(6)-H(6A) 109.5

N(1)-C(6)-H(6B) 109.5

H(6A)-C(6)-H(6B) 109.5

N(1)-C(6)-H(6C) 109.5

H(6A)-C(6)-H(6C) 109.5

H(6B)-C(6)-H(6C) 109.5

C(1)-C(7)-H(7A) 109.5

C(1)-C(7)-H(7B) 109.5

H(7A)-C(7)-H(7B) 109.5

C(1)-C(7)-H(7C) 109.5

H(7A)-C(7)-H(7C) 109.5

H(7B)-C(7)-H(7C) 109.5

Table A.3. Anisotropic displacement parameters ($Å^2$x 10^3) for 3-Hydroxy-1,2-dimethyl-4-pyridone (**1**). The anisotropic displacement factor exponent takes the form: $-2\pi^2[h^2a^{*2}U^{11} + ... + 2 h k a^* b^* U^{12}]$

	U^{11}	U^{22}	U^{33}	U^{23}	U^{13}	U^{12}
O(1)	20(1)	18(1)	10(1)	-1(1)	0(1)	3(1)
O(2)	22(1)	14(1)	10(1)	-1(1)	2(1)	4(1)
N(1)	14(1)	14(1)	10(1)	-2(1)	1(1)	0(1)
C(1)	10(1)	13(1)	13(1)	0(1)	1(1)	-1(1)
C(2)	11(1)	11(1)	13(1)	0(1)	1(1)	0(1)
C(3)	11(1)	14(1)	12(1)	0(1)	0(1)	-1(1)
C(4)	15(1)	12(1)	12(1)	1(1)	0(1)	0(1)
C(5)	14(1)	11(1)	14(1)	-2(1)	1(1)	0(1)
C(6)	22(1)	19(1)	10(1)	-3(1)	2(1)	0(1)
C(7)	16(1)	16(1)	12(1)	2(1)	0(1)	1(1)

Table A.4.Hydrogen coordinates (x 10^4) and isotropic displacement parameters ($Å^2$x 10^3) for 3-Hydroxy-1,2-dimethyl-4-pyridone (**1**).

	x	y	z	U(eq)
H(2)	10007	-529	5907	23
H(4)	7703	2637	6198	16
H(5)	7678	2842	7848	16
H(6A)	8171	2333	9380	25
H(6B)	9736	1502	9530	25
H(6C)	7634	1171	9553	25
H(7A)	10661	-94	8965	22
H(7B)	10082	-936	8198	22
H(7C)	8607	-506	8938	22

Table A. 5. Torsion angles [°] for 3-Hydroxy-1,2-dimethyl-4-pyridone (**1**).

C(5)-N(1)-C(1)-C(2)	0.71(17)
C(6)-N(1)-C(1)-C(2)	-178.60(11)
C(5)-N(1)-C(1)-C(7)	-178.36(11)
C(6)-N(1)-C(1)-C(7)	2.33(17)
N(1)-C(1)-C(2)-O(2)	-179.29(11)
C(7)-C(1)-C(2)-O(2)	-0.26(18)
N(1)-C(1)-C(2)-C(3)	-1.60(18)
C(7)-C(1)-C(2)-C(3)	177.43(11)
O(2)-C(2)-C(3)-O(1)	0.60(18)
C(1)-C(2)-C(3)-O(1)	-177.09(12)
O(2)-C(2)-C(3)-C(4)	178.96(11)
C(1)-C(2)-C(3)-C(4)	1.27(17)
O(1)-C(3)-C(4)-C(5)	178.21(12)
C(2)-C(3)-C(4)-C(5)	-0.08(17)
C(1)-N(1)-C(5)-C(4)	0.47(18)
C(6)-N(1)-C(5)-C(4)	179.79(11)
C(3)-C(4)-C(5)-N(1)	-0.77(19)

Table A.6. Hydrogen bonds for 3-Hydroxy-1,2-dimethyl-4-pyridone (**1**) [Å and °].

D-H...A	d(D-H)	d(H...A)	d(D...A)	<(DHA)
O(2)-H(2)...O(1)$^{\#1}$	0.82	1.93	2.6712(13)	150.7

Symmetry transformations used to generate equivalent atoms: #1 -x+2,-y,-z+1

B. Data for 1-Ethyl-3-hydroxy-2-methyl-4-pyridone (2)

Table B.1. Atomic coordinates (x 10^4) and equivalent isotropic displacement parameters ($Å^2$x 10^3) for 1-Ethyl-3-hydroxy-2-methyl-4-pyridone (**2**). U(eq) is defined as one third of the trace of the orthogonalized U^{ij} tensor.

	x	y	z	U(eq)
O(1)	8937(1)	740(1)	5528(1)	18(1)
O(2)	10327(1)	1387(1)	3812(1)	18(1)
N(1)	8842(1)	4169(1)	4366(1)	15(1)
C(1)	9575(1)	3343(1)	3888(1)	15(1)
C(4)	8147(1)	2706(1)	5609(1)	18(1)
C(3)	8893(1)	1809(1)	5183(1)	14(1)
C(5)	8136(1)	3839(1)	5193(1)	17(1)
C(6)	8719(1)	5406(1)	3942(1)	18(1)
C(2)	9608(1)	2194(1)	4287(1)	14(1)
C(8)	10321(1)	3726(1)	2952(1)	20(1)
C(7)	7762(1)	5485(1)	3097(1)	21(1)

Table B.2. Bond lengths [Å] and angles [°] for 1-Ethyl-3-hydroxy-2-methyl-4-pyridone (**2**).

O(1)-C(3)	1.2669(13)
O(2)-C(2)	1.3562(13)
N(1)-C(5)	1.3554(14)
N(1)-C(1)	1.3814(14)
N(1)-C(6)	1.4816(14)
C(1)-C(2)	1.3727(15)
C(1)-C(8)	1.4992(15)
C(4)-C(5)	1.3637(16)
C(4)-C(3)	1.4188(15)
C(3)-C(2)	1.4424(14)
C(6)-C(7)	1.5191(15)
C(5)-N(1)-C(1)	120.46(9)
C(5)-N(1)-C(6)	117.43(9)
C(1)-N(1)-C(6)	121.91(9)

C(2)-C(1)-N(1)	119.06(9)
C(2)-C(1)-C(8)	121.71(9)
N(1)-C(1)-C(8)	119.22(9)
C(5)-C(4)-C(3)	121.27(10)
O(1)-C(3)-C(4)	124.20(10)
O(1)-C(3)-C(2)	120.98(9)
C(4)-C(3)-C(2)	114.82(9)
N(1)-C(5)-C(4)	121.91(10)
N(1)-C(6)-C(7)	111.38(9)
O(2)-C(2)-C(1)	118.79(9)
O(2)-C(2)-C(3)	118.77(9)
C(1)-C(2)-C(3)	122.43(9)

Table B.3. Anisotropic displacement parameters ($Å^2 x\ 10^3$) for 1-Ethyl-3-hydroxy-2-methyl-4-pyridone (**2**). The anisotropic displacement factor exponent takes the form: $-2\pi^2[\ h^2 a^{*2} U^{11} + ... + 2\ h\ k\ a^*\ b^*\ U^{12}\ ]$

	U11	U22	U33	U23	U13	U12
O(1)	20(1)	14(1)	19(1)	2(1)	2(1)	0(1)
O(2)	20(1)	16(1)	19(1)	3(1)	6(1)	4(1)
N(1)	17(1)	12(1)	16(1)	1(1)	-2(1)	0(1)
C(1)	13(1)	17(1)	14(1)	0(1)	-2(1)	-1(1)
C(4)	20(1)	18(1)	16(1)	0(1)	4(1)	0(1)
C(3)	16(1)	13(1)	14(1)	0(1)	-1(1)	-1(1)
C(5)	18(1)	17(1)	17(1)	-2(1)	1(1)	2(1)
C(6)	20(1)	13(1)	21(1)	2(1)	-3(1)	0(1)
C(2)	14(1)	15(1)	14(1)	-1(1)	-1(1)	0(1)
C(8)	20(1)	20(1)	20(1)	6(1)	2(1)	1(1)
C(7)	21(1)	25(1)	18(1)	3(1)	-2(1)	4(1)

Table B.4. Hydrogen coordinates ($x\ 10^4$) and isotropic displacement parameters ($Å^2 x\ 10^3$) for 1-Ethyl-3-hydroxy-2-methyl-4-pyridone (**2**).

	x	y	z	U(eq)
H(2)	10326	748	4173	28

H(4)	7645	2512	6195	22
H(5)	7618	4414	5493	21
H(6A)	9463	5664	3614	21
H(6B)	8540	5957	4549	21
H(8A)	9831	4073	2383	30
H(8B)	10736	3029	2663	30
H(8C)	10882	4327	3200	30
H(7A)	7964	4984	2472	32
H(7B)	7674	6320	2861	32
H(7C)	7030	5203	3413	32

Table B.5. Torsion angles [°] for 1-Ethyl-3-hydroxy-2-methyl-4-pyridone (**2**).

C(5)-N(1)-C(1)-C(2)	-2.17(14)
C(6)-N(1)-C(1)-C(2)	-176.88(9)
C(5)-N(1)-C(1)-C(8)	178.24(9)
C(6)-N(1)-C(1)-C(8)	3.53(14)
C(5)-C(4)-C(3)-O(1)	-179.47(10)
C(5)-C(4)-C(3)-C(2)	-0.68(15)
C(1)-N(1)-C(5)-C(4)	2.23(15)
C(6)-N(1)-C(5)-C(4)	177.18(10)
C(3)-C(4)-C(5)-N(1)	-0.75(16)
C(5)-N(1)-C(6)-C(7)	-85.05(12)
C(1)-N(1)-C(6)-C(7)	89.82(12)
N(1)-C(1)-C(2)-O(2)	179.80(8)
C(8)-C(1)-C(2)-O(2)	-0.62(15)
N(1)-C(1)-C(2)-C(3)	0.70(15)
C(8)-C(1)-C(2)-C(3)	-179.72(9)
O(1)-C(3)-C(2)-O(2)	0.42(15)
C(4)-C(3)-C(2)-O(2)	-178.41(9)
O(1)-C(3)-C(2)-C(1)	179.52(9)
C(4)-C(3)-C(2)-C(1)	0.69(14)

Table B.6. Hydrogen bonds for 1-Ethyl-3-hydroxy-2-methyl-4-pyridone (**2**) [Å and °].

D-H...A	d(D-H)	d(H...A)	d(D...A)	<(DHA)
O(2)-H(2)...O(1)$^{\#1}$	0.84	1.90	2.6464(14)	147.4

Symmetry transformations used to generate equivalent atoms: #1 -x+2,-y,-z+1

C. Data for 2-Ethyl-3-hydroxy-1-methyl-4-pyridone (4)

Table C.1. Atomic coordinates (x 10^4) and equivalent isotropic displacement parameters (Å^{2}x 10^3) for 2-Ethyl-3-hydroxy-1-methyl-4-pyridone (**4**). U(eq) is defined as one third of the trace of the orthogonalized U^{ij} tensor.

	x	y	z	U(eq)
O(1A)	1572(1)	4942(1)	9172(1)	18(1)
O(1B)	-3757(1)	11342(1)	5768(1)	19(1)
O(2B)	-6639(1)	9857(1)	6345(1)	22(1)
O(2A)	-1292(1)	6332(1)	8729(1)	21(1)
N(1A)	374(1)	7010(1)	5964(1)	16(1)
C(1A)	-676(1)	7014(1)	6820(1)	15(1)
C(2A)	-255(1)	6310(1)	7892(1)	15(1)
C(3B)	-4170(1)	11608(1)	6789(1)	16(1)
N(1B)	-5157(1)	12079(1)	9060(1)	17(1)
C(4A)	2248(1)	5616(1)	7233(1)	17(1)
C(1B)	-6114(1)	11032(1)	8262(1)	17(1)
C(3A)	1233(1)	5564(1)	8164(1)	14(1)
C(6A)	-11(1)	7713(1)	4785(1)	20(1)
C(2B)	-5661(1)	10839(1)	7141(1)	16(1)
C(5A)	1800(1)	6341(1)	6183(1)	18(1)
C(6B)	-5627(2)	12397(2)	10251(1)	22(1)
C(7A)	-2269(1)	7737(1)	6571(1)	21(1)
C(7B)	-7599(1)	10087(1)	8633(1)	20(1)
C(4B)	-3253(1)	12646(1)	7671(1)	20(1)
C(5B)	-3769(1)	12861(1)	8759(1)	20(1)
C(8B)	-9183(1)	10880(2)	8345(1)	25(1)
C(8A)	-3602(2)	6583(2)	5892(1)	34(1)

Table C.2. Bond lengths [Å] and angles [°] for 2-Ethyl-3-hydroxy-1-methyl-4-pyridone (**4**).

O(1A)-C(3A)	1.2687(12)
O(1B)-C(3B)	1.2654(12)
O(2B)-C(2B)	1.3552(13)
O(2A)-C(2A)	1.3535(12)
N(1A)-C(5A)	1.3536(14)

N(1A)-C(1A)	1.3774(13)
N(1A)-C(6A)	1.4729(13)
C(1A)-C(2A)	1.3735(14)
C(1A)-C(7A)	1.5026(15)
C(2A)-C(3A)	1.4372(15)
C(3B)-C(4B)	1.4187(15)
C(3B)-C(2B)	1.4437(14)
N(1B)-C(5B)	1.3553(14)
N(1B)-C(1B)	1.3798(14)
N(1B)-C(6B)	1.4725(13)
C(4A)-C(5A)	1.3657(15)
C(4A)-C(3A)	1.4227(14)
C(1B)-C(2B)	1.3759(14)
C(1B)-C(7B)	1.5095(15)
C(7A)-C(8A)	1.5302(18)
C(7B)-C(8B)	1.5294(17)
C(4B)-C(5B)	1.3649(15)
C(5A)-N(1A)-C(1A)	120.47(9)
C(5A)-N(1A)-C(6A)	117.76(9)
C(1A)-N(1A)-C(6A)	121.76(9)
C(2A)-C(1A)-N(1A)	118.69(10)
C(2A)-C(1A)-C(7A)	120.81(9)
N(1A)-C(1A)-C(7A)	120.48(9)
O(2A)-C(2A)-C(1A)	118.09(9)
O(2A)-C(2A)-C(3A)	118.87(9)
C(1A)-C(2A)-C(3A)	123.05(9)
O(1B)-C(3B)-C(4B)	124.55(10)
O(1B)-C(3B)-C(2B)	120.84(10)
C(4B)-C(3B)-C(2B)	114.61(9)
C(5B)-N(1B)-C(1B)	120.62(9)
C(5B)-N(1B)-C(6B)	118.25(9)
C(1B)-N(1B)-C(6B)	121.12(9)

C(5A)-C(4A)-C(3A)	120.72(10)
C(2B)-C(1B)-N(1B)	118.72(10)
C(2B)-C(1B)-C(7B)	121.05(10)
N(1B)-C(1B)-C(7B)	120.20(9)
O(1A)-C(3A)-C(4A)	124.73(10)
O(1A)-C(3A)-C(2A)	120.59(9)
C(4A)-C(3A)-C(2A)	114.68(9)
O(2B)-C(2B)-C(1B)	118.49(9)
O(2B)-C(2B)-C(3B)	118.80(9)
C(1B)-C(2B)-C(3B)	122.69(10)
N(1A)-C(5A)-C(4A)	122.37(10)
C(1A)-C(7A)-C(8A)	112.42(10)
C(1B)-C(7B)-C(8B)	114.23(9)
C(5B)-C(4B)-C(3B)	121.25(10)
N(1B)-C(5B)-C(4B)	122.00(10)

Table C.3. Anisotropic displacement parameters ($Å^2 x\ 10^3$) for 2-Ethyl-3-hydroxy-1-methyl-4-pyridone (**4**). The anisotropic displacement factor exponent takes the form: $-2\pi^2[\ h^2 a^{*2} U^{11} + ... + 2\ h\ k\ a^*\ b^*\ U^{12}\ ]$

	U^{11}	U^{22}	U^{33}	U^{23}	U^{13}	U^{12}
O(1A)	17(1)	22(1)	14(1)	2(1)	1(1)	2(1)
O(1B)	19(1)	22(1)	15(1)	-2(1)	4(1)	-1(1)
O(2B)	20(1)	26(1)	18(1)	-7(1)	7(1)	-7(1)
O(2A)	19(1)	30(1)	16(1)	6(1)	7(1)	8(1)
N(1A)	15(1)	18(1)	14(1)	2(1)	3(1)	-1(1)
C(1A)	14(1)	16(1)	16(1)	0(1)	3(1)	0(1)
C(2A)	14(1)	16(1)	15(1)	-1(1)	4(1)	0(1)
C(3B)	16(1)	16(1)	15(1)	1(1)	2(1)	2(1)
N(1B)	19(1)	20(1)	14(1)	-1(1)	2(1)	3(1)
C(4A)	13(1)	21(1)	18(1)	0(1)	3(1)	2(1)
C(1B)	18(1)	16(1)	16(1)	1(1)	3(1)	2(1)
C(3A)	14(1)	14(1)	14(1)	-2(1)	1(1)	-1(1)
C(6A)	20(1)	25(1)	15(1)	5(1)	2(1)	-2(1)
C(2B)	17(1)	15(1)	16(1)	-2(1)	2(1)	0(1)
C(5A)	15(1)	21(1)	17(1)	0(1)	5(1)	-1(1)
C(6B)	24(1)	30(1)	14(1)	-3(1)	4(1)	7(1)
C(7A)	19(1)	25(1)	21(1)	6(1)	5(1)	8(1)
C(7B)	22(1)	20(1)	20(1)	1(1)	7(1)	0(1)
C(4B)	18(1)	22(1)	19(1)	-2(1)	2(1)	-4(1)
C(5B)	20(1)	21(1)	18(1)	-4(1)	0(1)	-1(1)
C(8B)	19(1)	28(1)	27(1)	1(1)	4(1)	0(1)
C(8A)	15(1)	35(1)	49(1)	11(1)	-3(1)	3(1)

Table C.4. Hydrogen coordinates (x 10^4) and isotropic displacement parameters ($Å^2$x 10^3) for 2-Ethyl-3-hydroxy-1-methyl-4-pyridone (**4**).

	x	y	z	U(eq)
H(2B)	-6182	9755	5728	33
H(2A)	-911	5862	9339	31
H(4A)	3250	5141	7344	21
H(6AA)	-689	6924	4253	31
H(6AB)	1003	8025	4447	31
H(6AC)	-602	8656	4869	31
H(5A)	2514	6377	5584	21
H(6BA)	-6731	12739	10167	33
H(6BB)	-4863	13242	10658	33
H(6BC)	-5598	11421	10718	33
H(7AA)	-2107	8712	6098	25
H(7AB)	-2628	8057	7336	25
H(7BA)	-7417	9916	9503	24
H(7BB)	-7727	9024	8230	24
H(4B)	-2261	13202	7500	24
H(5B)	-3135	13582	9322	24
H(8BA)	-9400	11015	7482	37
H(8BB)	-9078	11927	8750	37
H(8BC)	-10085	10205	8620	37
H(8AA)	-3295	6336	5104	50
H(8AB)	-4632	7079	5797	50
H(8AC)	-3733	5596	6339	50

Table C.5. Torsion angles [°] for 2-Ethyl-3-hydroxy-1-methyl-4-pyridone (**4**).

C(5A)-N(1A)-C(1A)-C(2A)	-0.77(15)
C(6A)-N(1A)-C(1A)-C(2A)	178.71(9)
C(5A)-N(1A)-C(1A)-C(7A)	-179.16(10)
C(6A)-N(1A)-C(1A)-C(7A)	0.32(16)
N(1A)-C(1A)-C(2A)-O(2A)	179.55(9)
C(7A)-C(1A)-C(2A)-O(2A)	-2.07(16)
N(1A)-C(1A)-C(2A)-C(3A)	-0.09(16)
C(7A)-C(1A)-C(2A)-C(3A)	178.30(10)
C(5B)-N(1B)-C(1B)-C(2B)	-2.15(16)
C(6B)-N(1B)-C(1B)-C(2B)	176.78(10)
C(5B)-N(1B)-C(1B)-C(7B)	176.07(10)
C(6B)-N(1B)-C(1B)-C(7B)	-5.00(15)
C(5A)-C(4A)-C(3A)-O(1A)	-178.62(10)
C(5A)-C(4A)-C(3A)-C(2A)	0.44(15)
O(2A)-C(2A)-C(3A)-O(1A)	-0.28(15)

C(1A)-C(2A)-C(3A)-O(1A)	179.35(10)
O(2A)-C(2A)-C(3A)-C(4A)	-179.39(9)
C(1A)-C(2A)-C(3A)-C(4A)	0.24(15)
N(1B)-C(1B)-C(2B)-O(2B)	-177.48(9)
C(7B)-C(1B)-C(2B)-O(2B)	4.33(16)
N(1B)-C(1B)-C(2B)-C(3B)	4.08(16)
C(7B)-C(1B)-C(2B)-C(3B)	-174.11(10)
O(1B)-C(3B)-C(2B)-O(2B)	-1.81(16)
C(4B)-C(3B)-C(2B)-O(2B)	178.32(10)
O(1B)-C(3B)-C(2B)-C(1B)	176.63(10)
C(4B)-C(3B)-C(2B)-C(1B)	-3.24(16)
C(1A)-N(1A)-C(5A)-C(4A)	1.50(16)
C(6A)-N(1A)-C(5A)-C(4A)	-178.00(10)
C(3A)-C(4A)-C(5A)-N(1A)	-1.33(17)
C(2A)-C(1A)-C(7A)-C(8A)	-95.48(13)
N(1A)-C(1A)-C(7A)-C(8A)	82.87(13)
C(2B)-C(1B)-C(7B)-C(8B)	-88.83(13)
N(1B)-C(1B)-C(7B)-C(8B)	93.00(12)
O(1B)-C(3B)-C(4B)-C(5B)	-179.31(11)
C(2B)-C(3B)-C(4B)-C(5B)	0.55(16)
C(1B)-N(1B)-C(5B)-C(4B)	-0.48(17)
C(6B)-N(1B)-C(5B)-C(4B)	-179.44(11)
C(3B)-C(4B)-C(5B)-N(1B)	1.25(18)

Table C.6. Hydrogen bonds for 2-Ethyl-3-hydroxy-1-methyl-4-pyridone (**4**) [Å and °].

D-H...A	d(D-H)	d(H...A)	d(D...A)	<(DHA)
O(2B)-H(2B)...O(1B)$^{\#1}$	0.84	1.91	2.6508(11)	146.3
O(2A)-H(2A)...O(1A)$^{\#2}$	0.84	1.94	2.6370(11)	139.8

Symmetry transformations used to generate equivalent atoms:
#1 -x-1,-y+2,-z+1 #2 -x,-y+1,-z+2

D. Data for 1,2-Diethyl-3-hydroxy-4-pyridone (5)

Table D. 1. Atomic coordinates (x 10^4) and equivalent isotropic displacement parameters ($Å^2$x 10^3) for 1,2-Diethyl-3-hydroxy-4-pyridone(**5**). U(eq) is defined as one third of the trace of the orthogonalized U^{ij} tensor.

	x	y	z	U(eq)
O(1)	1454(1)	6320(1)	5295(1)	24(1)
O(2)	-1206(1)	5046(1)	6420(1)	21(1)
C(2)	-174(1)	6173(1)	6775(1)	16(1)
C(4)	2178(1)	7996(1)	6596(1)	21(1)
C(1)	-449(1)	6627(1)	7730(1)	17(1)
C(3)	1187(1)	6813(1)	6154(1)	17(1)
N(1)	573(1)	7781(1)	8103(1)	17(1)
C(5)	1850(1)	8428(1)	7540(1)	20(1)
C(6)	421(1)	8280(1)	9144(1)	22(1)
C(8)	-1882(1)	5890(1)	8339(1)	22(1)
C(9)	-3891(1)	6409(1)	8070(1)	29(1)
C(7)	1683(2)	7410(1)	9866(1)	30(1)

Table D.2. Bond lengths [Å] and angles [°] for 1,2-Diethyl-3-hydroxy-4-pyridone (**5**).

O(1)-C(3)	1.2653(11)
O(2)-C(2)	1.3548(10)
C(2)-C(1)	1.3751(12)
C(2)-C(3)	1.4388(12)
C(4)-C(5)	1.3632(13)
C(4)-C(3)	1.4227(12)
C(1)-N(1)	1.3785(11)
C(1)-C(8)	1.5050(12)
N(1)-C(5)	1.3523(12)
N(1)-C(6)	1.4835(11)
C(6)-C(7)	1.5196(14)
C(8)-C(9)	1.5299(14)
O(2)-C(2)-C(1)	117.89(8)
O(2)-C(2)-C(3)	119.10(8)
C(1)-C(2)-C(3)	122.99(8)
C(5)-C(4)-C(3)	120.89(8)

C(2)-C(1)-N(1)	118.89(8)
C(2)-C(1)-C(8)	119.91(8)
N(1)-C(1)-C(8)	121.18(8)
O(1)-C(3)-C(4)	124.68(8)
O(1)-C(3)-C(2)	120.89(8)
C(4)-C(3)-C(2)	114.42(8)
C(5)-N(1)-C(1)	120.09(7)
C(5)-N(1)-C(6)	118.01(8)
C(1)-N(1)-C(6)	121.74(8)
N(1)-C(5)-C(4)	122.67(8)
N(1)-C(6)-C(7)	111.32(8)
C(1)-C(8)-C(9)	111.92(8)

Table D. 3. Anisotropic displacement parameters ($Å^2 x\ 10^3$)for 1,2-Diethyl-3-hydroxy-4-pyridone (**5**). The anisotropic displacement factor exponent takes the form: $-2\pi^2[h^2 a^{*2} U^{11} + ... + 2 h k a^* b^* U^{12}]$

	U^{11}	U^{22}	U^{33}	U^{23}	U^{13}	U^{12}
O(1)	24(1)	30(1)	19(1)	-7(1)	6(1)	-6(1)
O(2)	26(1)	21(1)	18(1)	-5(1)	5(1)	-7(1)
C(2)	16(1)	16(1)	17(1)	0(1)	0(1)	0(1)
C(4)	18(1)	24(1)	20(1)	-1(1)	3(1)	-4(1)
C(1)	16(1)	17(1)	17(1)	0(1)	0(1)	1(1)
C(3)	16(1)	20(1)	16(1)	-1(1)	1(1)	1(1)
N(1)	16(1)	20(1)	16(1)	-3(1)	1(1)	1(1)
C(5)	18(1)	21(1)	22(1)	-3(1)	0(1)	-3(1)
C(6)	23(1)	27(1)	17(1)	-8(1)	3(1)	-1(1)
C(8)	25(1)	24(1)	17(1)	-1(1)	5(1)	-5(1)
C(9)	21(1)	29(1)	38(1)	-7(1)	9(1)	-5(1)
C(7)	27(1)	44(1)	18(1)	-4(1)	-3(1)	-1(1)

Table D.4. Hydrogen coordinates ($x\ 10^4$) and isotropic displacement parameters ($Å^2 x\ 10^3$) for 1,2-Diethyl-3-hydroxy-4-pyridone (**5**).

	x	y	z	U(eq)
H(2)	-933	4873	5831	32
H(4)	3081	8491	6227	25
H(5)	2547	9215	7815	24

H(6A)	-906	8197	9332	26
H(6B)	787	9301	9191	26
H(8A)	-1576	6073	9056	26
H(8B)	-1814	4845	8228	26
H(9A)	-4199	6230	7361	44
H(9B)	-3977	7436	8204	44
H(9C)	-4783	5892	8471	44
H(7A)	3004	7528	9700	45
H(7B)	1333	6398	9814	45
H(7C)	1525	7744	10548	45

Table D.5. Torsion angles [°] for 1,2-Diethyl-3-hydroxy-4-pyridone (**5**).

O(2)-C(2)-C(1)-N(1)	-179.36(7)
C(3)-C(2)-C(1)-N(1)	2.36(13)
O(2)-C(2)-C(1)-C(8)	-0.91(12)
C(3)-C(2)-C(1)-C(8)	-179.18(8)
C(5)-C(4)-C(3)-O(1)	-177.64(9)
C(5)-C(4)-C(3)-C(2)	1.43(13)
O(2)-C(2)-C(3)-O(1)	-1.46(13)
C(1)-C(2)-C(3)-O(1)	176.79(8)
O(2)-C(2)-C(3)-C(4)	179.42(8)
C(1)-C(2)-C(3)-C(4)	-2.32(13)
C(2)-C(1)-N(1)-C(5)	-1.42(12)
C(8)-C(1)-N(1)-C(5)	-179.85(8)
C(2)-C(1)-N(1)-C(6)	-176.71(8)
C(8)-C(1)-N(1)-C(6)	4.85(13)
C(1)-N(1)-C(5)-C(4)	0.61(14)
C(6)-N(1)-C(5)-C(4)	176.07(8)
C(3)-C(4)-C(5)-N(1)	-0.67(15)
C(5)-N(1)-C(6)-C(7)	-92.48(10)
C(1)-N(1)-C(6)-C(7)	82.91(10)
C(2)-C(1)-C(8)-C(9)	-80.47(11)
N(1)-C(1)-C(8)-C(9)	97.95(10)

Table D.6. Hydrogen bonds for 1,2-Diethyl-3-hydroxy-4-pyridone (**5**) [Å and °].

D-H...A	d(D-H)	d(H...A)	d(D...A)	<(DHA)
O(2)-H(2)...O(1)$^{\#1}$	0.84	1.90	2.6318(9)	144.9

Symmetry transformations used to generate equivalent atoms: #1 -x,-y+1,-z+1

E. Data for 2-Ethyl-3-hydroxy-1-isopropyl-4-pyridone (6)

Table E.1. Atomic coordinates (x 10^4) and equivalent isotropic displacement parameters ($Å^2$x 10^3) for 2-Ethyl-3-hydroxy-1-isopropyl-4-pyridone (**6**). U(eq) is defined as one third of the trace of the orthogonalized U^{ij} tensor.

	x	y	z	U(eq)
O(1A)	4340(1)	-394(1)	362(1)	23(1)
O(2A)	4070(1)	1381(1)	-4(1)	22(1)
N(1A)	1595(1)	1408(1)	563(1)	19(1)
C(5A)	1745(1)	546(1)	747(1)	23(1)
C(1A)	2396(1)	1695(1)	313(1)	17(1)
C(3A)	3491(1)	153(1)	428(1)	18(1)
C(6A)	567(1)	2030(1)	647(1)	23(1)
C(4A)	2649(1)	-68(1)	689(1)	24(1)
C(7A)	-513(1)	1410(1)	614(1)	38(1)
C(2A)	3307(1)	1083(1)	244(1)	16(1)
C(9A)	2262(1)	2652(1)	108(1)	23(1)
C(8A)	688(1)	2489(1)	1015(1)	28(1)
C(10A)	1560(1)	2493(1)	-228(1)	33(1)
O(1B)	9129(1)	1965(1)	1734(1)	18(1)
O(2B)	8281(1)	181(1)	1471(1)	24(1)
N(1B)	5998(1)	1882(1)	1255(1)	16(1)
C(2B)	7678(1)	1046(1)	1446(1)	17(1)
C(3B)	8151(1)	1947(1)	1594(1)	15(1)
C(1B)	6634(1)	1012(1)	1281(1)	17(1)
C(10B)	6792(1)	-233(1)	777(1)	34(1)
C(5B)	6392(1)	2739(1)	1405(1)	18(1)
C(6B)	4831(1)	1876(1)	1095(1)	20(1)
C(4B)	7421(1)	2793(1)	1569(1)	18(1)
C(8B)	3968(1)	1590(1)	1380(1)	27(1)
C(9B)	6215(1)	37(1)	1127(1)	23(1)
C(7B)	4537(1)	2871(1)	921(1)	23(1)
O(2C)	10861(1)	1271(1)	2082(1)	21(1)
O(1C)	10520(1)	-44(1)	1517(1)	19(1)
N(1C)	13390(1)	-248(1)	2134(1)	15(1)
C(1C)	12575(1)	465(1)	2213(1)	15(1)
C(6C)	14432(1)	-367(1)	2360(1)	18(1)
C(2C)	11622(1)	544(1)	2001(1)	15(1)
C(3C)	11412(1)	-116(1)	1706(1)	15(1)
C(5C)	13220(1)	-889(1)	1860(1)	18(1)
C(4C)	12277(1)	-842(1)	1650(1)	17(1)
C(8C)	14232(1)	-1194(1)	2631(1)	24(1)
C(9C)	12736(1)	1171(1)	2520(1)	18(1)
C(7C)	15487(1)	-540(1)	2133(1)	22(1)
C(10C)	13417(1)	2101(1)	2414(1)	24(1)

Table E.2. Bond lengths [Å] and angles [°] for 2-Ethyl-3-hydroxy-1-isopropyl-4-pyridone (**6**).

O(1A)-C(3A)	1.2614(15)
O(2A)-C(2A)	1.3532(15)
N(1A)-C(5A)	1.3547(17)
N(1A)-C(1A)	1.3834(16)
N(1A)-C(6A)	1.4979(16)
C(5A)-C(4A)	1.3595(19)
C(1A)-C(2A)	1.3702(17)
C(1A)-C(9A)	1.5000(17)
C(3A)-C(4A)	1.4218(18)
C(3A)-C(2A)	1.4378(17)
C(6A)-C(8A)	1.5185(19)
C(6A)-C(7A)	1.519(2)
C(9A)-C(10A)	1.523(2)
O(1B)-C(3B)	1.2642(15)
O(2B)-C(2B)	1.3588(14)
N(1B)-C(5B)	1.3562(16)
N(1B)-C(1B)	1.3849(15)
N(1B)-C(6B)	1.4960(16)
C(2B)-C(1B)	1.3729(17)
C(2B)-C(3B)	1.4382(17)
C(3B)-C(4B)	1.4209(17)
C(1B)-C(9B)	1.5072(17)
C(10B)-C(9B)	1.523(2)
C(5B)-C(4B)	1.3581(18)
C(6B)-C(8B)	1.5203(19)
C(6B)-C(7B)	1.5218(18)
O(2C)-C(2C)	1.3543(14)
O(1C)-C(3C)	1.2690(15)
N(1C)-C(5C)	1.3539(15)
N(1C)-C(1C)	1.3817(15)
N(1C)-C(6C)	1.4975(15)
C(1C)-C(2C)	1.3765(17)
C(1C)-C(9C)	1.5029(16)
C(6C)-C(8C)	1.5202(18)
C(6C)-C(7C)	1.5207(18)
C(2C)-C(3C)	1.4355(17)
C(3C)-C(4C)	1.4204(17)
C(5C)-C(4C)	1.3615(17)
C(9C)-C(10C)	1.5294(18)

C(5A)-N(1A)-C(1A)	119.52(11)
C(5A)-N(1A)-C(6A)	117.93(11)
C(1A)-N(1A)-C(6A)	122.54(10)
N(1A)-C(5A)-C(4A)	122.14(12)
C(2A)-C(1A)-N(1A)	119.65(11)
C(2A)-C(1A)-C(9A)	119.53(11)
N(1A)-C(1A)-C(9A)	120.80(11)
O(1A)-C(3A)-C(4A)	124.39(12)
O(1A)-C(3A)-C(2A)	121.65(11)
C(4A)-C(3A)-C(2A)	113.95(11)
N(1A)-C(6A)-C(8A)	109.83(11)
N(1A)-C(6A)-C(7A)	110.73(12)
C(8A)-C(6A)-C(7A)	111.91(12)
C(5A)-C(4A)-C(3A)	121.92(12)

O(2A)-C(2A)-C(1A)	118.19(11)
O(2A)-C(2A)-C(3A)	119.04(11)
C(1A)-C(2A)-C(3A)	122.76(11)
C(1A)-C(9A)-C(10A)	111.32(11)
C(5B)-N(1B)-C(1B)	119.67(10)
C(5B)-N(1B)-C(6B)	118.92(10)
C(1B)-N(1B)-C(6B)	121.17(10)
O(2B)-C(2B)-C(1B)	117.95(10)
O(2B)-C(2B)-C(3B)	118.90(11)
C(1B)-C(2B)-C(3B)	123.15(11)
O(1B)-C(3B)-C(4B)	124.08(11)
O(1B)-C(3B)-C(2B)	121.89(11)
C(4B)-C(3B)-C(2B)	114.04(11)
C(2B)-C(1B)-N(1B)	119.00(11)
C(2B)-C(1B)-C(9B)	119.54(10)
N(1B)-C(1B)-C(9B)	121.45(11)
N(1B)-C(5B)-C(4B)	122.48(11)
N(1B)-C(6B)-C(8B)	109.23(11)
N(1B)-C(6B)-C(7B)	112.09(10)
C(8B)-C(6B)-C(7B)	111.75(11)
C(5B)-C(4B)-C(3B)	121.56(11)
C(1B)-C(9B)-C(10B)	112.94(11)
C(5C)-N(1C)-C(1C)	119.73(10)
C(5C)-N(1C)-C(6C)	118.94(10)
C(1C)-N(1C)-C(6C)	121.23(10)
C(2C)-C(1C)-N(1C)	119.50(11)
C(2C)-C(1C)-C(9C)	119.85(10)
N(1C)-C(1C)-C(9C)	120.62(10)
N(1C)-C(6C)-C(8C)	109.33(10)
N(1C)-C(6C)-C(7C)	111.33(10)
C(8C)-C(6C)-C(7C)	113.05(10)
O(2C)-C(2C)-C(1C)	117.50(10)
O(2C)-C(2C)-C(3C)	119.97(11)
C(1C)-C(2C)-C(3C)	122.53(11)
O(1C)-C(3C)-C(4C)	123.88(11)
O(1C)-C(3C)-C(2C)	121.81(11)
C(4C)-C(3C)-C(2C)	114.31(11)
N(1C)-C(5C)-C(4C)	122.12(11)
C(5C)-C(4C)-C(3C)	121.74(11)
C(1C)-C(9C)-C(10C)	111.98(10)

Table E.3. Anisotropic displacement parameters ($Å^2 \times 10^3$) for 2-Ethyl-3-hydroxy-1-isopropyl-4-pyridone (**6**). The anisotropic displacement factor exponent takes the form: $-2\pi^2[h^2 a^{*2} U^{11} + ... + 2 h k a^* b^* U^{12}]$

	U^{11}	U^{22}	U^{33}	U^{23}	U^{13}	U^{12}
O(1A)	21(1)	22(1)	28(1)	4(1)	3(1)	5(1)
O(2A)	21(1)	17(1)	28(1)	3(1)	7(1)	1(1)
N(1A)	20(1)	19(1)	17(1)	1(1)	2(1)	4(1)
C(5A)	24(1)	24(1)	21(1)	5(1)	5(1)	2(1)
C(1A)	20(1)	17(1)	15(1)	-1(1)	-2(1)	-1(1)
C(3A)	18(1)	18(1)	19(1)	-1(1)	-2(1)	0(1)
C(6A)	21(1)	25(1)	23(1)	2(1)	3(1)	8(1)
C(4A)	27(1)	21(1)	24(1)	6(1)	4(1)	4(1)

C(7A)	23(1)	45(1)	48(1)	-4(1)	-6(1)	5(1)
C(2A)	17(1)	17(1)	15(1)	-1(1)	-2(1)	-2(1)
C(9A)	28(1)	19(1)	23(1)	3(1)	5(1)	5(1)
C(8A)	33(1)	23(1)	28(1)	-2(1)	8(1)	5(1)
C(10A)	34(1)	42(1)	23(1)	8(1)	1(1)	13(1)
O(1B)	16(1)	18(1)	20(1)	-1(1)	-3(1)	1(1)
O(2B)	16(1)	14(1)	42(1)	-3(1)	-7(1)	2(1)
N(1B)	14(1)	14(1)	20(1)	-2(1)	-2(1)	2(1)
C(2B)	17(1)	13(1)	21(1)	0(1)	2(1)	1(1)
C(3B)	16(1)	16(1)	14(1)	1(1)	2(1)	-1(1)
C(1B)	17(1)	13(1)	22(1)	-1(1)	1(1)	1(1)
C(10B)	33(1)	28(1)	39(1)	-16(1)	-3(1)	-2(1)
C(5B)	20(1)	13(1)	22(1)	-2(1)	-1(1)	2(1)
C(6B)	16(1)	19(1)	25(1)	-4(1)	-5(1)	2(1)
C(4B)	20(1)	13(1)	21(1)	-3(1)	-1(1)	-1(1)
C(8B)	18(1)	25(1)	39(1)	4(1)	0(1)	0(1)
C(9B)	18(1)	15(1)	36(1)	-5(1)	-4(1)	0(1)
C(7B)	22(1)	25(1)	21(1)	-1(1)	-4(1)	4(1)
O(2C)	18(1)	24(1)	21(1)	-7(1)	-5(1)	7(1)
O(1C)	16(1)	23(1)	19(1)	-4(1)	-3(1)	1(1)
N(1C)	14(1)	15(1)	17(1)	0(1)	-2(1)	0(1)
C(1C)	16(1)	14(1)	16(1)	0(1)	1(1)	-1(1)
C(6C)	15(1)	17(1)	21(1)	-1(1)	-5(1)	1(1)
C(2C)	16(1)	14(1)	16(1)	0(1)	2(1)	0(1)
C(3C)	15(1)	16(1)	15(1)	2(1)	1(1)	-3(1)
C(5C)	18(1)	13(1)	22(1)	-2(1)	1(1)	1(1)
C(4C)	18(1)	16(1)	18(1)	-3(1)	0(1)	-2(1)
C(8C)	22(1)	27(1)	23(1)	5(1)	-3(1)	2(1)
C(9C)	19(1)	17(1)	17(1)	-3(1)	-3(1)	1(1)
C(7C)	16(1)	26(1)	25(1)	1(1)	-2(1)	-1(1)
C(10C)	30(1)	17(1)	25(1)	-2(1)	-5(1)	-3(1)

Table E. 4. Hydrogen coordinates (x 10^4) and isotropic displacement parameters (Å^{2}x 10^3) for 2-Ethyl-3-hydroxy-1-isopropyl-4-pyridone (**6**).

	x	y	z	U(eq)
H(2A)	4514	921	-46	33
H(5A)	1212	368	919	28
H(6A)	527	2576	473	28
H(4A)	2720	-650	823	29
H(7AA)	-523	1080	387	58
H(7AB)	-1165	1841	633	58
H(7AC)	-534	918	800	58
H(9AA)	3008	2907	44	28
H(9AB)	1892	3147	258	28
H(8AA)	689	1967	1191	42
H(8AB)	62	2934	1059	42
H(8AC)	1390	2855	1028	42
H(10A)	1522	3108	-360	49
H(10B)	804	2286	-164	49
H(10C)	1910	1986	-372	49
H(2B)	8941	308	1526	36
H(10D)	6614	264	601	50

H(10E)	6525	-875	698	50
H(10F)	7602	-258	811	50
H(5B)	5942	3311	1394	22
H(6B)	4814	1358	910	24
H(4B)	7652	3398	1668	22
H(8BA)	4154	942	1474	41
H(8BB)	3220	1571	1276	41
H(8BC)	3985	2076	1568	41
H(9BA)	5399	82	1089	27
H(9BB)	6349	-495	1298	27
H(7BA)	4441	3374	1101	34
H(7BB)	3843	2803	788	34
H(7BC)	5142	3065	763	34
H(2C)	10371	1296	1927	31
H(6C)	14543	259	2492	21
H(5C)	13764	-1378	1814	21
H(4C)	12198	-1296	1464	21
H(8CA)	13568	-1039	2770	36
H(8CB)	14882	-1246	2785	36
H(8CC)	14119	-1818	2510	36
H(9CA)	13130	826	2711	21
H(9CB)	11996	1376	2609	21
H(7CA)	15433	-1180	2018	33
H(7CB)	16152	-525	2282	33
H(7CC)	15541	-23	1956	33
H(10G)	13024	2450	2227	36
H(10H)	14157	1902	2331	36
H(10I)	13497	2533	2617	36

Table E.5. Torsion angles [°] for 2-Ethyl-3-hydroxy-1-isopropyl-4-pyridone (**6**).

C(1A)-N(1A)-C(5A)-C(4A)	-1.6(2)
C(6A)-N(1A)-C(5A)-C(4A)	179.73(13)
C(5A)-N(1A)-C(1A)-C(2A)	2.62(18)
C(6A)-N(1A)-C(1A)-C(2A)	-178.79(11)
C(5A)-N(1A)-C(1A)-C(9A)	-179.24(12)
C(6A)-N(1A)-C(1A)-C(9A)	-0.65(18)
C(5A)-N(1A)-C(6A)-C(8A)	69.45(15)
C(1A)-N(1A)-C(6A)-C(8A)	-109.15(13)
C(5A)-N(1A)-C(6A)-C(7A)	-54.65(16)
C(1A)-N(1A)-C(6A)-C(7A)	126.74(13)
N(1A)-C(5A)-C(4A)-C(3A)	-0.6(2)
O(1A)-C(3A)-C(4A)-C(5A)	-179.54(13)
C(2A)-C(3A)-C(4A)-C(5A)	1.58(19)
N(1A)-C(1A)-C(2A)-O(2A)	179.43(11)
C(9A)-C(1A)-C(2A)-O(2A)	1.26(17)
N(1A)-C(1A)-C(2A)-C(3A)	-1.53(18)
C(9A)-C(1A)-C(2A)-C(3A)	-179.70(11)
O(1A)-C(3A)-C(2A)-O(2A)	-0.41(18)
C(4A)-C(3A)-C(2A)-O(2A)	178.50(11)
O(1A)-C(3A)-C(2A)-C(1A)	-179.45(12)
C(4A)-C(3A)-C(2A)-C(1A)	-0.53(17)
C(2A)-C(1A)-C(9A)-C(10A)	90.28(14)
N(1A)-C(1A)-C(9A)-C(10A)	-87.86(14)
O(2B)-C(2B)-C(3B)-O(1B)	2.92(18)
C(1B)-C(2B)-C(3B)-O(1B)	-177.76(12)

O(2B)-C(2B)-C(3B)-C(4B)	-176.72(11)
C(1B)-C(2B)-C(3B)-C(4B)	2.60(17)
O(2B)-C(2B)-C(1B)-N(1B)	179.28(11)
C(3B)-C(2B)-C(1B)-N(1B)	-0.05(18)
O(2B)-C(2B)-C(1B)-C(9B)	-1.77(18)
C(3B)-C(2B)-C(1B)-C(9B)	178.90(12)
C(5B)-N(1B)-C(1B)-C(2B)	-2.65(18)
C(6B)-N(1B)-C(1B)-C(2B)	-176.90(11)
C(5B)-N(1B)-C(1B)-C(9B)	178.42(12)
C(6B)-N(1B)-C(1B)-C(9B)	4.17(18)
C(1B)-N(1B)-C(5B)-C(4B)	2.67(19)
C(6B)-N(1B)-C(5B)-C(4B)	177.05(12)
C(5B)-N(1B)-C(6B)-C(8B)	-89.31(13)
C(1B)-N(1B)-C(6B)-C(8B)	84.98(14)
C(5B)-N(1B)-C(6B)-C(7B)	35.10(15)
C(1B)-N(1B)-C(6B)-C(7B)	-150.61(11)
N(1B)-C(5B)-C(4B)-C(3B)	0.13(19)
O(1B)-C(3B)-C(4B)-C(5B)	177.73(12)
C(2B)-C(3B)-C(4B)-C(5B)	-2.63(17)
C(2B)-C(1B)-C(9B)-C(10B)	-76.05(16)
N(1B)-C(1B)-C(9B)-C(10B)	102.87(14)
C(5C)-N(1C)-C(1C)-C(2C)	-2.87(17)
C(6C)-N(1C)-C(1C)-C(2C)	-179.20(10)
C(5C)-N(1C)-C(1C)-C(9C)	178.76(11)
C(6C)-N(1C)-C(1C)-C(9C)	2.43(16)
C(5C)-N(1C)-C(6C)-C(8C)	-80.74(13)
C(1C)-N(1C)-C(6C)-C(8C)	95.62(13)
C(5C)-N(1C)-C(6C)-C(7C)	44.88(14)
C(1C)-N(1C)-C(6C)-C(7C)	-138.76(11)
N(1C)-C(1C)-C(2C)-O(2C)	-178.27(10)
C(9C)-C(1C)-C(2C)-O(2C)	0.11(16)
N(1C)-C(1C)-C(2C)-C(3C)	2.49(17)
C(9C)-C(1C)-C(2C)-C(3C)	-179.13(11)
O(2C)-C(2C)-C(3C)-O(1C)	-0.36(17)
C(1C)-C(2C)-C(3C)-O(1C)	178.87(11)
O(2C)-C(2C)-C(3C)-C(4C)	179.82(10)
C(1C)-C(2C)-C(3C)-C(4C)	-0.96(17)
C(1C)-N(1C)-C(5C)-C(4C)	1.82(17)
C(6C)-N(1C)-C(5C)-C(4C)	178.23(11)
N(1C)-C(5C)-C(4C)-C(3C)	-0.29(19)
O(1C)-C(3C)-C(4C)-C(5C)	-179.98(11)
C(2C)-C(3C)-C(4C)-C(5C)	-0.16(17)
C(2C)-C(1C)-C(9C)-C(10C)	-91.88(14)
N(1C)-C(1C)-C(9C)-C(10C)	86.48(14)

Table E.6. Hydrogen bonds for 2-Ethyl-3-hydroxy-1-isopropyl-4-pyridone (**6**) [Å and °].

D-H...A	d(D-H)	d(H...A)	d(D...A)	<(DHA)
O(2A)-H(2A)...O(1A)$^{\#1}$	0.82	1.93	2.6491(14)	146.6
O(2B)-H(2B)...O(1C)	0.82	1.91	2.6517(17)	149.4
O(2C)-H(2C)...O(1B)	0.82	1.86	2.5879(14)	148.0

Symmetry transformations used to generate equivalent atoms: #1 -x+1,-y,-z

F. Data for Bis(1-ethyl-3-hydroxy-2-methyl-4-pyridinonato) copper(II) (8)

Table F. 1. Atomic coordinates (x 10^4) and equivalent isotropic displacement parameters ($Å^2$x 10^3) for Bis(1-ethyl-3-hydroxy-2-methyl-4-pyridinonato)copper(II) (**8**). U(eq) is defined as one third of the trace of the orthogonalized U^{ij} tensor.

	x	y	z	U(eq)
Cu(1)	0	5000	5000	13(1)
Cu(2)	5000	0	0	13(1)
O(1B)	2694(2)	327(2)	522(1)	16(1)
O(2B)	6370(2)	706(2)	1535(1)	17(1)
O(2A)	1652(2)	4852(2)	3938(2)	17(1)
O(1A)	-1223(2)	6442(2)	3943(2)	19(1)
N(1A)	1640(3)	6884(2)	1303(2)	14(1)
N(2B)	4338(3)	2047(2)	3869(2)	13(1)
C(2A)	1203(3)	5759(2)	3063(2)	14(1)
C(1A)	-370(3)	6625(2)	3079(2)	16(1)
C(2B)	5129(3)	1099(2)	2147(2)	14(1)
C(3B)	5706(3)	1654(2)	3298(2)	14(1)
C(11A)	2582(4)	7032(2)	296(2)	18(1)
C(3A)	2201(3)	5907(2)	2178(2)	15(1)
C(4B)	2455(3)	1861(2)	3348(2)	16(1)
C(1B)	3138(3)	883(2)	1593(2)	14(1)
C(11B)	4878(3)	2635(2)	5108(2)	16(1)
C(5A)	-837(4)	7617(2)	2182(2)	19(1)
C(4A)	176(3)	7714(2)	1314(2)	17(1)
C(12B)	5059(4)	1578(2)	6086(2)	21(1)
C(5B)	1814(3)	1280(2)	2235(2)	16(1)
C(31B)	7785(3)	1809(3)	3910(2)	24(1)
C(12A)	1777(4)	6094(3)	-756(2)	25(1)
C(31A)	3905(4)	5055(3)	2197(2)	21(1)

Table F.2. Bond lengths [Å] and angles [°] for Bis(1-ethyl-3-hydroxy-2-methyl-4-pyridinonato)copper(II) (**8**).

Cu(1)-O(2A)$^{\#1}$	1.9061(17)
Cu(1)-O(2A)	1.9061(17)
Cu(1)-O(1A)$^{\#1}$	1.9426(16)
Cu(1)-O(1A)	1.9426(16)
Cu(2)-O(2B)$^{\#2}$	1.9083(16)
Cu(2)-O(2B)	1.9083(16)
Cu(2)-O(1B)$^{\#2}$	1.9342(16)
Cu(2)-O(1B)	1.9342(16)
O(1B)-C(1B)	1.303(3)
O(2B)-C(2B)	1.329(3)
O(2A)-C(2A)	1.323(3)
O(1A)-C(1A)	1.296(3)
N(1A)-C(4A)	1.352(3)
N(1A)-C(3A)	1.379(3)

N(1A)-C(11A)	1.478(3)
N(2B)-C(4B)	1.350(3)
N(2B)-C(3B)	1.372(3)
N(2B)-C(11B)	1.485(3)
C(2A)-C(3A)	1.385(3)
C(2A)-C(1A)	1.437(3)
C(1A)-C(5A)	1.401(3)
C(2B)-C(3B)	1.385(3)
C(2B)-C(1B)	1.432(3)
C(3B)-C(31B)	1.492(3)
C(11A)-C(12A)	1.524(3)
C(11A)-H(11A)	0.9700
C(11A)-H(11B)	0.9700
C(3A)-C(31A)	1.496(3)
C(4B)-C(5B)	1.362(3)
C(4B)-H(4B)	0.9300
C(1B)-C(5B)	1.402(3)
C(11B)-C(12B)	1.518(3)
C(11B)-H(11C)	0.9700
C(11B)-H(11D)	0.9700
C(5A)-C(4A)	1.372(3)
C(5A)-H(5A)	0.9300
C(4A)-H(4A)	0.9300
C(12B)-H(12D)	0.9600
C(12B)-H(12E)	0.9600
C(12B)-H(12F)	0.9600
C(5B)-H(5B)	0.9300
C(31B)-H(31D)	0.9600
C(31B)-H(31E)	0.9600
C(31B)-H(31F)	0.9600
C(12A)-H(12A)	0.9600
C(12A)-H(12B)	0.9600
C(12A)-H(12C)	0.9600
C(31A)-H(31A)	0.9600
C(31A)-H(31B)	0.9600
C(31A)-H(31C)	0.9600

O(2A)$^{\#1}$-Cu(1)-O(2A)	180.0
O(2A)$^{\#1}$-Cu(1)-O(1A)$^{\#1}$	86.00(7)
O(2A)-Cu(1)-O(1A)$^{\#1}$	94.00(7)
O(2A)$^{\#1}$-Cu(1)-O(1A)	94.00(7)
O(2A)-Cu(1)-O(1A)	86.00(7)
O(1A)$^{\#1}$-Cu(1)-O(1A)	179.999(1)
O(2B)$^{\#2}$-Cu(2)-O(2B)	180.0
O(2B)$^{\#2}$-Cu(2)-O(1B)$^{\#2}$	86.70(7)
O(2B)-Cu(2)-O(1B)$^{\#2}$	93.30(7)
O(2B)$^{\#2}$-Cu(2)-O(1B)	93.30(7)
O(2B)-Cu(2)-O(1B)	86.70(7)
O(1B)$^{\#2}$-Cu(2)-O(1B)	180.0
C(1B)-O(1B)-Cu(2)	109.51(14)
C(2B)-O(2B)-Cu(2)	109.18(13)
C(2A)-O(2A)-Cu(1)	110.16(14)
C(1A)-O(1A)-Cu(1)	109.91(14)
C(4A)-N(1A)-C(3A)	121.3(2)
C(4A)-N(1A)-C(11A)	117.57(19)
C(3A)-N(1A)-C(11A)	121.1(2)
C(4B)-N(2B)-C(3B)	121.25(19)
C(4B)-N(2B)-C(11B)	117.52(19)
C(3B)-N(2B)-C(11B)	121.17(18)
O(2A)-C(2A)-C(3A)	122.8(2)

O(2A)-C(2A)-C(1A)	116.8(2)
C(3A)-C(2A)-C(1A)	120.3(2)
O(1A)-C(1A)-C(5A)	125.0(2)
O(1A)-C(1A)-C(2A)	117.1(2)
C(5A)-C(1A)-C(2A)	117.9(2)
O(2B)-C(2B)-C(3B)	122.4(2)
O(2B)-C(2B)-C(1B)	117.4(2)
C(3B)-C(2B)-C(1B)	120.2(2)
N(2B)-C(3B)-C(2B)	119.0(2)
N(2B)-C(3B)-C(31B)	120.7(2)
C(2B)-C(3B)-C(31B)	120.4(2)
N(1A)-C(11A)-C(12A)	112.4(2)
N(1A)-C(11A)-H(11A)	109.1
C(12A)-C(11A)-H(11A)	109.1
N(1A)-C(11A)-H(11B)	109.1
C(12A)-C(11A)-H(11B)	109.1
H(11A)-C(11A)-H(11B)	107.9
N(1A)-C(3A)-C(2A)	118.9(2)
N(1A)-C(3A)-C(31A)	120.5(2)
C(2A)-C(3A)-C(31A)	120.6(2)
N(2B)-C(4B)-C(5B)	122.1(2)
N(2B)-C(4B)-H(4B)	118.9
C(5B)-C(4B)-H(4B)	118.9
O(1B)-C(1B)-C(5B)	124.9(2)
O(1B)-C(1B)-C(2B)	117.1(2)
C(5B)-C(1B)-C(2B)	118.0(2)
N(2B)-C(11B)-C(12B)	110.68(19)
N(2B)-C(11B)-H(11C)	109.5
C(12B)-C(11B)-H(11C)	109.5
N(2B)-C(11B)-H(11D)	109.5
C(12B)-C(11B)-H(11D)	109.5
H(11C)-C(11B)-H(11D)	108.1
C(4A)-C(5A)-C(1A)	119.7(2)
C(4A)-C(5A)-H(5A)	120.2
C(1A)-C(5A)-H(5A)	120.2
N(1A)-C(4A)-C(5A)	121.8(2)
N(1A)-C(4A)-H(4A)	119.1
C(5A)-C(4A)-H(4A)	119.1
C(11B)-C(12B)-H(12D)	109.5
C(11B)-C(12B)-H(12E)	109.5
H(12D)-C(12B)-H(12E)	109.5
C(11B)-C(12B)-H(12F)	109.5
H(12D)-C(12B)-H(12F)	109.5
H(12E)-C(12B)-H(12F)	109.5
C(4B)-C(5B)-C(1B)	119.4(2)
C(4B)-C(5B)-H(5B)	120.3
C(1B)-C(5B)-H(5B)	120.3
C(3B)-C(31B)-H(31D)	109.5
C(3B)-C(31B)-H(31E)	109.5
H(31D)-C(31B)-H(31E)	109.5
C(3B)-C(31B)-H(31F)	109.5
H(31D)-C(31B)-H(31F)	109.5
H(31E)-C(31B)-H(31F)	109.5
C(11A)-C(12A)-H(12A)	109.5
C(11A)-C(12A)-H(12B)	109.5
H(12A)-C(12A)-H(12B)	109.5
C(11A)-C(12A)-H(12C)	109.5
H(12A)-C(12A)-H(12C)	109.5
H(12B)-C(12A)-H(12C)	109.5
C(3A)-C(31A)-H(31A)	109.5

C(3A)-C(31A)-H(31B)	109.5
H(31A)-C(31A)-H(31B)	109.5
C(3A)-C(31A)-H(31C)	109.5
H(31A)-C(31A)-H(31C)	109.5
H(31B)-C(31A)-H(31C)	109.5

Symmetry transformations used to generate equivalent atoms:
#1 -x,-y+1,-z+1 #2 -x+1,-y,-z

Table F.3. Anisotropic displacement parameters ($Å^2$ x 10^3)for Bis(1-ethyl-3-hydroxy-2-methyl-4-pyridinonato)copper(II) (**8**). The anisotropic displacement factor exponent takes the form: $-2\pi^2[h^2 a^{*2} U^{11} + ... + 2 h k a^* b^* U^{12}]$

	U^{11}	U^{22}	U^{33}	U^{23}	U^{13}	U^{12}
Cu(1)	16(1)	12(1)	13(1)	3(1)	5(1)	1(1)
Cu(2)	14(1)	13(1)	11(1)	1(1)	4(1)	-1(1)
O(1B)	15(1)	17(1)	14(1)	-1(1)	3(1)	-1(1)
O(2B)	14(1)	23(1)	14(1)	-2(1)	4(1)	-2(1)
O(2A)	20(1)	14(1)	18(1)	5(1)	8(1)	3(1)
O(1A)	20(1)	18(1)	20(1)	6(1)	9(1)	4(1)
N(1A)	18(1)	13(1)	13(1)	2(1)	4(1)	-2(1)
N(2B)	13(1)	13(1)	11(1)	0(1)	2(1)	-1(1)
C(2A)	16(1)	12(1)	13(1)	2(1)	3(1)	-2(1)
C(1A)	15(1)	15(1)	15(1)	1(1)	3(1)	-1(1)
C(2B)	14(1)	14(1)	14(1)	2(1)	5(1)	1(1)
C(3B)	13(1)	16(1)	15(1)	0(1)	4(1)	-3(1)
C(11A)	21(1)	16(1)	16(1)	2(1)	7(1)	-3(1)
C(3A)	16(1)	13(1)	15(1)	1(1)	2(1)	-2(1)
C(4B)	15(1)	16(1)	18(1)	1(1)	7(1)	2(1)
C(1B)	16(1)	11(1)	14(1)	2(1)	3(1)	1(1)
C(11B)	17(1)	15(1)	16(1)	-2(1)	5(1)	-1(1)
C(5A)	19(1)	17(1)	20(1)	3(1)	5(1)	4(1)
C(4A)	19(1)	15(1)	15(1)	5(1)	2(1)	0(1)
C(12B)	25(1)	21(1)	16(1)	2(1)	5(1)	0(1)
C(5B)	12(1)	17(1)	18(1)	1(1)	2(1)	0(1)
C(31B)	16(1)	35(2)	21(1)	-8(1)	5(1)	-3(1)
C(12A)	36(2)	22(1)	19(1)	-2(1)	9(1)	-4(1)
C(31A)	24(1)	20(1)	23(1)	7(1)	12(1)	5(1)

Table F.4. Hydrogen coordinates (x 10^4) and isotropic displacement parameters ($Å^2$x 10^3) for Bis(1-ethyl-3-hydroxy-2-methyl-4-pyridinonato)copper(II) (**8**).

	x	y	z	U(eq)
H(11A)	3945	6867	609	21
H(11B)	2415	7932	-9	21
H(4B)	1567	2138	3761	19
H(11C)	3913	3275	5181	19

H(11D)	6089	3091	5226	19
H(5A)	-1829	8206	2176	23
H(4A)	-154	8368	717	20
H(12D)	5406	1976	6879	31
H(12E)	6029	952	6021	31
H(12F)	3855	1135	5975	31
H(5B)	510	1149	1905	19
H(31D)	7930	2207	4696	36
H(31E)	8364	2359	3415	36
H(31F)	8399	959	4013	36
H(12A)	2428	6224	-1386	38
H(12B)	433	6266	-1081	38
H(12C)	1962	5201	-462	38
H(31A)	4419	5291	1523	32
H(31B)	3525	4148	2128	32
H(31C)	4863	5181	2951	32

Table F.5. Torsion angles [°] for Bis(1-ethyl-3-hydroxy-2-methyl-4-pyridinonato)copper(II) (**8**).

O(2B)$^{\#2}$-Cu(2)-O(1B)-C(1B)	-177.96(15)
O(2B)-Cu(2)-O(1B)-C(1B)	2.04(15)
O(1B)$^{\#2}$-Cu(2)-O(1B)-C(1B)	-36(8)
O(2B)$^{\#2}$-Cu(2)-O(2B)-C(2B)	-85(9)
O(1B)$^{\#2}$-Cu(2)-O(2B)-C(2B)	177.65(14)
O(1B)-Cu(2)-O(2B)-C(2B)	-2.35(14)
O(2A)$^{\#1}$-Cu(1)-O(2A)-C(2A)	40(24)
O(1A)$^{\#1}$-Cu(1)-O(2A)-C(2A)	-179.21(15)
O(1A)-Cu(1)-O(2A)-C(2A)	0.79(15)
O(2A)$^{\#1}$-Cu(1)-O(1A)-C(1A)	179.04(15)
O(2A)-Cu(1)-O(1A)-C(1A)	-0.96(15)
O(1A)$^{\#1}$-Cu(1)-O(1A)-C(1A)	86(14)
Cu(1)-O(2A)-C(2A)-C(3A)	178.24(18)
Cu(1)-O(2A)-C(2A)-C(1A)	-0.5(2)
Cu(1)-O(1A)-C(1A)-C(5A)	-177.50(19)
Cu(1)-O(1A)-C(1A)-C(2A)	0.9(2)
O(2A)-C(2A)-C(1A)-O(1A)	-0.3(3)
C(3A)-C(2A)-C(1A)-O(1A)	-179.1(2)
O(2A)-C(2A)-C(1A)-C(5A)	178.2(2)
C(3A)-C(2A)-C(1A)-C(5A)	-0.5(3)
Cu(2)-O(2B)-C(2B)-C(3B)	179.88(18)
Cu(2)-O(2B)-C(2B)-C(1B)	2.3(2)
C(4B)-N(2B)-C(3B)-C(2B)	2.3(3)
C(11B)-N(2B)-C(3B)-C(2B)	179.4(2)
C(4B)-N(2B)-C(3B)-C(31B)	-177.1(2)
C(11B)-N(2B)-C(3B)-C(31B)	0.0(3)
O(2B)-C(2B)-C(3B)-N(2B)	179.44(19)
C(1B)-C(2B)-C(3B)-N(2B)	-3.0(3)
O(2B)-C(2B)-C(3B)-C(31B)	-1.1(3)
C(1B)-C(2B)-C(3B)-C(31B)	176.4(2)
C(4A)-N(1A)-C(11A)-C(12A)	-95.6(2)
C(3A)-N(1A)-C(11A)-C(12A)	82.5(3)
C(4A)-N(1A)-C(3A)-C(2A)	1.7(3)
C(11A)-N(1A)-C(3A)-C(2A)	-176.3(2)
C(4A)-N(1A)-C(3A)-C(31A)	-176.0(2)
C(11A)-N(1A)-C(3A)-C(31A)	5.9(3)

O(2A)-C(2A)-C(3A)-N(1A)	-179.7(2)
C(1A)-C(2A)-C(3A)-N(1A)	-1.0(3)
O(2A)-C(2A)-C(3A)-C(31A)	-1.9(3)
C(1A)-C(2A)-C(3A)-C(31A)	176.7(2)
C(3B)-N(2B)-C(4B)-C(5B)	-0.1(3)
C(11B)-N(2B)-C(4B)-C(5B)	-177.3(2)
Cu(2)-O(1B)-C(1B)-C(5B)	178.72(18)
Cu(2)-O(1B)-C(1B)-C(2B)	-1.3(2)
O(2B)-C(2B)-C(1B)-O(1B)	-0.7(3)
C(3B)-C(2B)-C(1B)-O(1B)	-178.3(2)
O(2B)-C(2B)-C(1B)-C(5B)	179.31(19)
C(3B)-C(2B)-C(1B)-C(5B)	1.6(3)
C(4B)-N(2B)-C(11B)-C(12B)	85.8(2)
C(3B)-N(2B)-C(11B)-C(12B)	-91.5(2)
O(1A)-C(1A)-C(5A)-C(4A)	179.8(2)
C(2A)-C(1A)-C(5A)-C(4A)	1.4(3)
C(3A)-N(1A)-C(4A)-C(5A)	-0.8(3)
C(11A)-N(1A)-C(4A)-C(5A)	177.3(2)
C(1A)-C(5A)-C(4A)-N(1A)	-0.8(4)
N(2B)-C(4B)-C(5B)-C(1B)	-1.3(4)
O(1B)-C(1B)-C(5B)-C(4B)	-179.5(2)
C(2B)-C(1B)-C(5B)-C(4B)	0.5(3)

Symmetry transformations used to generate equivalent atoms:

#1 -x,-y+1,-z+1 #2 -x+1,-y,-z

G. Data for Bis(2-ethyl-3-hydroxy-1-isopropyl-4-pyridinonato)copper(II) (9)

Table G.1. Atomic coordinates (x 10^4) and equivalent isotropic displacement parameters (Å^{2}x 10^3) for Bis(2-ethyl-3-hydroxy-1-isopropyl-4-pyridinonato)copper(II) (**9**). U(eq) is defined as one third of the trace of the orthogonalized U^{ij} tensor.

	x	y	z	U(eq)
Cu(1)	0	0	0	13(1)
O(2)	40(1)	-1877(1)	861(1)	16(1)
O(3)	-3440(1)	2995(1)	-917(1)	26(1)
O(1)	-1780(1)	265(1)	-135(1)	17(1)
N(1)	-2633(1)	-3637(2)	1436(1)	16(1)
C(2)	-1121(1)	-2123(2)	900(1)	14(1)
C(1)	-1397(1)	-3461(2)	1440(1)	15(1)
C(6)	-3015(1)	-5041(2)	1995(1)	19(1)
C(5)	-3569(1)	-2541(2)	916(1)	20(1)
C(9)	-345(1)	-4722(2)	1958(1)	17(1)
C(4)	-3334(1)	-1207(2)	375(1)	20(1)
C(8)	-3588(2)	-4195(2)	2680(1)	25(1)
C(3)	-2102(1)	-955(2)	358(1)	15(1)
C(11)	-2777(2)	4397(2)	-1176(1)	27(1)
C(7)	-3919(2)	-6353(2)	1330(1)	28(1)
C(10)	-289(2)	-6302(2)	1336(1)	24(1)

Table G.2. Bond lengths [Å] and angles [°] for Bis(2-ethyl-3-hydroxy-1-isopropyl-4-pyridinonato)copper(II) (**9**).

Cu(1)-O(2)$^{\#1}$	1.9094(9)
Cu(1)-O(2)	1.9094(9)
Cu(1)-O(1)$^{\#1}$	1.9300(9)
Cu(1)-O(1)	1.9300(9)
O(2)-C(2)	1.3245(15)
O(3)-C(11)	1.4185(18)
O(3)-H(3)	0.8200
O(1)-C(3)	1.3050(16)
N(1)-C(5)	1.3531(17)
N(1)-C(1)	1.3786(17)
N(1)-C(6)	1.5007(17)
C(2)-C(1)	1.3921(18)
C(2)-C(3)	1.4258(18)
C(1)-C(9)	1.5054(18)
C(6)-C(7)	1.520(2)
C(6)-C(8)	1.521(2)
C(6)-H(6)	0.9800
C(5)-C(4)	1.3735(19)
C(5)-H(5)	0.9300
C(9)-C(10)	1.5295(19)
C(9)-H(9A)	0.9700
C(9)-H(9B)	0.9700
C(4)-C(3)	1.3920(18)
C(4)-H(4)	0.9300
C(8)-H(8A)	0.9600
C(8)-H(8B)	0.9600
C(8)-H(8C)	0.9600
C(11)-H(11A)	0.9600
C(11)-H(11B)	0.9600
C(11)-H(11C)	0.9600
C(7)-H(7A)	0.9600
C(7)-H(7B)	0.9600
C(7)-H(7C)	0.9600
C(10)-H(10A)	0.9600
C(10)-H(10B)	0.9600
C(10)-H(10C)	0.9600
O(2)$^{\#1}$-Cu(1)-O(2)	180.00(7)
O(2)$^{\#1}$-Cu(1)-O(1)$^{\#1}$	86.37(4)
O(2)-Cu(1)-O(1)$^{\#1}$	93.63(4)
O(2)$^{\#1}$-Cu(1)-O(1)	93.63(4)
O(2)-Cu(1)-O(1)	86.37(4)
O(1)$^{\#1}$-Cu(1)-O(1)	180.0
C(2)-O(2)-Cu(1)	109.52(8)
C(11)-O(3)-H(3)	109.5
C(3)-O(1)-Cu(1)	109.57(8)
C(5)-N(1)-C(1)	120.95(11)
C(5)-N(1)-C(6)	116.57(11)
C(1)-N(1)-C(6)	122.48(11)
O(2)-C(2)-C(1)	122.50(11)
O(2)-C(2)-C(3)	117.14(11)
C(1)-C(2)-C(3)	120.36(12)
N(1)-C(1)-C(2)	118.91(11)
N(1)-C(1)-C(9)	122.64(11)

C(2)-C(1)-C(9)	118.36(11)
N(1)-C(6)-C(7)	110.04(11)
N(1)-C(6)-C(8)	110.09(11)
C(7)-C(6)-C(8)	112.55(12)
N(1)-C(6)-H(6)	108.0
C(7)-C(6)-H(6)	108.0
C(8)-C(6)-H(6)	108.0
N(1)-C(5)-C(4)	121.84(12)
N(1)-C(5)-H(5)	119.1
C(4)-C(5)-H(5)	119.1
C(1)-C(9)-C(10)	111.31(11)
C(1)-C(9)-H(9A)	109.4
C(10)-C(9)-H(9A)	109.4
C(1)-C(9)-H(9B)	109.4
C(10)-C(9)-H(9B)	109.4
H(9A)-C(9)-H(9B)	108.0
C(5)-C(4)-C(3)	119.77(12)
C(5)-C(4)-H(4)	120.1
C(3)-C(4)-H(4)	120.1
C(6)-C(8)-H(8A)	109.5
C(6)-C(8)-H(8B)	109.5
H(8A)-C(8)-H(8B)	109.5
C(6)-C(8)-H(8C)	109.5
H(8A)-C(8)-H(8C)	109.5
H(8B)-C(8)-H(8C)	109.5
O(1)-C(3)-C(4)	124.57(12)
O(1)-C(3)-C(2)	117.25(11)
C(4)-C(3)-C(2)	118.17(12)
O(3)-C(11)-H(11A)	109.5
O(3)-C(11)-H(11B)	109.5
H(11A)-C(11)-H(11B)	109.5
O(3)-C(11)-H(11C)	109.5
H(11A)-C(11)-H(11C)	109.5
H(11B)-C(11)-H(11C)	109.5
C(6)-C(7)-H(7A)	109.5
C(6)-C(7)-H(7B)	109.5
H(7A)-C(7)-H(7B)	109.5
C(6)-C(7)-H(7C)	109.5
H(7A)-C(7)-H(7C)	109.5
H(7B)-C(7)-H(7C)	109.5
C(9)-C(10)-H(10A)	109.5
C(9)-C(10)-H(10B)	109.5
H(10A)-C(10)-H(10B)	109.5
C(9)-C(10)-H(10C)	109.5
H(10A)-C(10)-H(10C)	109.5
H(10B)-C(10)-H(10C)	109.5

Symmetry transformations used to generate equivalent atoms: #1 -x,-y,-z

Table G.3. Anisotropic displacement parameters ($Å^2 \times 10^3$) for Bis(2-ethyl-3-hydroxy-1-isopropyl-4-pyridinonato)copper(II) (**9**). The anisotropic displacement factor exponent takes the form: $-2\pi^2[h^2 a^{*2} U^{11} + ... + 2 h k a^* b^* U^{12}]$

	U^{11}	U^{22}	U^{33}	U^{23}	U^{13}	U^{12}
Cu(1)	13(1)	13(1)	14(1)	2(1)	5(1)	0(1)

O(2)	14(1)	17(1)	17(1)	4(1)	6(1)	1(1)
O(3)	21(1)	21(1)	38(1)	10(1)	11(1)	5(1)
O(1)	16(1)	16(1)	20(1)	5(1)	6(1)	1(1)
N(1)	17(1)	15(1)	18(1)	2(1)	7(1)	-1(1)
C(2)	15(1)	14(1)	13(1)	-2(1)	4(1)	0(1)
C(1)	16(1)	13(1)	14(1)	-1(1)	4(1)	0(1)
C(6)	20(1)	17(1)	21(1)	6(1)	9(1)	-1(1)
C(5)	15(1)	21(1)	23(1)	3(1)	7(1)	0(1)
C(9)	17(1)	17(1)	16(1)	4(1)	5(1)	2(1)
C(4)	16(1)	19(1)	23(1)	6(1)	5(1)	4(1)
C(8)	30(1)	28(1)	20(1)	3(1)	11(1)	-2(1)
C(3)	17(1)	13(1)	15(1)	0(1)	5(1)	-1(1)
C(11)	24(1)	22(1)	34(1)	4(1)	9(1)	2(1)
C(7)	34(1)	22(1)	32(1)	-3(1)	17(1)	-9(1)
C(10)	30(1)	19(1)	24(1)	2(1)	9(1)	6(1)

Table G.4. Hydrogen coordinates (x 10^4) and isotropic displacement parameters ($Å^2$ x 10^3) for Bis(2-ethyl-3-hydroxy-1-isopropyl-4-pyridinonato)copper(II) (**9**).

	x	y	z	U(eq)
H(3)	-2945	2176	-697	39
H(6)	-2243	-5683	2367	23
H(5)	-4395	-2694	925	24
H(9A)	-488	-5143	2524	20
H(9B)	468	-4105	2151	20
H(4)	-3996	-475	22	24
H(8A)	-2982	-3388	3088	38
H(8B)	-3793	-5100	3055	38
H(8C)	-4351	-3564	2331	38
H(11A)	-2602	5315	-707	40
H(11B)	-3292	4865	-1778	40
H(11C)	-1986	3961	-1218	40
H(7A)	-4714	-5776	997	41
H(7B)	-4072	-7326	1689	41
H(7C)	-3542	-6785	883	41
H(10A)	-1046	-7007	1217	36
H(10B)	450	-7007	1655	36
H(10C)	-236	-5884	747	36

Table G.5. Torsion angles [°] for Bis(2-ethyl-3-hydroxy-1-isopropyl-4-pyridinonato)copper(II) (**9**).

Cu(1)-O(2)-C(2)-C(1)	177.06(10)
Cu(1)-O(2)-C(2)-C(3)	-2.69(14)
C(5)-N(1)-C(1)-C(2)	0.31(19)
C(6)-N(1)-C(1)-C(2)	179.93(12)

C(5)-N(1)-C(1)-C(9)	-176.00(12)
C(6)-N(1)-C(1)-C(9)	3.63(19)
O(2)-C(2)-C(1)-N(1)	-179.51(11)
C(3)-C(2)-C(1)-N(1)	0.25(19)
O(2)-C(2)-C(1)-C(9)	-3.04(19)
C(3)-C(2)-C(1)-C(9)	176.71(12)
C(5)-N(1)-C(6)-C(7)	65.98(16)
C(1)-N(1)-C(6)-C(7)	-113.66(14)
C(5)-N(1)-C(6)-C(8)	-58.63(16)
C(1)-N(1)-C(6)-C(8)	121.72(13)
C(1)-N(1)-C(5)-C(4)	-0.3(2)
C(6)-N(1)-C(5)-C(4)	-179.94(13)
N(1)-C(1)-C(9)-C(10)	87.95(15)
C(2)-C(1)-C(9)-C(10)	-88.37(15)
N(1)-C(5)-C(4)-C(3)	-0.3(2)
Cu(1)-O(1)-C(3)-C(4)	-176.23(11)
Cu(1)-O(1)-C(3)-C(2)	2.62(14)
C(5)-C(4)-C(3)-O(1)	179.66(13)
C(5)-C(4)-C(3)-C(2)	0.8(2)
O(2)-C(2)-C(3)-O(1)	0.03(18)
C(1)-C(2)-C(3)-O(1)	-179.73(12)
O(2)-C(2)-C(3)-C(4)	178.96(12)
C(1)-C(2)-C(3)-C(4)	-0.80(19)

Symmetry transformations used to generate equivalent atoms: #1 -x,-y,-z

Table G.6. Hydrogen bonds for Bis(2-ethyl-3-hydroxy-1-isopropyl-4-pyridinonato)copper(II) (**9**) [Å and °].

D-H...A	d(D-H)	d(H...A)	d(D...A)	<(DHA)
O(3)-H(3)...O(1)	0.82	1.93	2.7520(14)	177.9
C(5)-H(5)...O(3)#2	0.93	2.41	3.3419(17)	177.9
C(9)-H(9B)...O(2)	0.97	2.49	2.8271(16)	100.4
C(11)-H(11C)...O(2)#1	0.96	2.58	3.4829(18)	156.5

Symmetry transformations used to generate equivalent atoms:

#1 -x,-y,-z #2 -x-1,-y,-z